**Characterizing Chromosome Instability in Chemonaïve, Chemosensitive and Chemoresistant High-Grade Serous Ovarian Cancer**

by

Claire R. Morden

A Thesis submitted to the Faculty of Graduate Studies of

The University of Manitoba

In partial fulfillment of the requirements of the degree of

**Master of Science**

Department of Biochemistry and Medical Genetics

University of Manitoba

Winnipeg, Manitoba, Canada

**ABSTRACT**

High-grade serous ovarian cancer (HGSOC) is the most common and lethal gynaecological malignancy in women. The high level of mortality in HGSOC patients is attributed to late stage diagnoses, highly aggressive metastatic disease, disease recurrence and drug resistance. Currently, little is known about the underlying mechanisms driving tumor recurrence and drug resistance in HGSOC. Chromosome instability (CIN; an increased rate of chromosome gains and losses) is one mechanism associated with multi-drug resistance and tumor recurrence in many cancer types, but has only just begun to be characterized in HGSOC. I hypothesize that CIN is prevalent in HGSOC, is associated with HGSOC progression and will increase in recurrent and chemoresistant disease. Using a combination of quantitative imaging microscopy and cytogenetic approaches, I investigate the prevalence and unique temporal dynamics of CIN in ascites derived patient samples and solid tumor samples collected from HGSOC patients, encompassing chemonaïve, chemosensitive and chemoresistant disease. CIN was prevalent in 92.5% of HGSOC ascites derived patient samples and 100% of HGSOC solid tumors. Further in-depth analyses demonstrated that serial ascites derived HGSOC patient samples exhibit statistically significant changes over time (*i.e.* temporal dynamics). Importantly, aneuploidy and CIN increases with disease progression and recurrence, and CIN exhibits varied dynamics during and following chemotherapy, highlighting CIN as a potential biomarker of disease progression.

**ACKNOWLEDGEMENTS**

First and foremost, I would like to express my deepest gratitude to my supervisors and mentors, Dr. Kirk McManus and Dr. Mark Nachtigal. Thank you both for your time, advice and unwavering support throughout my graduate degree. You both have pushed me to grow, move out of my comfort zone, and reach my full potential as a student and person – I am extremely privileged to have worked with you both. I would also like to acknowledge and thank my advisory committee; Dr. Tamra Ogilvie and Dr. Yvonne Myal, for their time, questions, feedback, advice, support and laughter during meetings. You both helped keep me grounded, reflect on my growth and gain confidence in my abilities as a student.

I would like to thank all lab members of the McManus and Nachtigal labs, past and present; Zelda Lichtensztejn, Mirka Sliwowski, Dr. Raghvendra Vishwakarma, Dr. Laura Thompson, Lucile Jeusset, Nicole Wilson, Chloe Lepage, Manisha Bungsy, Michaela Palmer, Kailee Rutherford, Ally Farrell, Nicole Neudorf and all summer and co-op students I have had an opportunity to work with. Thank you for all of your kindness, support, laughter and fun over my graduate degree. This process would have been a lot harder without each of you. I would especially like to thank Zelda for training me and helping me trouble shoot my experiments, Mirka for establishing, growing and maintaining patient samples, and Ally for your hard work and significant contributions to my research project.

A special thank you goes out to Andrea Fristensky, Shannon Kornelsen, the Manitoba Tumor Bank, and the women who generously donated their biologic samples. Without you I would not have access to or information on the precious clinical samples I used for this study.

This research was funded by the Manitoba Graduate Scholarship, Diagnostic Services Manitoba, CancerCare Manitoba Foundation and the University of Manitoba. I would also like to thank the donors that provided funding for the Women's Health Research Foundation of Canada Graduate Scholarship, Arnold Portigal Award, the 1st Place Basic Sciences Poster Presentation Award, and all travel awards from the Faculty of Graduate Studies, Biochemistry and Medical Genetics, and the University of Manitoba Graduate Students Association.

Lastly, I would like to thank my family and friends, especially my mom and Braden. Thank you for your love, encouragement, patience, kindness and support in my life and studies. This has been a long and hard process, and each of you played an important role by reminding me that there is life outside of school, and by encouraging me to take time to rest and recuperate.

**DEDICATION**

*This thesis is dedicated to my mom,*

*Marie Annette Morden,*

*with love.*

*Thank you for being an inspiration, role model, and friend.*

*I could not have made it this far without you.*

**TABLE OF CONTENTS**

## LIST OF ABBREVIATIONS

| | |
|---|---|
| 2D | 2-dimensional |
| 3D | 3-dimensional |
| ~ | Approximately |
| ASI | Applied spectral imaging |
| COEUR | Canadian Ovarian Experimental Unified Resource |
| CA125 | Cancer antigen 125 |
| cm | Centimeter(s) (size) |
| xg | Centrifugal force |
| CEPs | Chromosome enumeration probes |
| CIN | Chromosome instability |
| *CS* | Chromosome instability score |
| $CS_8$ | Chromosome instability score chromosome 8 |
| $CS_{11}$ | Chromosome instability score chromosome 11 |
| $CS_{17}$ | Chromosome instability score chromosome 17 |
| ctDNA | Circulating tumor DNA |
| CIMP | CpG island methylator phenotype |
| $CS_c$ | Combined chromosome instability score |
| CGH | Comparative genomic hybridization |
| CT | Computerized tomography |
| °C | Degrees Celsius |
| DNA | Deoxyribonucleic acid |
| DAPI | 4',6-diamidino-2-phenylindole |
| DMEM | Dulbecco's Modified Eagle's Medium |
| *et al.* | Et alia (and others) |
| *e.g.* | exempli gratia |
| EOC | Epithelial ovarian cancer |
| FTF | Fallopian tube fimbriae |
| FT | Fallopian tube secretory epithelial (cell lines) |
| FTSEC | Fallopian tube secretory epithelial cells (patient samples; negative control) |
| FIGO | Federation of Gynecology and Obstetrics |
| FBS | Fetal bovine serum |
| Fig | Figure |
| FISH | Fluorescence *in situ* hybridization |
| FFPE | Formalin fixed paraffin embedded |
| HIPC | Heat intraperitoneal chemotherapy |
| H&E | Hematoxylin and eosin |
| HE4 | Human epididymis protein 4 |
| HGSOC | High-grade serous ovarian cancer |
| HRR | Homologous recombination repair |
| h | Hour |
| *i.e.* | Id est |
| ITH | Intratumoral heterogeneity |
| IP | Intraperitoneal |
| IV | Intravenous |

| | |
|---|---|
| KS | Kolmogorov-Smirnov |
| L | Liver core marker |
| MRI | Magnetic resonance imaging |
| MOBP | Manitoba Ovarian Biobank Program |
| MW | Mann-Whitney |
| µg | Microgram(s) (weight) |
| µL | Microliter(s) (volume) |
| µm | Micrometer(s) (size) |
| $\mu m^2$ | Micrometer(s) squared (area) |
| MSI | Microsatellite instability |
| mL | Milliliter(s) (volume) |
| mm | Millimeter(s) (size) |
| mM | Millimolar(s) (concentration) |
| min | Minute(s) |
| M | Molar (concentration) |
| nm | Nanometer(s) (size) |
| N/A | Not applicable |
| NOS | Not otherwise specified |
| ns | Not significant |
| NAs | Nuclear areas |
| n | Number of nuclei analyzed |
| N | Number of replicates |
| N-CIN | Numerical chromosome instability |
| pg. | Page |
| % | Percent |
| PBS | Phosphate buffered saline |
| PARP | Poly ADP-ribose polymerase |
| PET-CT | Positron emission tomography-computerized tomography |
| *p*-value | Probability value |
| QuantIM | Quantitative imaging microscopy |
| RT | Room temperature |
| SSC | Saline sodium citrate |
| SEE-FIM | Sectioning and Extensively Examining the Fimbriated End |
| SD | Standard deviation |
| S-CIN | Structural chromosome instability |
| STIC | Serous tubal intraepithelial carcinoma |
| TERT | Telomerase reverse transcriptase |
| tiff | Tagged image file format |
| TMA | Tissue microarray(s) |
| TCPS2 | Tri-council policy statement |
| VEGF | Vascular endothelial growth factor |
| vs. | Versus |

**LIST OF TABLES**

## LIST OF FIGURES

## USED WITH PERMISSIONS and CONTRIBUTION OF AUTHOR

***PREFACE**:*

This thesis contains material, images, and/or ideas from one article published in the peer-reviewed journal *Cancers*, of which Claire Morden was co-first author. This journal applies the Creative Commons Attribution (CC BY) license to articles and other works, such that articles can be reused in whole or in part for any purpose.

## CONTRIBUTION OF AUTHOR

***CHAPTER 1 AND CHAPTER 7:***

Lepage, C.C., **Morden, C.R.**, Palmer, M.C.L., Nachtigal, M.W., and McManus, K.J. Detecting Chromosome Instability in Cancer: Approaches to Resolve Cell-to-Cell Heterogeneity. Cancers. 11, (2019).

Contribution: Claire Morden contributed to original draft preparation (40%) and editing (40%).

# CHAPTER 1: INTRODUCTION

## 1.1.0 Overview of Ovarian Cancer

In Canada, cancer is the leading cause of death and it is predicted that 1 in 2 Canadians will develop cancer in their lifetime, and 1 in 4 Canadians will die of cancer[1]. More specifically, 220,400 Canadians were diagnosed with cancer and 82,100 died from the disease in 2019 alone[1]. Ovarian cancer is the 8th most common cancer in women, accounting for ~3000 Canadian (~90 Manitoban) women or 2.8% of newly diagnosed cancer cases annually, and it is predicted that 1 in 75 women will develop the disease in their lifetime[1]. Additionally, ovarian cancer is the 5th leading cause of death, accounting for ~1900 Canadian (~65 Manitoban) women or 4.9% of all cancer deaths in women annually, making it the most lethal gynecologic malignancy[1]. Ovarian cancer is a nonspecific term used to describe an assortment of tumors involving the reproductive tract that may involve the ovary. More specifically, ovarian cancers can occur in the two cell types that comprise the ovaries, including germ cells[2] and sex-cord stromal cells[3] (Figure [Fig] 1-1); however, 90% of ovarian cancers are categorised as epithelial ovarian cancer (EOC)[4] and arise from cells not associated with the ovary[5] (*detailed below in Section 1.1.1*).

EOC is a highly heterogeneous disease that consists of two biologically distinct histological subtypes termed type I and type II[6,7] (Fig 1-1). Type I tumors account for ~25% of all EOCs and includes low-grade serous ovarian cancer, endometrioid carcinoma, clear-cell carcinoma, mucinous carcinoma, and rare malignant Brenner tumours[6,7] (Fig 1-1). Type I tumors typically grow more slowly compared to type II tumors and have a high frequency of early stage diagnoses (stage I) while the tumor is still confined to the ovary[6,7]. Additionally, type I tumors are characterized by a number of defined genetic alterations, including *BRAS*[8], *KRAF*[8], and *PTEN*[9] mutations, but retain wild-type *TP53* status[10]. Type II tumors account for ~75% of newly

diagnosed cases, and include high-grade serous ovarian cancer (HGSOC), as well as rare undifferentiated carcinomas and carcinosarcomas (Fig 1-1)[6,7]. Importantly, HGSOC represents the majority of type II tumors, accounting for ~70% of all EOC diagnoses (~60 Manitoban women annually[1]). Unfortunately, HGSOC also accounts for ~70-80% of all EOC deaths[11] (~50 Manitoban women annually[1]), as patients typically present with highly aggressive metastases throughout the peritoneal cavity[12], are diagnosed at late stages (stage III and IV)[13], and generally have a poor prognosis and outcomes[12,14]. Due to its high prevalence, HGSOC will be the focus for the remainder of this study.

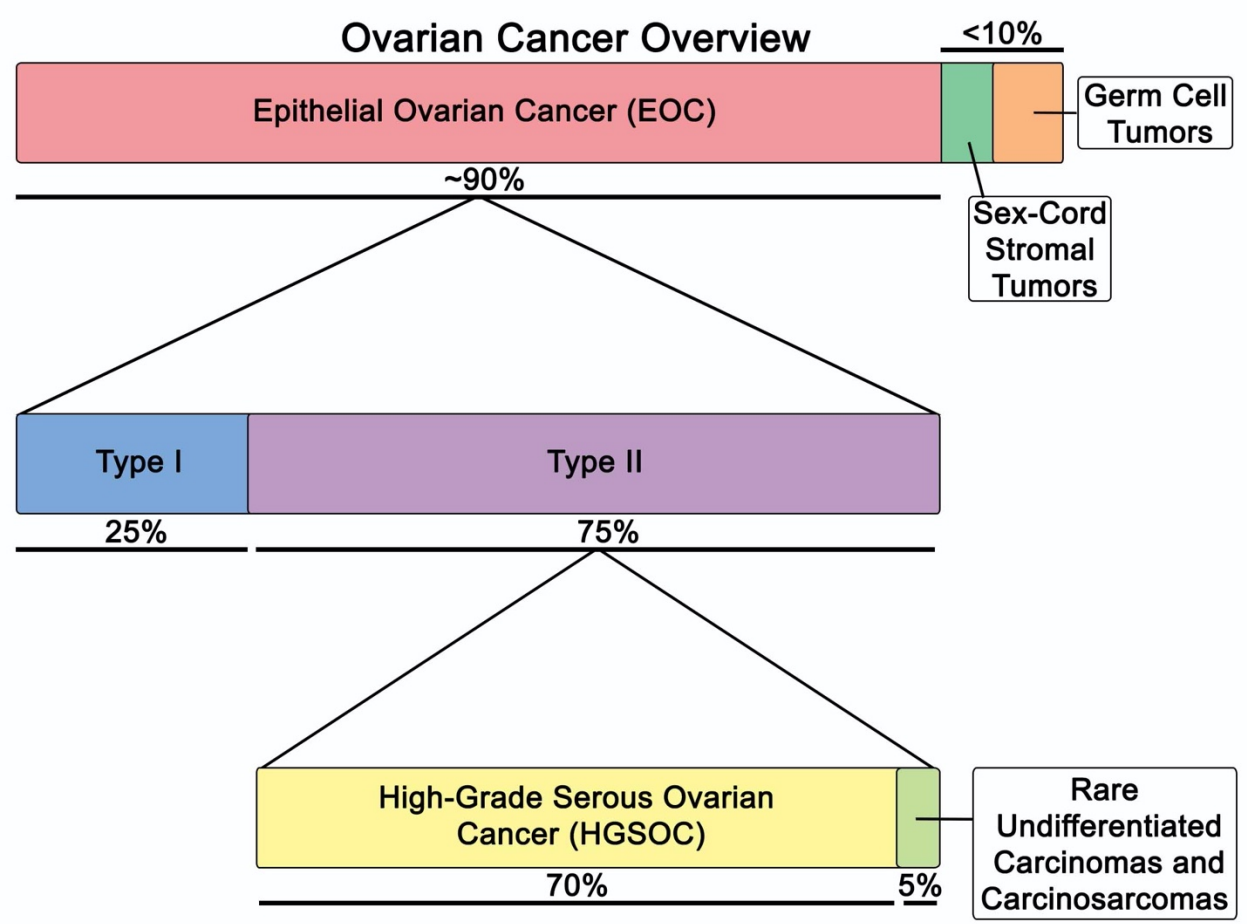


**Figure 1-1. Ovarian Cancer Histological Subtypes Overview.**
Schematic depicting the division of ovarian cancer subtypes. Note the size of the bars represent the disease frequencies for each subtype. Ovarian cancers can occur in epithelial cells, sex-cord stromal cells and germ cells. EOC is the most common form of ovarian cancer and is further subdivided into Type I and Type II EOC tumors. HGSOC is the most common subtype of EOC and represents 70% of all EOC diagnoses.

### 1.1.1 Molecular Pathogenesis, Cells of Origin and Risk Factors of HGSOC

Compared to type I EOCs, HGSOC has few recurrent somatic or germline mutations and is characterized by widespread copy number gains and losses involving all chromosomes[12,15], with the exception of somatic mutations in *TP53*, which occur in > 96% of HGSOCs[15–18]. Mutations in *TP53* are thought to be an early event in HGSOC pathogenesis as they occur in precursor lesions[5,7,19]. Type II EOCs were previously believed to arise from the ovarian surface epithelium[6,7,20]; however, more recent studies have determined that HGSOC likely arises from secretory epithelial cells located at the distal end of the fallopian tube that have transformed into a serous tubal intraepithelial carcinoma (STIC)[5,7,19–23]. Following transformation, STIC lesions can subsequently implant into the ovarian surface epithelium, but more commonly grow so large that the ovary is encompassed by the tumor[5,7,19–23]. These findings were confirmed by immunohistochemistry studies, which showed the same *TP53* mutations in benign fallopian tube secretory epithelial cells, STICs and HGSOC lesions[17,18,22,24]. Additional immunohistochemical studies have determined that HGSOCs are positive for PAX8 labeling (a Müllerian epithelial marker, which includes the fallopian tube epithelium) and negative for calretinin labeling (an ovarian surface epithelium mesothelial marker), further confirming fallopian tube secretory epithelial cells as HGSOC precursor cells[23].

*BRCA1* and *BRCA2* are two distinct tumor suppressor genes and functional studies show that the proteins they encode play a role in chromatin remodeling, transcriptional control, cell cycle regulation, and DNA repair processes (*e.g.* homologous recombination repair [HRR])[25,26]. Importantly, germline and somatic *BRCA1* and *BRCA2* mutations occur in ~12% and ~11% of HGSOCs[15], respectively, and loss of *BRCA1/2* function results in genome instability, tumour initiation and tumor evolution (*i.e.* increased intratumoral heterogeneity [ITH])[26,27]. Additionally,

germline mutations of *BRCA1* and *BRCA2* are associated with increased lifetime risk of breast and ovarian cancer. More specifically, the estimated lifetime risk of developing ovarian cancer ranges from 40-60% and 11-35% for individuals with germline mutations in the *BRCA1* and *BRCA2* gene, respectively[25]. Interestingly, studies have shown that exons 11-13 in both *BRCA1* and *BRCA2* harbour a large proportion of clinically relevant mutations and are highly important for the tumor suppressor function of the proteins[25,26]. Additional studies expanded on these findings and determined that mutations in exon 11 of both *BRCA1*/2 are associated with increased risk of ovarian cancer over breast cancer and correlates to an earlier diagnosis[26,28]. Further, epigenetic modifications of *BRCA1* promoters through DNA hypermethylation prevents gene expression, while additional somatic mutations to genes that function in HRR occurs in 40-50% of HGSOCs[7,20].

### 1.1.2 HGSOC Early Detection, Diagnosis, Staging and Prognosis

HGSOC patients are typically post-menopausal women with ~75% of cases diagnosed at late stages (stage III or IV; *staging detailed below*)[11]. Unfortunately, late stage diagnoses are common due to the fact that early stage HGSOCs are often asymptomatic and late stage HGSOCs have nonspecific and vague symptoms, such as back pain, abdominal pain/bloating, constipation, and/or urinary symptoms that could be accredited to conditions other than cancer[29]. Additionally, Ovarian Cancer Canada states there are occasional symptoms, such as changes in bowel habits, extreme fatigue and/or unexplained weight loss that can occur and recommends that women contact their doctor if any of the symptoms mentioned above are persistent for more than 3 weeks[30]. Moreover, many women are diagnosed at later stages because there are a limited number screening modalities and a lack of early detection technologies[29]. For example, current screening

procedures, including transvaginal ultrasound and serial measurements of cancer antigen 125 (CA125), are used for individuals with increased risk of ovarian cancer (*i.e.* women harbouring *BRCA1/2* germline mutations)[29]. These modalities are not used to screen average risk women as it does not decrease mortality risk, is associated with false-positives and increased harm due to unnecessary surgical intervention of benign lesions, increased infections, and cardiovascular/pulmonary complications[29].

In order to diagnose ovarian cancer, symptomatic women are assessed for risk factors, family history of cancer, and undergo a complete physical examination for pelvic and/or abdominal masses[29]. While physical examination plays an important role in diagnosis, it lacks the sensitivity to detect small masses[29]. Imaging technologies provide additional evidence for ovarian cancer diagnosis, including: 1) transvaginal ultrasound, which can be used to assess ovarian architecture and vascularity, distinguish between benign (cystic) and malignant (solid masses) lesions, and detect ascites (*detailed below in Section 1.1.3*)[29,31]; 2) computerized tomography (CT) scan, which is the recommended imaging modality, can be used to determine the size of the primary tumors, size and location of any peritoneal metastases (provided the tumors are > 1 cm in size) and investigate lymph node involvement[31]; 3) magnetic resonance imaging (MRI), which can be used to detect lesions that cannot be determined by ultrasound or CT scans and plays an important role in determining the extent of peritoneal dissemination in preoperative patients[31]; and 4) positron emission tomography-CT (PET-CT), which can be used for staging, detecting recurrence (provided the tumors are > 1 cm in size), and selecting optimal surgical candidates[31].

Following imagining, women with suspected ovarian cancer undergo laboratory testing of serum biomarkers, such as human epididymis protein 4 (HE4) and CA125[29,32,33]. Both HE4 and CA125 are glycoproteins that are increased in 33% and 80% of late stage EOCs, respectively, and

are used for diagnoses, to assess disease progression and to monitor disease recurrance[29,32]. Unfortunately, both HE4 and CA125 have a limited capacity to identify ovarian cancers as HE4 is only increased in < 50% of late stage patients and CA125 is only increased in 50% of early stage EOCs and can be elevated in benign conditions such as endometriosis and fibroids[29,32]. Therefore, laparoscopy (*e.g.* a small tube with a camera) can be used to obtain biopsies and confirm HGSOC diagnoses through hematoxylin and eosin (H&E) staining or immunohistochemistry (*i.e.* PAX8 positive staining)[29,34], although, in most clinical settings, diagnoses through biopsies of large ovarian masses is discouraged due to the potential of tumor spreading and upstaging patients (*i.e.* changing the stage used to describe a patients cancer from a lower stage to a higher stage and more widespread disease)[14].

HGSOC staging is based on the 2014 International Federation of Gynecology and Obstetrics (FIGO) staging for ovarian, fallopian tube and peritoneal cancer or the 2018 American Joint Committee on Cancer TNM (tumor, nodes and metastasis) staging system and is assigned during surgical intervention (*i.e.* laparotomy) for HGSOC[31,34,35]. Importantly, surgical staging confirms diagnoses, provides a better understanding of the severity of a patient's clinical condition, and is used to predict patient outcomes and plan for adequate treatments[31,34,35]. Stage I describes tumors that are confined to the ovaries and fallopian tube(s) and is divided into three subcategories, IA, IB, and IC[31,34,35]. Stage IA and IB represent tumors that involve one or both ovaries, respectively, with the capsule intact, and no malignant cells in the ascites or peritoneal washings[31,34,35]. Stage IC is divided into three subcategories and describes tumors that are confined to the ovaries or fallopian tubes with any of the following: 1) surgical spill intraoperatively (IC1); 2) capsule ruptured before surgery (IC2); and 3) malignant cells present in the ascites or peritoneal washings (IC3)[31,34,35]. Stage II HGSOC describes tumors involving one or both ovaries or fallopian

tubes with pelvic extension, or primary peritoneal cancer, and is divided into two subcategories, IIA and IIB[31,34,35]. Stage IIA defines tumor extensions and/or implants on the uterus, fallopian tubes or ovarian surface, while stage IIB involves tumor extensions to other pelvic peritoneal tissues[31,34,35]. Stage I and II account for ~13% of all EOC diagnoses and have a 5- and 10-year survival rate of 92% and 55%, respectively[4,36]. Stage III disease describes tumors that have spread to the peritoneum outside of the pelvis and/or metastasized to the retroperitoneal lymph nodes, and is divided into three subcategories, IIIA, IIIB, and IIIC[31,34,35]. Stage IIIA describes metastases involving the retroperitoneal lymph nodes with or without microscopic peritoneal involvement above the pelvic brim, stage IIIB is associated with macroscopic (< 2 cm) metastases to the peritoneal above the pelvic brim, and stage IIIC represents macroscopic (> 2 cm) metastases to the peritoneal above the pelvic brim[31,34,35]. More than 50% of all new HGSOC diagnoses are at stage III, which has 5- and 10-year survival rates of 46%[37] and 15%[36], respectively. Finally, stage IV disease involves distant metastasis (excluding peritoneal metastases) and is divided into two subcategories, IVA and IVB[31,34,35]. Stage IVA disease describes pleural effusion with positive cytology, while stage IVB is associated with metastases to extra-abdominal organs, inguinal nodes, and lymph nodes outside the abdominal cavity[31,34,35]. Unfortunately, ~30% of all new diagnoses are stage IV, which has 5- and 10-year survival rates of 26%[37] and 15%[36], respectively. Collectively, the above information highlights that the majority (~80%) of all new HGSOC diagnoses occur at late stages (III and IV), when chemotherapy may be the only viable option.

### 1.1.3 Production, Treatment, Composition and Utility of Ascites

Ascites is the excess accumulation of fluid in the peritoneal cavity and is a symptom of many diseases including, hepatic cirrhosis (81%), heart failure (3%), tuberculosis (2%), and

malignant cancers (10%)[13,38]. Ovarian cancer is the most common cancer associated with ascites production, and ~30% of HGSOC patients present with ascites upon disease diagnosis[13,38]. Under normal conditions, the lymphatic system and capillaries located in the peritoneal lining secrete fluid to lubricate the abdominal cavity and the majority of this fluid is reabsorbed into the lymphatic channels[13,38]. However, ascites production can increase and accumulate in some HGSOC patients due to increased leaky vasculature and an inability of a patient to reabsorb fluid due to metastatic tumors obstructing lymphatic vessels[13,38]. Unfortunately, ascites production can cause abdominal pain/discomfort, early satiety, affect respiratory, gastrointestinal and urinary systems, negatively impact quality of life, is indicative of chemoresistance and recurrence, and is often a sign of advanced disease and poor prognosis[13,38]. Ascites accumulation is combated by standard HGSOC treatments, such as surgery and chemotherapy (*detailed below in Section 1.1.4*); however, as the disease progresses and becomes less responsive to treatments, large volumes (*e.g.* > 5 L) of ascites are often removed by paracentesis in order to alleviate symptoms[13,38].

Ascites is comprised of a heterogenous mix of various cell types and soluble components, such as tumor cells (singles cells and small multicellular aggregates [*i.e.* spheroids]), cancer stem-like cells[39], cancer-associated fibroblasts[40], macrophages/monocytes, inflammatory cells (*e.g.* T-cells), cytokines (*e.g.* IL-6, IL-8 and IL-10)[41,42], chemokines, growth factors (*e.g.* vascular endothelial growth factor [VEGF])[43], lysophosphatidic acid[44] and extra-cellular membrane fragments[13,38]. Each of these components constitute part of the tumor microenvironment and impact tumor proliferation, intraperitoneal dissemination, treatment response, drug resistance, and disease recurrence[13,38,39,41]. Importantly, the accessibility of ascites and the ability to isolate[45] and analyze its components render it a unique and insightful source for tumor investigation[13,38]. Studies are now able to employ ascites to identify novel therapeutic

targets, as well as prognostic and predictive biomarkers[13,38,41,43]. Additionally, since ascites production corresponds with disease progression, collection and assessment of factors within ascites can enable unique insight into the dynamics of these novel targets and biomarkers over time, during treatment, in response to treatment, upon disease recurrence and following a diagnosis of drug resistance[13,38,46].

### 1.1.4 Surgery and First-Line Chemotherapy Treatments for HGSOC

The gold standard of care for HGSOC patients is optimal surgical cytoreduction of all tumors combined with chemotherapy[14,34,47] (*treatments detailed further below*). The goal of surgical intervention is to confirm diagnosis, stage the disease, and achieve microscopic resection of all tumor masses that have disseminated to the peritoneal cavity, lymph nodes and pelvis (*i.e.* below the pelvic brim) of the patient[14,34,47]. During surgery patients often undergo a complete hysterectomy, bilateral salpingo-oophorectomy (*e.g.* surgery to remove both ovaries and fallopian tubes), pelvic and para-aortic lymph node dissection, omentectomy (*e.g.* surgery to remove the omentum) and examination of peritoneal surfaces of the diaphragm and pelvis[34]. Ideally, successful surgery involves complete resection of all tumors and the absence of any macroscopic residual disease; however, in practice, optimal cytoreduction is defined as resection of the tumors to < 1 cm of residual disease[14,34,47]. Surgical intervention resulting in > 1 cm of residual disease is considered suboptimal cytoreduction[14,34,47]. Importantly, surgical resection of tumors is the most significant prognostic factor associated with patient outcomes and the main component impacting overall survival in patients[14,34,47]. Individuals with optimal cytoreduction (< 1 cm) have worse outcomes than those with complete resection, but have better outcomes than individuals with suboptimal cytoreduction (> 1 cm)[14,34,47]. Unfortunately, some patients are not ideal surgical

candidates and have high perioperative risks (*e.g.* old age, hypertension, diabetes mellitus, and/or cardiac/pulmonary complications[48]) and low likelihood of optimal resection of the tumors to < 1 cm of residual disease[14,34]. Therefore, it is recommended that these women undergo neoadjuvant chemotherapy and interval surgical cytoreduction (*i.e.* surgery following chemotherapy)[14,34]. Interval surgical cytoreduction should be performed following three cycles of neoadjuvant chemotherapy in women who responded to initial treatments (*i.e.* women with reduced tumor burden) or with stable disease[14,34]. Importantly, neoadjuvant chemotherapy is associated with less peri- and post-operative morbidity and mortality, as well as shorter post-operative hospitalizations; however, it results in shorter overall survival compared to primary surgical cytoreduction candidates[14,34,47,49].

The gold standard for both adjuvant and neoadjuvant first-line chemotherapy in HGSOC patients is a regime of intravenous (IV) or intraperitoneal (IP) carboplatin and paclitaxel[14,34,50]. Carboplatin is a platinum agent that interferes with cell replication and division by cross-linking guanine bases in DNA double-helix strands[51]. Cross-linking guanine bases makes the DNA strands unable to uncoil and separate, interrupting replication and transcription resulting in DNA damage[51]. The DNA damage elicits DNA damage repair and apoptosis when repair is impossible[51]. Paclitaxel is a cytoskeletal drug that targets tubulin (*i.e.* the building block of microtubules) by hyper-stabilizing the microtubule structure and preventing its disassembly[51]. The resulting stabilization adversely affects the cells as microtubule dynamics are necessary for critical cell functions like mitosis[51]. Prolonged activation of mitotic checkpoints during mitosis due to hyper-stabilization triggers apoptosis and cell death[51]. A combination of IV/IP chemotherapy or IV chemotherapy alone can be used to treat patients with complete or optimal tumor resection, while IV chemotherapy is recommended for those with suboptimal tumor resection[14,34]. IP delivery

of chemotherapy is associated with a 23% reduced risk of death[34] and recently, large hospitals have started using heated intraperitoneal chemotherapy (HIPC)[52]. HIPC is based on the principle that heat is directly cytotoxic to tumors, induces protein damage, disrupts the microtubule system, and is synergistic with drug action[52]. Mechanisms of synergy include: 1) increased membrane permeability; 2) enhanced transcellular transport; and 3) deep tumor penetration[52]. Importantly, HIPC is given at the time of primary or interval cytoreductive surgery, is administered under anesthesia, shortens the time between surgery and chemotherapy treatment, and reduces the number of postoperative patients that experience hypothermia from long surgeries[52]. Nevertheless, both IP and HIPC are considered controversial and have not been widely implemented at a number of hospitals and clinics due to the lack of infrastructure, excessive system toxicities associate with IP chemotherapy and the large number of patients admitted to hospital due to adverse reactions and IP port complications[34]. Although most patients initially respond to IV/IP first-line combination chemotherapy, most (80-90%) will ultimately relapse within two years[14,47,50].

### 1.1.5 Recurrence and Second-line Chemotherapies for HGSOC

Diagnosis of recurrent disease poses similar challenges to those of initial diagnosis, as there are no specific symptoms or biomarkers. Many patients often report comparable symptoms to those at initial diagnosis, while others are asymptomatic or report new symptoms, including swelling of limbs (*i.e.* lymphoedema)[14]. Similar to the initial diagnosis, a recurrent diagnosis is based on imaging (*e.g.* CT or MRI), physical examination, or increasing concentrations of HE4 or CA125 biomarkers[14,47]. Once recurrence is suspected or diagnosed, HGSOC patients are categorized into one of three groups based on their response to initial therapy and time to recurrent disease: 1) chemorefractory; 2) chemoresistant, or 3) chemosensitive disease[14]. First,

chemorefractory disease describes patients with tumors that fail to respond to first-line chemotherapy and have continued tumor growth. These patients are treated with second-line chemotherapies or transition to end-of-life palliative care. Unsurprisingly, patients with refractory disease have very poor prognosis with an overall survival of < 12 months[14]. Second, chemoresistant disease describes patients with disease recurrence < 6 months following completion of the initial chemotherapy[14]. Similar to chemorefractory patients, these individuals are treated with second-line chemotherapies. Finally, chemosensitive disease describes patients that have recurrence > 6 months following completion of initial chemotherapy[14]. These patients have the best prognosis compared to chemorefractory and chemoresistant disease, as many chemosensitive patients are likely to respond to additional first-line chemotherapy as well as multiple second-line chemotherapies[14]. Additionally, chemosensitive patients that experience recurrence > 12 months following initial chemotherapy, have good performance (*e.g.* fully active and able to carry on all pre-disease performance without restriction[53]), are typically younger in age, have no co-morbidities, have tumors less than < 10 cm in size, < 500 mL ascites and no unresectable lesions (based on CT or MRI imaging) are candidates for secondary cytoreductive surgery[54].

Currently, there are number of second-line chemotherapies used to treat recurrent HGSOC, including: 1) cisplatin, a platinum drug that functions as a crosslinking agent similar to carboplatin[51,55]; 2) docetaxel, an antineoplastic drug that stabilizes microtubules and prevents disassembly similar to paclitaxel[51,55]; 3) gemcitabine, an antimetabolite that inhibits thymidylate synthetase and DNA replication[51,55]; 4) pegylated liposomal doxorubicin, a DNA intercalating agent that inhibits topoisomerase II[51,56]; 5) topotecan, a DNA intercalating agent that inhibits topoisomerase I[51,57]; 6) olaparib, a poly ADP-ribose polymerase (PARP) inhibitor used as a

targeted therapy to treat *BRCA1/2* mutants and individuals that are HRR deficient[14,47,50,51,58,59]; 7) bevacizumab, a monoclonal antibody that inhibits VEGF-A signaling, used as an antiangiogenic targeted therapy[14,47,50,55,60]; 8) tamoxifen, a selective estrogen receptor modulator[51,61,62]; 9) letrozole, an aromatase inhibitor[51,61,62]; and 10) megestrol acetate, a synthetic progestin used for its antianorexic and anticachexia properties as a palliative care treatment[51,62]. Importantly, many of these second-line treatments can be used alone or in combination with one another[14].

### 1.1.6 Chemoresistance in HGSOC

Despite having multiple treatment options for HGSOC, the majority of patients with recurrent disease ultimately develop and succumb to chemoresistant disease. Due to the high morbidity and mortality associated with chemoresistant disease, many studies have focused on molecular characterization of recurrent disease and elucidating the mechanisms of resistance[63–65]. Similar to primary HGSOCs, chemoresistant HGSOCs have few recurrent somatic or germline mutations, but rather, are characterized by widespread gene copy number gains and losses involving all chromosomes, with the exception of *TP53, BRCA1* and *BRCA2* (*Section 1.1.1)* and a cluster of localized breakpoints involving the long arm of chromosome 19 resulting in *CCNE1* (Cyclin E1) amplification[63]. Importantly, *CCNE1* encodes a cell cycle regulatory protein[66] that is involved in DNA replication[67], is associated with poor prognosis[68] and intrinsic drug resistance in ~20% of chemoresistant HGSOCs[63,64]. Additional acquired mechanisms of resistance in recurrent HGSOC include: 1) increased efflux or sequestering of platinum chemotherapies by copper exporters (*i.e.* ATP7A and ATP7B)[64]; 2) decreased platinum chemotherapy uptake due to loss or internalization of the copper transporter 1 protein from the plasma membrane[64]; 3) acquisition of secondary mutations in *BRCA1/2*, or decreased *BRCA1* promoter methylation, that restore HRR

(*i.e.* reversion mutations)[63]; 4) promoter fusions resulting in upregulation of *ABCB1* gene, which encodes the multidrug resistance efflux pump protein, MDR1; and 5) genome instability resulting in extensive intratumoral heterogeneity (ITH), clonal evolution and survival advantages (*i.e.* drug resistance; *detailed further below*)[64].

### 1.2.0 Chromosome Instability (CIN) in Cancer

Genome instability is an enabling feature in cancer[69], and it refers to a state of increased mutations, copy number changes, and epigenetic alterations within a cell[70,71]. Genome instability exhibits critical roles in cancer initiation, progression, evolution and drug resistance (reviewed previously[69,70,72–74]) and is characteristic of many cancer types[71,75–77]. Traditionally, genome instability has been categorized into three distinct forms: 1) microsatellite instability (MSI); 2) CpG island methylator phenotype (CIMP); and 3) chromosome instability (CIN)[70,71]. While MSI arises due to defects in DNA mismatch repair genes (*MLH1, MSH2, MSH6* and *PMS2*) that underlie DNA mismatches, as well as expansions and/or contractions of repetitive DNA sequences termed microsatellites[70,73] (reviewed previously[78]), CIMP is characterized by extensive DNA methylation (CpG dinucleotides) within promoter regions, leading to transcriptional silencing (reviewed previously[79])[70,71]. CIN is a third form of genome instability and is defined as an increase in the rate at which whole chromosomes or large parts thereof are gained or lost[69,80–82]. Collectively, all three forms of genome instability contribute to cancer pathogenesis by altering the expression and/or encoded functions of key genes, and thus they are significant contributors to the aberrant genetic and epigenetic landscapes contained within cancer cells[69,71,83]. CIN has a particular profound impact on genome instability by inducing simultaneous and ongoing copy number changes in large cohorts of genes (*e.g.* oncogenes, tumor suppressor genes, DNA repair

genes and apoptotic genes) that promote oncogenesis[71,84–86]. Thus, CIN is a dynamic phenotype that increases the probability of acquiring the myriad of genetic changes that are required to initiate and drive the development and progression of cancer[71,84,87–90].

The chromosomal alterations associated with CIN can be broadly classified as either: 1) numerical (N-CIN), involving gains and/or losses of whole chromosomes[71,81]; or, 2) structural (S-CIN), involving amplifications, deletions, inversions, and translocations of chromosomal regions that can range in size from single genes to whole chromosome arms[70,71,81,91]. Conceptually, the ongoing chromosome gains, losses or structural alterations associated with CIN promote the production of genetically distinct (*i.e.* heterogeneous) populations of daughter cells[71]. Therefore, within the context of cancer, CIN increases ITH[92,93] that under certain conditions may confer a selective growth advantage (*e.g.* increased cell proliferation, metastatic potential, or intrinsic/acquired drug resistance) to a subpopulation of cells[71,94]. Consequently, under certain selective pressures (*e.g.* chemotherapy), cells harbouring specific growth advantages (*e.g.* drug resistance), will continue to proliferate and may ultimately produce a highly aggressive or drug-resistant tumor[71,95]. In agreement with this possibility, CIN is frequently associated with disease recurrence, multi-drug resistance[94,96–99] and poor patient outcomes[71,96,100–102]. It has been suggested that extreme levels of chromosomal changes, or high rates of CIN may not be compatible with viability and cancer cells with inherently high levels of CIN die and are lost from the tumor cell population[71,103,104]. In this regard, CIN may represent a therapeutic vulnerability that can be leveraged to induce cancer-specific cell killing[71,105–108]. Therefore, identifying CIN and the causative genes and pathways are of tremendous clinical interest, as they may represent valuable diagnostic/prognostic biomarker with implications for healthcare delivery and treatment decisions[71]. Unfortunately, the prevalence of CIN and its associations with tumor progression,

treatment response and drug resistance has only just begun to be evaluated in HGSOC[46]. Thus, the current study is focused on evaluating CIN in a larger patient cohort to gain further insight into CIN and its potential association with HGSOC recurrence and chemoresistance.

### 1.2.1 Methods to Evaluate CIN

Many traditional techniques, like comparative genomic hybridization (CGH), single nucleotide polymorphism arrays, polymerase chain reaction-based methods, or flow cytometry, employ population-based averaging to identify gene copy number changes or aneuploidy within pooled samples, and erroneously equate these findings with CIN[71,109–113]. However, CIN refers to an ongoing *rate* of change that drives cell-to-cell heterogeneity rather than a static *state* such as aneuploidy[71]. Unfortunately, the population averaging associated with many of these classical studies effectively masks the cell-to-cell heterogeneity contained within the pooled samples, rendering it impossible to accurately assess CIN[71,114]. This concept is more clearly demonstrated in a study by Bakker *et al.*[71,114], where CIN was analyzed in mouse T-cell lymphoblastic lymphomas using both CGH (population-based approached) and single cell whole genome sequencing. Comparison of these approaches revealed that CGH, a common technique used to identify aneuploidy and/or copy number alterations, failed to detect the level of karyotypic heterogeneity and CIN identified by single cell whole genome sequencing[71,114]. These findings underscore the importance of assessing CIN at the single cell level using techniques that are capable of capturing the full spectrum of heterogeneity and CIN existing within a given sample[71].

In general, there are two central approaches that are used to assess CIN: 1) tracking chromosome numbers within a single cell and its progeny over time; and 2) quantitatively assessing cell-to-cell heterogeneity within a given population[71]. A fundamental benefit of the first

concept is that it allows for the calculation of an exact rate of chromosomal gains/losses over time, but this requires the use of experimental approaches, like live cell approaches and transgenic chromosome markers that do not adversely impinge upon cell proliferation or viability[71]. The second concept operates under the premise that CIN drives karyotypic heterogeneity, which in a given cellular population, can be readily detected through the use of quantitative, single cell approaches[70], including: 1) cytogenetic approaches, such as Giemsa banding, fluorescence *in situ* hybridization (FISH), and spectral karyotyping; 2) quantitative and high-throughput imaging cytometry, such as quantitative imaging microscopy (QuantIM) evaluating changes in nuclear areas (NAs) and micronuclei (*e.g.* small extra-nuclear bodies), and imaging flow cytometry; and 3) single cell genomic sequencing[71]. Due to the inherent complexities of the first approach, the latter approaches are more commonly employed as they are easily adapted to traditional endpoint analyses (live or fixed), and they can be readily employed on a wide variety of samples including precious clinical specimens[71].

## CHAPTER 2: RESEARCH RATIONALE, HYPOTHESIS AND AIMS

### 2.1.0 Rationale

In 2017, the McManus and Nachtigal laboratories showed that CIN is associated and dynamic in primary cell cultures isolated from five women with EOC[46]. In that study, they utilized both QuantIM and cytogenetic approaches (*e.g.* FISH) to assess changes in NAs and *CIN Score* (*CS*) values (*detailed further in Section 3.9.1*) within serial samples isolated from the ascites of women over time, including those with responsive, recurrent and drug resistant EOC. Interestingly, they determined that CIN increased with disease progression and drug resistance, suggesting CIN may be a novel biomarker of disease progression and/or treatment response[46]. To firmly establish the relationship between CIN and EOC and determine its potential as a novel biomarker with clinical relevance, I now seek to expand this initial work by evaluating CIN in a larger patient cohort and by focusing specifically on HGSOC due to its prevalence and poor prognosis. I will also evaluate CIN within a Manitoba EOC tissue microarray (TMA) recently developed by the Nachtigal and McManus laboratories.

### 2.2.0 Hypothesis

My literature summary and our preliminary findings suggest that CIN is associated with tumor progression, treatment response and drug resistance in EOC[46]. I hypothesize that CIN is prevalent in HGSOC, is associated with HGSOC progression and will increase in recurrent and chemoresistant disease.

### 2.3.0 Aims

*Aim 1*: To validate CEP specificity in diploid and aneuploid cell lines.

*Aim 2*: To determine the prevalence and dynamics of CIN in Manitoba HGSOC Cohort – Ascites Derived Patient Samples.

*Aim 3*: To determine the prevalence of CIN in the Manitoba EOC (HGSOC) Cohort TMA

# CHAPTER 3: MATERIALS AND METHODS

## 3.1.0 Ethics Approval Statement

This study, including the collection and use of HGSOC ascites derived patient samples and archived clinical EOC tissue samples, was approved by the University of Manitoba Research Ethics Board (ethics number HS21178). Prior to starting this study, I completed the Tri-Council Policy Statement (TCPS2) Course on Research Ethics.

## 3.2.0 Reagents

Appendix A contains a list of the solutions and the reagents used throughout this study (pg. 161). In general, reagents were purchased through ThermoFisher Scientific, Fisherbrand, Sarstedt, Gibco, Sigma-Aldrich and Vysis (Inter Medico).

## 3.3.0 Cell Culture

Human immortalized fallopian tube secretory epithelial (FT) cell lines FT190, FT194, FT237, and FT246 were utilized in this study and the general properties for each cell line are summarized in Table 3-1. All cell lines were generously provided by Dr. Ronny Drapkin (University of Pennsylvania, Philadelphia). All cell lines were cultured in Dulbecco's Modified Eagle's Medium (DMEM) (ThermoFisher Scientific), F12 supplemented with 2% Ultroser G (PALL).

**Table 3-1. Common Properties of FT190, FT194, FT237 and FT246 Cell Lines.**

| Properties | FT190 | FT194 | FT237 | FT246 |
|---|---|---|---|---|
| Organism | Human | Human | Human | Human |
| Cell Type | Immortalized Fallopian Tube Secretory Epithelial Cells | Immortalized Fallopian Tube Secretory Epithelial Cells | Immortalized Fallopian Tube Secretory Epithelial Cells | Immortalized Fallopian Tube Secretory Epithelial Cells |
| Alterations | TERT[B] + SV40 TAg | TERT + SV40 TAg | TERT + p53 shRNA, CDK4-R24C | TERT + p53 shRNA, CDK4-R24C |
| Required Medium | DMEM, F12 + 2% Ultroser G | DMEM, F12 + 2% Ultroser G | DMEM, F12 + 2% Ultroser G | DMEM, F12 + 2% Ultroser G |
| Approximate Doubling Time | ~48 h | ~24 h | ~48 h | ~40 h |
| Modal Karyotype[A] | Hypotetraploid 78, XX | Diploid 46, XX | Near Diploid 44, XX | Near Diploid 46, XX |
| Chromosome Range | 76 – 85 | 44 – 47 | 43 – 45 | 43 – 47 |

[A]The modal karyotypes have been determined for each cell line from mitotic chromosome spreads. N = 2, n = 50.
[B]Telomerase Reverse Transcriptase (TERT)

### 3.3.1 Cell Passaging

Cells were grown on 10 cm tissue culture dishes (Sarstedt) and initially seeded at 20-40% confluency. Cells were maintained in a humidified Sanyo $CO_2$ incubator at 37°C and 5.0% $CO_2$, until confluency reached > 80%. Cells were passaged in a biological safety cabinet and reseeded every 2-3 days. Medium was aspirated from the tissue culture dish and adherent cells were washed with sterile phosphate buffered saline (1x PBS). Following the aspiration of 1x PBS, 1.5 mL of 0.05% trypsin containing ethylenediaminetetraacetic acid (Gibco; Life Technologies) was added for 5-10 minutes (min) at 37 °C to detach cells from the tissue culture dish. Cells were monitored using an inverted ID03 microscope (Zeiss) and 10x objective to ensure cells had rounded up and detached from the culture dish prior to transferring to a 15 mL conical tube (ThermoFisher Scientific). Trypsin was neutralized in 3 mL of complete medium supplemented with Ultroser G and was transferred into a 15 mL conical tube. The residual cells were washed with 3 mL of 1x PBS to collect the remainder of detached cells and was transferred into the 15 mL conical tube. A total suspended volume of ~ 7 mL was centrifuged at 140x*g* for 5 min using a Thermo Scientific Legend XFR centrifuge at room temperature (RT). Supernatant was aspirated and the cell pellet was resuspended in 3 mL of 1x PBS. Approximately 1 mL of cell suspension was added back to the 10 cm culture dish containing 10 mL of fresh medium and cell culture dishes were returned to the incubator.

### 3.3.2 Generating Mitotic Chromosome Spreads

FT190, FT194, FT237 and FT246 were utilized to generate mitotic chromosome spreads. First, cells were harvested as described above (*Section 3.3.1*). Following centrifugation and aspiration of the supernatant, the pelleted cells were resuspended in aliquots of 1-2 mL of 1x PBS.

Cells were mixed by gently pipetting and flicking the tubes to minimize cell clumping. Approximately 250 µL of the cellular suspension was seeded into each well of a 2-well chamber slide (ThermoFisher Scientific), with each well containing 2 mL of medium, and allowed to grow for 24 hours (h) in the incubator. The cells were enriched in mitosis through the addition of mitotic arresting agents (*e.g.* colcemid) to the growth medium. KaryoMAX colcemid (Gibco; 10 µg/mL), which depolymerizes microtubules and disrupts spindle fiber formation and chromosome segregation, was added to the medium of asynchronously growing cells at a working concentration of 0.1 µg/mL. Empirical tests determined that 3.5 h was the optimal time for colcemid treatment in FT190 and FT246 cells and 2.5 h was optimal in FT194 and FT237 cells. Following enrichment, the colcemid containing growth medium was aspirated and 2 mL of hypotonic solution (75 mM KCl) was added to the chamber slides prior to fixation. The hypotonic solution causes the nuclei to swell and burst, and subsequently spread the mitotic chromosomes. Empirical tests determined that 11 min was the optimal time for the hypotonic treatment in FT190 and FT194 cells and 10 min was optimal in FT237 and FT246 cells.

### 3.4.0 Manitoba HGSOC Cohort – Ascites Derived Patient Samples

The Manitoba HGSOC cohort used for this study consists of 34 unique ascites derived patient samples, 12 of which include serial (*i.e.* multiple) collections and were used to assess the prevalence and temporal kinetics of CIN. The samples were provided in an anonymized fashion with additional clinical information provided by the Manitoba Ovarian Biobank Program (MOBP) administered by the Manitoba Tumor Bank (CancerCare Manitoba). Clinical information associated with each sample, included: age, date of birth, diagnosis date, primary site, tumor type,

histological grade and stage, surgery date and type, genetic test results, treatment history, CA125 results, and last known vital status.

### 3.4.1 Isolation and Cryopreservation of Patient Samples

To evaluate CIN in patient samples, tumor cells were isolated from ascites according to the protocol of Shepherd *et al.*[45] by Mirka Sliwowski, laboratory cell culture expert for the MOBP. Briefly, ascites collected by paracentesis was poured from the sterile vacuum bottles into sterile centrifuge bottles and cells were pelleted at 2500x*g* for 6 min at RT. Following centrifugation, 20 mL of supernatant was removed for cell resuspension and the remaining supernatant was aspirated. The pelleted cells were resuspended in 20 mL of supernatant, seeded into two T-75 flasks (Sarstedt) each containing 10 mL of medium, and were maintained in a humidified Fisher Scientific Isotemp incubator at 37°C and 5.0% $CO_2$. All patient samples were cultured using a 50:50 mixture of Medium 199 (Gibco) and MCDB 105 Medium (Sigma), supplemented with 10% fetal bovine serum (FBS) (Wisent). After 3-5 days of growth, the medium was aspirated, and 20 mL of medium was added to each of the two T-75 flasks. Cells were grown for 1-2 weeks in the incubator until confluency reached > 80%. During this time, 50% of the medium was replaced every 2-3 days or as needed. Once > 80% confluency was reached patient samples were harvested for cryopreservation (*detailed below*) and were stored in liquid nitrogen until ready for analysis. Briefly, cells were harvested as detailed in *Section 3.3.1*. Following centrifugation (140x*g*, 5 min) and aspiration, the pelleted cells were resuspended in 1.5 mL of freezing medium (Medium 199 + MCDB 105 Medium + 20% FBS + 10% dimethyl sulfoxide) and transferred to a Nalgene Cryoware cryogenic vial (Thermo Scientific). The cells were placed in the -80°C freezer for 24 h and moved to liquid nitrogen for long-term storage.

### 3.4.2 Seeding of Patient Samples

Primary HGSOC cell cultures were removed from cryogenic storage (liquid nitrogen) and placed into a 37°C water bath for 5 min by Mirka Sliwowski. In the biological safety cabinet, the thawed cells (~1.5 mL) were added to a 15 mL conical tube containing 3 mL of medium and centrifuged (140x*g*, 5 min). The supernatant was aspirated, the cells were resuspended in 5 mL of medium, seeded into a T-25 flask (Sarstedt) and maintained in a humidified Fisher Scientific Isotemp incubator at 37°C and 5.0% $CO_2$. After 24 h the medium was aspirated, and 5 mL of medium was added to the T-25 flask and allowed to grow as detailed above (*Section 3.4.1*). Cells were harvested as detailed in *Section 3.3.1*. The pelleted cells were provided by Mirka Sliwowski and were resuspended in aliquots of 500 µL to 1 mL of 1x PBS depending on the pellet size. Cells were mixed by gently pipetting and flicking the tubes to minimize cell clumping. Cells were seeded into a single well of a 4-well chamber slide (ThermoFisher Scientific), with each well containing 1 mL of culture medium, at 80-90% confluency and allowed to grow for 24 h.

### 3.5.0 Cell Fixation

Following the hypotonic treatment (mitotic chromosome spreads) and seeding of interphase cells, the cells were fixed using freshly prepared fixative (3:1 methanol:acetic acid). The hypotonic solution (mitotic chromosome spreads) or media (interphase cells) was aspirated and 2 mL of 1x PBS was added to the chamber slides. 3-5 drops of fixative were added to each well for 30 seconds. The 1x PBS/fixative was aspirated, and 2 mL of fixative was added for 10 min. This process was repeated two more times and each well was treated for 30 min with fixative. Following the third and final cycle of fixative, the solution was aspirated, and slides were allowed to air dry before processing and analysis.

### 3.6.0 Assessing Chromosome Instability in Cells

#### 3.6.1 Fluorescence *in situ* Hybridization (FISH) Probes

DNA FISH probes (chromosome enumeration probes [CEPs]) specifically recognizing the α satellite DNA within the pericentromeric regions of chromosomes 8, 11, and 17 (Fig. 3-1), were purchased from Vysis (Inter Medico). Each CEP harbors unique fluorescence properties (Table 3-2), which allows them to be combined in a multiplexed manner. These CEPs were chosen because the centromere is an essential chromosome structure and genes on these chromosomes are mutated or have altered expression in HGSOC, including *MTDH*[115] (chromosome 8), *WT1*[116] (chromosome 11), and *TP53*[16–18] and *BRCA1*[117] (chromosome 17).

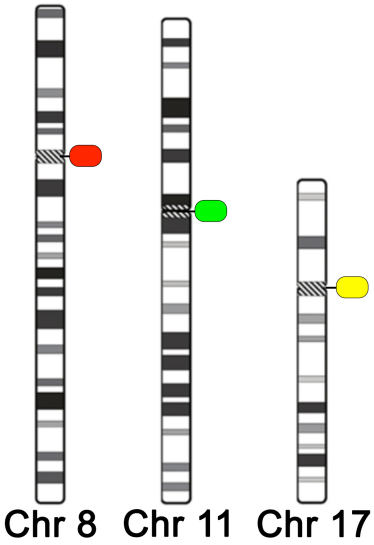


**Figure 3-1. Ideogram Depicting the Location and Pseudocolors of the DNA Probe Set.**
CEPs that hybridize to the pericentromeric α satellite DNA of chromosomes 8, 11, and 17 were employed in cell lines and patient samples and are pseudocolored red, green, and yellow, respectively[46,118].

**Table 3-2. Pericentromeric α Satellite DNA FISH Probes.**

| Properties | Chromosome 8 | Chromosome 11 | Chromosome 17 |
|---|---|---|---|
| Probe | Vysis CEP 8 | Vysis CEP 11 | Vysis CEP 17 |
| Band Region | 8p11.1-q11.1 | 11p11.11-q11 | 17p11.1-q11.1 |
| Vysis Probe Spectrum | SpectrumOrange | SpectrumGreen | SpectrumAqua |
| Excitation Peak,<br>Emission Peak | 559,<br>588 | 509,<br>538 | 433,<br>480 |
| Chroma Filter,<br>Excitation,<br>Emission | Cy3,<br>530 ± 30,<br>570 | FITC,<br>493 ± 16,<br>525 | CFP,<br>436 ± 20,<br>476 |
| Pseudocolored | Red | Green | Yellow |

### 3.6.2 FISH in Human Cell Lines and Primary Ascites Patient Samples

Mitotic chromosome spreads and interphase cells from FT190, FT194, FT237 and FT246 cell lines were used to validate the specificity of the three FISH probes employed in this study (Table 3-2). Following validation, the three FISH probes were employed in ascites derived patient samples. Briefly, slides were generated as detailed in *Sections 3.3.2, 3.4.2* and *3.4.3* and were rinsed twice with 2x saline sodium citrate buffer solution (2xSSC) (Vysis) for 5 min, with shaking. Next pepsin (50 µg/mL) (Sigma-Aldrich), a proteolytic enzyme that digests proteins including histones and other DNA-associated proteins, was added to pre-warmed 0.01 M HCl (Fisherbrand) (37°C). The acidic pH of the HCl solution was matched to the optimal pH for pepsin activity (pH 2.0). The optimal pepsin incubation time was previously determined to be 10 min at 37°C[46]. Following the pepsin treatment, the samples were washed twice with 1x PBS, and once with 1x PBS/50 mM $MgCl_2$ for 5 min each with shaking at RT. Next, slides were submerged into freshly prepared 1% formaldehyde/1x PBS/50 mM $MgCl_2$ (SigmaAldrich) for 10 min. The samples were washed for 5 min in 1x PBS with shaking, and dehydrated in serial washes of 70%, 90% and 100% ethanol (3 min each) and air dried for 5 min. The DNA was further denatured by pre-warming the slides at 70°C in a ThermoBrite slide processing system (Abbott Molecular) (5 min). Next, 100 µl of 70% formamide/2x SSC (Sigma-Aldrich) was added to each slide before gently being covered by a 22x50mm (Fisherbrand) coverslip and warmed at 70°C in a ThermoBrite slide processing system (2 min). Samples were fixed using ice cold 70%, 90% and 100% ethanol (3 min each) and air dried at RT.

The FISH probes comprising the DNA probe set (*Section 3.6.1*) were supplied pre-denatured by the manufacturer (Vysis). To prepare the multiplexed cocktail of probes, the probes were first thawed on ice and protected from the light to minimize bleaching. The

chromosome 8 FISH probe was purchased pre-diluted in hybridization buffer and was the solution into which the chromosome 11 and 17 FISH probes were added. One µL each of the chromosome 11 and 17 FISH probes were added to 8 µL of the chromosome 8 FISH probe/sample, mixed and transferred to a 0.5 mL microcentrifuge tube (Fisher Scientific). The multiplexed cocktail was subsequently mixed by vortexing and briefly centrifuged (Biofuge; Fresco) to collect the probes. A total of 10 µL of the DNA probe set was transferred to each sample contained on the four-well chamber slide before gently being covered by a 22x12.5 mm coverslip (22x50 mm coverslip cut into four using a diamond pen) on the marked region of the denatured slide. The edges of the coverslips were sealed with rubber cement (Elmers) to prevent desiccation, and the samples were incubated overnight at 37°C in the dark, in a ThermoBrite slide processing system. The following day, excess FISH probes were removed through three 5 min washes in 50% formamide/2x SSC at 42°C with shaking, followed by two additional rinses in 1x SSC (5 min) with shaking, at RT. As a final step, the DNA was counterstained through the addition of 50 µL of 4',6-diamidino-2-phenylindole (DAPI) (Sigma-Aldrich, 0.1 µg/mL), a DNA intercalating dye that was added to the slide before gently placing a coverslip and incubated for 5 min at RT. The coverslip was removed and a drop of Vectashield anti-fade mounting medium (Vector Laboratories) was placed on the marked region of the slide before placing a coverslip. The slides were stored at -20°C, prior to imaging (*Section 3.8.0*).

### 3.7.0 CIN Analysis in HGSOC Tissue Samples

#### 3.7.1 Manitoba Epithelial Ovarian Cancer Cohort Samples

A FISH-based approach was employed to determine the prevalence of CIN within a Manitoba EOC cohort comprised of EOC type I and type II solid tumors. Archived clinical formalin fixed paraffin embedded (FFPE) tissue blocks were supplied through the MOBP. The Manitoba EOC cohort consists of 52 unique patient samples and includes: two carcinosarcoma, five clear cell carcinoma, five endometroid carcinoma, 34 HGSOC, two HGSOC mixed, three mucinous adenocarcinoma and low grade mucinous, and one possible gastrointestinal metastasis. For the purpose of this study, my project focuses on the 36 type II EOC tumor samples (HGSOC). Additionally, it should be noted that 10 patient samples have associated ascites available.

#### 3.7.2 Tissue Microarrays (TMA)

The EOC solid tumor samples contained on the EOC tissue microarray (TMA) were supplied as archived clinical FFPE tissue blocks with corresponding H&E stained slides. Haematoxylin is a basic dye that stains acidic structures, most predominantly the nucleic acids of DNA, a deep purple/blue color. Eosin is an acidic dye and works by counterstaining basic cellular components, often referred to as eosinophilic structures, shades of pink. All slides from the EOC cohort were reviewed by the study collaborator and pathologist Dr. Cyrille Bicamumpaka (University of Manitoba and Manitoba Shared Health, Winnipeg). EOC solid tumor FFPE blocks were reviewed and tumour regions were marked with a felt pen by Dr. Bicamumpaka for subsequent coring.

To facilitate the CIN enumeration, two “mini-TMAs” were generated for this study by the Manitoba Tumor Bank. Mini-TMAs were generated to contain a manageable number of samples

to ensure that samples could be labeled and imaged with minimal photobleaching. Briefly, each mini-TMA contains 20-30 unique patient tumor samples, cored in duplicate, as 0.6 mm tumour cores (*e.g.* 20-30 unique patient samples x 2 cores/patient = 40-60 cores/mini-TMA). Figure 3-2 depicts the maps and histotypes of mini-TMA-1, and -2. Liver marker tissue was included in each mini-TMA (designated L) for orientation purposes. Each mini-TMA was subsequently sectioned by the Manitoba Tumor Bank at a thickness of 5 µm, a thickness previously determined to include intact (*i.e.* complete) nuclei and be compatible with the FISH probes labeling protocol[118] (Fig 3-1, Table 3-2).

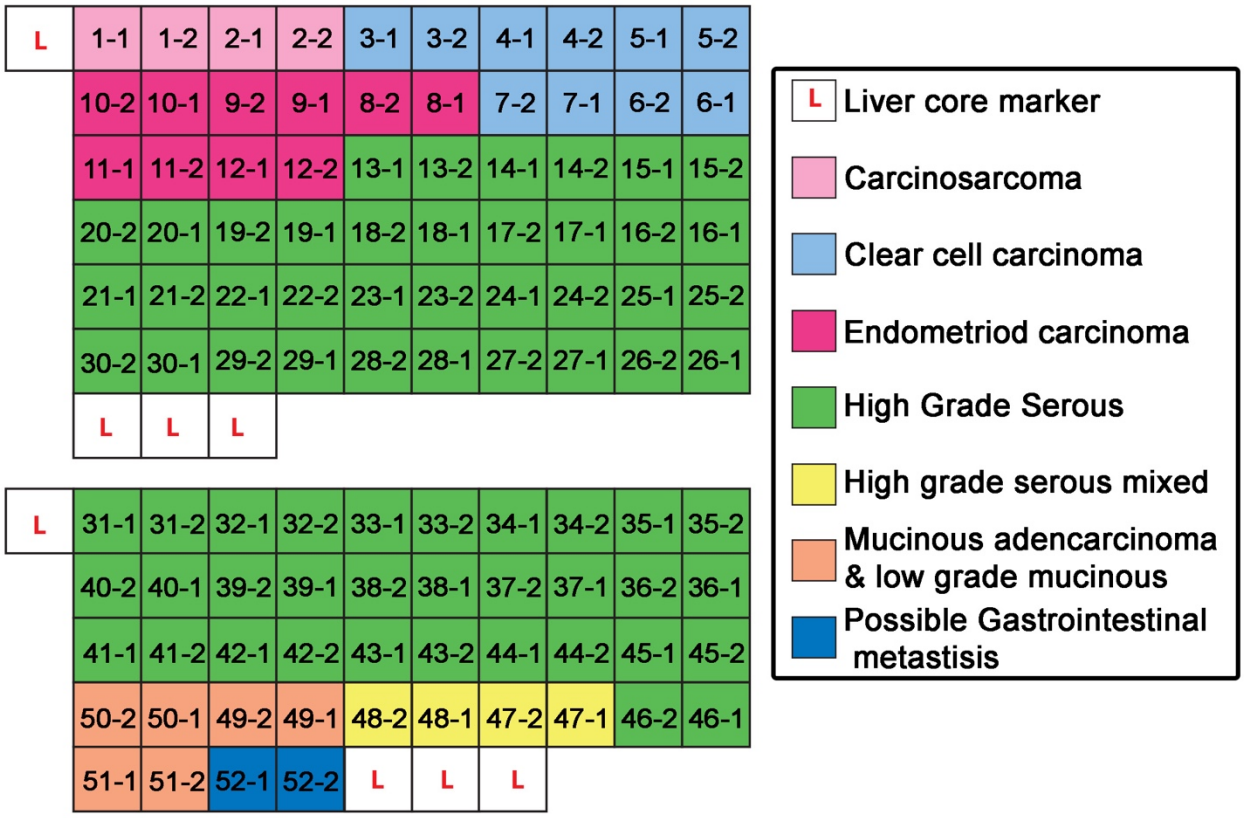


**Figure 3-2. The Manitoba EOC Cohort Contained on the Mini-TMAs.**
Map presenting the histotypes and positions for each of the 52 unique EOC samples contained within mini-TMA-1 (top) and mini-TMA-2 (bottom). The mini-TMAs include EOC samples cored in duplicate (*i.e.* #-1 and #-2 are two cores from the same patient archived clinical FFPE tissue block), and liver core markers (L) used for orientation purposes.

### 3.7.3 FISH of Formalin-Fixed, Paraffin Embedded HGSOC Samples

FISH was initially performed and optimized using 5 µm test tissue sections (granulosa cell tumor – borderline malignancy) and subsequently applied to each of the two mini-TMAs. First, paraffin was removed from the samples through two washes in xylene (10 min each) (Fisher Scientific), followed by two washes in 100% ethanol (2 x 10 min), and allowed to air dry. To prepare the DNA for hybridization with the DNA probe set, samples were incubated in a 10 mM citric acid buffer for 1 h at 80°C, followed by two 5 min washes in 2x SSC (pH 7.0), one 3 min wash in double distilled $H_20$, and a 30 min pepsin (0.5 mg/mL) treatment. Pepsin was added to pre-warmed 0.2 M HCl (pH 2.0, 37°C water bath), immediately prior to use. After two 5 min washes in 2x SSC (pH 7.0) and a serial dehydration in 70%, 90%, and 100% ethanol, the samples were hybridized with the CEPs, as detailed in *Section 3.6.2*. Next, samples were incubated at 77°C for 10 min in the ThermoBrite slide processing system, followed by an overnight incubation at 37°C. The following day, excess probe was removed through three 10 min washes in 50% formamide/2x SSC (46 °C), followed by three washes in 1x SSC (46°C) for 5 min, and one 2x SSC/01% NP-40 (VWR, 46°C) for 5 min. The samples were washed with 1x SSC (5 min, RT), followed by the addition of 150 µL of Vector TrueVIEW Autoflorescence Quenching Kit (Vector Laboratories) to reduce non-specific binding of the DNA probe set and autofluorescence in the background, and was applied to slides according to the manufacturer. Finally, nuclei were counterstained with DAPI (5 µg/mL) before placing a coverslip (22x22 mm) and left to incubate for 10 min at RT. The coverslip was removed and a drop of Vectashield Vibrance (Vector Laboratories) was placed on the marked region of the slide before placing a coverslip and incubated for 1 – 2 h at RT prior to being stored in the dark at -20°C for imaging.

### 3.8.0 Fluorescence Imaging Microscopy

#### 3.8.1 Two-Dimensional Image Acquisition

2-dimensional (2D) fluorescent images of mitotic chromosome spreads were utilized for karyotype analysis and subsequent examination of the CEP specificity. 2D images were acquired with a Zeiss AxioImager.Z2 widefield fluorescence microscope equipped with a Zeiss Axiocam MRm camera. 2D images of cell lines were acquired using a 63x Plan-Neofluar oil-immersion objective lens (numerical aperture 1.40) with Zeiss Immersol 518F immersion oil (refractive index 1.518). Images were analyzed using the Case Data Manager software from ASI (Applied Spectral Imaging). The identification of chromosomes as well as the generation of the karyotypes was performed by a trained cytogeneticist, Zelda Lichtensztejn. The remaining 2D images of interphase nuclei were acquired with a Zeiss AxioImager.Z2 widefield fluorescence microscope equipped with a Zeiss Axiocam 702 mono camera. 2D images captured from cell lines and ascites derived patient samples were acquired using a 20x Plan-Neofluar objective lens (0.5 numerical aperture), exported as a tagged image file format (tiff) and imported directly into Imaris version 7.7.2 (Bitplane) image visualization software for NA analysis and FISH probe enumeration purposes (detailed in *Section 3.9.1*).

#### 3.8.2 Three-Dimensional Image Acquisition and Deconvolution

3-dimensional (3D) images captured from the mini-TMAs were acquired using a Zeiss AxioImager.Z2 widefield fluorescence microscope equipped with a Zeiss Axiocam 702 mono camera. Orientation of the mini-TMAs was performed using a 20x objective for position and image registration, and subsequently changed to the 40x Plan-Neofluar oil-immersion objective lens (numerical aperture 1.30) with Zeiss Immersol 518F immersion oil for 3D image acquisition. The

optical sections of the 3D images were previously optimized[118], and 400 nm intervals was determined to be sufficient to visualize the fluorescent probes while minimizing photo-bleaching of the samples (Fig 3-3). The total thickness of the 3D images was determined by setting the centre of the optical sections, optimized for each image collected and ranged from 0.9 μm - 0.11 μm. Due to the 3D orientation of the cells in the mini-TMAs, each 3D image series consisted of ~21-28 optical sections. Depending on the cellularity of each core within the mini-TMAs, 3-6 distinct regions were imaged from each core. Imaging systematically across the mini-TMAs (*i.e.* starting a top [left], image counter-clockwise) ensured that nuclei were only imaged once. Image series of the various fluorophores were collected using fluorescent filters for DAPI, and those specific to the DNA probe set, Cy3, FITC, and CFP (Table 3-1). To account for sample variability and autofluorescence, the exposure time for each probe was independently optimized. All 3D images were exported as tiff files for image deconvolution and were imported and processed by image deconvolution in AutoQuant X3 (Media Cybernetics) (Fig 3-3). The deconvolution software employs a constrained iterative algorithm and theoretical point spread functions for each of the fluorescent channels, DAPI (461 nm), Cy3 (570 nm), FITC (525 nm), and CFP (476 nm). Each image was saved as a 16-bit IMS (Bitplane) file that could be imported directly into Imaris image visualization software for FISH probe enumeration purposes.

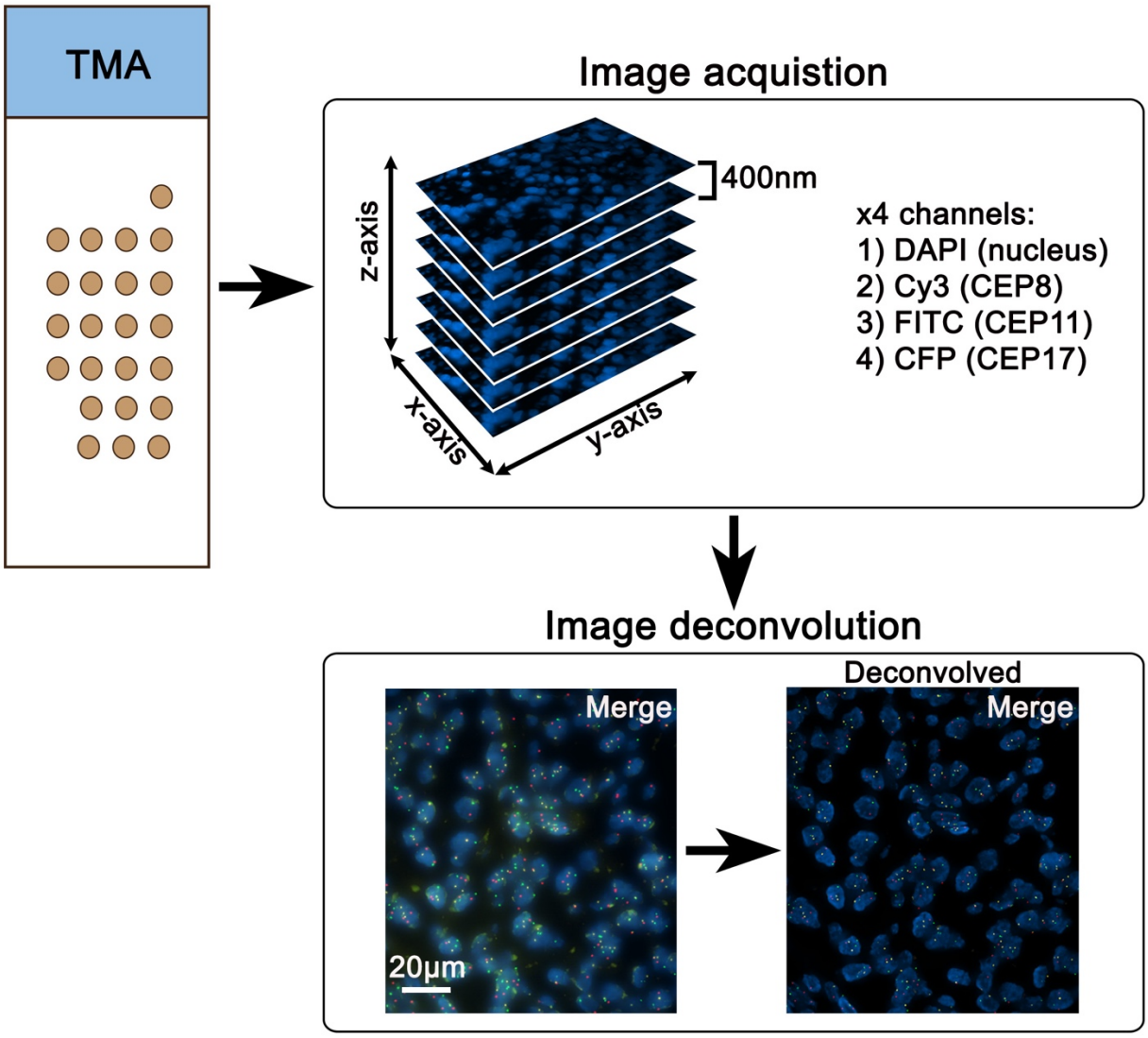


**Figure 3-3. TMA 3D Image Acquisition and Deconvolution.**
Schematic depicting 3D image acquisition (top) and deconvolution (bottom). 3D images are acquired (top) for each channel corresponding to the nucleus (DAPI), CEP8 (Cy3), CEP11 (FITC), and CEP17 (CFP) at an optimal step size of 400 nm. The merged images (bottom, left) is deconvolved to reassign out-of-focus light. Deconvolved merged images (bottom, right) are used for analysis.

### 3.9.0 Evaluating CIN

#### 3.9.1 Automated Two-Dimensional Image Analysis

Imaris was employed for NA analysis and the enumeration of the DNA probe set. All 2D images were automatically enumerated using previously established protocols[46] (*i.e.* nuclear mask generation, vesicle detection and rendered images) (Fig 3-4), in order to quantify NAs and enumerate CEP foci in > 200 nuclei/sample. Briefly, the cell detection function was used to quantify NAs and generate nuclear masks. Size exclusion filters were employed to eliminate apoptotic bodies and overlapping nuclei, while signal intensity thresholds were applied to remove brightly fluorescing apoptotic bodies and mitotic cells. Additionally, an edge filter was also applied to remove partial nuclei located along the periphery of each image, so that only intact interphase nuclei were included in the downstream analyses. Following the generation of a nuclear masks, the vesicle (*i.e.* spot) detection function was used to enumerate CEP foci contained within the nuclear masks. Once nuclear masks and vesicle detection has been applied, rendered images were automatically generated with NA quantification and CEP foci counts.

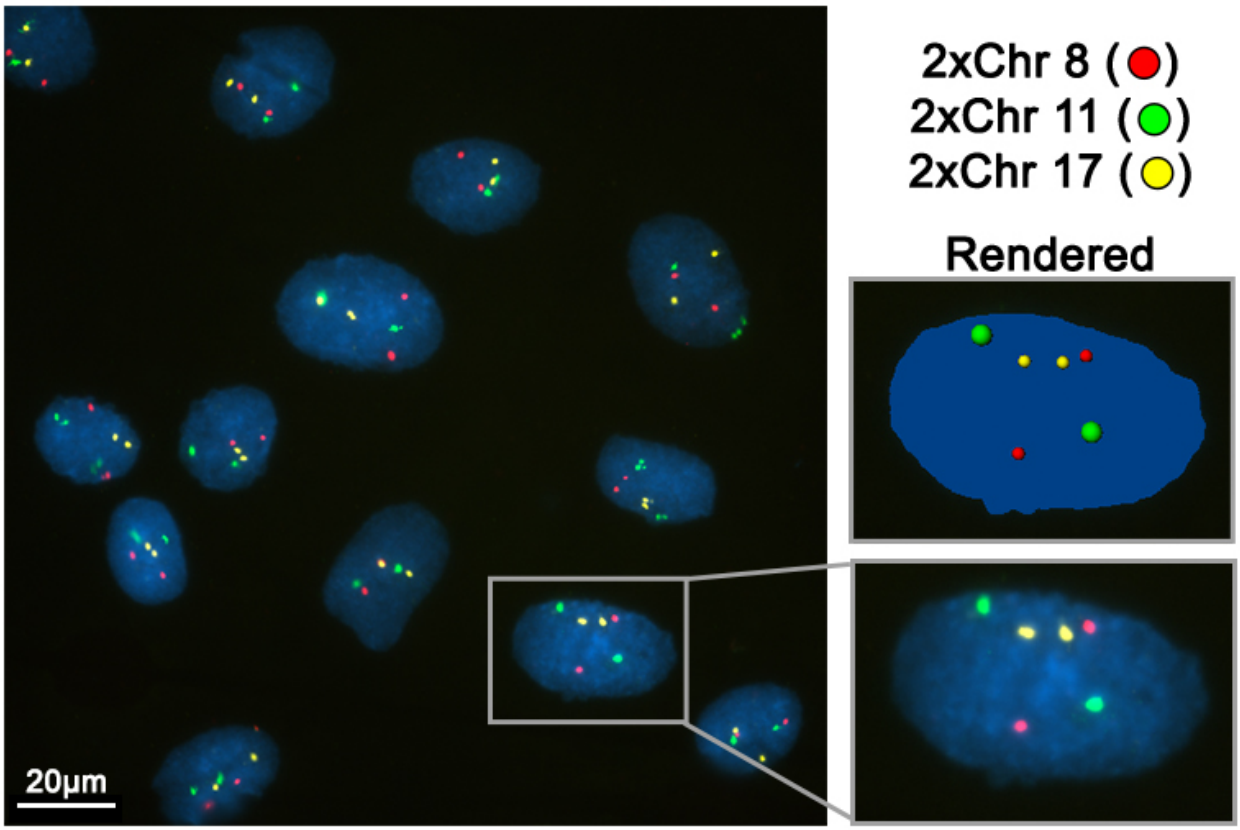


**Figure 3-4. Automated Image Analysis Used to Assess NAs and Enumerate CEP Foci.** Representative portion of an image (left) showing nuclei labelled with CEPs recognizing chromosomes 8 (red), 11 (green) and 17 (yellow). The single diploid nucleus highlighted by the bounding box harbors the expected 2 CEP foci/chromosome/nucleus. In general, image analysis software generates a nuclear mask in which all CEP foci are automatically enumerated. This automated approach is applied to all nuclei within an image and to all images from a given sample.

### 3.9.2 Manual Three-Dimensional Image Analysis

Imaris was employed for the enumeration of the DNA probe set. All 3D images were manually enumerated by myself and an undergraduate summer student, Ally Farrell. Briefly, each channel (*i.e.* CEP) was independently scored and 100 intact nuclei were analyzed from each core. Surface renderings were generated from the DAPI channel to ensure that only intact nuclei were included in the enumeration process, and only foci contained within the nuclear boundaries, as defined by the DAPI signal intensity, were enumerated (Fig 3-5). To ensure that each nucleus was only analyzed once, each enumerated nucleus was assigned a number and the enumeration data were assembled in Excel (Microsoft). 3D projections (*i.e.* "maps") were generated for each image enumerated and opened in Photoshop CS6 (Adobe) to record the assigned numbers for each nucleus that was enumerated. All image panels were also generated in Photoshop CS6 and the figures and maps were saved as JPEG files.

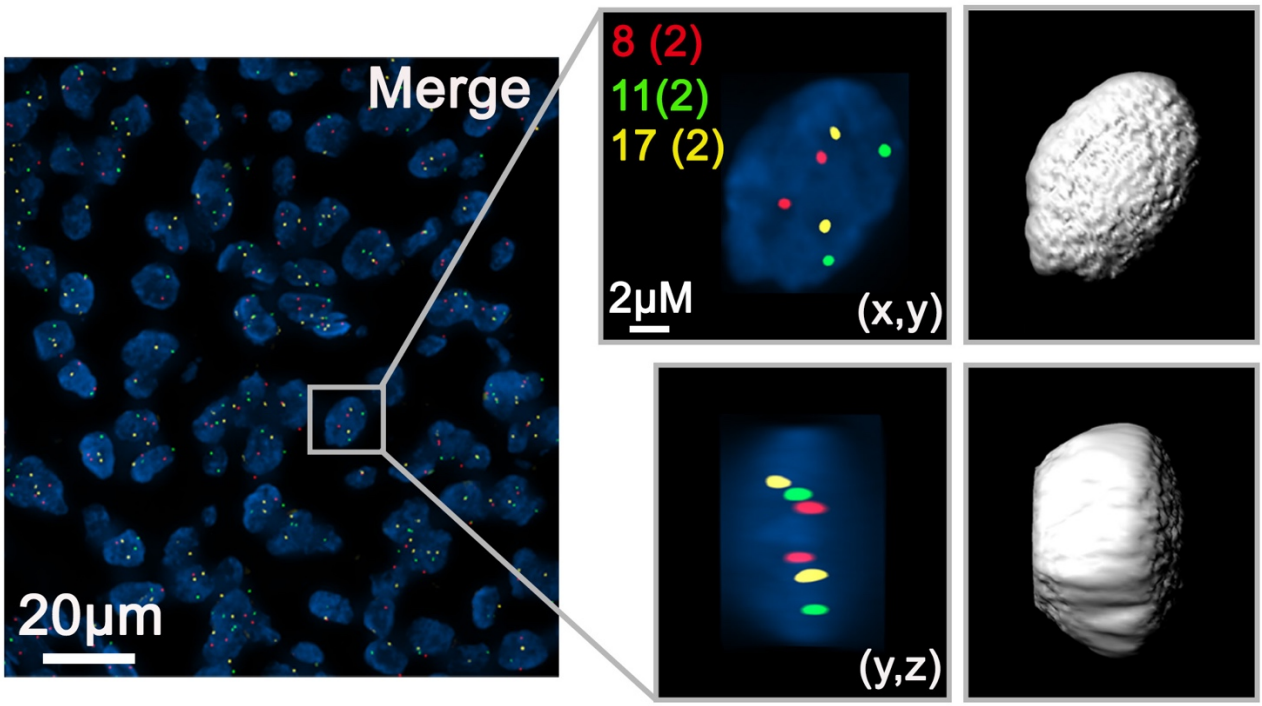


**Figure 3-5. Manual Enumeration and Surface Rendering in TMA.**
Following deconvolution (left), CEPs were manually enumerated from 100 intact nuclei/sample. The representative diploid nucleus (centre) can be rotated on its axis to ensure CEPs are within the nucleus. Intact nuclei were identified based on their surface rendering (right).

### 3.9.3 Determining *CIN Scores* (*CS*)

In order to determine the prevalence of CIN within HGSOC, the McManus and Nachtigal laboratories previously developed a metric called a *CIN score* (*CS*)[46,118] that describes the extent of both chromosome gains and losses. Briefly, a *CS* was devised to measure the deviations from the expected two CEP foci/chromosome/nucleus. The *CS* can be calculated for each individual CEP (*i.e.* $CS_{8,}$ $CS_{11,}$ and $CS_{17}$) or all three CEPs combined ($CS_c$). A CEP-specific *CS* value (*e.g.* $CS_8$) is calculated by the following formula, ($CS_8 = e_{\text{Chr8}} - o_{\text{Chr8}}$), where the *CS* is equal to the observed (*o*) number of CEP8 foci subtracted from the expected (*e*) number of two CEP8 foci, while a $CS_c$ value is generated by summing the absolute values of the three CEP-specific *CS* values (*e.g.* $CS_c = |CS_8| + |CS_{11}| + |CS_{17}|$). By definition, a $CS_c = 0$ defines a diploid state (*i.e.* two copies of each of CEPs 8, 11, and 17), and thus gains or losses in any CEP foci will result in deviations from the diploid state (*i.e.* $CS_c \neq 0$)[46,118]. Therefore, for the purpose of this study samples with a median $CS_c = 0$ do not exhibit CIN and samples with a median $CS_c \geq 1$ indicate CIN is prevalent. Additionally, a median $CS_c \geq 3$ identifies a CIN state where the three chromosomes under investigation are gained or lost in combination with one another, representing extreme levels of aneuploidy. Chromosomes 8, 11, and 17 were enumerated in >200 nuclei from cell lines and ascites derived patient samples and ~100 nuclei/core in the mini-TMAs. Importantly, nuclei harbouring both gains and losses are captured by the *CS* and were not scored as diploid/normal. Finally, the data were imported to Prism v6 (GraphPad) and scatterplots and cumulative distributions frequencies were generated to evaluate CIN in HGSOC.

### 3.10.0 Statistical Analysis

All data collected from the 12 serial collections of The Manitoba HGSOC cohort were imported into Prism where standard statistics were generated including mean, standard deviation, median, and Student's *t*-tests. Differences between the cumulative distribution frequencies for NA were statistically compared using a two-sample Kolmogorov-Smirnov (KS) test with a confidence interval of 0.05 ($\alpha$ statistic) and *p*-values < 0.05 were considered statistically significant. Differences between the ranked values for the *CS* values (individual [$CS_8$, $CS_{11}$, and $CS_{17}$] and combined [$CS_c$]) (scatterplots) were statistically compared using a two-sample Mann-Whitney (MW) test with a confidence interval of 0.05 ($\alpha$ statistic) and *p*-values < 0.05 were considered statistically significant.

# CHAPTER 4: AIM 1 RESULTS

## 4.1.0 Aim 1: To validate CEP Specificity in Diploid and Aneuploid Cell Lines.

***Rationale:*** Prior to evaluating CIN in patient samples, it was first essential to confirm the specificity of the DNA probe set (CEPs), which hybridizes to the α satellite DNA within the pericentromeric regions of chromosomes 8, 11, and 17 (Fig. 3-1), and validate that they accurately detect changes in chromosome numbers within interphase cells, as the vast majority of patient samples were interphase cells[119].

## 4.1.1 Confirming the Specificity of the DNA Probe Set

The specificity of the individual FISH probes was confirmed utilizing four distinct hTERT immortalized, fallopian tube secretory epithelial (FT) human cell lines, namely FT190 (hypotetraploid), FT194 (diploid), FT237 (near diploid), and FT246 (near diploid) (see Table 3-1 for additional cell line properties, pg. 22). FT cells were used as they are a cellular precursor to HGSOC[5,21] and therefore are relevant to the disease. Mitotic cells were used to confirm correct FISH probe localization and position (*i.e.* pericentromeric regions) within the corresponding chromosomes. Mitotic chromosome spreads of FT194 were generated and evaluated as detailed in Materials and Methods (*Sections 3.3.2, 3.5.0*, *3.6.1* and *3.8.1*) and revealed that the three FISH probes hybridize to the expected pericentromeric regions of chromosomes 8, 11 and 17 with high specificity (Fig 4-1).

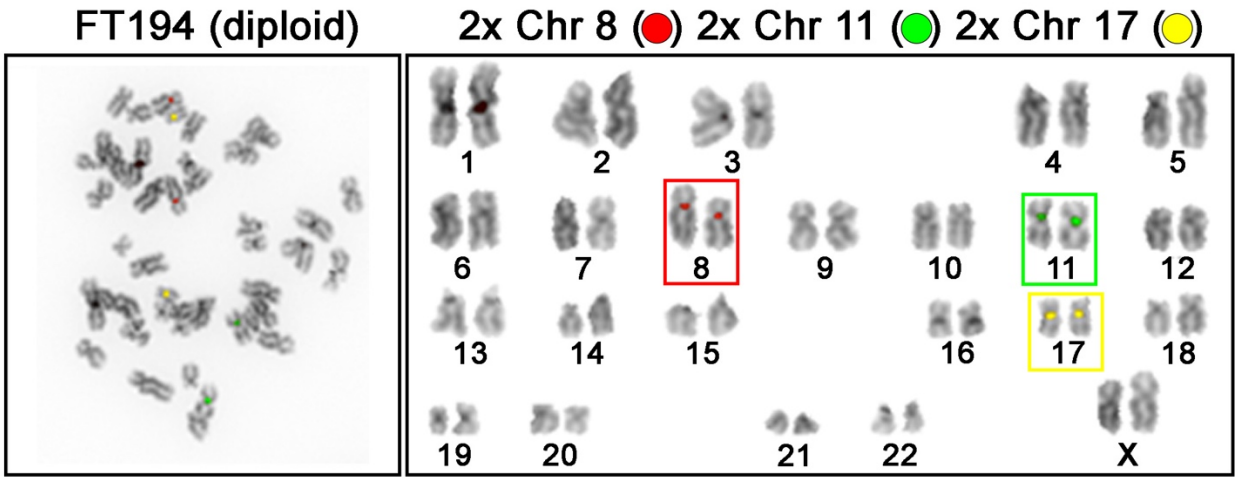


**Figure 4-1. Confirming the Specificity of CEPs within FT194.**
The representative mitotic chromosome spread (left) depicts the localization pattern of CEP8 (red), CEP11 (green), and CEP17 (yellow) obtained from the cell line FT194 and is presented as a karyotype (right) confirming CEP efficacy and specificity.

### 4.1.2 Evaluating the DNA Probe Set to Detect Changes in Chromosome Numbers

Following validation of the DNA probe set specificity (*i.e.* the CEPs hybridize to the correct chromosomes and pericentromeric regions) in mitotic chromosome spreads, it was essential to evaluate their ability to reflect changes in chromosome numbers within interphase cells, as the HGSOC tumor samples to be evaluated are predominately comprised of interphase cells[119]. Consequently, the FISH protocol (*Section 3.6.1*) was performed on both mitotic chromosome spreads and interphase cells from FT190, FT194, FT237, and FT246 cell lines. When hybridized with the DNA probe set, interphase FT194 cells produce the expected two CEP foci/chromosome/nucleus (Fig 4-2A). The foci within the interphase cells reflected similar numbers as observed within the mitotic chromosome spreads indicating that this approach is capable of accurately detecting chromosome copy numbers for each of the three chromosomes evaluated. Similar results were obtained in FT237 and FT246, which are diploid for chromosomes 8, 11 and 17 (Table 4-1). FT190 cells were also evaluated using the DNA probe set and provided additional support that the protocol can be employed to enumerate abnormal chromosome numbers and visualize aneusomy, as deviations from the expected two CEP foci/chromosome/nucleus were frequently detected (Fig 4-2B). In fact, most interphase FT190 cells evaluated had four copies of chromosome 8, three copies of chromosome 11, and four copies of chromosome 17, which correlates with what is observed within the mitotic chromosome spreads (Table 4-1). Collectively, the above data indicate that this approach is ideally suited to the analysis of CIN within interphase populations from both cell lines and HGSOC patient samples.

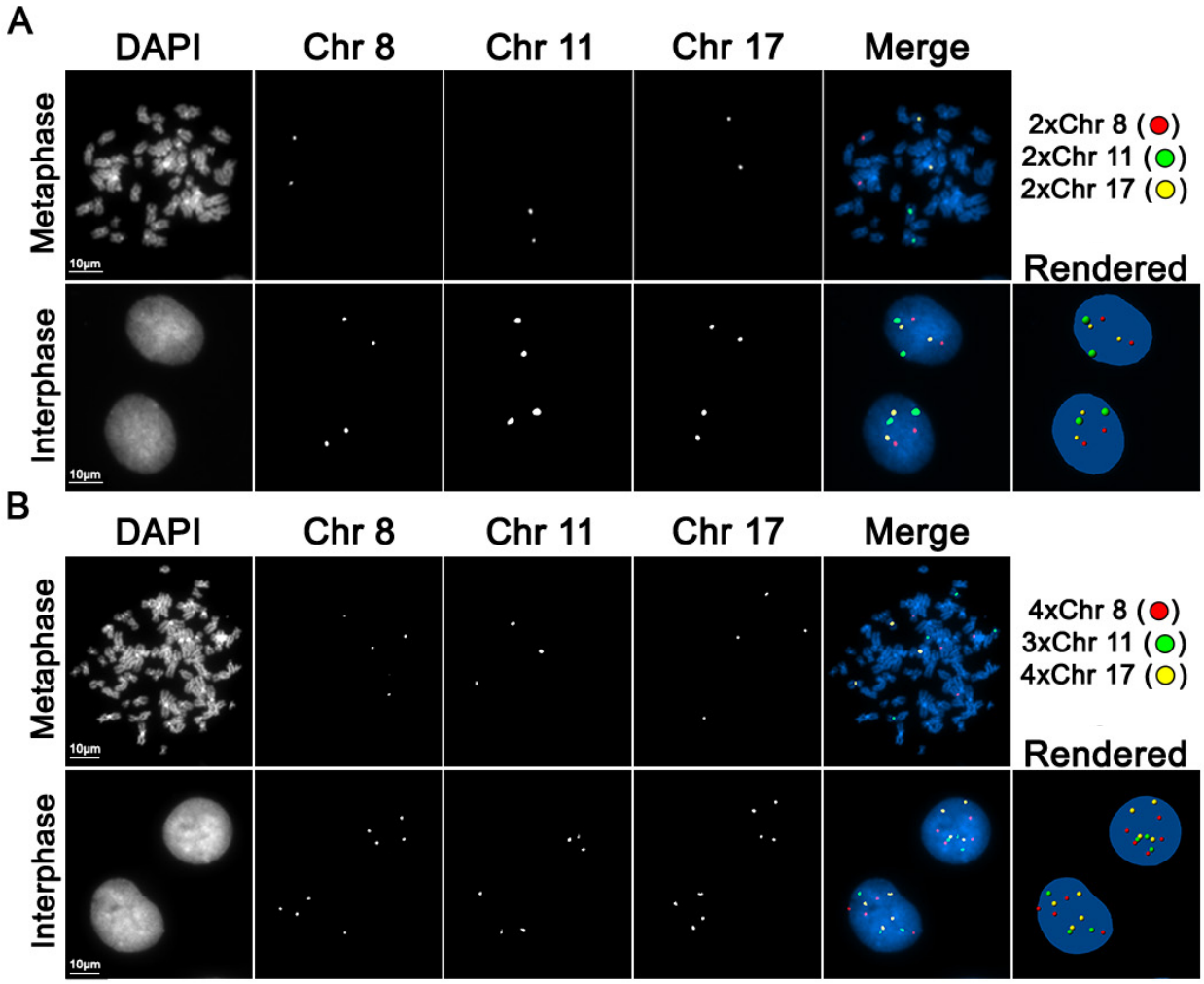


**Figure 4-2. Establishing the Enumeration Capabilities of CEPs Within Diploid and Aneuploid FT Cell Lines.**

***(A)*** The CEP-based approach was employed in mitotic (top) and interphase (bottom) FT194 cells. FT194 have the expected two CEP foci/chromosome (N = 2, n ≥ 100). ***(B)*** The CEP-based approach was employed mitotic (top) and interphase (bottom) FT190 cells. FT190 have an aberrant number of CEP foci/chromosome (N = 2, n ≥ 100).

**Table 4-1. Chromosome Copy Numbers in FT190, FT194, FT237 and FT246 Cell Lines.**

| | Number of Chromosomes[A] | | |
|---|---|---|---|
| Cell Line | Chromosome 8 | Chromosome 11 | Chromosome 17 |
| FT190 | 4 | 3 | 4 |
| FT194 | 2 | 2 | 2 |
| FT237 | 2 | 2 | 2 |
| FT246 | 2 | 2 | 2 |

[A]Observed in both mitotic chromosome spreads and interphase nuclei.

### 4.1.3 Evaluating CIN in FT Cell Lines

Following confirmation of enumeration capabilities of both diploid and aneuploid interphase chromosomes, CIN was evaluated in FT190, FT194, FT237, and FT246 cell lines. More specifically, NA quantification and *CS* values were used to evaluate CIN. Importantly, NA heterogeneity is an indicator of large-scale chromosome content changes and is suggestive of CIN[105]; however, must be used in combination with *CS* to determine if CIN was prevalent within cell lines and patient samples. Additionally, a *CS* was devised to measure the deviations from the expected two CEP foci/chromosome/nucleus. Therefore, for the purpose of this study samples with a median $CS_c = 0$ do not exhibit CIN and samples with a median $CS_c \geq 1$ indicate CIN is prevalent. Additionally, a $CS_c \geq 3$ identifies a CIN state where the three chromosomes under investigation are gained or lost in combination with one another, representing extreme levels of aneuploidy. In general, cell-to-cell heterogeneity was observed for NAs within each of the FT cell lines (Fig 4-3A). The total NA range observed for each cell line was 1,954 $\mu m^2$ (FT190), 2,106 $\mu m^2$ (FT194), 1,858 $\mu m^2$ (FT237), and 1,820 $\mu m^2$ (FT246) (Table S4-1). Similarly, $CS_c$ values were evaluated in FT190, FT194, FT237, and FT246 cell lines (Fig 4-3B) (Table S4-2). FT190 exhibited a large overall $CS_c$ distribution range (maximum $CS_c = 18$) and had a median $CS_c = 4$ (Fig 4-3B). In general, the remaining FT cell lines exhibited a smaller overall $CS_c$ distribution range (maximum $CS_c = 7$) and had median $CS_c = 0$. Similar trends were also observed for the individual *CS* values (Fig 4-3C). FT190 exhibited frequent gains in chromosomes 8, 11, and 17 and had median individual *CS* values of $CS_8 = 2$, $CS_{11} = 1$, and $CS_{17} = 2$, respectively. In general, the remaining FT cell lines exhibited some gains and losses in chromosomes 8, 11, and 17, but had median individual *CS* values of $CS_8 = 0$, $CS_{11} = 0$, and $CS_{17} = 0$, respectively. Overall, these data show that FT190 exhibits CIN (supported by NA heterogeneity and a median $CS_c = 4$) and FT194, FT237, and

FT246 exhibit a baseline variation in both NAs and *CS*s, which is expected due to NA changes throughout the cell cycle[119] and cell culture variation, but do not exhibit CIN ($CS_c = 0$).

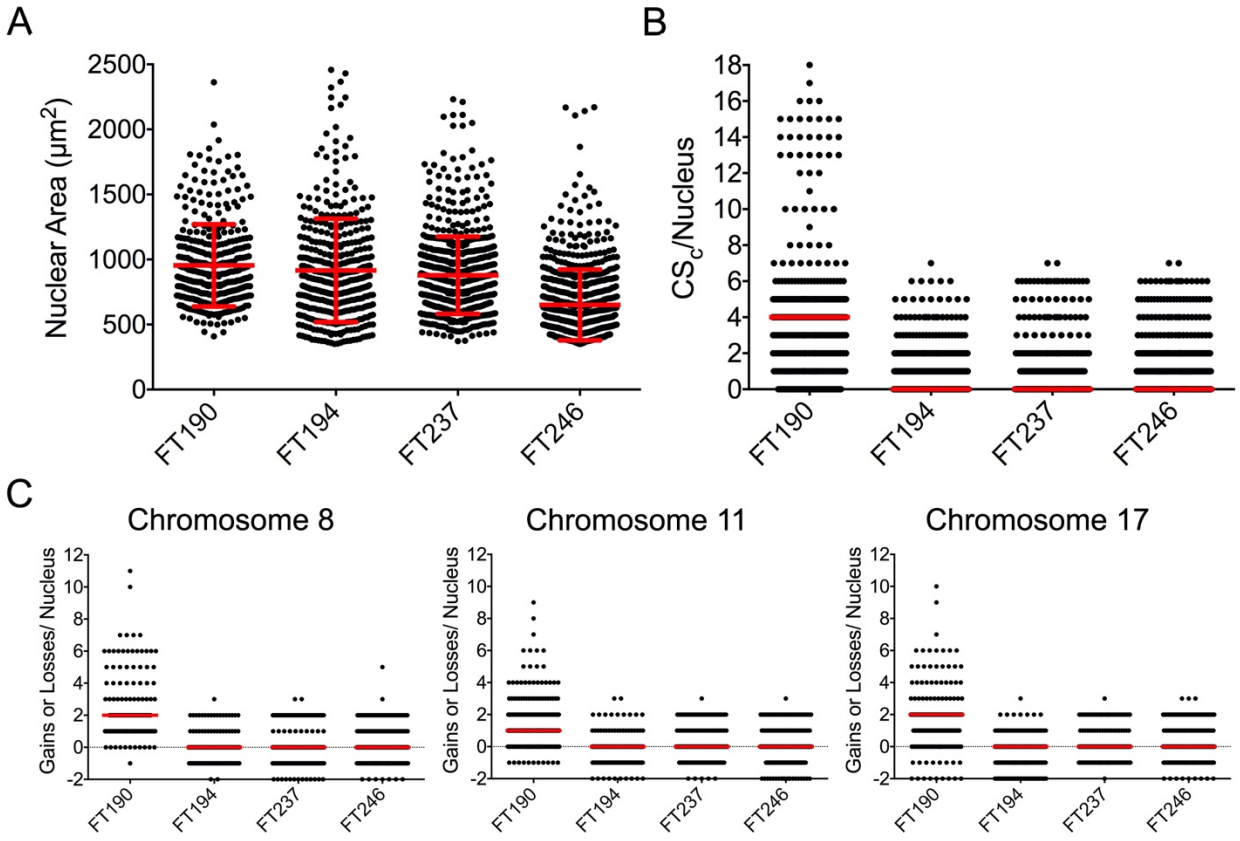


**Figure 4-3. FT Cells Lines Exhibit NA and *CS* Heterogeneity.**
***(A)*** Dot plot presenting the NAs determined for the four FT cell lines (x-axis). Red bars indicate the mean ± standard deviation (SD) (N = 2; n >100). ***(B)*** Dot plot presenting the $CS_c$ values for each nucleus evaluated in four FT cell lines. Red bars indicate the median $CS_c$. ***(C)*** Dot plot presenting the individual *CS* values (chromosome 8 [left], 11 [middle], and 17 [right]) for each nucleus evaluated in four FT cell lines. Red bars indicate the median individual *CS* values.

### 4.2.0 Supporting Information

### 4.2.1 Supporting Tables

**Table S4-1. Nuclear Area Descriptive Statistics for FT Cell Lines.**

| Cell Line | n[A] | Nuclear Area (μm$^2$) | | | | | |
|---|---|---|---|---|---|---|---|
| | | 25$^{th}$ Percentile | Median | 75$^{th}$ Percentile | Total Range | Mean | SD[B] |
| FT190 | 352 | 737.2 | 862.2 | 1103 | 1954 | 954.6 | 315.8 |
| FT194 | 391 | 634.7 | 846.0 | 1114 | 2106 | 916.0 | 397.5 |
| FT237 | 704 | 686.3 | 829.9 | 998.2 | 1858 | 878.6 | 297.3 |
| FT246 | 694 | 457.0 | 575.7 | 773.2 | 1820 | 650.5 | 272.0 |

[A]Number of nuclei analyzed (n)
[B]Standard deviation (SD)

**Table S4-2. *CIN Score* Descriptive Statistics for FT Cell Lines.**

| Cell Line | n[A] | Median | | | | Total $CS_c$ Range |
|---|---|---|---|---|---|---|
| | | $CS_8$ | $CS_{11}$ | $CS_{17}$ | $CS_c$ | |
| FT190 | 352 | 2 | 1 | 2 | 4 | 18 |
| FT194 | 391 | 0 | 0 | 0 | 0 | 7 |
| FT237 | 704 | 0 | 0 | 0 | 0 | 7 |
| FT246 | 694 | 0 | 0 | 0 | 0 | 7 |

[A]Number of nuclei analyzed (n)

# CHAPTER 5: AIM 2 RESULTS

## 5.1.0 Aim 2: To Determine the Prevalence and Dynamics of CIN in the Manitoba HGSOC Cohort – Ascites Derived Patient Samples

***Rationale:*** Patient samples provide unique opportunities to gain novel insight into the temporal dynamics of CIN in response to disease progression, treatment and disease recurrence.

### 5.1.1 Assessing CIN within Ascites Derived HGSOC Patient Samples

Using the validated FISH-based approach from *Aim* 1, NAs and *CS* values were determined in both single and serial ascites samples derived from HGSOC patients. Ascites is the accumulation of fluid in the peritoneal cavity and is routinely removed by paracentesis[38]. Ascites derived cell cultures were generated as detailed above (*Section 3.4.1*) and are readily available from the MOBP. The Manitoba HGSOC cohort used for this study consists of 34 unique ascites samples, including 22 single patient samples (10 chemonaïve, six chemosensitive, and six chemoresistant) (Table S5-1) and 12 serial patient samples (2-12 samples/patient, 46 total samples, categorized into the five groups as detailed in *Section 5.1.6*) (Table S5-2) that were used to assess the prevalence and temporal kinetics of CIN.

### 5.1.2 Determining the Prevalence of CIN in Single Chemonaïve HGSOC Patient Samples

Chemonaïve HGSOC patient samples are ascites samples that were collected prior to patients receiving any chemotherapy treatment. To assess whether CIN exhibits specific dynamics in chemonaïve ascites samples NAs and $CS_c$ values were assessed. In general, NA heterogeneity was present within each of the single samples for 10 chemonaïve HGSOC patients (Fig 5-1A). The minimum overall NA range was 796.1 $\mu m^2$ (OV205A), while the maximum range was 2,128 $\mu m^2$

(OV169A) (Table S5-3). Similarly, $CS_c$ values were evaluated in the 10 single chemonaïve HGSOC patient samples. OV177A and OV246A exhibited large $CS_c$ distribution ranges (maximum $CS_c = 9$ and $CS_c = 19$, respectively) and median $CS_c$ values = 2. OV021A, OV058A, OV118A, OV184A, OV205A, and OV247A had variable $CS_c$ distribution ranges (maximum $CS_c = 22$, $CS_c = 14$, $CS_c = 8$, $CS_c = 18$, $CS_c = 11$, and $CS_c = 6$, respectively) and median $CS_c$ values = 1. The remaining patient samples, OV060A and OV169A, exhibited large $CS_c$ distribution ranges (maximum $CS_c = 10$ and $CS_c = 17$, respectively) and had median $CS_c$ values = 0 (Fig 5-1B) (Table S5-4). Similar trends were also observed for the individual *CS* values (Fig 5-1C). In general, all 10 samples exhibited gains and losses in chromosomes 8, 11, and 17 and had median individual *CS* values of $CS_8 = 0$, $CS_{11} = 0$, and $CS_{17} = 0$, respectively, excluding OV021A, which had an individual $CS_8 = 0.5$ and OV247A that had an individual $CS_{17} = -1$. Overall, these data show that CIN is prevalent in 80% of single chemonaïve HGSOC patient samples (*i.e.* OV021A, OV058A, OV118A, OV177A, OV184A, OV205A, OV246A and OV247A), which is supported by NA heterogeneity and median $CS_c$ values $\geq 1$. The remaining chemonaïve patient samples, OV060A and OV169A, do not exhibit CIN as defined by a median $CS_c = 0$. It should be noted that OV169A is positive for Lynch Syndrome, which is associated with MSI[120], therefore a median $CS_c = 0$ is in agreement with observations indicating that CIN and MSI tend to be mutually exclusive[121].

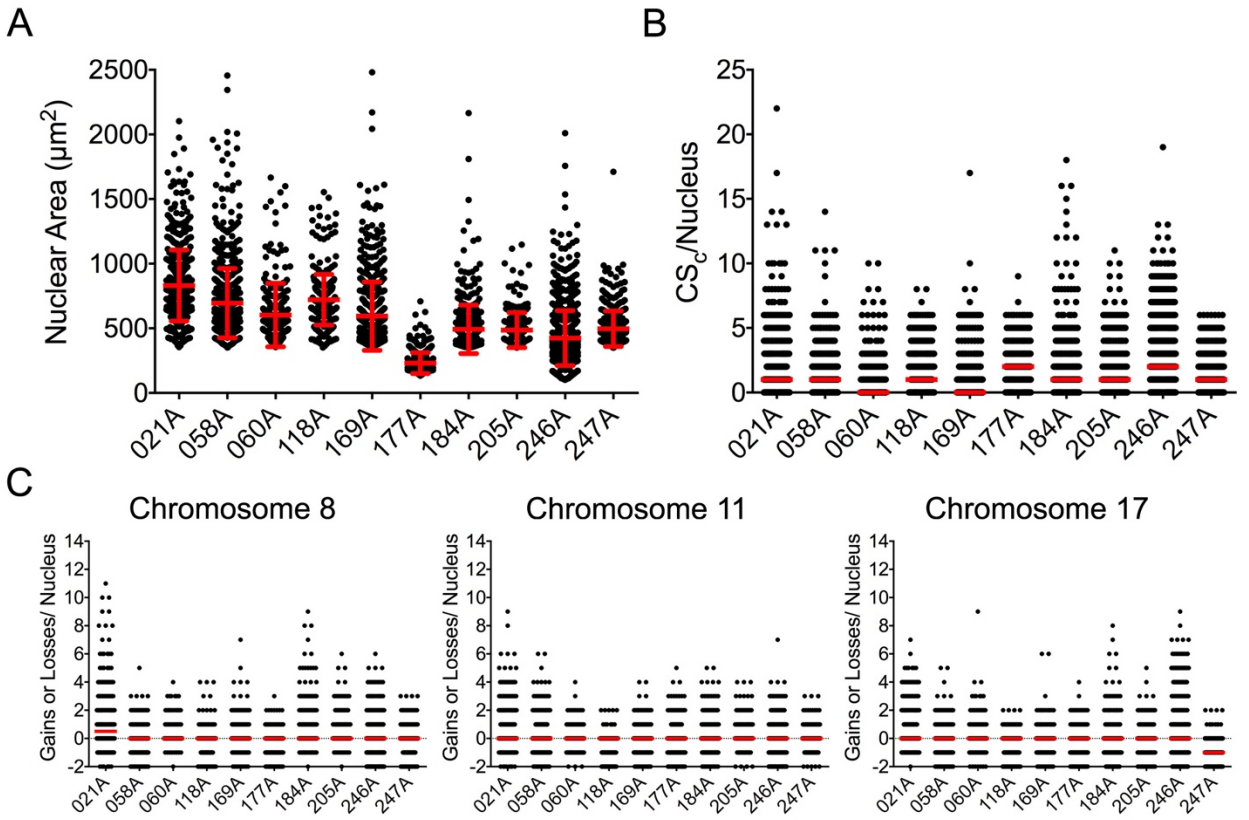


**Figure 5-1. Chemonaïve HGSOC Patient Samples Exhibit NA and *CS* Heterogeneity.**
***(A)*** Dot plot presenting the NAs determined for the 10 chemonaïve HGSOC patient samples. Red bars indicate the mean ± SD (N = 2; n >200). ***(B)*** Dot plot presenting the $CS_c$ values for each nucleus evaluated. Red bars indicate the median $CS_c$. ***(C)*** Dot plot presenting the individual *CS* values (chromosome 8 [left], 11 [middle], and 17 [right]) for each nucleus evaluated. Red bars indicate the median individual *CS* values.

### 5.1.3 Determining the Prevalence of CIN in Single Chemosensitive HGSOC Patient Samples

Chemosensitive HGSOC patient samples are ascites samples that were collected > 6 months following the completion of a chemotherapy treatment[122]. To assess whether CIN exhibits specific dynamics in chemosensitive ascites samples NAs and $CS_c$ values were assessed. In general, NA heterogeneity was present within each of the single samples for six chemosensitive HGSOC patients (Fig 5-2A). The minimum NA range observed was 496.4 $\mu m^2$ (OV069A), while the maximum range was 1,719 $\mu m^2$ (OV067A) (Table S5-3). Similarly, $CS_c$ values were evaluated in the six single chemosensitive HGSOC patient samples. OV196A exhibited a large overall $CS_c$ distribution range (maximum $CS_c = 16$) and a median $CS_c = 2$. The remaining five patient samples exhibited a variable $CS_c$ distribution ranges (maximum $CS_c = 8$ [OV059A], $CS_c = 6$ [OV067A], $CS_c = 12$ [OV069A], $CS_c = 8$ [OV171B], and $CS_c = 23$ [OV189A]), but had median $CS_c$ values = 1 (Fig 5-2B) (Table S5-4). Similar trends were also observed for the individual *CS* values (Fig 5-2C). In general, all six samples exhibited gains and losses in chromosomes 8, 11, and 17 and had median individual *CS* values of $CS_8 = 0$, $CS_{11} = 0$, and $CS_{17} = 0$, excluding OV067A and OV196A which had an individual $CS_{17} = -1$. Overall, these data show that CIN is prevalent in 100% of single chemosensitive HGSOC patient samples, which is supported by NA heterogeneity and median $CS_c$ values $\geq 1$.

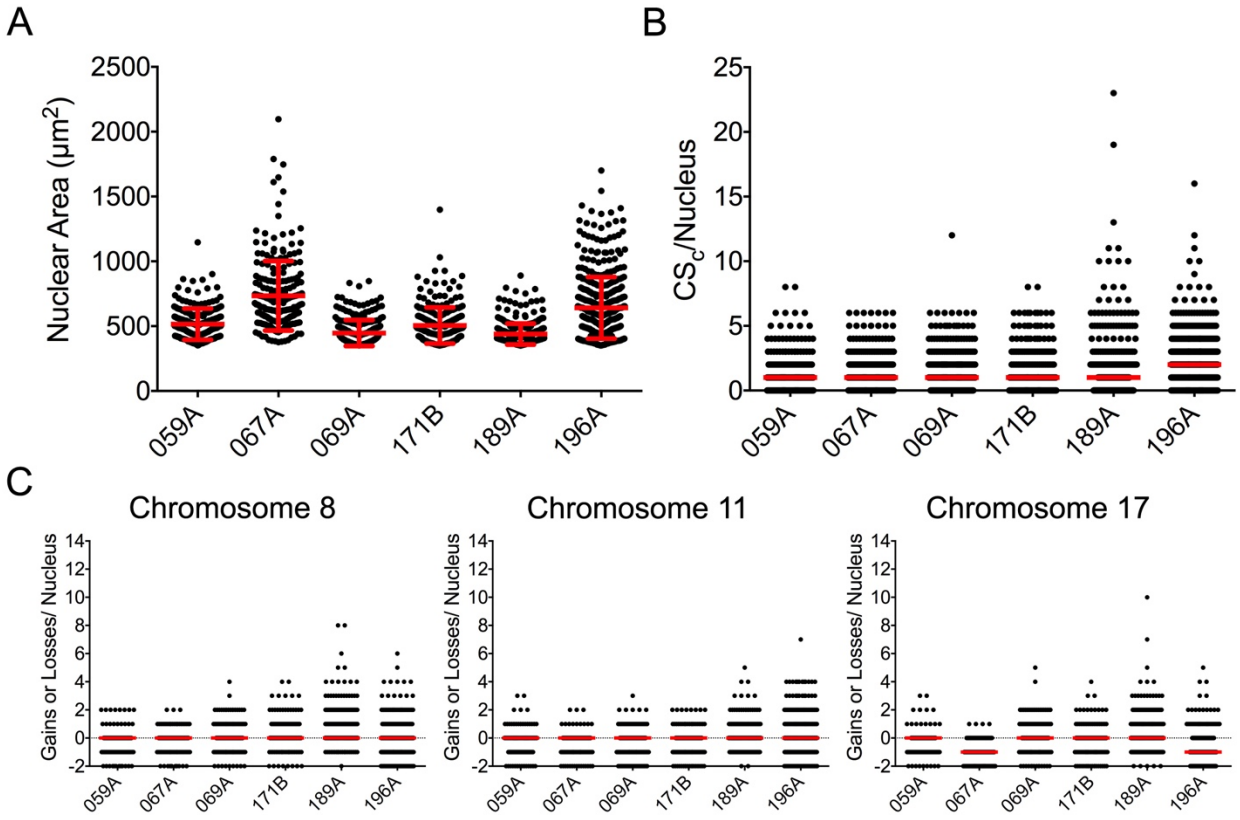


**Figure 5-2. Chemosensitive HGSOC Patient Samples Exhibit NA and CS Heterogeneity.** ***(A)*** Dot plot presenting the NAs determined for the six chemosensitive HGSOC patient samples. Red bars indicate the mean ± SD (N = 2; n > 200). ***(B)*** Dot plot presenting the $CS_c$ values for each nucleus evaluated. Red bars indicate the median $CS_c$. ***(C)*** Dot plot presenting the individual *CS* values (chromosome 8 [left], 11 [middle], and 17 [right]) for each nucleus evaluated. Red bars indicate the median individual *CS* values.

### 5.1.4 Determining the Prevalence of CIN in Single Chemoresistant HGSOC Patient Samples

Chemoresistant HGSOC patient samples are ascites samples that were collected < 6 months following the completion of chemotherapy treatments[122]. To assess whether CIN exhibits specific dynamics in chemoresistant ascites samples NAs and $CS_c$ values were assessed. In general, NA heterogeneity was present within each of the six chemoresistant samples (Fig 5-3A). The minimum NA range observed was 761.7 $\mu m^2$ (OV073C), while the maximum range was 2,148 $\mu m^2$ (OV146A) (Table S5-3). Similarly, $CS_c$ values were evaluated in all six samples. OV073C and OV103E exhibited large overall $CS_c$ ranges (maximum $CS_c = 11$ and $CS_c = 16$, respectively) and had median $CS_c$ values = 2. The remaining four samples exhibited variable $CS_c$ ranges (maximum $CS_c = 9$ [OV053A], $CS_c = 20$ [OV109A], $CS_c = 10$ [OV146A], and $CS_c = 10$ [OV230A]) and had median $CS_c$ values = 1 (Fig 5-3B) (Table S5-4). Similar trends were observed for the individual *CS* values (Fig 5-3C). In general, all six samples exhibited both gains and losses in chromosomes 8, 11, and 17, but had median individual *CS* values of $CS_8 = 0$, $CS_{11} = 0$, and $CS_{17} = 0$, excluding OV073C which had a $CS_{17} = 1$ and OV103E that had an individual $CS_{17} = -1$. Overall, these data show that CIN is prevalent in 100% of single chemoresistant HGSOC patient samples, which is supported by NA heterogeneity and median $CS_c$ values $\geq 1$.

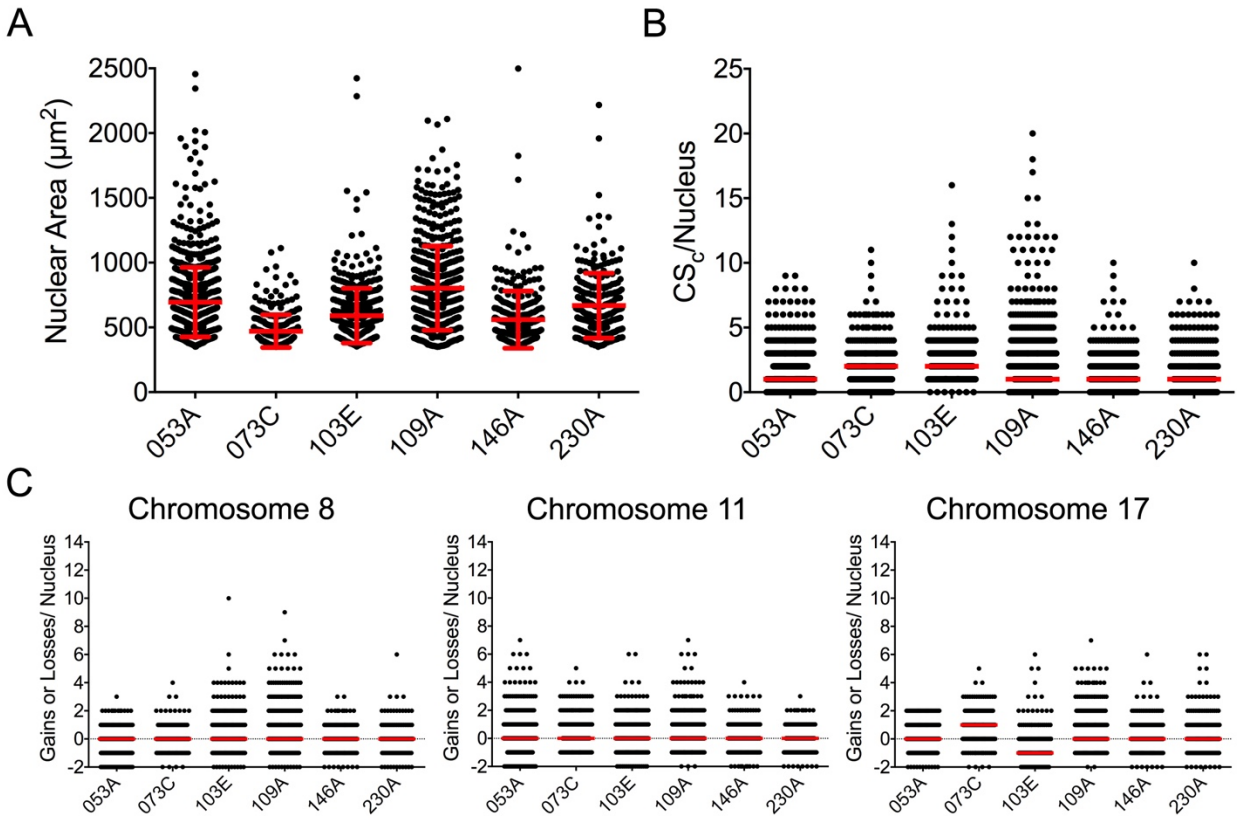


**Figure 5-3. Chemoresistant HGSOC Patient Samples Exhibit NA and CS Heterogeneity.** ***(A)*** Dot plot presenting the NAs determined for the six chemoresistant HGSOC patient samples. Red bars indicate the mean ± SD (N = 2; n >200). ***(B)*** Dot plot presenting the $CS_c$ values for each nucleus evaluated. Red bars indicate the median $CS_c$. ***(C)*** Dot plot presenting the individual *CS* values (chromosome 8 [left], 11 [middle], and 17 [right]) for each nucleus evaluated. Red bars indicate the median individual *CS* values.

### 5.1.5 Conclusion

Overall, the above data shows that CIN is prevalent in 91% of single HGSOC patient samples (eight chemonaïve, six chemosensitive, and six chemoresistant), which is supported by NA heterogeneity (Table S5-3) and median $CS_c$ values $\geq 1$ (Table S5-4). Importantly, CIN is prevalent at a high frequency in single HGSOC patient samples regardless of chemotherapy status and in general, the majority (68%) of CIN positive samples have a median $CS_c = 1$ (23% of patients have a median $CS_c = 2$).

### 5.1.6 Analysis of Serial Samples Collected from HGSOC Patients; Patient Profiles

In addition to the 22 single samples from HGSOC patients (10 chemonaïve, six chemosensitive, and six chemoresistant) described above, serial samples from 12 individual HGSOC patients (2-12 samples/patient, total 46 samples) (Table S5-2) were used to assess the prevalence and temporal kinetics of CIN. Importantly, production of ascites is dependent on the individual patient, and its production often changes throughout the course of the disease and with treatment response[46]. Due to the heterogenous production of ascites, patients were sorted into one of five groups based on the collection of their ascites samples (*i.e.* patient profiles), including ascites samples collected: 1) within 10 months of diagnosis, with rapid progression to death (Group 1, Fig 5-4); 2) within 2 months of diagnosis, with survival (Group 2, Fig 5-5); 3) early following diagnosis and across disease following chemotherapy treatments (Group 3, Fig 5-6); 4) in late stage disease following multiple chemotherapy treatments (Group 4, Fig 5-7); and 5) from patients harbouring *BRCA1/BRCA2* mutations (Group 5, Fig 5-8). It should be noted that some serial patient samples are included in more than one group (*e.g.* OV173 is included in Group 2 and Group 5) and six single *BRCA1* or *BRCA2* positive patient samples (OV069, OV073, OV109, OV177, OV189, and OV246) are included in Group 5.

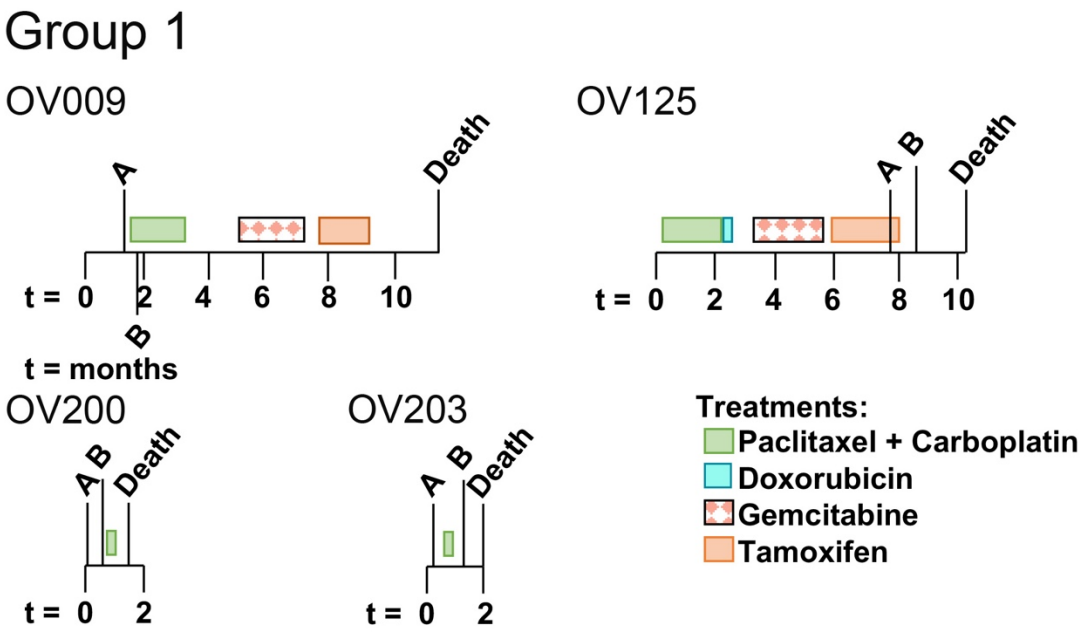


**Figure 5-4. Group 1 – Ascites Samples Collected Within 10 Months of Diagnosis, with Rapid Progression to Death.**

Timelines (t = months) presenting the serial ascites sample collection times (A and B) relative to surgery, treatments, recurrence and death for patients OV009, OV125, OV200 and OV203.

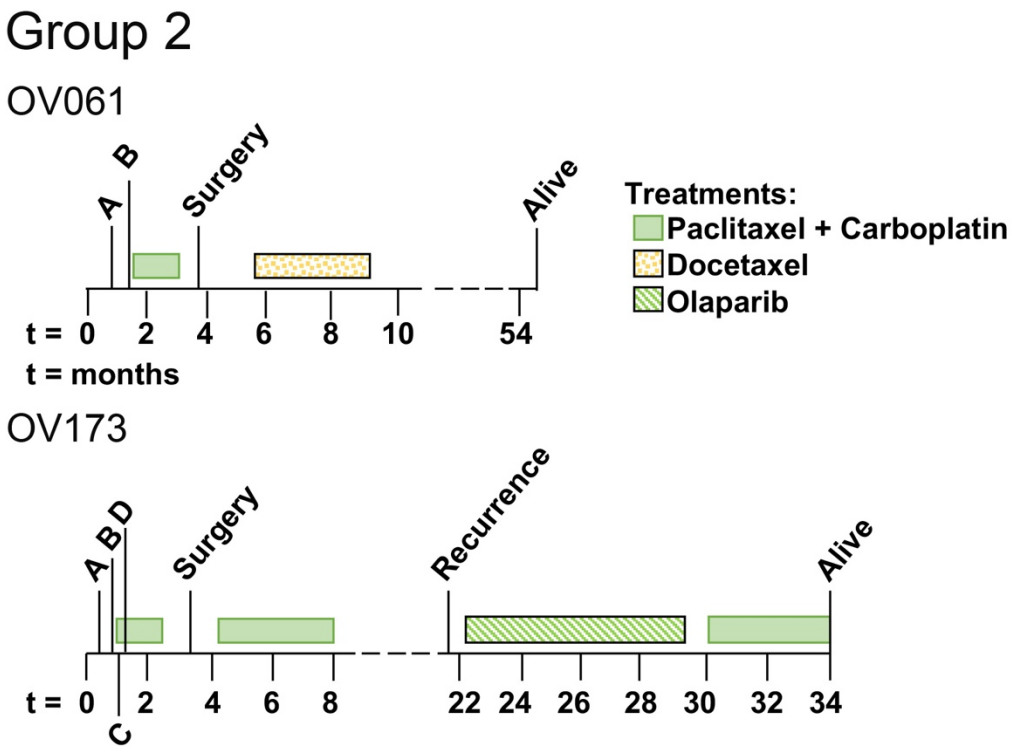


**Figure 5-5. Group 2 – Ascites Samples Collected Within 2 Months of Diagnosis, with Survival.**

Timelines presenting the serial sample collection times relative to surgery, treatments, and recurrence for patients OV061 and OV173. Note both patients were alive as of their last known update (OV061, August 13, 2018; OV173, February 4, 2019).

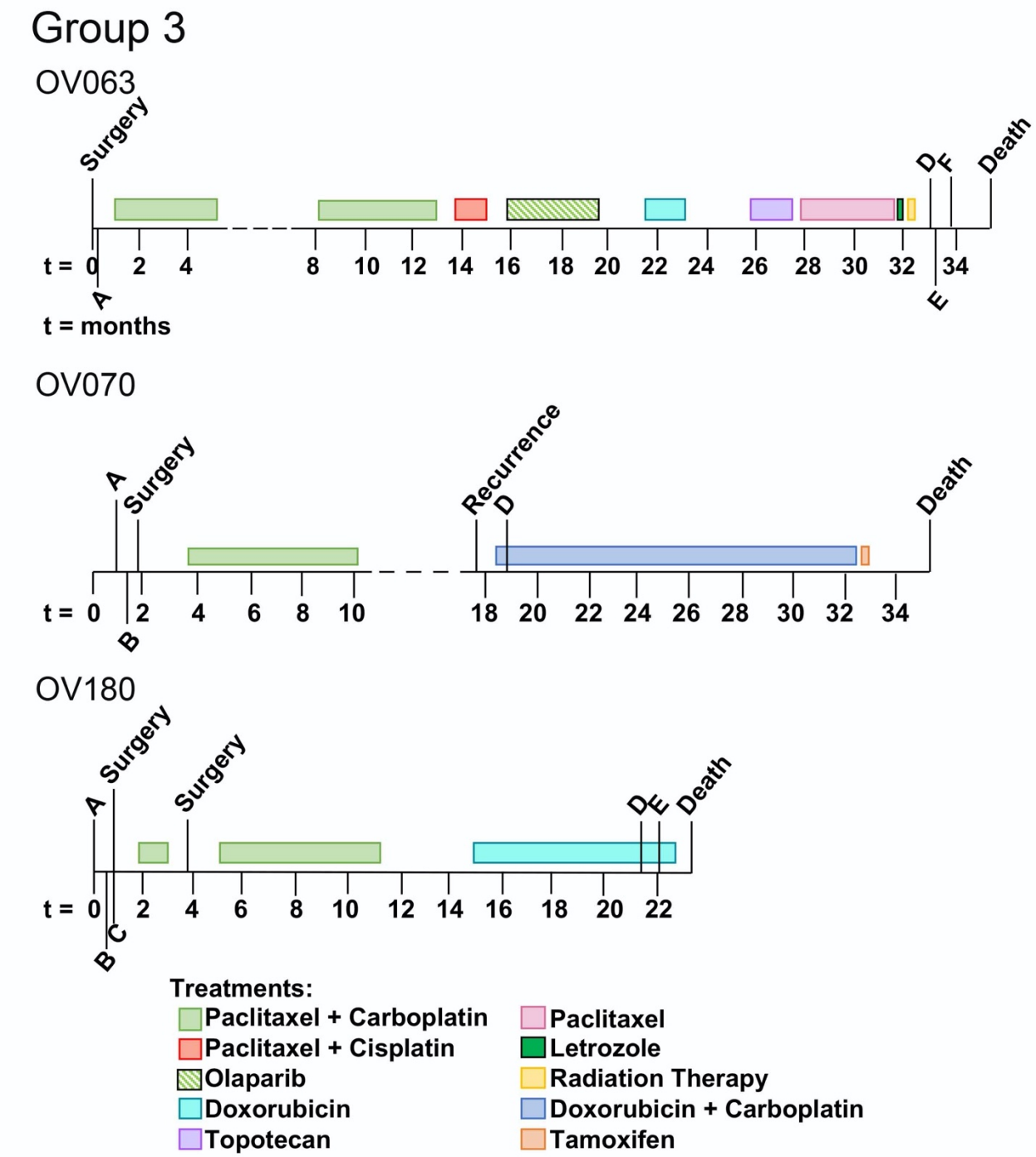


**Figure 5-6. Group 3 – Ascites Samples Collected Early Following Diagnosis and Across Disease Following Chemotherapy Treatments.**
Timelines presenting the serial sample collection times relative to surgery, treatments, recurrence and death for patients OV063, OV070, and OV180.

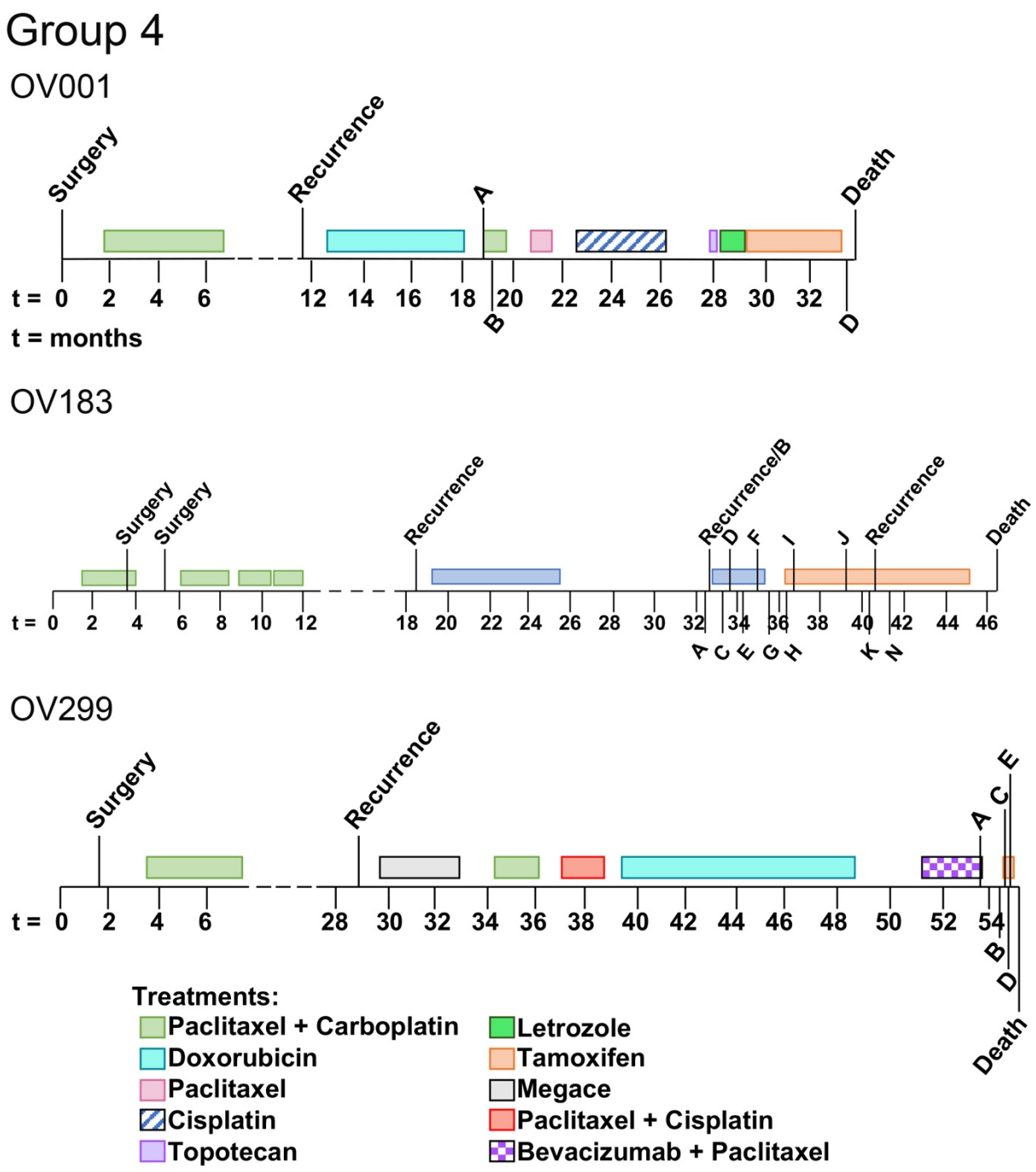


**Figure 5-7. Group 4 – Ascites Samples Collected in Late Stage Disease Following Multiple Chemotherapy Treatments.**
Timelines presenting the serial sample collection times relative to surgery, treatments, recurrence and death for patients OV001, OV183 and OV299.

# Group 5

## OV063

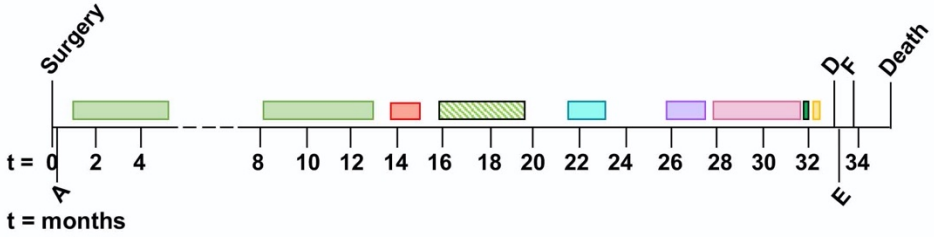


## OV069

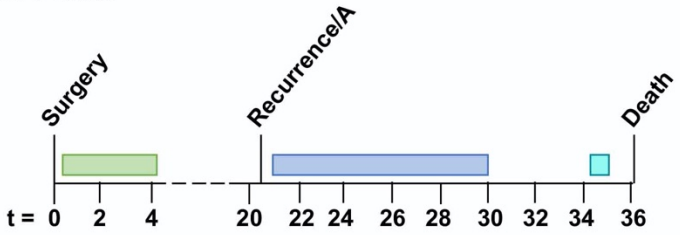


## OV073

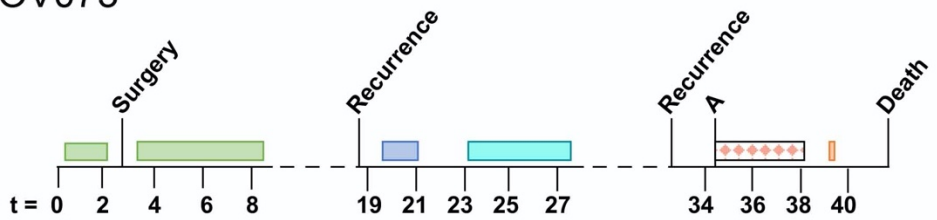


## OV109

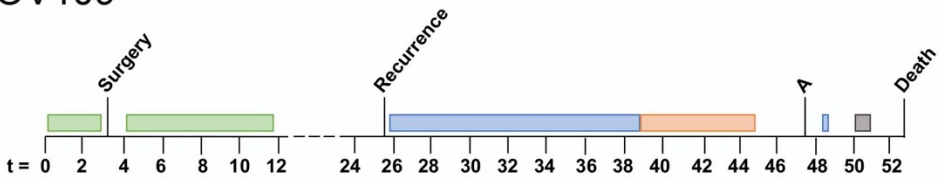


**Treatments:**

- Paclitaxel + Carboplatin
- Paclitaxel + Cisplatin
- Olaparib
- Doxorubicin
- Topotecan
- Paclitaxel
- Letrozole
- Radiation Therapy
- Doxorubicin + Carboplatin
- Gemcitabine
- Tamoxifen
- Carboplatin

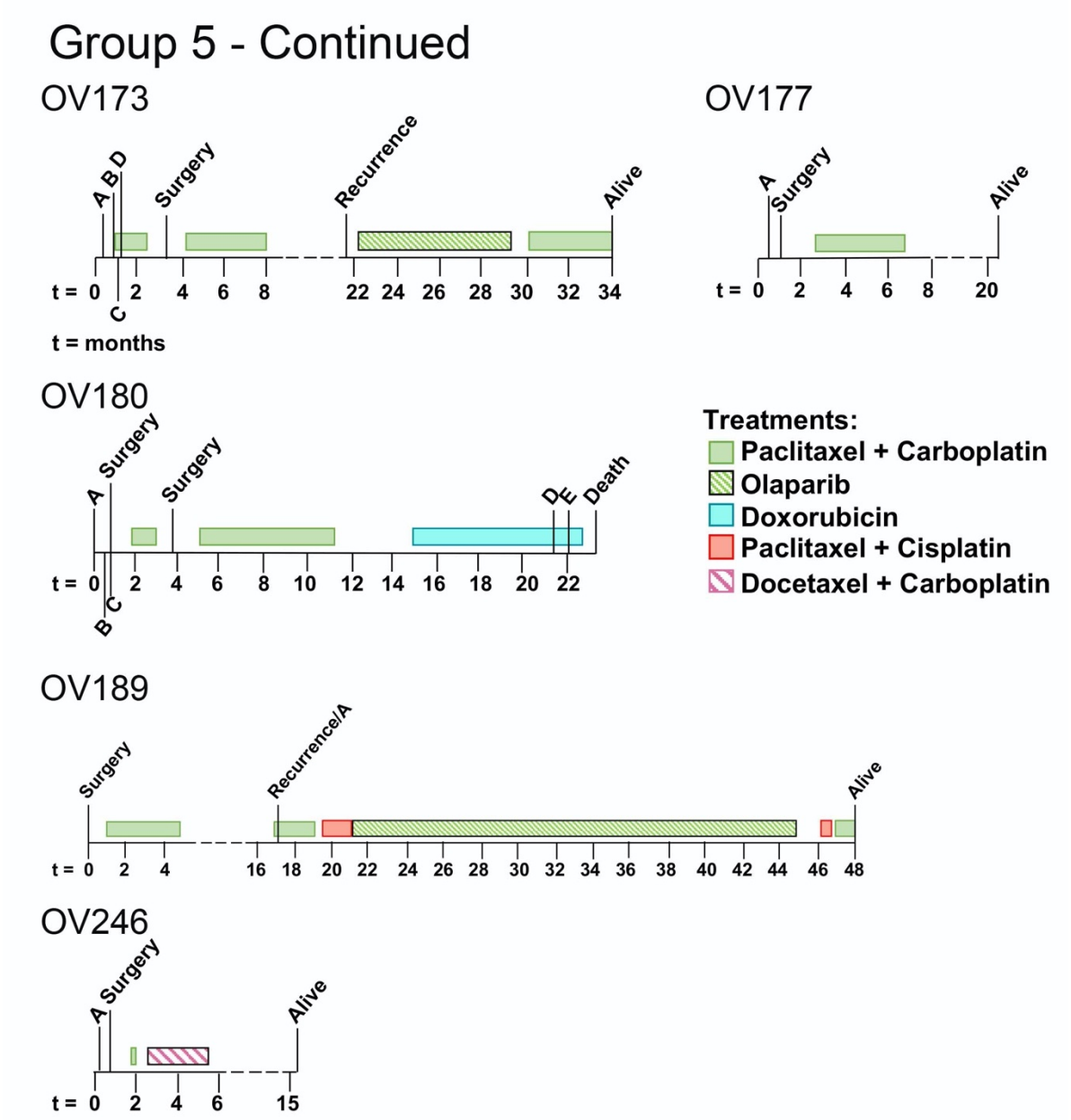


**Figure 5-8. Group 5 – Ascites Samples Collected from Patients with a *BRCA1* or *BRCA2* Positive Mutation.**

Timelines presenting the serial sample collection times relative to surgery, treatments, recurrence and death for patients OV063, OV069, OV073, OV109, OV173, OV177, OV180, OV189 and OV246. Note four patients were alive as of their last known update (OV173, February 4, 2019; OV177, February 22, 2018; OV189, January 18, 2019; OV246, November 13, 2018).

### 5.1.7 CIN is Prevalent and Dynamic in Patient Samples Collected Within 10 Months of Diagnosis, With Rapid Progression to Death

Group 1 (Fig 5-4) consists of ascites samples collected within 10 months of diagnosis, with rapid progression to death (*i.e.* chemorefractory disease). To assess the temporal dynamics of CIN in Group 1 samples, similar analyses to those detailed above (NAs and *CS* values) were performed on serial samples collected from four HGSOC patients OV009, OV125, OV200, and OV203. Figure 5-9 shows a timeline of serial samples collected from patient OV200 and quantified NA and *CS* values, which serves as a representative example of Group 1 HGSOC patients. Briefly, two serial samples were isolated and analyzed (Fig 5-9A). NA analysis revealed cell-to-cell heterogeneity, and OV200A and OV200B exhibited a total range of 1,967 $\mu m^2$ and 1,813 $\mu m^2$, respectively (Fig 5-9B) (Table S5-5). A two sample KS test comparing the NA distributions (Fig 5-10) of A and B was statistically significant ($p$-value < 0.05) (Table S5-6). In general, similar results were observed in OV125 (Fig S5-1) and OV203 (Fig S5-2), with the exception of OV009 (Fig S5-3). Two sample KS test comparing the NA distributions of samples A and B was statistically significant for OV125 ($p$-value < 0.0001) (Fig S5-4) (Table S5-7) and OV203 ($p$-value < 0.0001) (Fig S5-5) (Table S5-8), while OV009 was not significant ($p$-value > 0.05) (Fig S5-6) (Table S5-9).

Next, *CS* values were evaluated and exhibited cell-to-cell heterogeneity. OV200A exhibited a large overall $CS_c$ distribution range (maximum $CS_c = 12$) and had a median $CS_c = 2$, while OV200B exhibited a larger overall $CS_c$ distribution range (maximum $CS_c = 33$) and had a median $CS_c = 3$ (Fig 5-9C) (Table S5-10). Two sample MW test comparing the $CS_c$ ranked values (Fig 5-9C) was statistically significant ($p$-value < 0.0001) (Table S5-11). In general, similar results were also obtained in OV009 (Fig S5-3) and OV203 (Fig S5-2), with the exception of OV125

(Fig S5-1). Two sample MW test comparing the $CS_c$ ranked values of samples A and B was statistically significant for OV009 ($p$-value < 0.0001) (Table S5-12) and OV203 ($p$-value < 0.05) (Table S5-13), while OV125 was not significant ($p$-value > 0.05) (Table S5-14). Similar trends were also observed for the individual *CS* values (Fig 5-9D). OV200A exhibited gains and losses in chromosomes 8, 11, and 17 and had median individual *CS* values of $CS_8 = 0$, $CS_{11} = -1$, and $CS_{17} = 0$, respectively. Similarly, OV200B exhibited gains and losses in chromosomes 8, 11, and 17 and had median individual *CS* values of $CS_8 = 1$, $CS_{11} = -1$, and $CS_{17} = 0$, respectively. In general, the remaining Group 1 HGSOC patient samples exhibited gains and losses in chromosomes 8, 11, and 17 and had median individual *CS* values of $CS_8 = 0$, $CS_{11} = 0$, and $CS_{17} = 0$, respectively, excluding OV125A that had an individual $CS_8 = 0.5$ and OV203A that had an individual $CS_{11} = 1$.

Overall, these data show that CIN is prevalent in 87.5% of Group 1 HGSOC patient samples, which is supported by NA heterogeneity and median $CS_c$ values ≥ 1, and each HGSOC patient sample exhibits unique CIN dynamics. More specifically, based on NA and $CS_c$ values, OV200 shows an increase in aneuploidy (shift toward smaller NAs and increase in median $CS_c$) with disease progression, OV009 shows a reduction in aneuploidy (stable NAs and decrease in median $CS_c$ from sample A [$CS_c = 2$] to B [$CS_c = 0$]) during paclitaxel and carboplatin treatment, OV125 shows CIN persisted (shift toward smaller NAs and stable median $CS_c$) and there was no disease response following multiple treatments, and OV203 shows CIN persisted (shift toward larger NAs and stable median $CS_c$) as the disease progresses.

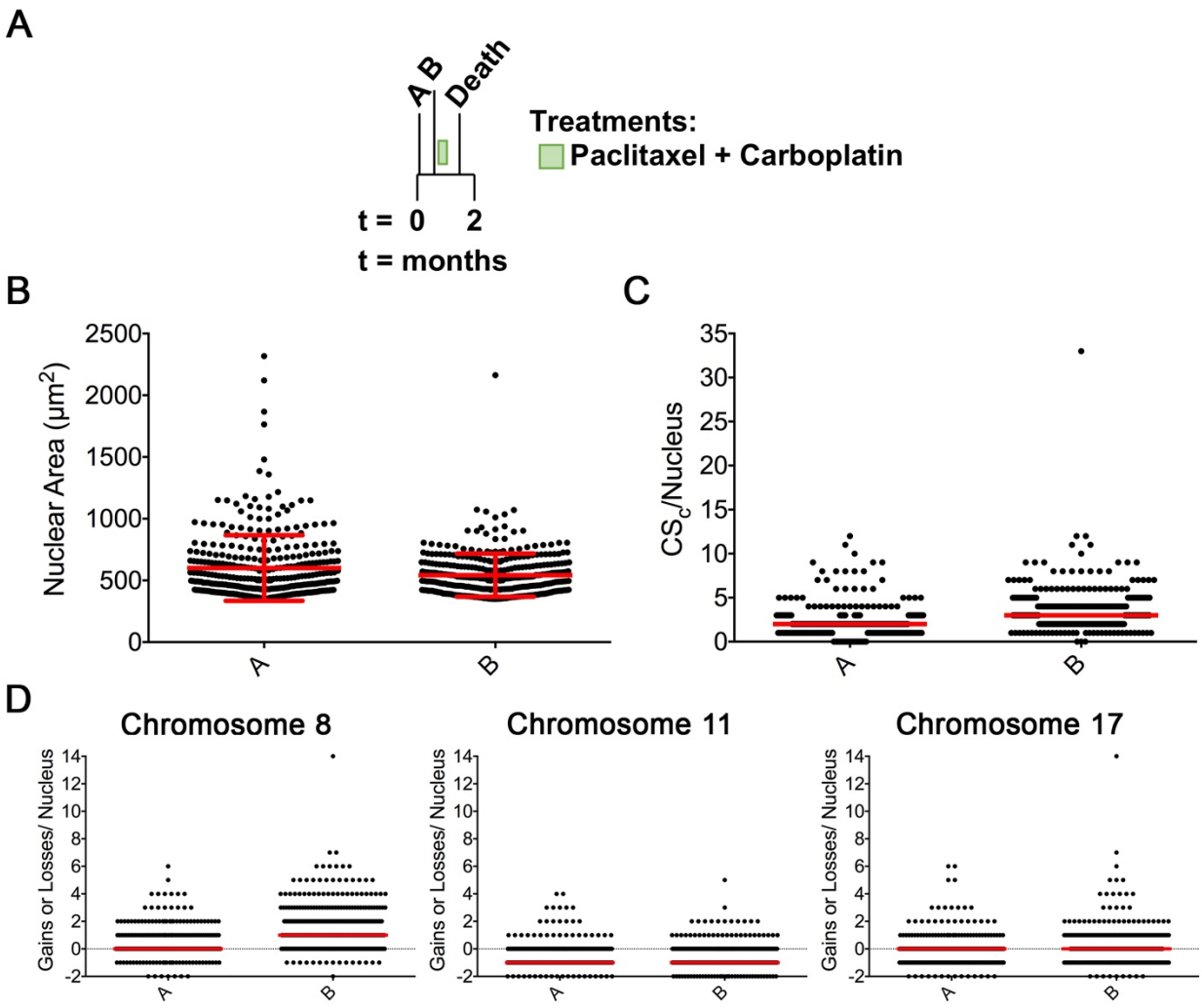


**Figure 5-9. CIN is Prevalent and Increases with Disease Progression in OV200.**
***(A)*** Timeline indicating the collection times for two samples relative to surgery, treatments, recurrence and death. ***(B)*** Dot plot presenting the NAs determined from two serial samples. Red bars indicate the mean ± SD (N = 2; n >200). ***(C)*** Dot plot presenting the $CS_c$ values for each nucleus evaluated. Red bars indicate the median $CS_c$. ***(D)*** Dot plot presenting the individual *CS* values (chromosome 8 [left], 11 [middle], and 17 [right]) for each nucleus evaluated. Red bars indicate the individual *CS* values.

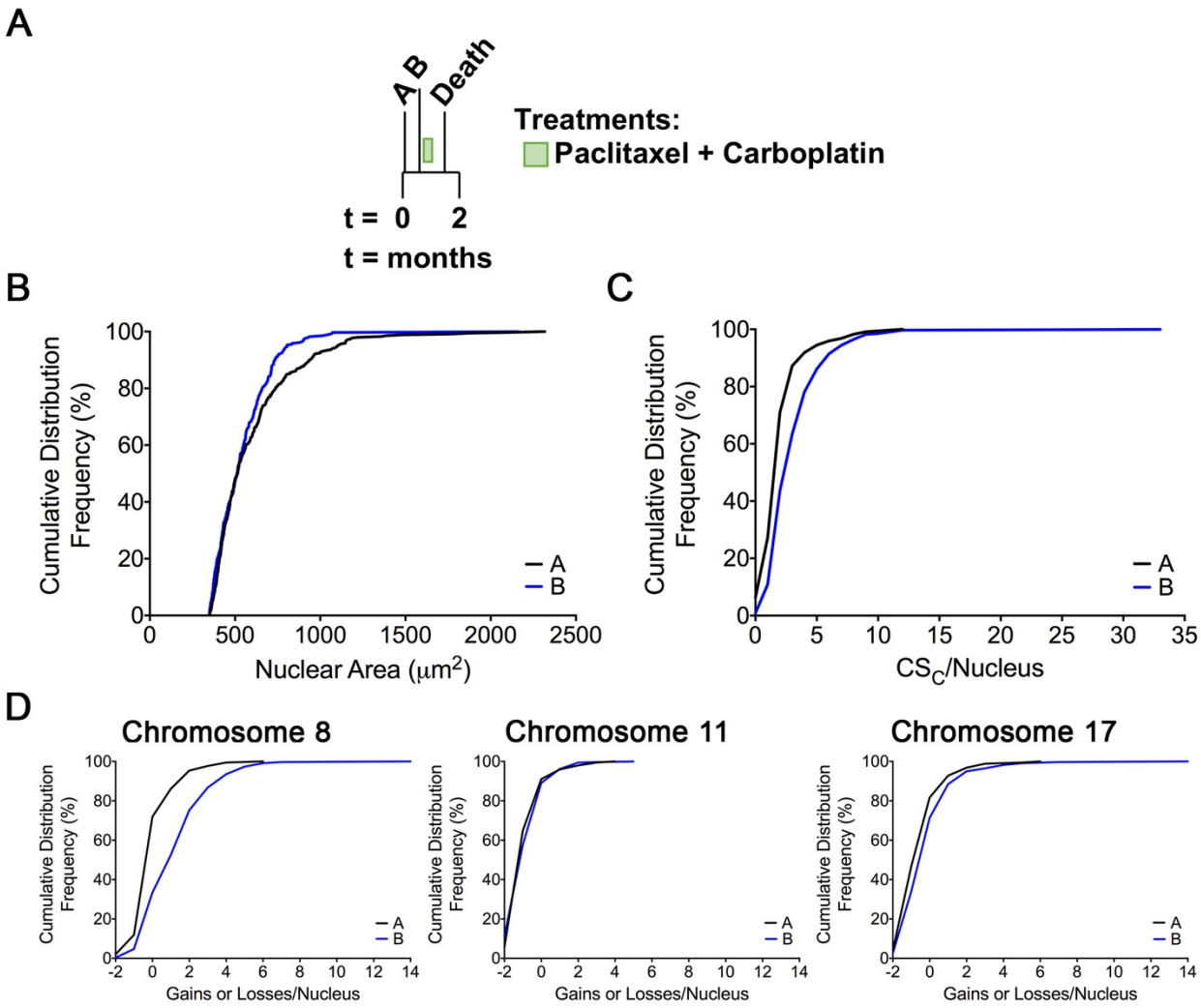


**Figure 5-10. Cumulative Distribution Frequencies for patient OV200.**
***(A)*** Timeline indicating the collection times for two samples. ***(B)*** Cumulative NA distribution frequencies of two serial samples (N = 2; n >200). ***(C)*** Cumulative $CS_c$ distribution frequencies for each of the two serial samples evaluated. ***(D)*** Cumulative distribution frequencies for each individual *CS* value (*i.e.* $CS_8$ [left], $CS_{11}$ [middle], and $CS_{17}$ [right]).

### 5.1.8 CIN is Prevalent and Dynamic in Patient Samples Collected Within 2 Months of Diagnosis, With Survival

The above observations suggest CIN is associated with chemorefractory disease, poor treatment response and rapid progression to death in HGSOC patient samples. To assess whether CIN exhibits specific dynamics in Group 2 (Fig 5-5) ascites samples, NAs and $CS_c$ values were evaluated, and includes two serial HGSOC patient samples OV061 and OV173. Figure 5-11 shows a timeline of serial samples collected from patient OV173 and quantified NA and *CS* values, which serves as a representative example of Group 2 HGSOC. Briefly, four serial samples were isolated and analyzed (Fig 5-11A). NA analysis revealed cell-to-cell heterogeneity, and the minimum total NA range observed was 659.0 $\mu m^2$ (OV173B), and the maximum total NA range observed was 1,984 $\mu m^2$ (OV173C) (Table S5-15). Two sample KS test comparing the NA distributions (Fig S5-7) of all pairwise combinations were statistically significant ($p$-value < 0.0001) (Table S5-16) with the exception of samples A vs. D that was not significant ($p$-value > 0.05). In general, similar results were observed in OV061 (Fig S5-8), and two sample KS test comparing the NA distributions of samples A and B was not statistically significant ($p$-value > 0.05) (Fig S5-9) (Table S5-17).

Next, *CS* values were evaluated and revealed cell-to-cell heterogeneity. In particular, OV173A exhibited the largest overall $CS_c$ distribution range (maximum $CS_c$ = 17) and had a median $CS_c$ = 1 and OV173D exhibited the smallest overall $CS_c$ distribution range (maximum $CS_c$ = 6) and had a median $CS_c$ = 1 (Fig 5-11C) (Table S5-18). Two sample MW test comparing the $CS_c$ ranked values (Fig 5-11C) of A vs. B and B vs. C were statistically significant ($p$-value < 0.01) (Table S5-19). All other pairwise combinations for OV173 were not statistically significant ($p$-value > 0.05) (Table S5-19). In general, similar results were observed in OV061 (Fig S5-8) and

two sample MW test comparing the $CS_c$ ranked values of samples A and B was statistically significant ($p$-value < 0.01) (Table S5-20). Similar trends were also observed for the individual *CS* values (Fig 5-11D). All four samples from OV173 exhibited gains and losses in chromosomes 8, 11, and 17 and had median individual *CS* values of $CS_8 = 0$, $CS_{11} = 0$, and $CS_{17} = 0$, respectively. Similarly, both samples from OV061 exhibited gains and losses in chromosomes 8, 11, and 17 and had median individual *CS* values of $CS_8 = 0$, $CS_{11} = 0$, and $CS_{17} = 0$, respectively.

Overall, these data show that CIN is prevalent in 100% of Group 2 HGSOC patient samples, which is supported by NA heterogeneity and median $CS_c$ values ≥ 1, and both HGSOC patient samples exhibit similar dynamics. More specifically, OV173 shows CIN was dynamic (shift towards smaller NAs from sample A to B and stable median $CS_c$) as the disease progresses and (shift towards larger NAs from sample B to C, shift towards smaller NAs from C to D and stable median $CS_c$) persisted during paclitaxel and carboplatin treatment, and OV061 shows CIN persisted (shift toward smaller NAs and stable median $CS_c$) as the disease progresses prior to any treatment.

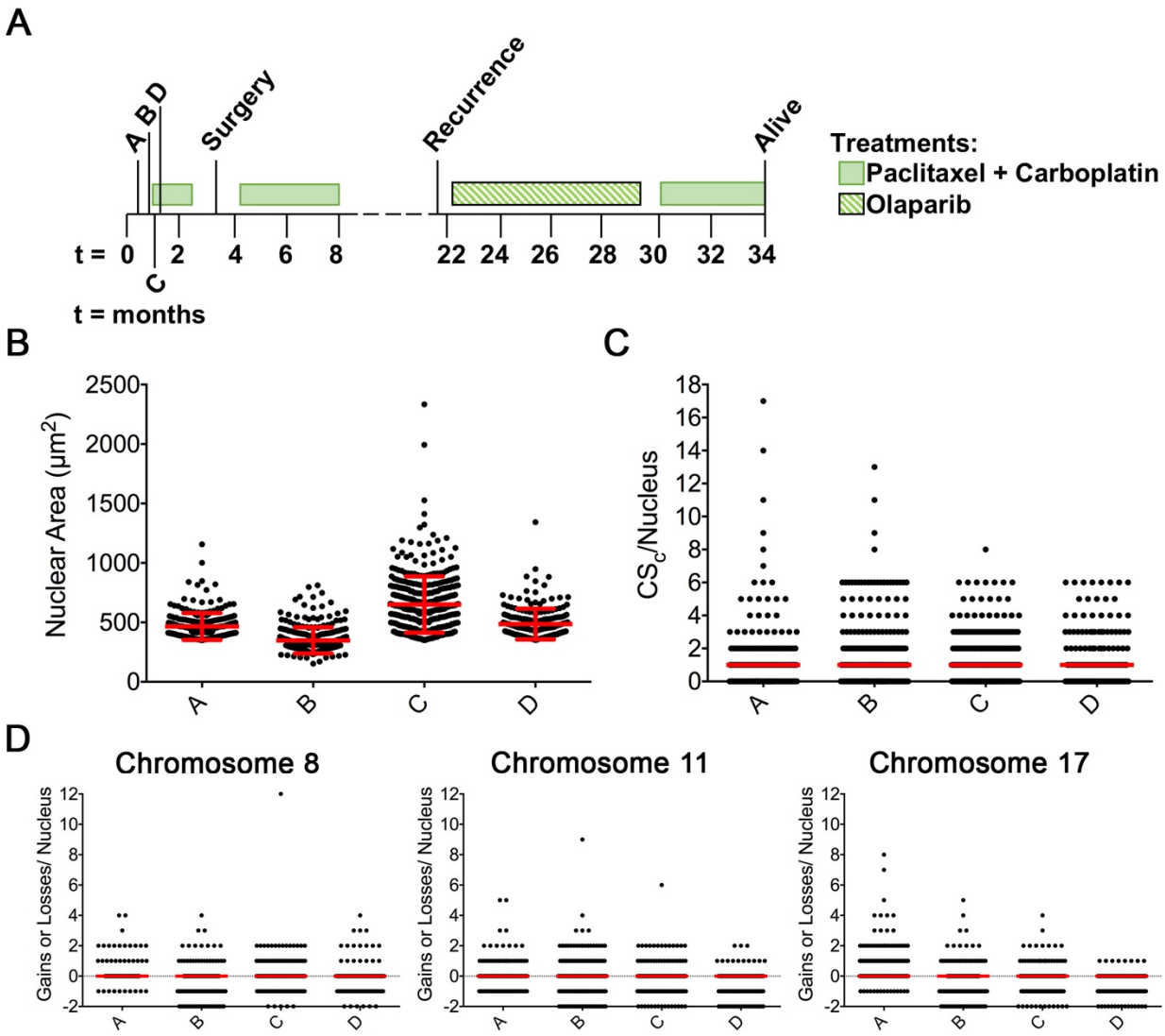


**Figure 5-11. OV173 Exhibits CIN Dynamics as Disease Progresses and During Initial Chemotherapy Treatments.**

***(A)*** Timeline indicating the collection times for four samples. Note this patient was alive as of their last known update (February 4, 2019). ***(B)*** Dot plot presenting the NAs determined from four serial samples. Red bars indicate the mean ± SD (N = 2; n >200). ***(C)*** Dot plot presenting the $CS_c$ values for each nucleus evaluated. Red bars indicate the median $CS_c$. ***(D)*** Dot plot presenting the individual *CS* values (chromosome 8 [left], 11 [middle], and 17 [right]) for each nucleus evaluated. Red bars indicate the individual *CS* values.

### 5.1.9 CIN is Prevalent and Dynamic in Patient Samples Collected Within 2 Months of Diagnosis and Following Chemotherapy Treatments

The above observations suggest CIN has varied dynamics as the disease progresses and in response to treatment in HGSOC patient samples collected within 10 months of diagnosis (Groups 1 and 2). To assess whether CIN exhibits specific dynamics in Group 3 (Fig 5-6) ascites samples, NAs and $CS_c$ values were evaluated, and includes three serial HGSOC patient samples OV063, OV070 and OV180. Figure 5-12 shows a timeline of serial samples collected from patient OV070 and quantified NA and *CS* values, which serves as a representative example of Group 3 HGSOC patients. Briefly, three serial samples were isolated and analyzed (Fig 5-12A). NA analysis revealed cell-to-cell heterogeneity, and the minimum total NA range observed was 1,084 $\mu m^2$ (OV070D), and the maximum total NA range observed was 1,179 $\mu m^2$ (OV070B) (Table S5-21). Two sample KS test comparing the NA distributions (Fig S5-10) of all pairwise combinations were statistically significant ($p$-value < 0.0001) (Table S5-22). In general, similar results were observed in OV063 (Fig S5-11) and OV180 (Fig S5-12). Two sample KS test comparing the NA distributions of all pairwise comparisons was statistically significant for OV063 ($p$-value < 0.01) (Fig S5-13) (Table S5-23) with the exception of samples D vs. E and E vs. F that were not statistically significant ($p$-value > 0.05). Two sample KS test comparing the NA distributions of all pairwise comparisons was statistically significant for OV180 ($p$-value < 0.01) (Fig S5-14) (Table S5-24).

Next, *CS* values were calculated for Group 3 samples and showed cell-to-cell heterogeneity. OV070B exhibited the largest overall $CS_c$ distribution range (maximum $CS_c = 21$) and had a median $CS_c = 1$ and OV070A exhibited the smallest overall $CS_c$ distribution range (maximum $CS_c = 9$) and had a median $CS_c = 0$ (Fig 5-12C) (Table S5-25). Two sample MW test

comparing the $CS_c$ ranked values (Fig 5-12C) of all pairwise combinations for OV070 were statistically significant ($p$-value < 0.0001) (Table S5-26). In general, similar results were observed in OV063 (Fig S5-11) and OV180 (Fig S5-12). Two sample MW test comparing the $CS_c$ ranked values of all pairwise combinations for OV063 were statistically significant ($p$-value < 0.05) (Table S5-27) with the exception of samples E vs. F that was not statistically significant ($p$-value > 0.05). Two sample MW test comparing the $CS_c$ ranked values of all pairwise combinations for OV063 were statistically significant ($p$-value < 0.05) (Table S5-28) with the exception of samples B vs. C and B vs. E that were not statistically significant ($p$-value > 0.05).

Overall, these data show that CIN is prevalent in 83.3% of Group 3 HGSOC patient samples, which is supported by NA heterogeneity and median $CS_c$ values ≥ 1, and each HGSOC patient sample exhibits varied dynamics. More specifically, OV070 shows an increase in aneuploidy (shift toward smaller NAs and increase in median $CS_c$) as the disease progresses and following disease recurrence, OV063 shows an increase in aneuploidy (stable NAs and increase in median $CS_c$ from sample A [$CS_c = 0$] to B [$CS_c = 1$]) as the disease progresses and remains stable at a median $CS_c = 1$ following disease recurrence and multiple treatments, and OV180 shows CIN is dynamic (shift towards larger NAs from sample A to B, shift towards smaller NAs from B to C, and a decrease in median $CS_c$ from sample A [$CS_c = 2$] to B [$CS_c = 1$]) following diagnosis and persisted (shift towards smaller NAs from sample C to D, stable NAs from D to E, and stable median $CS_c = 1$) as disease progresses and during doxorubicin treatment.

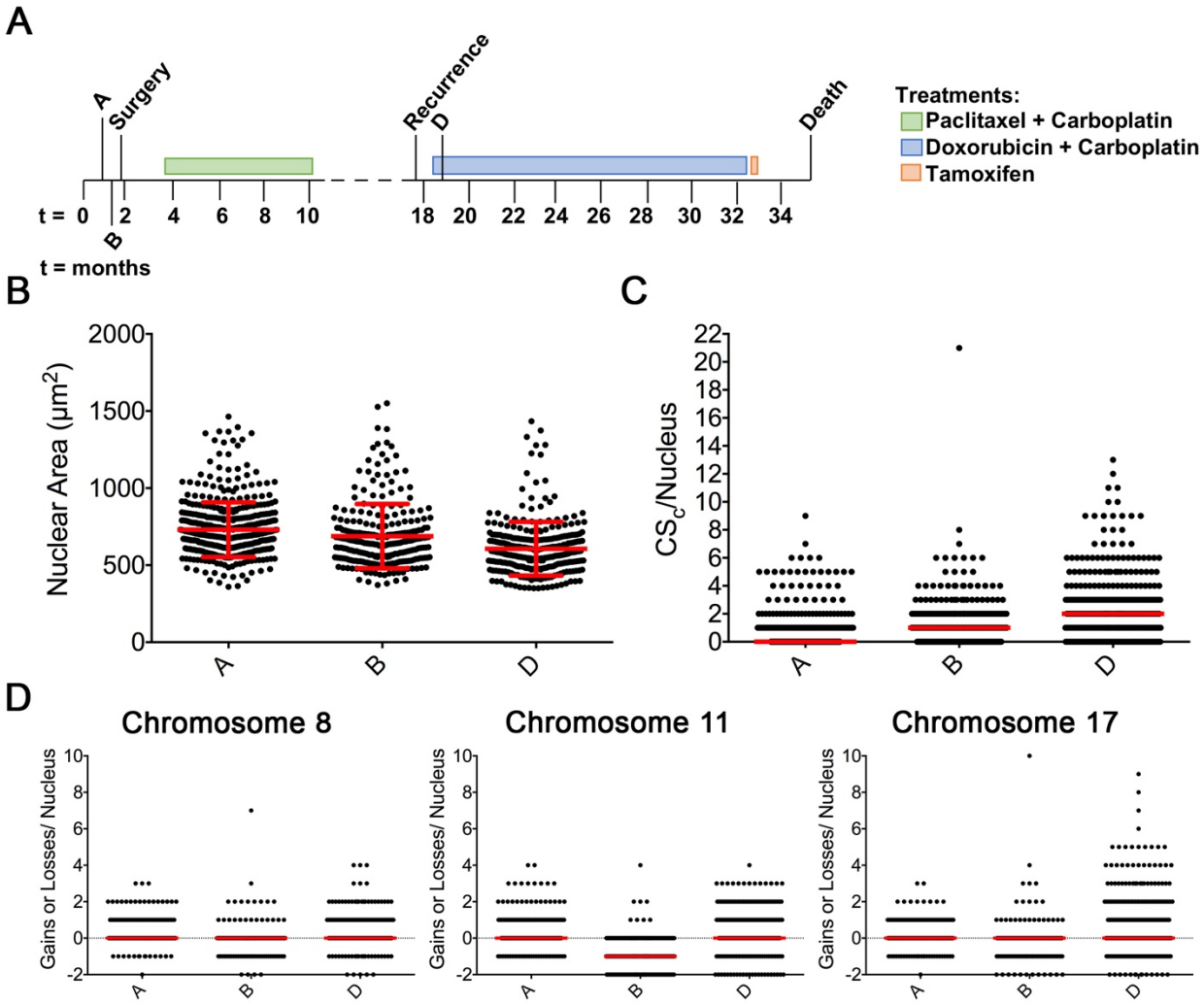


**Figure 5-12. CIN is Prevalent and Increases with Disease Progression in OV070.**
***(A)*** Timeline indicating the collection times for three samples. ***(B)*** Dot plot presenting the NAs determined from three serial samples. Red bars indicate the mean ± SD (N = 2; n >200). ***(C)*** Dot plot presenting the $CS_c$ values for each nucleus evaluated. Red bars indicate the median $CS_c$. ***(D)*** Dot plot presenting the individual *CS* values (chromosome 8 [left], 11 [middle], and 17 [right]) for each nucleus evaluated. Red bars indicate the individual *CS* values.

### 5.1.10 CIN is Prevalent and Dynamic in Patient Samples Collected in Late Stage Disease, Following Multiple Chemotherapy Treatments

The above observations suggest CIN increases as the disease progresses and upon disease recurrence in HGSOC patient samples collected within 2 months of diagnosis and following chemotherapy treatments (Groups 3). To assess whether CIN exhibits specific dynamics in Group 4 (Fig 5-7) ascites samples, NAs and $CS_c$ values were evaluated, and includes three serial HGSOC patient samples OV001, OV183 and OV299. Figure 5-13 shows a timeline of serial samples collected from patient OV183 and quantified NA and *CS* values, which serves as a representative example of Group 4 HGSOC patients. Briefly, 12 serial samples were isolated and analyzed (Fig 5-13A). NA analysis revealed cell-to-cell heterogeneity, and the minimum total NA range observed was 1,577 $\mu m^2$ (OV183B), and the maximum total NA range observed was 2,140 $\mu m^2$ (OV183F) (Table S5-29). Two sample KS test comparing the NA distributions (Fig S5-15) of all pairwise combinations were statistically significant ($p$-value < 0.01) (Table S5-30), with the exception of samples C vs. F and J vs. K that were not statistically significant ($p$-value < 0.05). In general, similar results were observed in OV001 (Fig S5-16) and OV299 (Fig S5-17). Two sample KS test comparing the NA distributions of all pairwise comparisons was statistically significant for OV001 ($p$-value < 0.0001) (Fig S5-18) (Table S5-31). Two sample KS test comparing the NA distributions of all pairwise comparisons was statistically significant for OV299 ($p$-value < 0.0001) (Fig S5-19) (Table S5-32), with the exception of samples A vs. E. and D vs. E that were not statistically significant ($p$-value < 0.05).

Next, *CS* values were evaluated and exhibited cell-to-cell heterogeneity. OV183D exhibited the largest overall $CS_c$ distribution range (maximum $CS_c$ = 31) and had a median $CS_c$ = 3 and OV183K exhibited the smallest overall $CS_c$ distribution range (maximum $CS_c$ = 11)

and had a median $CS_c$ = 1 (Fig 5-13C) (Table S5-33). Two sample MW test comparing the $CS_c$ ranked values (Fig 5-14C) of all pairwise combinations for OV183 were statistically significant ($p$-value < 0.05) (Table S5-34), with the exception of samples A vs. H, B vs. I, J, and K, C vs. N, D vs. E and F, E vs. F, I vs. J and K, and J vs. K that were not statistically significant ($p$-value < 0.05). In general, similar results were observed in OV001 (Fig S5-16) and OV299 (Fig S5-17). Two sample MW test comparing the $CS_c$ ranked values of all pairwise combinations for OV001 were statistically significant ($p$-value < 0.0001) (Table S5-35). Two sample MW test comparing the $CS_c$ ranked values of all pairwise combinations for OV299 were statistically significant ($p$-value < 0.05) (Table S5-36) with the exception of samples A vs. D and E, C vs. E, and D vs. E that were not statistically significant ($p$-value > 0.05).

Overall, these data show that CIN is prevalent in 100% of Group 4 HGSOC patient samples, which is supported by NA heterogeneity and median $CS_c$ value*s* ≥ 1, and each HGSOC patient sample exhibits varied CIN dynamics. More specifically, OV183 shows CIN was prevalent (shift towards smaller NAs and stable median $CS_c$) and aneuploidy increased (shift towards larger NAs in samples C to E and an increase in median $CS_c$ from sample C [$CS_c$ = 2] to D [$CS_c$ = 3]) during doxorubicin and carboplatin treatments. Next, aneuploidy decreased following treatment (shift towards smaller NAs and a decrease in median $CS_c$ from sample F [$CS_c$ = 3] to G [$CS_c$ = 1]) and was maintained during tamoxifen treatments (stable NAs and stable median $CS_c$). Lastly, aneuploidy increased (shift towards larger NAs and an increase in median $CS_c$ from sample K [$CS_c$ = 1] to N [$CS_c$ = 2]) following disease recurrence. OV001 shows aneuploidy increased (shift towards larger NAs and increase in median $CS_c$ from sample A [$CS_c$ = 1] to B [$CS_c$ = 3]) during paclitaxel and carboplatin treatment and CIN persisted (shift towards larger NA and a decrease in median $CS_c$ from sample B [$CS_c$ = 3] to D [$CS_c$ = 2]) following multiple chemotherapy treatments,

and OV299 shows aneuploidy increased (shift towards smaller NAs and increase in median $CS_c$ from sample A [$CS_c$ = 1] to B [$CS_c$ = 2]) following bevacizumab and paclitaxel treatment, and decreased (shift towards larger NAs and decrease in median $CS_c$ from sample B [$CS_c$ = 2] to C [$CS_c$ = 1]) during tamoxifen treatment.

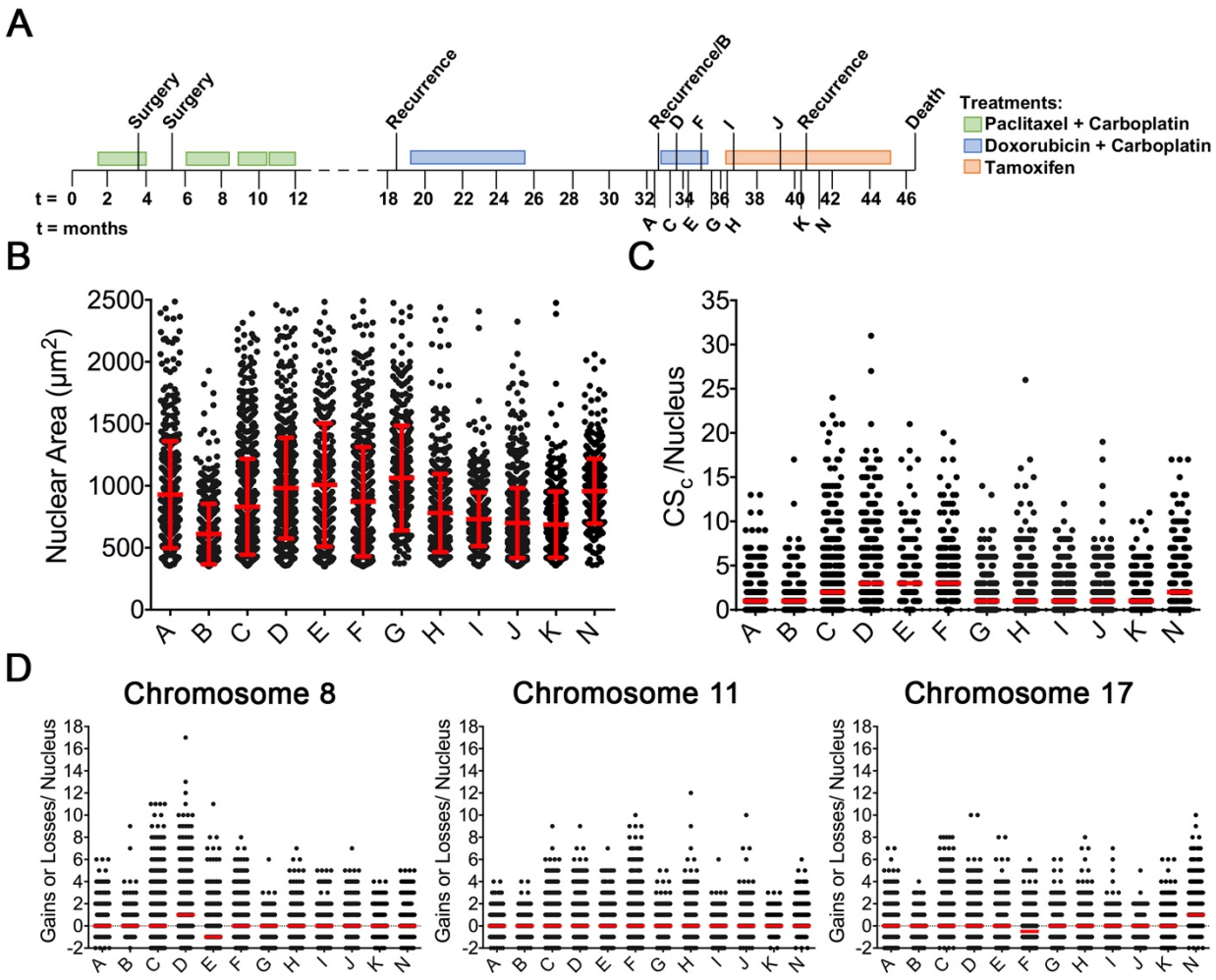


**Figure 5-13. CIN Increases as Disease Progresses and Upon Disease Recurrence and Decreases in Response to Treatment in OV183.**

***(A)*** Timeline indicating the collection times for 12 samples. ***(B)*** Dot plot presenting the NAs determined from 12 serial samples. Red bars indicate the mean ± SD (N = 2; n >200). ***(C)*** Dot plot presenting the $CS_c$ values for each nucleus evaluated. Red bars indicate the median $CS_c$. ***(D)*** Dot plot presenting the individual *CS* values (chromosome 8 [left], 11 [middle], and 17 [right]) for each nucleus evaluated. Red bars indicate the individual *CS* values.

### 5.1.11 CIN is Prevalent in Patient Samples with *BRCA1* and *BRCA2* Positive Mutations

The above observations suggest that CIN is associated with late stage disease and increases with disease progression and recurrence. To assess whether CIN is associated with Group 5 (Fig 5-8) ascites samples, NAs and $CS_c$ values were evaluated, and includes three serial HGSOC patient samples OV063 (four samples), OV173 (four samples) and OV180 (five samples) and six single HGSOC patient samples OV069, OV073, OV109, OV177, OV189 and OV246. NA analysis revealed cell-to-cell heterogeneity, and the minimum total NA range observed was 383.6 $\mu m^2$ (OV173B), and the maximum total NA range observed was 2,037 $\mu m^2$ (OV063A) (Fig 5-14A) (Table S5-37). Similarly, $CS_c$ values were evaluated in the 19 *BRCA* positive HGSOC patient samples. OV073C, OV177A, OV180A, and OV246A exhibited a varied overall $CS_c$ distribution range (maximum $CS_c = 11$, $CS_c = 9$, $CS_c = 21$, and $CS_c = 19$, respectively) and had a median $CS_c = 2$. The majority of samples (OV063D, E, and F, OV069A, OV109A, OV173A, B, C, and D, OV180B, C, D, and E, and OV189A) exhibited a varied overall $CS_c$ distribution range (from maximum $CS_c = 6$ [OV173D] to maximum $CS_c = 23$ [OV189A]). The remaining patient sample OV063A exhibited a large overall $CS_c$ distribution range (maximum $CS_c = 22$) and had a median $CS_c = 0$ (Fig 5-14B) (Table S5-38). Overall, these data show that CIN is prevalent in 94.7% of *BRCA* positive HGSOC patient samples, which is supported by NA heterogeneity and median $CS_c$ values $\geq 1$.

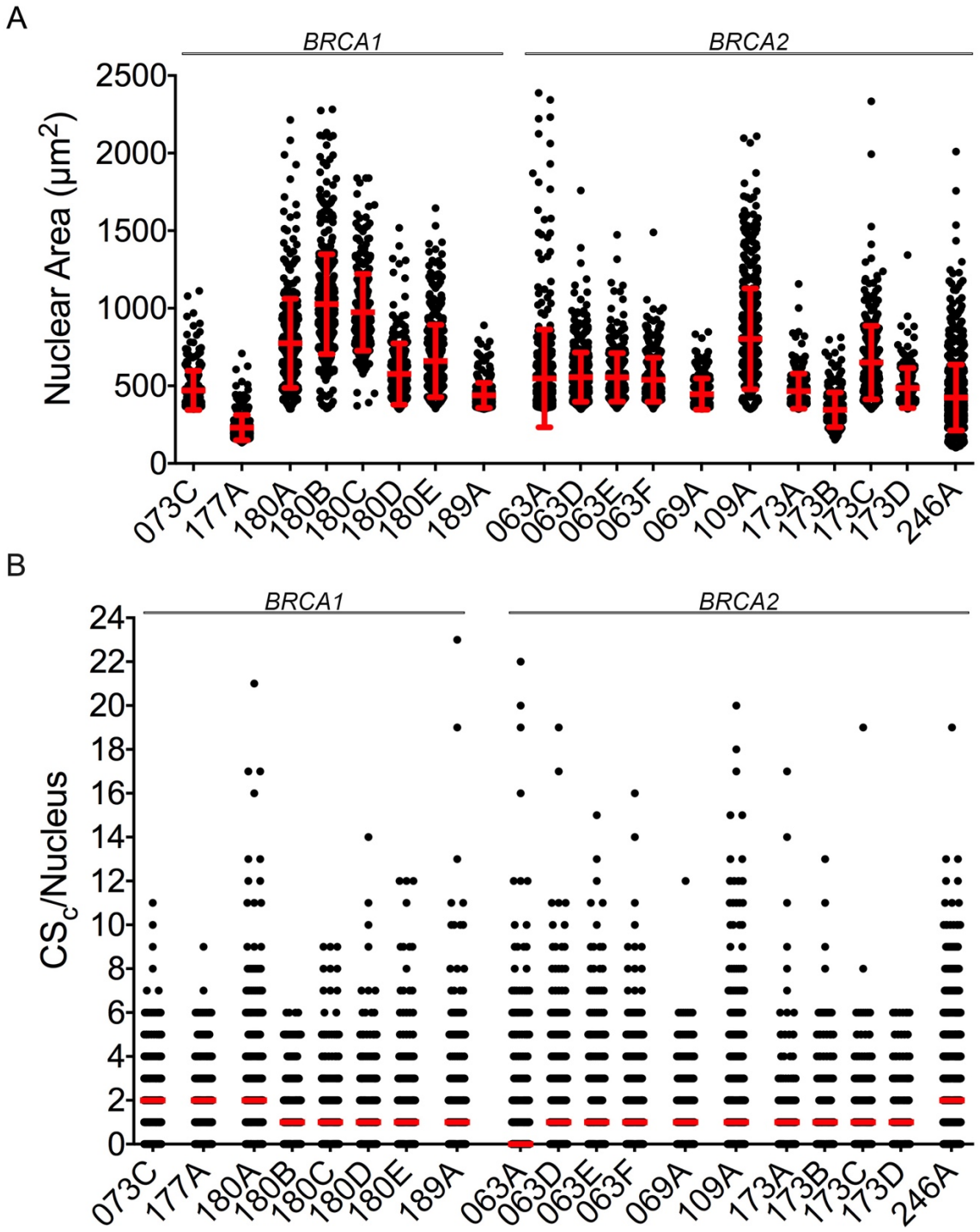


**Figure 5-14. CIN is Prevalent in *BRCA* Positive HGSOC Patient Samples.**
***(A)*** Dot plot presenting the NAs determined from three serial HGSOC patient samples (OV063, OV173, and OV180) and six single HGSOC patient samples (OV069A, OV073C, OV109A, OV177A, OV189A and OV246A) harbouring a *BRCA1* (left) or *BRCA2* (right) mutation. Red bars indicate the mean ± SD (N = 2; n >200). ***(B)*** Dot plot presenting the $CS_c$ values for each nucleus evaluated. Red bars indicate the median $CS_c$.

### 5.1.12 Conclusion

The central goal of *Aim 2* was to evaluate the prevalence and dynamics of CIN in both single and serial ascites samples derived from HGSOC patients. Overall, the above data show that CIN is prevalent in 92.5% of HGSOC ascites derived patient samples (20/22 single patient samples and 43/46 serial patient samples), which is supported by NA heterogeneity and median $CS_c$ values $\geq 1$. Importantly, CIN is prevalent at a high frequency in ascites derived HGSOC patient samples regardless of stage, grade, chemotherapy status, and *BRCA* mutations and in general, the majority (60.2%) of CIN positive samples have a median $CS_c = 1$ (25% of patients have a median $CS_c = 2$ and 7.4% of patients exhibit extreme CIN and have a median $CS_c = 3$). Additionally, serial HGSOC patient samples exhibit temporal dynamics and in general, aneuploidy and CIN increases with disease progression and recurrence, and have varied dynamics during treatments and following chemotherapy, similar to previously published results[46].

### 5.2.0 Supporting Information

### 5.2.1 Supporting Tables

**Table S5-1. Single HGSOC Patient Samples Clinical Details.**

| Patient ID | Histotype | Primary Site | Stage/Grade |
|---|---|---|---|
| | | *Chemonaïve* | |
| OV021A | Serous cystadenocarcinoma | Ovary (bilateral) | IV/high grade |
| OV058A | Serous cystadenocarcinoma | Ovary (left) | IIIC/high grade |
| OV060A | Serous cystadenocarcinoma | Peritoneum (unspecified) | IIIC/high grade |
| OV118A | Serous cystadenocarcinoma | Ovary (bilateral) | IIIC/high grade |
| OV169A[E] | Mixed cell adenocarcinoma | Ovary (Right) | IC/high grade |
| OV177A[B, D] | Mixed cell adenocarcinoma | Ovary (left) | IC/high grade |
| OV184A | Serous cystadenocarcinoma | Ovary (bilateral) | IV/high grade |
| OV205A | Serous cystadenocarcinoma | Ovary (bilateral) | IIIC/high grade |
| OV246A[C] | Papillary serous cystadenocarcinoma | Ovary (Right) | IIIC/ N/A[F] |
| OV247A | Serous cystadenocarcinoma | Ovary (Right) | IIINOS[G]/high grade |
| | | *Chemosensitive* | |
| OV059A | Serous cystadenocarcinoma | Fallopian tube (right) | IV/ N/A |
| OV067A | Serous cystadenocarcinoma | Ovary (bilateral) | IIIC/high grade |
| OV069A[C] | Serous cystadenocarcinoma | Ovary (unknown) | IIIC/high grade |
| OV171B[A] | Adenocarcinoma | Ovary (unknown) | IV/ N/A |
| OV189A[B] | Serous cystadenocarcinoma | Ovary (bilateral) | IIIC/high grade |
| OV196A | Serous cystadenocarcinoma | Ovary (bilateral) | IIIB/high grade |
| | | *Chemoresistant* | |
| OV053A | Mixed cell adenocarcinoma | Ovary (bilateral) | IIIC/high grade |
| OV073C[B] | Papillary serous cystadenocarcinoma | Ovary (bilateral) | IIIC/high grade |
| OV103E | Serous cystadenocarcinoma | Ovary (bilateral) | IIIC/high grade |
| OV109A[C] | Serous surface papillary carcinoma | Ovary (bilateral) | IIIC/high grade |
| OV146A | Serous cystadenocarcinoma | Peritoneum (unspecified) | IIINOS/ N/A |
| OV230A[A] | Adenocarcinoma | Ovary (Right) | IIIC/ N/A |

[A]No surgery
[B]*BRCA1* positive tumor
[C]*BRCA2* positive tumor
[D]*CDH1* positive tumor
[E]Positive for Lynch Syndrome
[F]Not applicable (N/A)
[G]Not otherwise specified (NOS)

**Table S5-2. Serial HGSOC Patient Samples Clinical Details.**

| Patient ID | Histotype | Primary Site | Stage/Grade |
|---|---|---|---|
| OV001 | Papillary adenocarcinoma | Peritoneum (unspecified) | Poorly differentiated |
| OV009[A] | Adenocarcinoma | Ovary (bilateral) | IV/high grade |
| OV061 | Serous cystadenocarcinoma | Ovary (bilateral) | IIIC/high grade |
| OV063[C] | Serous cystadenocarcinoma | Ovary (bilateral) | IIIA/high grade |
| OV070 | Serous cystadenocarcinoma | Ovary (bilateral) | IV/high grade |
| OV125[A] | Adenocarcinoma | Ovary (bilateral) | IIIA/ N/A[E] |
| OV173[C, D] | Serous cystadenocarcinoma | Ovary (bilateral) | IIIC/high grade |
| OV180[B] | Serous cystadenocarcinoma | Ovary (Right) | IIIC/high grade |
| OV183 | Serous cystadenocarcinoma | Ovary (bilateral) | IIIC/high grade |
| OV200[A] | Adenocarcinoma | Female genital organ (unspecified) | N/A |
| OV203[A] | Adenocarcinoma | Ovary (Right) | IV/ N/A |
| OV299 | Mixed cell adenocarcinoma | Ovary (left) | IC/high grade |

[A]No surgery
[B]*BRCA1* positive tumor
[C]*BRCA2* positive tumor
[D]*PALB2* positive tumor
[E]Not applicable (N/A)

**Table S5-3. NA Descriptive Statistics for Single HGSOC Patient Samples.**

| Patient ID | n[A] | Nuclear Area ($\mu m^2$) | | | | | |
|---|---|---|---|---|---|---|---|
| | | 25th Percentile | Median | 75th Percentile | Total Range | Mean | SD[B] |
| | | | | *Chemonaïve* | | | |
| OV021A | 598 | 634.6 | 795.1 | 974.1 | 1748 | 831.0 | 275.0 |
| OV058A | 823 | 530.0 | 630.9 | 773.2 | 2105 | 694.8 | 268.2 |
| OV060A | 237 | 432.0 | 526.7 | 680.2 | 1311 | 602.4 | 245.7 |
| OV118A | 348 | 616.0 | 704.2 | 790.3 | 1201 | 721.0 | 196.6 |
| OV169A | 604 | 428.7 | 501.3 | 654.6 | 2128 | 594.5 | 264.8 |
| OV177A | 383 | 178.3 | 206.4 | 253.0 | 574.9 | 230.6 | 81.26 |
| OV184A | 431 | 383.2 | 432.5 | 531.1 | 1815 | 492.6 | 187.6 |
| OV205A | 242 | 399.0 | 446.4 | 532.5 | 796.1 | 486.3 | 135.4 |
| OV246A | 1023 | 297.5 | 370.5 | 500.3 | 1909 | 424.4 | 212.1 |
| OV247A | 406 | 408.9 | 459.9 | 537.9 | 1361 | 496.5 | 137.7 |
| | | | | *Chemosensitive* | | | |
| OV059A | 215 | 423.3 | 494.9 | 577.4 | 794.9 | 514.9 | 120.7 |
| OV067A | 225 | 550.1 | 666.1 | 845.7 | 1719 | 734.3 | 268.3 |
| OV069A | 255 | 373.1 | 408.3 | 490.9 | 496.4 | 446.6 | 100.3 |
| OV171B | 250 | 396.2 | 475.8 | 567.8 | 1048 | 504.6 | 140.0 |
| OV189A | 400 | 386.2 | 418.1 | 468.4 | 539.6 | 438.8 | 80.84 |
| OV196A | 445 | 468.8 | 581.2 | 745.7 | 1350 | 614.3 | 237.8 |
| | | | | *Chemoresistant* | | | |
| OV053A | 892 | 530.0 | 630.9 | 773.2 | 2105 | 694.8 | 268.2 |
| OV073C | 296 | 381.6 | 435.0 | 510.0 | 761.7 | 470.7 | 126.5 |
| OV103E | 492 | 457.0 | 544.7 | 652.5 | 2071 | 589.7 | 211.3 |
| OV109A | 588 | 572.1 | 748.4 | 966.5 | 1759 | 802.6 | 325.2 |
| OV146A | 296 | 430.4 | 507.8 | 614.6 | 2148 | 559.6 | 220.7 |
| OV230A | 253 | 491.7 | 604.9 | 786.1 | 1868 | 668.1 | 250.6 |

[A]Number of nuclei analyzed (n)
[B]Standard deviation (SD)

**Table S5-4. *CS* Descriptive Statistics for Single HGSOC Patient Samples.**

| Patient ID | n[A] | Median | | | | Total $CS_c$ Range |
|---|---|---|---|---|---|---|
| | | $CS_8$ | $CS_{11}$ | $CS_{17}$ | $CS_c$ | |
| | | *Chemonaïve* | | | | |
| OV021A | 598 | 0.5 | 0 | 0 | 1 | 22 |
| OV058A | 823 | 0 | 0 | 0 | 1 | 14 |
| OV060A | 237 | 0 | 0 | 0 | 0 | 10 |
| OV118A | 348 | 0 | 0 | 0 | 1 | 8 |
| OV169A | 604 | 0 | 0 | 0 | 0 | 17 |
| OV177A | 383 | 0 | 0 | 0 | 2 | 9 |
| OV184A | 431 | 0 | 0 | 0 | 1 | 18 |
| OV205A | 242 | 0 | 0 | 0 | 1 | 11 |
| OV246A | 1023 | 0 | 0 | 0 | 2 | 19 |
| OV247A | 406 | 0 | 0 | -1 | 1 | 6 |
| | | *Chemosensitive* | | | | |
| OV059A | 215 | 0 | 0 | 0 | 1 | 8 |
| OV067A | 225 | 0 | 0 | -1 | 1 | 6 |
| OV069A | 255 | 0 | 0 | 0 | 1 | 12 |
| OV171B | 250 | 0 | 0 | 0 | 1 | 8 |
| OV189A | 400 | 0 | 0 | 0 | 1 | 23 |
| OV196A | 445 | 0 | 0 | -1 | 2 | 16 |
| | | *Chemoresistant* | | | | |
| OV053A | 892 | 0 | 0 | 0 | 1 | 9 |
| OV073C | 296 | 0 | 0 | 1 | 2 | 11 |
| OV103E | 492 | 0 | 0 | -1 | 2 | 16 |
| OV109A | 588 | 0 | 0 | 0 | 1 | 20 |
| OV146A | 296 | 0 | 0 | 0 | 1 | 10 |
| OV230A | 253 | 0 | 0 | 0 | 1 | 10 |

[A]Number of nuclei analyzed (n)

**Table S5-5. NA Descriptive Statistics for Group 1 Serial HGSOC Patient Samples.**

| Patient ID | n[A] | Nuclear Area (μm$^2$) | | | | | |
|---|---|---|---|---|---|---|---|
| | | 25$^{th}$ Percentile | Median | 75$^{th}$ Percentile | Total Range | Mean | SD[B] |
| OV009A | 206 | 381.7 | 420.5 | 504.4 | 1242 | 461.4 | 432.8 |
| OV009B | 312 | 373.2 | 407.4 | 452.0 | 555.2 | 130.0 | 86.47 |
| OV125A | 336 | 466.6 | 552.0 | 664.1 | 1994 | 618.2 | 261.8 |
| OV125B | 392 | 306.4 | 355.1 | 423.6 | 1854 | 394.0 | 178.1 |
| OV200A | 345 | 422.0 | 511.7 | 682.1 | 1967 | 600.5 | 265.5 |
| OV200B | 339 | 416.2 | 515.7 | 628.8 | 1813 | 542.6 | 174.4 |
| OV203A | 410 | 316.6 | 386.9 | 470.5 | 863.2 | 415.2 | 134.0 |
| OV203B | 215 | 374.0 | 445.2 | 594.9 | 2175 | 615.5 | 466.9 |

[A]Number of nuclei analyzed (n)
[B]Standard deviation (SD)

**Table S5-6. KS-test Comparing the Cumulative NA Distribution Frequencies in OV200[A].**

| | *vs.* Sample |
|---|---|
| Sample | B |
| A | * |

[A]Presented are the *p*-values calculated from two-sample KS-test for the indicated pairs with *p*-values < 0.05 considered statistically significant (*, *p*-value < 0.05).

**Table S5-7. KS-test Comparing the Cumulative NA Distribution Frequencies in OV125[A].**

| | *vs.* Sample |
|---|---|
| Sample | B |
| A | **** |

[A]Presented are the *p*-values calculated from two-sample KS-test for the indicated pairs with *p*-values < 0.05 considered statistically significant (****, *p*-value < 0.0001).

**Table S5-8. KS-test Comparing the Cumulative NA Distribution Frequencies in OV203[A].**

| | *vs.* Sample |
|---|---|
| Sample | B |
| A | **** |

[A]Presented are the *p*-values calculated from two-sample KS-test for the indicated pairs with *p*-values < 0.05 considered statistically significant (****, *p*-value < 0.0001).

**Table S5-9. KS-test Comparing the Cumulative NA Distribution Frequencies in OV009[A].**

| | *vs.* Sample |
|---|---|
| Sample | B |
| A | ns |

[A]Presented are the *p*-values calculated from two-sample KS-test for the indicated pairs with *p*-values < 0.05 considered statistically significant (ns, *p*-value > 0.05).

**Table S5-10. *CS* Descriptive Statistics for Serial Primary HGSOC Patient Samples – Patient Profile Group 1.**

| | | Median | | | | Total $CS_c$ |
|---|---|---|---|---|---|---|
| Patient ID | n[A] | $CS_8$ | $CS_{11}$ | $CS_{17}$ | $CS_c$ | Range |
| OV009A | 206 | 0 | 0 | 0 | 2 | 17 |
| OV009B | 312 | 0 | 0 | 0 | 0 | 15 |
| OV125A | 336 | 0.5 | 0 | 0 | 2 | 17 |
| OV125B | 392 | 0 | 0 | 0 | 2 | 16 |
| OV200A | 345 | 0 | -1 | 0 | 2 | 12 |
| OV200B | 339 | 1 | -1 | 0 | 3 | 33 |
| OV203A | 410 | 0 | 1 | 0 | 2 | 31 |
| OV203B | 215 | 0 | 0 | 0 | 2 | 17 |

[A]Number of nuclei analyzed (n)

**Table S5-11. MW-test Comparing the *CS* Ranked Values in OV200[A].**

| | *vs.* Sample |
|---|---|
| Sample | B |
| A | **** |

[A]Presented are the *p*-values calculated from two-sample MW-test for the indicated pairs with *p*-values < 0.05 considered statistically significant (****, *p*-value < 0.0001).

**Table S5-12. MW-test Comparing the *CS* Ranked Values in OV009[A].**

| | *vs.* Sample |
|---|---|
| Sample | B |
| A | **** |

[A]Presented are the *p*-values calculated from two-sample MW-test for the indicated pairs with *p*-values < 0.05 considered statistically significant (****, *p*-value < 0.0001).

**Table S5-13. MW-test Comparing the *CS* Ranked Values in OV203[A].**

| | *vs.* Sample |
|---|---|
| Sample | B |
| A | * |

[A]Presented are the *p*-values calculated from two-sample MW-test for the indicated pairs with *p*-values < 0.05 considered statistically significant (*, *p*-value < 0.05).

**Table S5-14. MW-test Comparing the *CS* Ranked Values in OV125[A].**

| | *vs.* Sample |
|---|---|
| Sample | B |
| A | ns |

[A]Presented are the *p*-values calculated from two-sample MW-test for the indicated pairs with *p*-values < 0.05 considered statistically significant (ns, *p*-value > 0.05).

**Table S5-15. NA Descriptive Statistics for Serial Primary HGSOC Patient Samples – Patient Profile Group 2.**

| | | Nuclear Area (μm$^2$) | | | | | |
|---|---|---|---|---|---|---|---|
| Patient ID | n[A] | 25$^{th}$ Percentile | Median | 75$^{th}$ Percentile | Total Range | Mean | SD[B] |
| OV061A | 307 | 483.6 | 568.3 | 753.2 | 1338 | 638.1 | 218.7 |
| OV061B | 270 | 456.8 | 553.9 | 705.5 | 1357 | 600.5 | 201.6 |
| OV173A | 230 | 390.1 | 431.2 | 505.6 | 806.3 | 465.9 | 112.8 |
| OV173B | 287 | 268.3 | 306.2 | 383.6 | 659.0 | 323.2 | 135.8 |
| OV173C | 378 | 472.0 | 610.0 | 763.2 | 1984 | 650.0 | 237.3 |
| OV173D | 202 | 397.3 | 450.8 | 535.7 | 1311 | 485.7 | 129.2 |

[A]Number of nuclei analyzed (n)
[B]Standard deviation (SD)

**Table S5-16. KS-test Comparing the Cumulative NA Distribution Frequencies in OV173[A].**

| | *vs.* Sample | | |
|---|---|---|---|
| Sample | B | C | D |
| A | **** | **** | ns |
| B | N/A[B] | **** | **** |
| C | | N/A | **** |

[A]Presented are the *p*-values calculated from two-sample KS-test for the indicated pairs with *p*-values < 0.05 considered statistically significant (ns, *p*-value > 0.05; ****, *p*-value < 0.0001).
[B]Not applicable (N/A)

**Table S5-17. KS-test Comparing the Cumulative NA Distribution Frequencies in OV061A.**

| | *vs.* Sample |
|---|---|
| Sample | B |
| A | ns |

[A]Presented are the *p*-values calculated from two-sample KS-test for the indicated pairs with *p*-values < 0.05 considered statistically significant (ns, *p*-value > 0.05).

**Table S5-18. *CS* Descriptive Statistics for Serial Primary HGSOC Patient Samples – Patient Profile Group 2.**

| | | Median | | | | Total $CS_c$ |
|---|---|---|---|---|---|---|
| Patient ID | n[A] | $CS_8$ | $CS_{11}$ | $CS_{17}$ | $CS_c$ | Range |
| OV061A | 307 | 0 | 0 | 0 | 1 | 7 |
| OV061B | 270 | 0 | 0 | 0 | 1 | 16 |
| OV173A | 230 | 0 | 0 | 0 | 1 | 17 |
| OV173B | 287 | 0 | 0 | 0 | 1 | 13 |
| OV173C | 378 | 0 | 0 | 0 | 1 | 8 |
| OV173D | 202 | 0 | 0 | 0 | 1 | 6 |

[A]Number of nuclei analyzed (n)

**Table S5-19. MW-test Comparing the *CS* Ranked Values in OV173[A].**

| | *vs.* Sample | | |
|---|---|---|---|
| Sample | B | C | D |
| A | * | ns | ns |
| B | N/A[B] | *** | ns |
| C | | N/A | ns |

[A]Presented are the *p*-values calculated from two-sample MW-test for the indicated pairs with *p*-values < 0.05 considered statistically significant (ns, *p*-value > 0.05; *, *p*-value < 0.05; ***, *p*-value < 0.001).
[B]Not applicable (N/A)

**Table S5-20. MW-test Comparing the *CS* Ranked Values in OV061[A].**

| | *vs.* Sample |
|---|---|
| Sample | B |
| A | ** |

[A]Presented are the *p*-values calculated from two-sample MW-test for the indicated pairs with *p*-values < 0.05 considered statistically significant (**, *p*-value < 0.01).

**Table S5-21. NA Descriptive Statistics for Serial Primary HGSOC Patient Samples – Patient Profile Group 3.**

| | | Nuclear Area (μm$^2$) | | | | | |
|---|---|---|---|---|---|---|---|
| Patient ID | n[A] | 25$^{th}$ Percentile | Median | 75$^{th}$ Percentile | Total Range | Mean | SD[B] |
| OV063A | 443 | 39.0 | 444.9 | 555.4 | 2037 | 547.9 | 314.7 |
| OV063D | 538 | 453.8 | 525.2 | 610.5 | 1409 | 556.1 | 159.0 |
| OV063E | 331 | 455.8 | 518.8 | 622.4 | 1119 | 554.8 | 155.9 |
| OV063F | 413 | 441.6 | 539.1 | 595.3 | 1136 | 539.1 | 141.4 |
| OV070A | 436 | 615.9 | 692.1 | 804.0 | 1105 | 730.1 | 177.9 |
| OV070B | 256 | 546.5 | 643.4 | 748.7 | 1179 | 688.0 | 208.8 |
| OV070D | 285 | 497.9 | 575.4 | 674.2 | 1084 | 606.6 | 174.3 |
| OV180A | 391 | 575.4 | 742.2 | 887.0 | 1862 | 774.5 | 287.7 |
| OV180B | 542 | 830.5 | 975.3 | 1163 | 1926 | 1026 | 321.6 |
| OV180C | 326 | 811.3 | 919.1 | 1071 | 1467 | 974.1 | 247.5 |
| OV180D | 253 | 435.5 | 519.8 | 664.0 | 1168 | 576.2 | 197.5 |
| OV180E | 434 | 504.4 | 599.0 | 747.2 | 1291 | 660.0 | 233.5 |

[A]Number of nuclei analyzed (n)
[B]Standard deviation (SD)

**Table S5-22. KS-test Comparing the Cumulative NA Distribution Frequencies in OV070[A].**

| | *vs.* Sample | |
|---|---|---|
| Sample | B | D |
| A | **** | **** |
| B | N/A[B] | **** |

[A]Presented are the *p*-values calculated from two-sample KS-test for the indicated pairs with *p*-values < 0.05 considered statistically significant (****, *p*-value < 0.0001).
[B]Not applicable (N/A)

**Table S5-23. KS-test Comparing the Cumulative NA Distribution Frequencies in OV063[A].**

| | *vs.* Sample | | |
|---|---|---|---|
| Sample | D | E | F |
| A | **** | **** | **** |
| D | N/A[B] | ns | ** |
| E | | N/A | ns |

[A]Presented are the *p*-values calculated from two-sample KS-test for the indicated pairs with *p*-values < 0.05 considered statistically significant (ns, *p*-value > 0.05; **, *p*-value < 0.01; ****, *p*-value < 0.0001).
[B]Not applicable (N/A)

**Table S5-24. KS-test Comparing the Cumulative NA Distribution Frequencies in OV180[A].**

| | *vs.* Sample | | | |
|---|---|---|---|---|
| Sample | B | C | D | E |
| A | **** | **** | **** | **** |
| B | N/A[B] | ** | **** | **** |
| C | | N/A | **** | **** |
| D | | | N/A | **** |

[A]Presented are the *p*-values calculated from two-sample KS-test for the indicated pairs with *p*-values < 0.05 considered statistically significant (**, *p*-value < 0.01; ****, *p*-value < 0.0001).
[B]Not applicable (N/A)

**Table S5-25. *CS* Descriptive Statistics for Serial Primary HGSOC Patient Samples – Patient Profile Group 3.**

| Patient ID | n[A] | Median | | | | Total $CS_c$ Range |
|---|---|---|---|---|---|---|
| | | $CS_8$ | $CS_{11}$ | $CS_{17}$ | $CS_c$ | |
| OV063A | 443 | 0 | 0 | 0 | 0 | 22 |
| OV063D | 538 | 0 | 0 | 0 | 1 | 19 |
| OV063E | 331 | 0 | 0 | 0 | 1 | 15 |
| OV063F | 413 | 0 | 0 | 0 | 1 | 16 |
| OV070A | 436 | 0 | 0 | 0 | 0 | 9 |
| OV070B | 256 | 0 | -1 | 0 | 1 | 21 |
| OV070D | 285 | 0 | 0 | 0 | 2 | 13 |
| OV180A | 391 | 0 | 0 | 0 | 2 | 21 |
| OV180B | 542 | 0 | 0 | 0 | 1 | 6 |
| OV180C | 326 | 0 | 0 | 0 | 1 | 9 |
| OV180D | 253 | 0 | 0 | 0 | 1 | 14 |
| OV180E | 434 | 0 | 0 | 0 | 1 | 12 |

[A]Number of nuclei analyzed (n)

**Table S5-26. MW-test Comparing the *CS* Ranked Values in OV070[A].**

| Sample | *vs.* Sample | |
|---|---|---|
| | B | D |
| A | **** | **** |
| B | N/A[B] | **** |

[A]Presented are the *p*-values calculated from two-sample MW-test for the indicated pairs with *p*-values < 0.05 considered statistically significant (****, *p*-value < 0.0001).
[B]Not applicable (N/A)

**Table S5-27. MW-test Comparing the *CS* Ranked Values in OV063[A].**

| | *vs.* Sample | | |
|---|---|---|---|
| Sample | D | E | F |
| A | * | **** | **** |
| D | N/A[B] | * | *** |
| E | | N/A | ns |

[A]Presented are the *p*-values calculated from two-sample MW-test for the indicated pairs with *p*-values < 0.05 considered statistically significant (ns, *p*-value > 0.05; *, *p*-value < 0.05; ***, *p*-value < 0.001; ****, *p*-value < 0.0001).
[B]Not applicable (N/A)

**Table S5-28. MW-test Comparing the *CS* Ranked Values in OV180[A].**

| | *vs.* Sample | | | |
|---|---|---|---|---|
| Sample | B | C | D | E |
| A | **** | **** | **** | **** |
| B | N/A[B] | ns | ** | ns |
| C | | N/A | **** | * |
| D | | | N/A | * |

[A]Presented are the *p*-values calculated from two-sample MW-test for the indicated pairs with *p*-values < 0.05 considered statistically significant (ns, *p*-value > 0.05; *, *p*-value < 0.05; **, *p*-value < 0.01; ****, *p*-value < 0.0001).
[B]Not applicable (N/A)

**Table S5-29. NA Descriptive Statistics for Serial Primary HGSOC Patient Samples – Patient Profile Group 4.**

| Patient ID | n[A] | Nuclear Area (μm$^2$) | | | | | |
|---|---|---|---|---|---|---|---|
| | | 25$^{th}$ Percentile | Median | 75$^{th}$ Percentile | Total Range | Mean | SD[B] |
| OV001A | 225 | 417.2 | 493.6 | 615.6 | 1913 | 578.3 | 301.7 |
| OV001B | 269 | 458.2 | 596.6 | 857.1 | 1993 | 731.0 | 392.9 |
| OV001D | 351 | 802.7 | 949.6 | 1143 | 2106 | 1019 | 347.2 |
| OV183A | 448 | 630.1 | 801.9 | 1127 | 2131 | 929.0 | 431.8 |
| OV183B | 498 | 437.2 | 537.6 | 702.2 | 1577 | 611.0 | 244.1 |
| OV183C | 909 | 549.3 | 719.1 | 1018 | 2035 | 830.5 | 386.4 |
| OV183D | 597 | 684.4 | 915.7 | 1201 | 2103 | 981.6 | 406.9 |
| OV183E | 296 | 585.8 | 888.6 | 1293 | 2134 | 1006 | 496.9 |
| OV183F | 596 | 527.6 | 754.7 | 1080 | 2140 | 872.1 | 440.8 |
| OV183G | 420 | 728.5 | 945.0 | 1339 | 2103 | 1062 | 422.4 |
| OV183H | 551 | 574.7 | 703.5 | 903.6 | 2078 | 780.7 | 316.7 |
| OV183I | 770 | 597.4 | 694.8 | 829.1 | 2055 | 730.9 | 216.8 |
| OV183J | 761 | 508.0 | 606.4 | 833.4 | 1974 | 699.5 | 282.5 |
| OV183K | 458 | 488.2 | 614.8 | 815.0 | 2118 | 686.9 | 266.9 |
| OV183N | 447 | 787.5 | 918.0 | 1091 | 1701 | 957.2 | 261.4 |
| OV299A | 487 | 582.0 | 685.0 | 845.4 | 2089 | 746.8 | 258.0 |
| OV299B | 439 | 550.2 | 613.6 | 677.5 | 906.1 | 618.1 | 119.7 |
| OV299C | 591 | 600.5 | 774.0 | 911.9 | 1708 | 792.9 | 283.5 |
| OV299D | 249 | 475.0 | 668.3 | 805.3 | 1932 | 702.3 | 310.9 |
| OV299E | 354 | 542.7 | 669.2 | 807.7 | 2006 | 741.7 | 311.3 |

[A]Number of nuclei analyzed (n)
[B]Standard deviation (SD)

**Table S5-30. KS-test Comparing the Cumulative NA Distribution Frequencies in OV183[A].**

| | *vs.* Sample | | | | | | | | | | |
|---|---|---|---|---|---|---|---|---|---|---|---|
| Sample | B | C | D | E | F | G | H | I | J | K | N |
| OV183A | **** | **** | **** | ** | **** | **** | **** | **** | **** | **** | **** |
| OV183B | N/A[B] | **** | **** | **** | **** | **** | **** | **** | **** | **** | **** |
| OV183C | | N/A | **** | **** | ns | **** | ** | **** | **** | **** | **** |
| OV183D | | | N/A | ** | **** | ** | **** | **** | **** | **** | **** |
| OV183E | | | | N/A | *** | **** | **** | **** | **** | **** | **** |
| OV183F | | | | | N/A | **** | **** | **** | **** | **** | **** |
| OV183G | | | | | | N/A | **** | **** | **** | **** | **** |
| OV183H | | | | | | | N/A | ** | **** | **** | **** |
| OV183I | | | | | | | | N/A | **** | **** | **** |
| OV183J | | | | | | | | | N/A | ns | **** |
| OV183K | | | | | | | | | | N/A | **** |

[A]Presented are the *p*-values calculated from two-sample KS-test for the indicated pairs with *p*-values < 0.05 considered statistically significant (ns, *p*-value > 0.05; **, *p*-value < 0.01; ****, *p*-value < 0.0001).
[B]Not applicable (N/A)

**Table S5-31. KS-test Comparing the Cumulative NA Distribution Frequencies in OV001[A].**

| | *vs.* Sample | |
|---|---|---|
| Sample | B | D |
| A | **** | **** |
| B | N/A[B] | **** |

[A]Presented are the *p*-values calculated from two-sample KS-test for the indicated pairs with *p*-values < 0.05 considered statistically significant (****, *p*-value < 0.0001).
[B]Not applicable (N/A)

**Table S5-32. KS-test Comparing the Cumulative NA Distribution Frequencies in OV299[A].**

| | *vs.* Sample | | | |
|---|---|---|---|---|
| Sample | B | C | D | E |
| A | **** | **** | **** | ns |
| B | N/A[B] | **** | **** | **** |
| C | | N/A | **** | **** |
| D | | | N/A | ns |

[A]Presented are the *p*-values calculated from two-sample KS-test for the indicated pairs with *p*-values < 0.05 considered statistically significant (ns, *p*-value > 0.05; ****, *p*-value < 0.0001)
[B]Not applicable (N/A)

**Table S5-33. *CS* Descriptive Statistics for Serial Primary HGSOC Patient Samples – Patient Profile Group 4.**

| | | Median | | | | Total $CS_c$ |
|---|---|---|---|---|---|---|
| Patient ID | n[A] | $CS_8$ | $CS_{11}$ | $CS_{17}$ | $CS_c$ | Range |
| OV001A | 225 | 0 | 0 | 0 | 1 | 6 |
| OV001B | 269 | 0 | 0 | 0 | 3 | 17 |
| OV001D | 351 | 0 | 0 | 0 | 2 | 16 |
| OV183A | 448 | 0 | 0 | 0 | 1 | 13 |
| OV183B | 498 | 0 | 0 | 0 | 1 | 17 |
| OV183C | 909 | 0 | 0 | 0 | 2 | 24 |
| OV183D | 597 | 1 | 0 | 0 | 3 | 31 |
| OV183E | 296 | -1 | 0 | 0 | 3 | 21 |
| OV183F | 596 | 0 | 0 | -0.5 | 3 | 20 |
| OV183G | 420 | 0 | 0 | 0 | 1 | 14 |
| OV183H | 551 | 0 | 0 | 0 | 1 | 25 |
| OV183I | 770 | 0 | 0 | 0 | 1 | 12 |
| OV183J | 761 | 0 | 0 | 0 | 1 | 19 |
| OV183K | 458 | 0 | 0 | 0 | 1 | 11 |
| OV183N | 447 | 0 | 0 | 1 | 2 | 17 |
| OV299A | 487 | 0 | 0 | 0 | 1 | 9 |
| OV299B | 439 | 0 | 0 | -1 | 2 | 7 |
| OV299C | 591 | 0 | 0 | 0 | 1 | 28 |
| OV299D | 249 | 0 | 0 | 0 | 1 | 12 |
| OV299E | 354 | 0 | 0 | 0 | 1 | 10 |

[A]Number of nuclei analyzed (n)

**Table S5-34. MW-test Comparing the *CS* Ranked Values in OV183[A].**

| | *vs.* Sample | | | | | | | | | | |
|---|---|---|---|---|---|---|---|---|---|---|---|
| Sample | B | C | D | E | F | G | H | I | J | K | N |
| OV183A | ** | **** | **** | **** | **** | ** | ns | **** | **** | ** | **** |
| OV183B | N/A[B] | **** | **** | **** | **** | **** | * | ns | ns | ns | **** |
| OV183C | | N/A | ** | **** | ns | **** | ** | **** | **** | **** | ns |
| OV183D | | | N/A | ns | ns | ** | **** | **** | **** | **** | *** |
| OV183E | | | | N/A | ns | **** | **** | **** | **** | **** | **** |
| OV183F | | | | | N/A | **** | **** | **** | **** | **** | **** |
| OV183G | | | | | | N/A | **** | **** | **** | **** | **** |
| OV183H | | | | | | | N/A | ** | **** | * | **** |
| OV183I | | | | | | | | N/A | ns | ns | **** |
| OV183J | | | | | | | | | N/A | ns | **** |
| OV183K | | | | | | | | | | N/A | **** |

[A]Presented are the *p*-values calculated from two-sample MW-test for the indicated pairs with *p*-values < 0.05 considered statistically significant (ns, *p*-value > 0.05; *, *p*-value < 0.05; **, *p*-value < 0.01; ***, *p*-value < 0.001; ****, *p*-value < 0.0001)
[B]Not applicable (N/A)

**Table S5-35. MW-test Comparing the *CS* Ranked Values in OV001[A].**

| | *vs.* Sample | |
|---|---|---|
| Sample | B | D |
| A | **** | **** |
| B | N/A[B] | **** |

[A]Presented are the *p*-values calculated from two-sample MW-test for the indicated pairs with *p*-values < 0.05 considered statistically significant (****, *p*-value < 0.000)
[B]Not applicable (N/A)

**Table S5-36. MW-test Comparing the *CS* Ranked Values in OV299[A].**

| | *vs.* Sample | | | |
|---|---|---|---|---|
| Sample | B | C | D | E |
| A | **** | ** | ns | ns |
| B | N/A[B] | *** | **** | **** |
| C | | N/A | * | ns |
| D | | | N/A | ns |

[A]Presented are the *p*-values calculated from two-sample MW-test for the indicated pairs with *p*-values < 0.05 considered statistically significant. $p > 0.05$ = ns, $p < 0.05$ = *, $p < 0.01$ = **, $p < 0.001$ = ***, and $p < 0.0001$ = ****

[B]Not applicable (N/A)

**Table S5-37. NA Descriptive Statistics for Serial Primary HGSOC Patient Samples – Patient Profile Group 5.**

| | | Nuclear Area (μm$^2$) | | | | | |
|---|---|---|---|---|---|---|---|
| Patient ID | n[A] | 25$^{th}$ Percentile | Median | 75$^{th}$ Percentile | Total Range | Mean | SD[B] |
| OV063A | 443 | 39.0 | 444.9 | 555.4 | 2037 | 547.9 | 314.7 |
| OV063D | 538 | 453.8 | 525.2 | 610.5 | 1409 | 556.1 | 159.0 |
| OV063E | 331 | 455.8 | 518.8 | 622.4 | 1119 | 554.8 | 155.9 |
| OV063F | 413 | 441.6 | 539.1 | 595.3 | 1136 | 539.1 | 141.4 |
| OV069A | 255 | 373.1 | 408.3 | 490.9 | 496.4 | 446.6 | 100.3 |
| OV073C | 296 | 381.6 | 435.0 | 510.0 | 761.7 | 470.7 | 126.5 |
| OV109A | 588 | 572.1 | 748.4 | 966.5 | 1759 | 802.6 | 325.2 |
| OV173A | 230 | 390.1 | 431.2 | 505.6 | 505.6 | 465.9 | 112.8 |
| OV173B | 287 | 268.3 | 306.2 | 383.6 | 383.6 | 323.2 | 135.8 |
| OV173C | 378 | 472.0 | 610.0 | 763.2 | 763.2 | 650.0 | 237.3 |
| OV173D | 202 | 397.3 | 450.8 | 535.7 | 535.7 | 485.7 | 129.2 |
| OV177A | 383 | 178.3 | 206.4 | 253.0 | 574.9 | 230.6 | 81.26 |
| OV180A | 391 | 575.4 | 742.2 | 887.0 | 1862 | 774.5 | 287.7 |
| OV180B | 542 | 830.5 | 975.3 | 1163 | 1926 | 1026 | 321.6 |
| OV180C | 326 | 811.3 | 919.1 | 1071 | 1467 | 974.1 | 247.5 |
| OV180D | 253 | 435.5 | 519.8 | 664.0 | 1168 | 576.2 | 197.5 |
| OV180E | 434 | 504.4 | 599.0 | 747.2 | 1291 | 660.0 | 233.5 |
| OV189A | 400 | 386.2 | 418.1 | 468.4 | 539.6 | 438.8 | 80.84 |
| OV246A | 1023 | 297.5 | 370.5 | 500.3 | 1909 | 424.4 | 212.1 |

[A]Number of nuclei analyzed (n)

[B]Standard deviation (SD)

**Table S5-38. *CS* Descriptive Statistics for Serial Primary HGSOC Patient Samples – Patient Profile Group 5.**

| | | Median | | | | Total $CS_c$ |
|---|---|---|---|---|---|---|
| Patient ID | n[A] | $CS_8$ | $CS_{11}$ | $CS_{17}$ | $CS_c$ | Range |
| OV063A | 443 | 0 | 0 | 0 | 0 | 22 |
| OV063D | 538 | 0 | 0 | 0 | 1 | 19 |
| OV063E | 331 | 0 | 0 | 0 | 1 | 15 |
| OV063F | 413 | 0 | 0 | 0 | 1 | 16 |
| OV069A | 255 | 0 | 0 | 0 | 1 | 12 |
| OV073C | 296 | 0 | 0 | 1 | 2 | 11 |
| OV109A | 588 | 0 | 0 | 0 | 1 | 20 |
| OV173A | 230 | 0 | 0 | 0 | 1 | 17 |
| OV173B | 287 | 0 | 0 | 0 | 1 | 13 |
| OV173C | 378 | 0 | 0 | 0 | 1 | 8 |
| OV173D | 202 | 0 | 0 | 0 | 1 | 6 |
| OV177A | 383 | 0 | 0 | 0 | 2 | 9 |
| OV180A | 391 | 0 | 0 | 0 | 2 | 21 |
| OV180B | 542 | 0 | 0 | 0 | 1 | 6 |
| OV180C | 326 | 0 | 0 | 0 | 1 | 9 |
| OV180D | 253 | 0 | 0 | 0 | 1 | 14 |
| OV180E | 434 | 0 | 0 | 0 | 1 | 12 |
| OV189A | 400 | 0 | 0 | 0 | 1 | 23 |
| OV246A | 1023 | 0 | 0 | 0 | 2 | 19 |

[A]Number of nuclei analyzed (n)

### 5.2.2 Supporting Figures

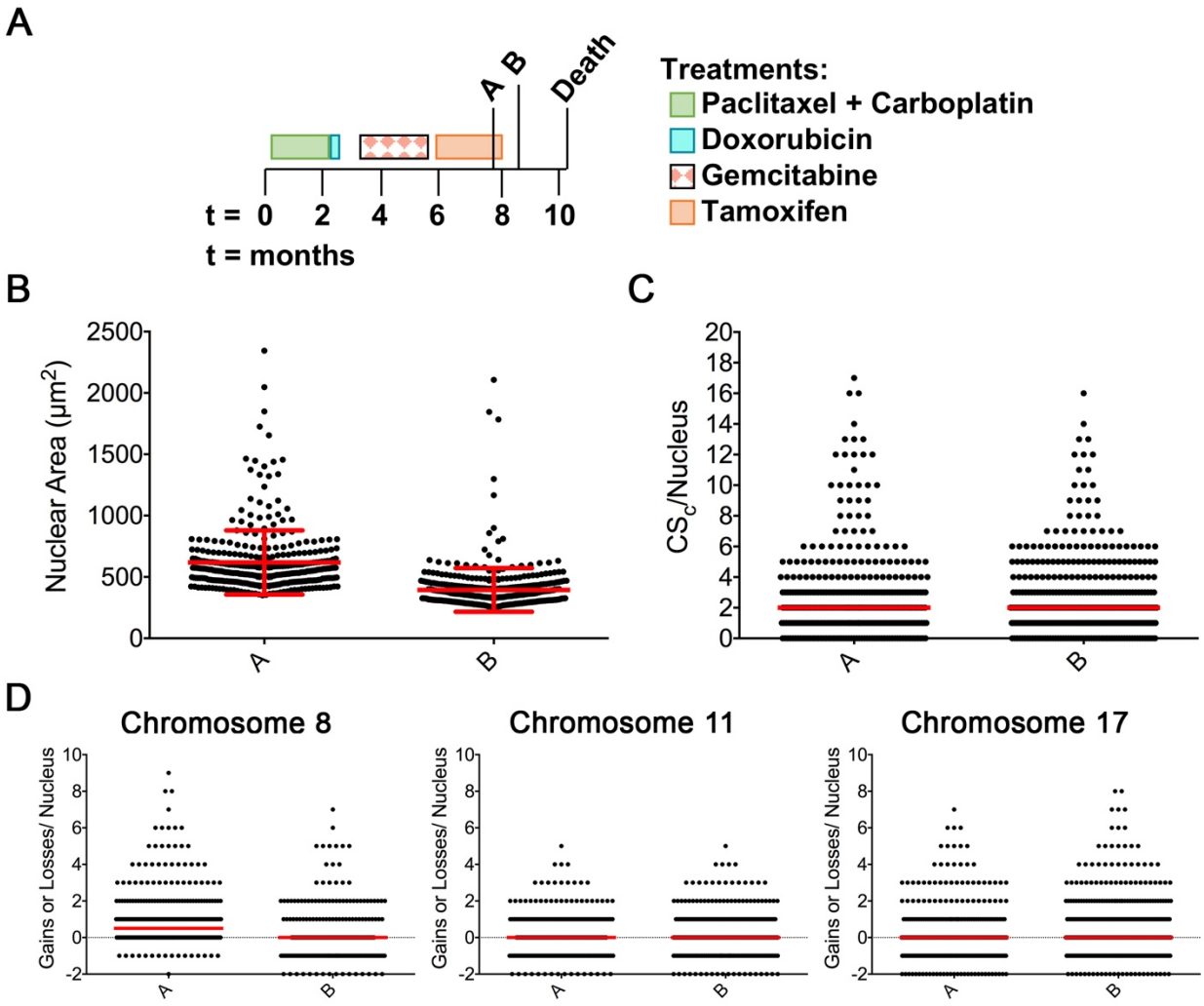


**Figure S5-1. OV125 Exhibits NA and *CS* Heterogeneity and is Not Responsive to Multiple Chemotherapy Treatments.**

***(A)*** Timeline indicating the collection times for two samples. ***(B)*** Dot plot presenting the NAs determined from two serial samples. Red bars indicate the mean ± SD (N = 2; n >200). ***(C)*** Dot plot presenting the $CS_c$ values for each nucleus evaluated. Red bars indicate the median $CS_c$. ***(D)*** Dot plot presenting the individual *CS* values (chromosome 8 [left], 11 [middle], and 17 [right]) for each nucleus evaluated. Red bars indicate the individual *CS* values.

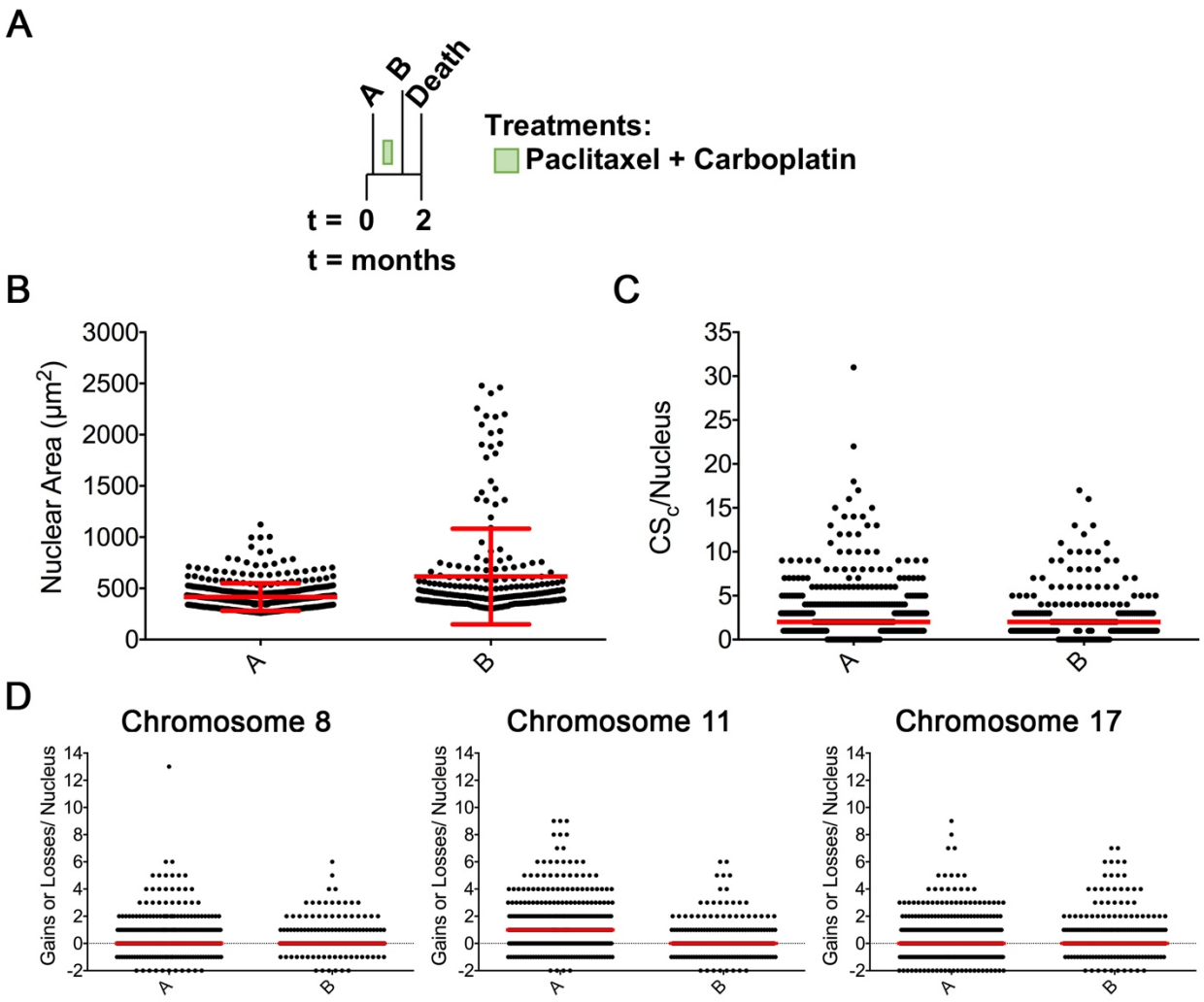


**Figure S5-2. OV203 Exhibits NA and *CS* Heterogeneity.**
***(A)*** Timeline indicating the collection times for two samples. ***(B)*** Dot plot presenting the NAs determined from two serial samples. Red bars indicate the mean ± SD (N = 2; n >200). ***(C)*** Dot plot presenting the $CS_c$ values for each nucleus evaluated. Red bars indicate the median $CS_c$. ***(D)*** Dot plot presenting the individual *CS* values (chromosome 8 [left], 11 [middle], and 17 [right]) for each nucleus evaluated. Red bars indicate the individual *CS* values.

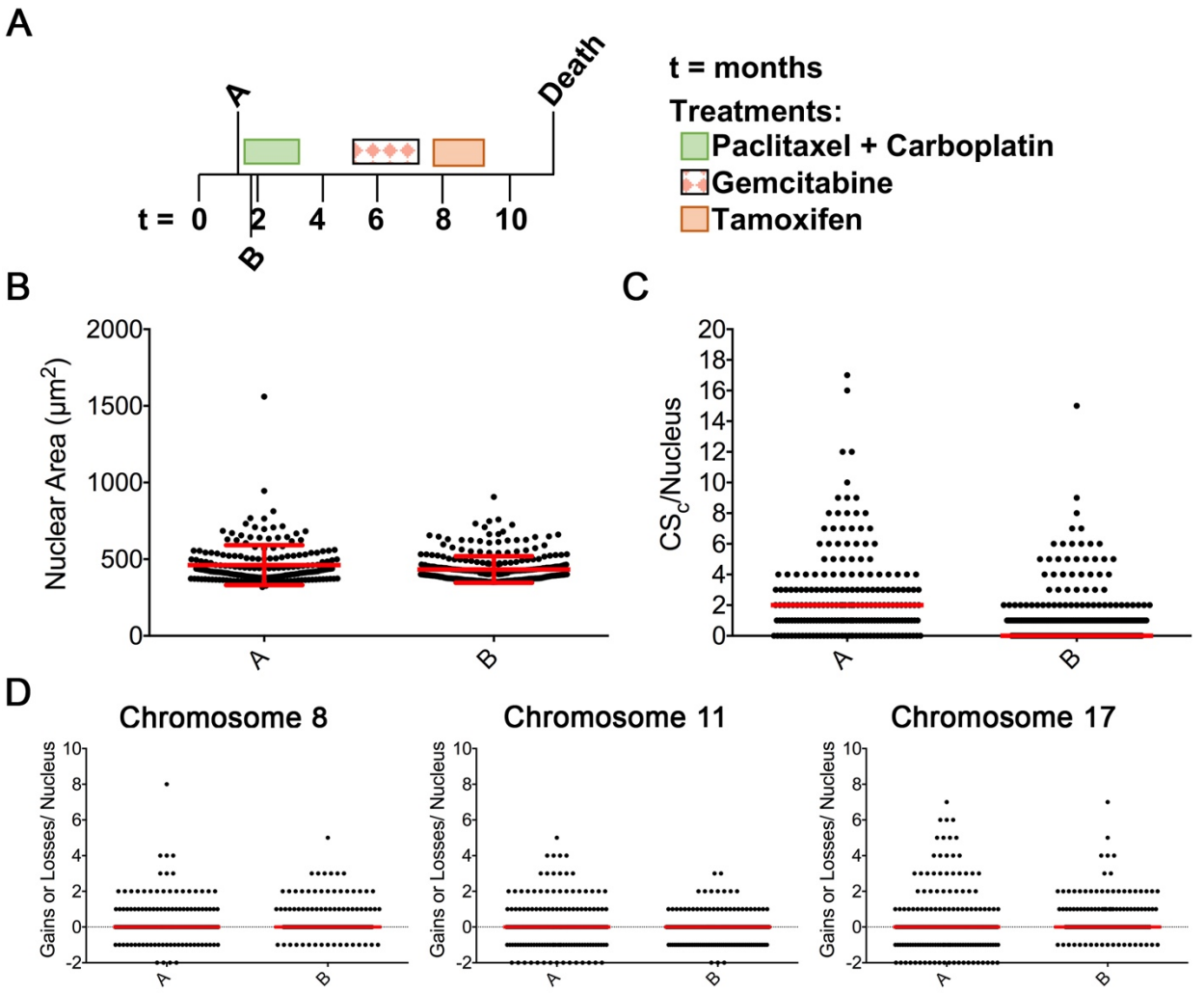


**Figure S5-3. CIN is Prevalent and Decreases During Treatment in OV009.**
***(A)*** Timeline indicating the collection times for two samples. ***(B)*** Dot plot presenting the NAs determined from two serial samples. Red bars indicate the mean ± SD (N = 2; n >200). ***(C)*** Dot plot presenting the $CS_c$ values for each nucleus evaluated. Red bars indicate the median $CS_c$. ***(D)*** Dot plot presenting the individual *CS* values (chromosome 8 [left], 11 [middle], and 17 [right]) for each nucleus evaluated. Red bars indicate the individual *CS* values.

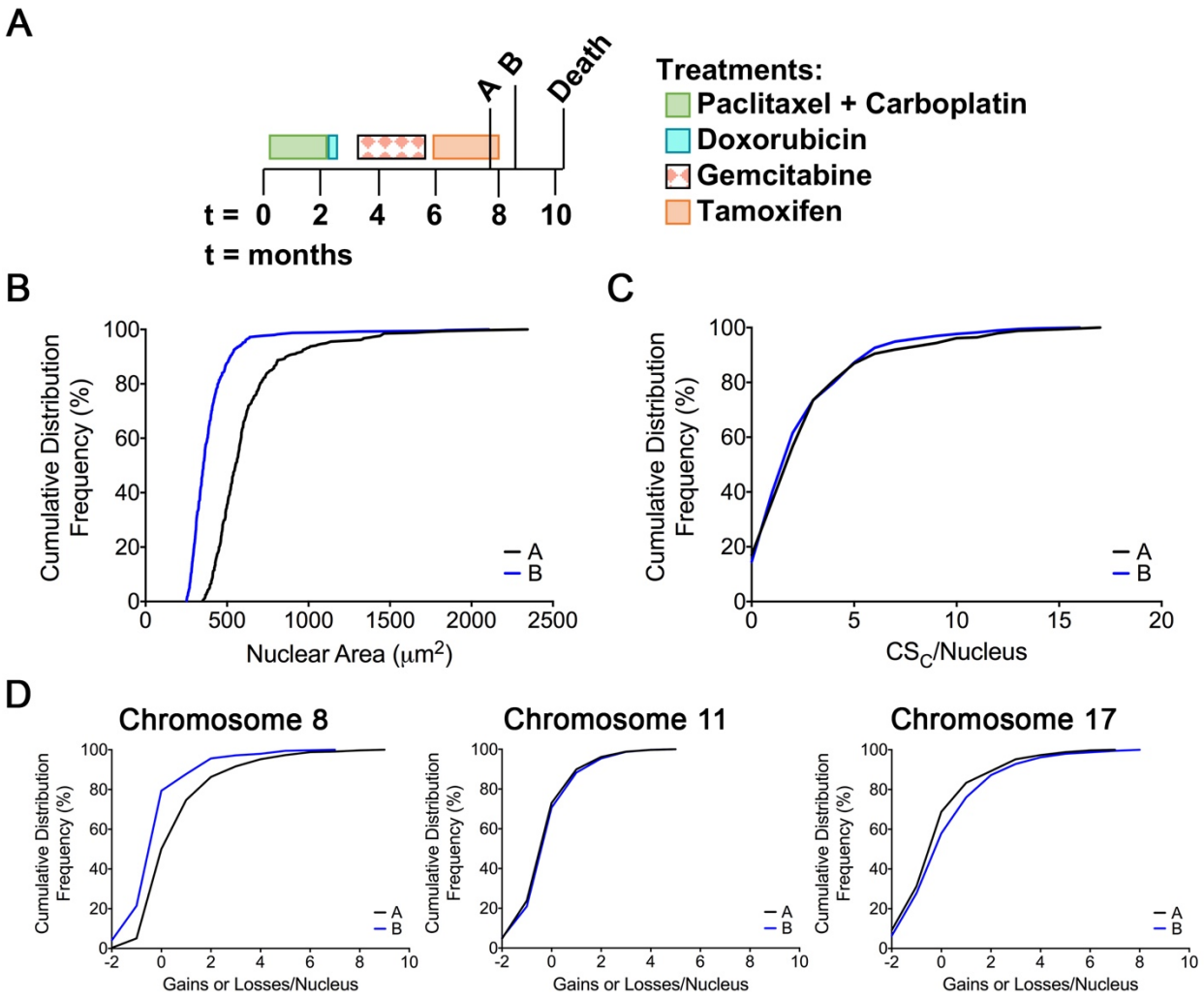


**Figure S5-4. Cumulative Distribution Frequencies for Patient OV125.**
***(A)*** Timeline indicating the collection times for two samples. ***(B)*** Cumulative NA distribution frequencies of two serial samples (N = 2; n >200). ***(C)*** Cumulative $CS_c$ distribution frequencies for each of the two serial samples evaluated. ***(D)*** Cumulative distribution frequencies for each individual *CS* value (*i.e.* $CS_8$ [left], $CS_{11}$ [middle], and $CS_{17}$ [right]) for the two samples.

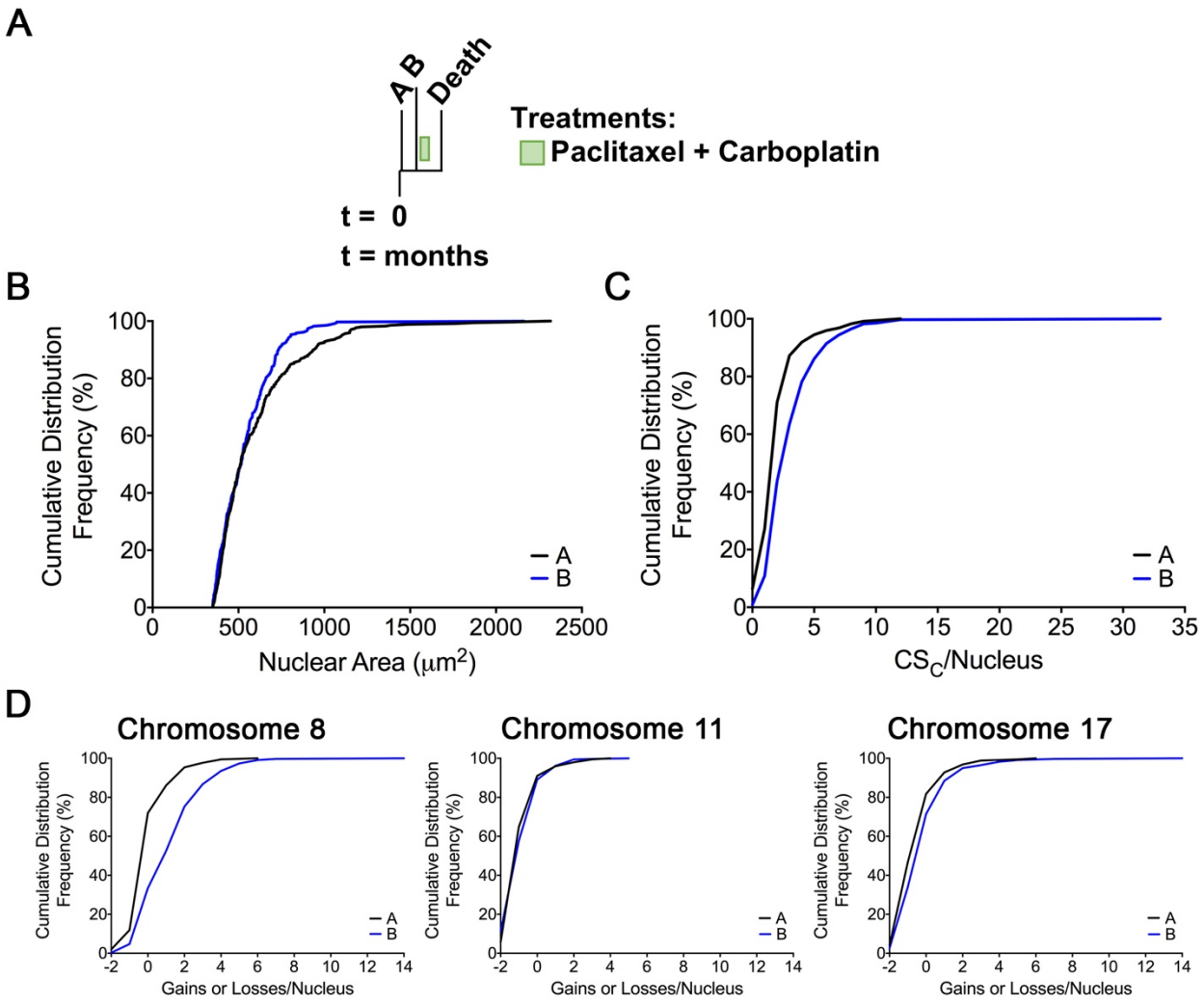


**Figure S5-5. Cumulative Distribution Frequencies for Patient OV203.**
***(A)*** Timeline indicating the collection times for two samples. ***(B)*** Cumulative NA distribution frequencies of two serial samples (N = 2; n >200). ***(C)*** Cumulative $CS_c$ distribution frequencies for each of the two serial samples evaluated. ***(D)*** Cumulative distribution frequencies for each individual *CS* value (*i.e.* $CS_8$ [left], $CS_{11}$ [middle], and $CS_{17}$ [right]) for the two samples.

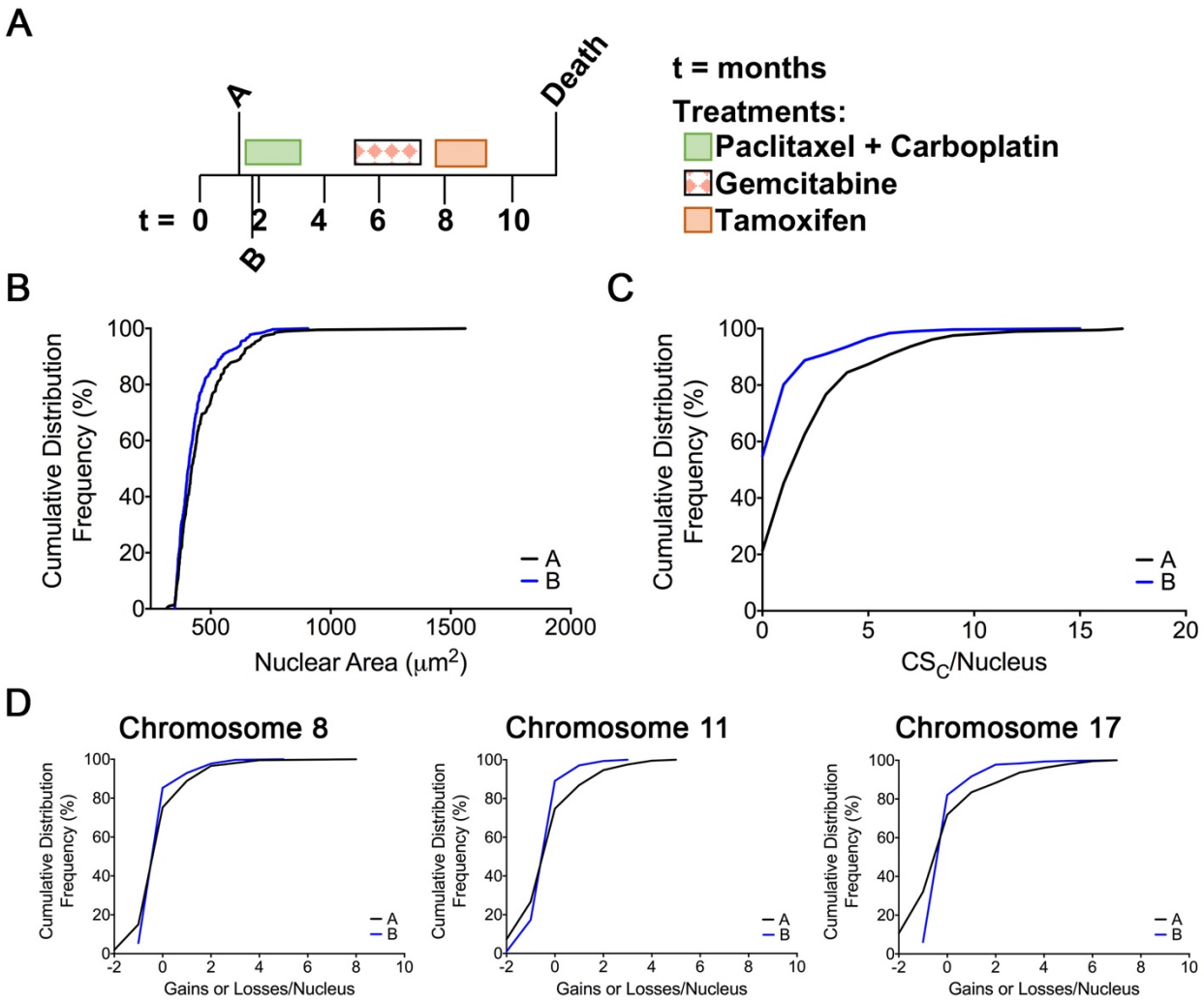


**Figure S5-6. Cumulative Distribution Frequencies for Patient OV009.**
***(A)*** Timeline indicating the collection times for two samples. ***(B)*** Cumulative NA distribution frequencies of two serial samples (N = 2; n >200). ***(C)*** Cumulative $CS_c$ distribution frequencies for each of the two serial samples evaluated. ***(D)*** Cumulative distribution frequencies for each individual *CS* value (*i.e.* $CS_8$ [left], $CS_{11}$ [middle], and $CS_{17}$ [right]) for the two samples.

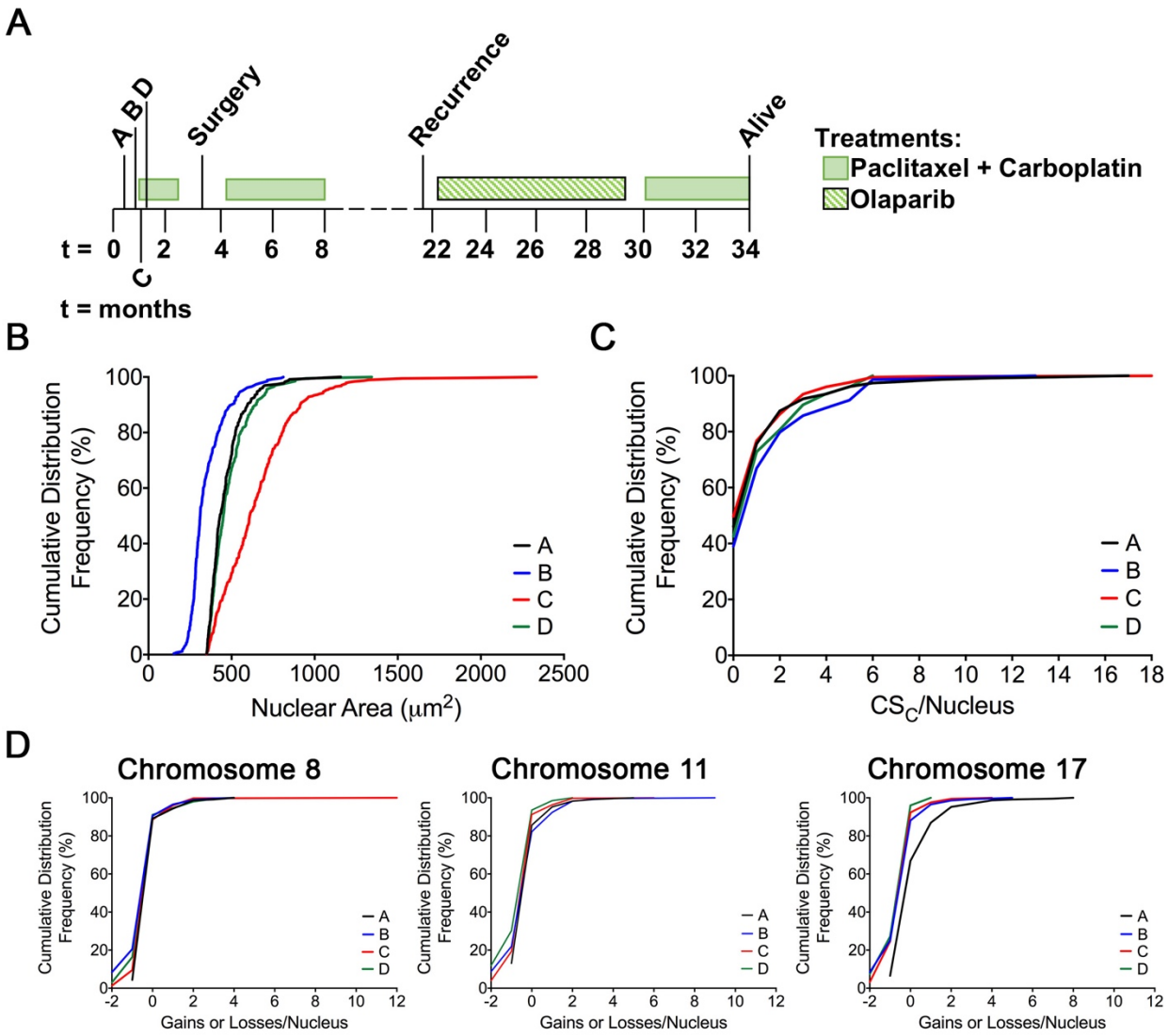


**Figure S5-7. Cumulative Distribution Frequencies for Patient OV173.**
***(A)*** Timeline indicating the collection times for four samples. Note this patient was alive as of their last known update (February 4, 2019). ***(B)*** Cumulative NA distribution frequencies of four serial samples (N = 2; n >200). ***(C)*** Cumulative $CS_c$ distribution frequencies for each of the four serial samples evaluated. ***(D)*** Cumulative distribution frequencies for each individual *CS* value (*i.e.* $CS_8$ [left], $CS_{11}$ [middle], and $CS_{17}$ [right]) for the four samples.

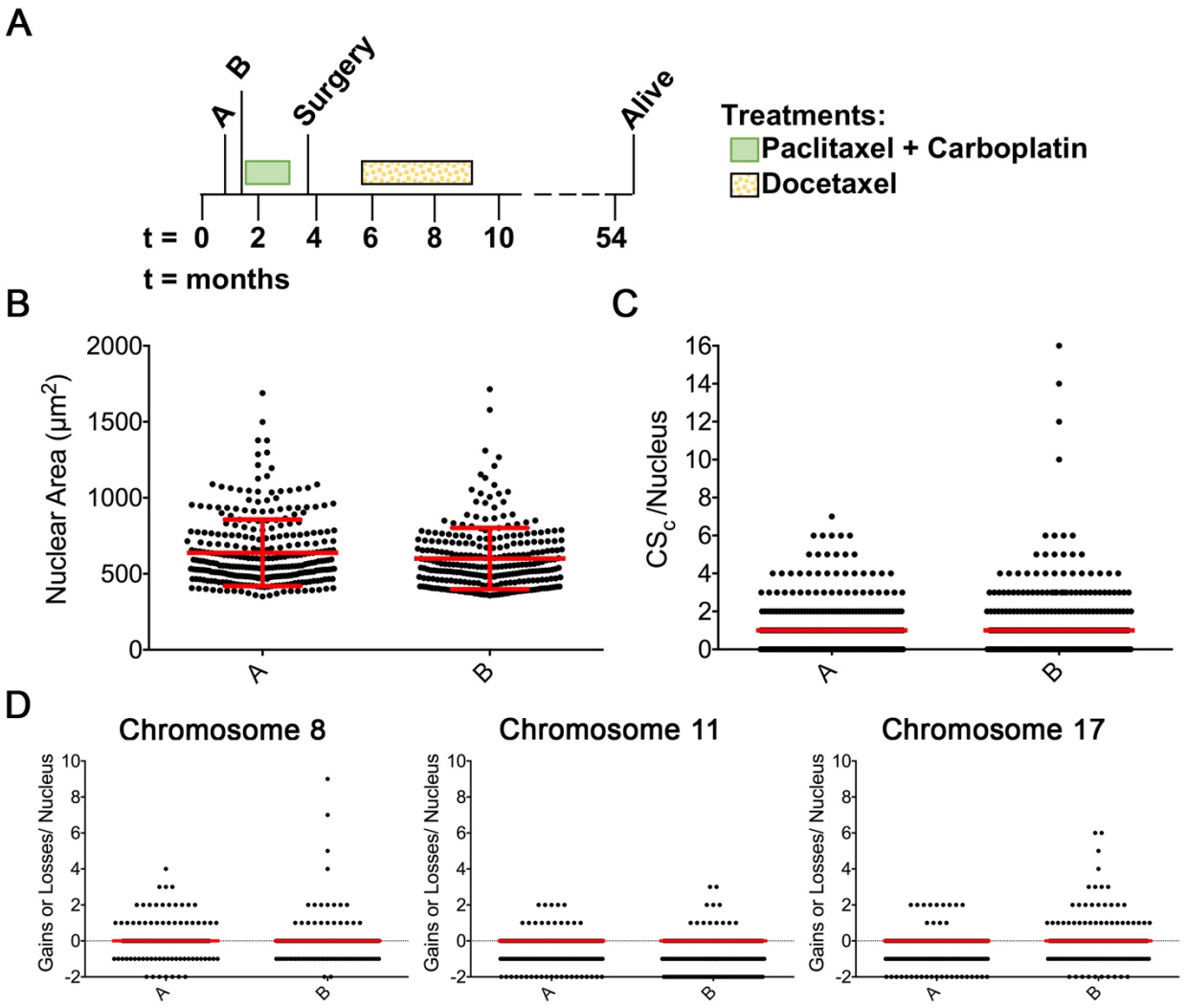


**Figure S5-8. OV061 Exhibits NA and *CS* Heterogeneity.**
***(A)*** Timeline indicating the collection times for two samples. Note this patient was alive as of their last known update (August 13, 2018). ***(B)*** Dot plot presenting the NAs determined from two serial samples. Red bars indicate the mean ± SD (N = 2; n >200). ***(C)*** Dot plot presenting the $CS_c$ values for each nucleus evaluated. Red bars indicate the median $CS_c$. ***(D)*** Dot plot presenting the individual *CS* values (chromosome 8 [left], 11 [middle], and 17 [right]) for each nucleus evaluated. Red bars indicate the individual *CS* values.

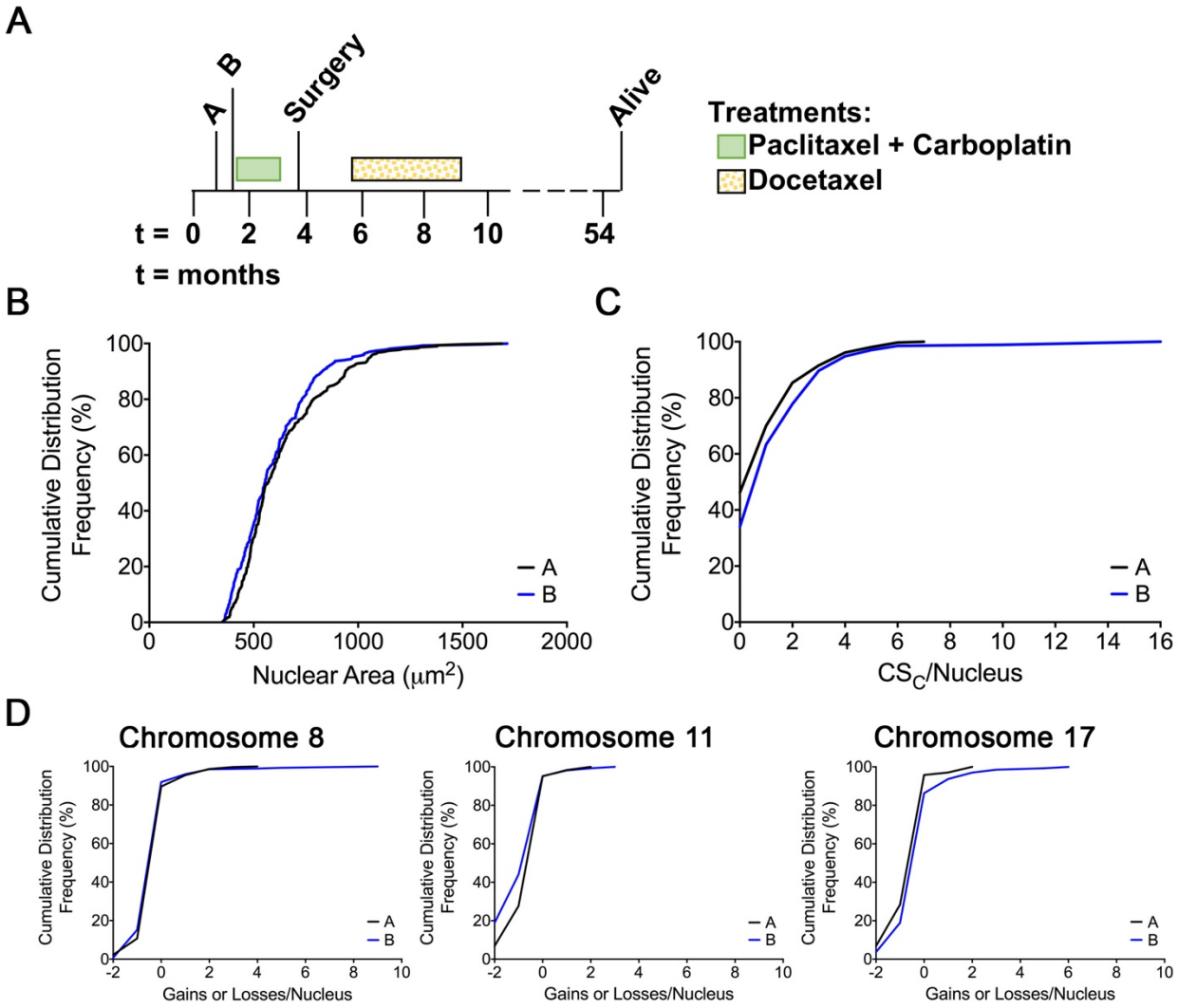


**Figure S5-9. Cumulative Distribution Frequencies for Patient OV061.**
***(A)*** Timeline indicating the collection times for two samples. Note this patient was alive as of their last known update (August 13, 2018). ***(B)*** Cumulative NA distribution frequencies of two serial samples (N = 2; n >200). ***(C)*** Cumulative $CS_c$ distribution frequencies for each of the two serial samples evaluated. ***(D)*** Cumulative distribution frequencies for each individual *CS* value (*i.e.* $CS_8$ [left], $CS_{11}$ [middle], and $CS_{17}$ [right]) for the two samples.

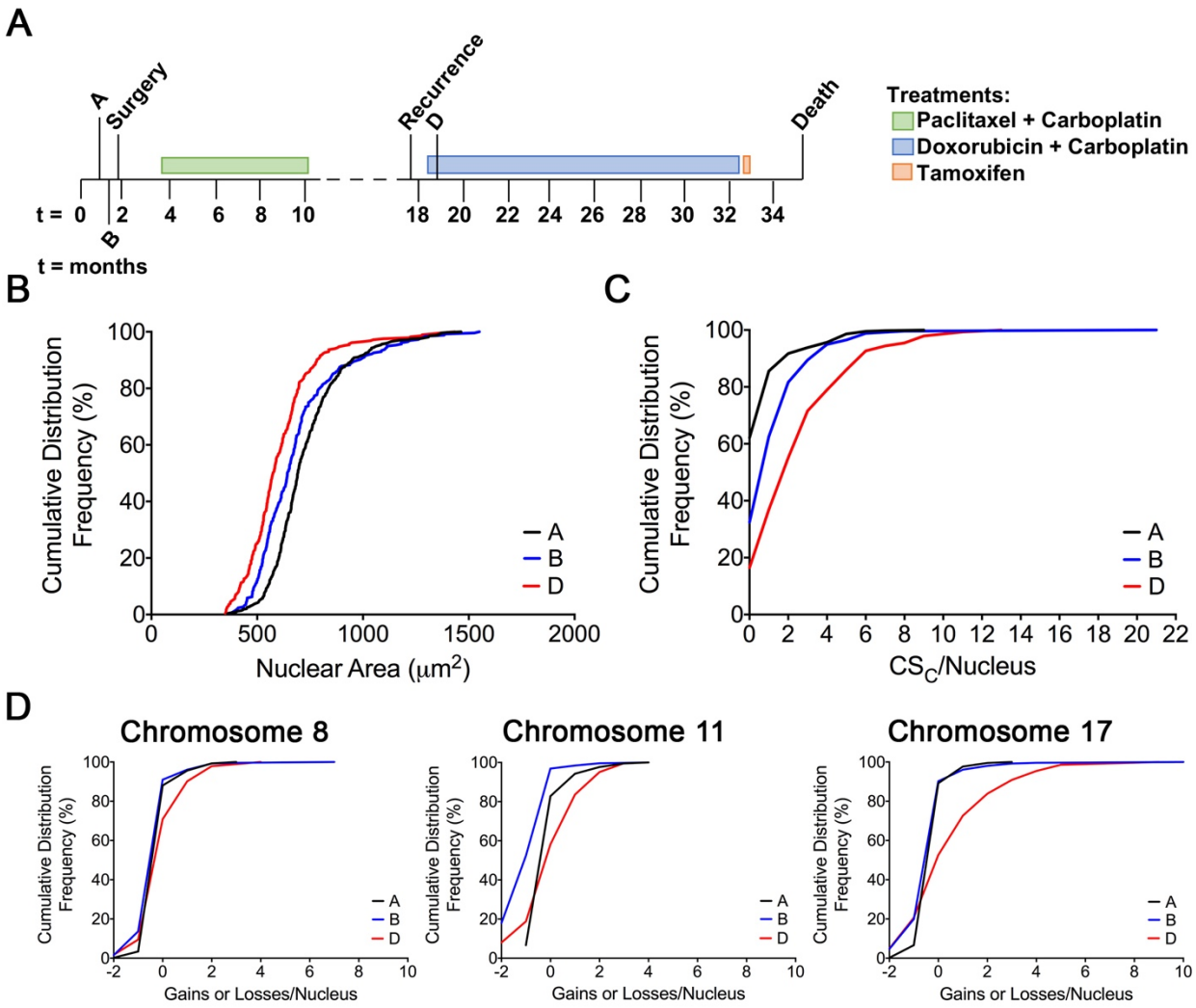


**Figure S5-10. Cumulative Distribution Frequencies for Patient OV070.**
***(A)*** Timeline indicating the collection times for three samples. ***(B)*** Cumulative NA distribution frequencies of three serial samples (N = 2; n >200). ***(C)*** Cumulative $CS_c$ distribution frequencies for each of the three serial samples evaluated. ***(D)*** Cumulative distribution frequencies for each individual *CS* value (*i.e.* $CS_8$ [left], $CS_{11}$ [middle], and $CS_{17}$ [right]) for the three samples.

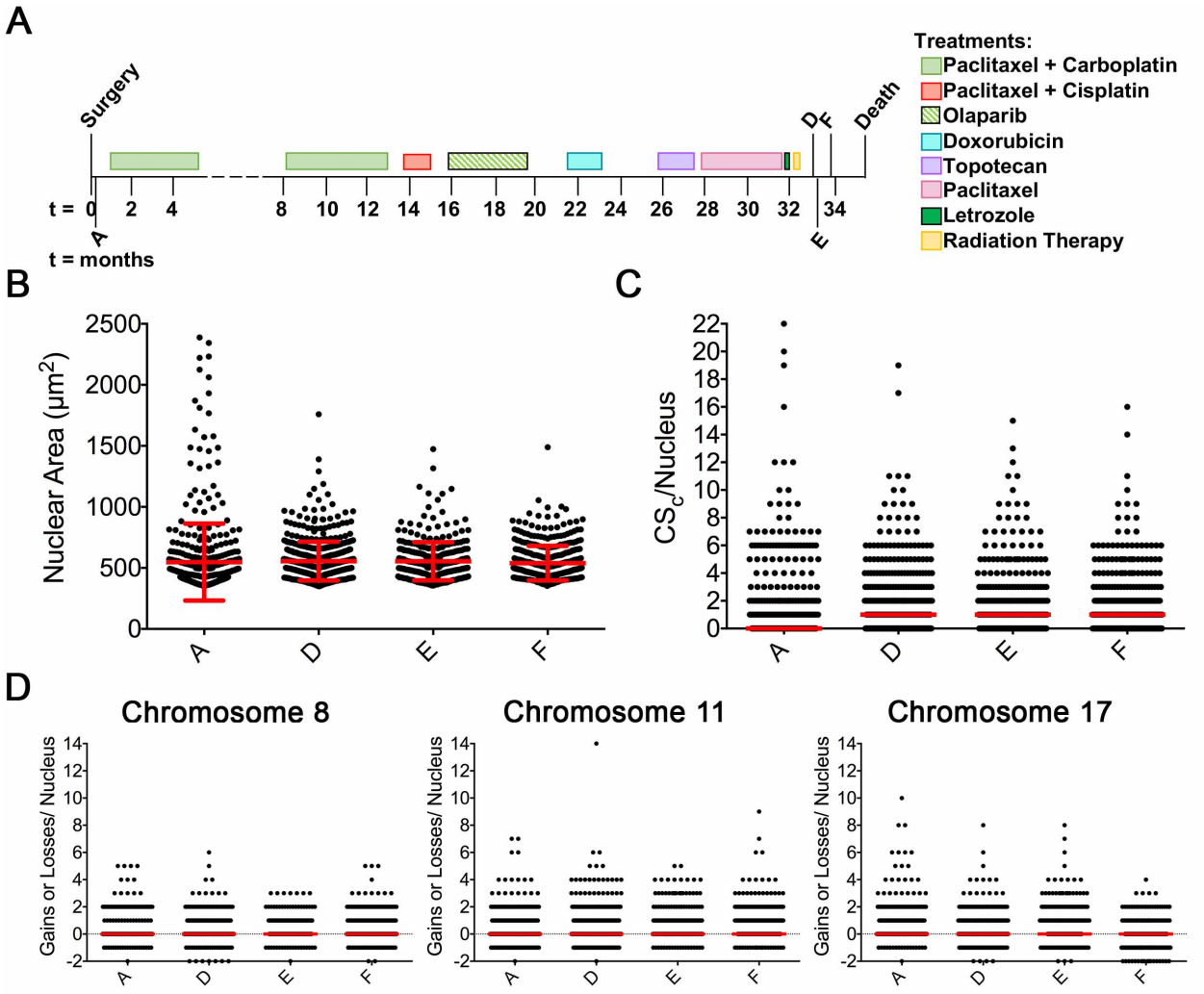


**Figure S5-11. CIN Increases as Disease Progresses in OV063.**
***(A)*** Timeline indicating the collection times for four samples. ***(B)*** Dot plot presenting the NAs determined from four serial samples. Red bars indicate the mean ± SD (N = 2; n >200). ***(C)*** Dot plot presenting the $CS_c$ values for each nucleus evaluated. Red bars indicate the median $CS_c$. ***(D)*** Dot plot presenting the individual *CS* values (chromosome 8 [left], 11 [middle], and 17 [right]) for each nucleus evaluated. Red bars indicate the individual *CS* values.

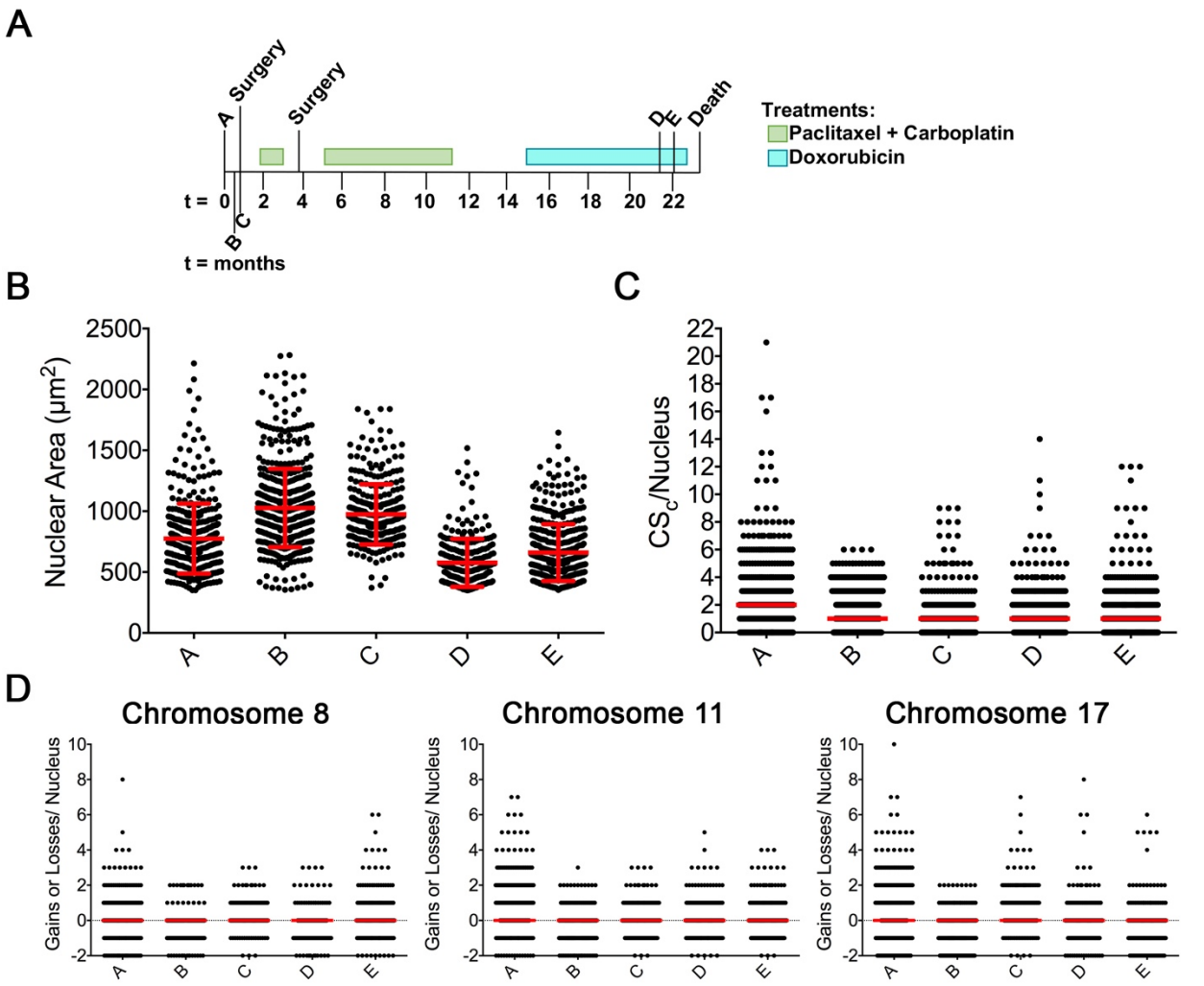


**Figure S5-12. CIN is Maintained Following First and Second Line Chemotherapy in OV180.** ***(A)*** Timeline indicating the collection times for five samples. ***(B)*** Dot plot presenting the NAs determined from five serial samples. Red bars indicate the mean ± SD (N = 2; n >200). ***(C)*** Dot plot presenting the $CS_c$ values for each nucleus evaluated. Red bars indicate the median $CS_c$. ***(D)*** Dot plot presenting the individual *CS* values (chromosome 8 [left], 11 [middle], and 17 [right]) for each nucleus evaluated. Red bars indicate the individual *CS* values.

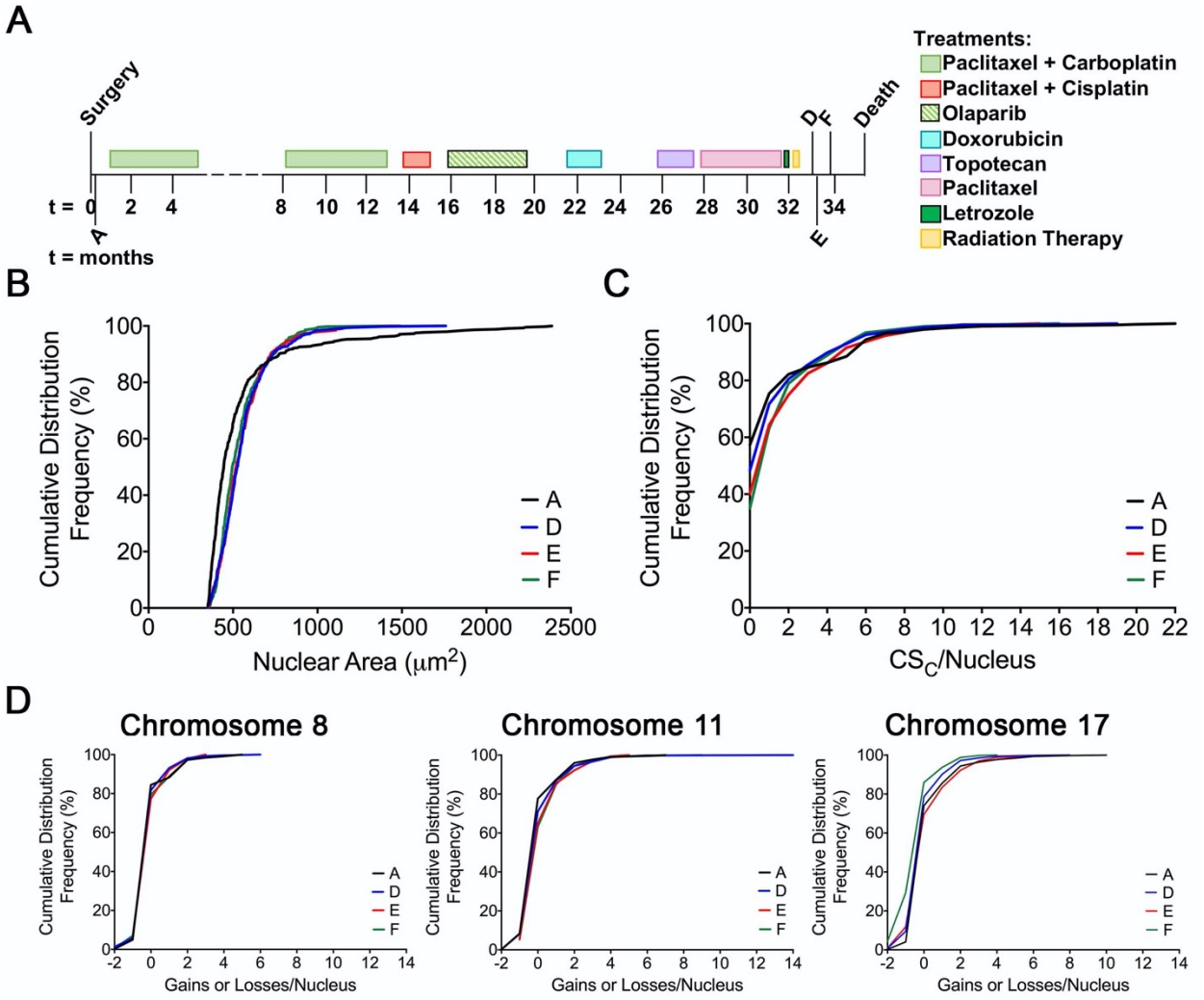


**Figure S5-13. Cumulative Distribution Frequencies for Patient OV063.**
***(A)*** Timeline indicating the collection times for four samples. ***(B)*** Cumulative NA distribution frequencies of four serial samples (N = 2; n >200). ***(C)*** Cumulative $CS_c$ distribution frequencies for each of the four serial samples evaluated. ***(D)*** Cumulative distribution frequencies for each individual *CS* value (*i.e.* $CS_8$ [left], $CS_{11}$ [middle], and $CS_{17}$ [right]) for the four samples.

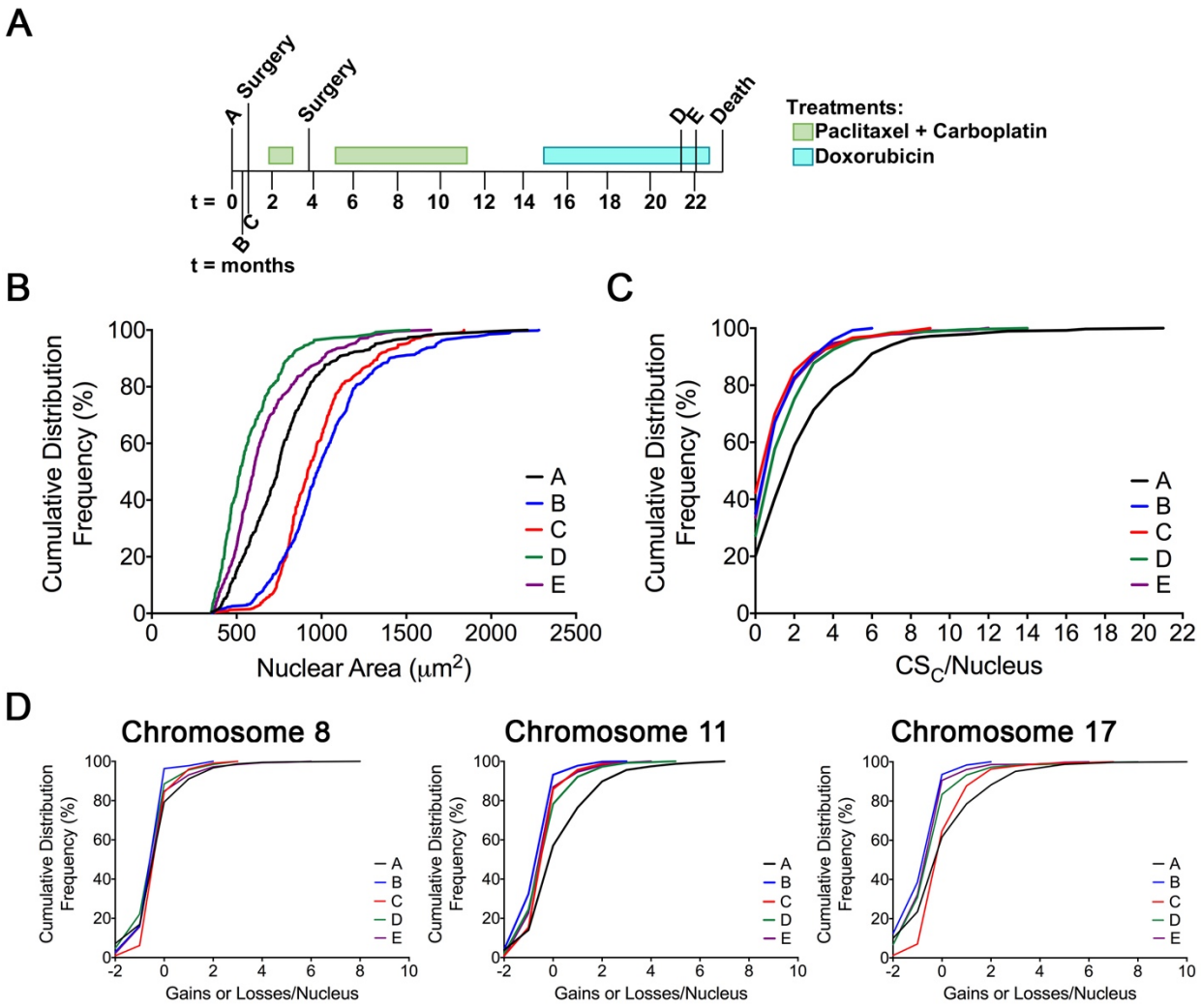


**Figure S5-14. Cumulative Distribution Frequencies for Patient OV180.**
***(A)*** Timeline indicating the collection times for five samples. ***(B)*** Cumulative NA distribution frequencies of five serial samples (N = 2; n >200). ***(C)*** Cumulative $CS_c$ distribution frequencies for each of the five serial samples evaluated. ***(D)*** Cumulative distribution frequencies for each individual *CS* value (*i.e.* $CS_8$ [left], $CS_{11}$ [middle], and $CS_{17}$ [right]) for the five samples.

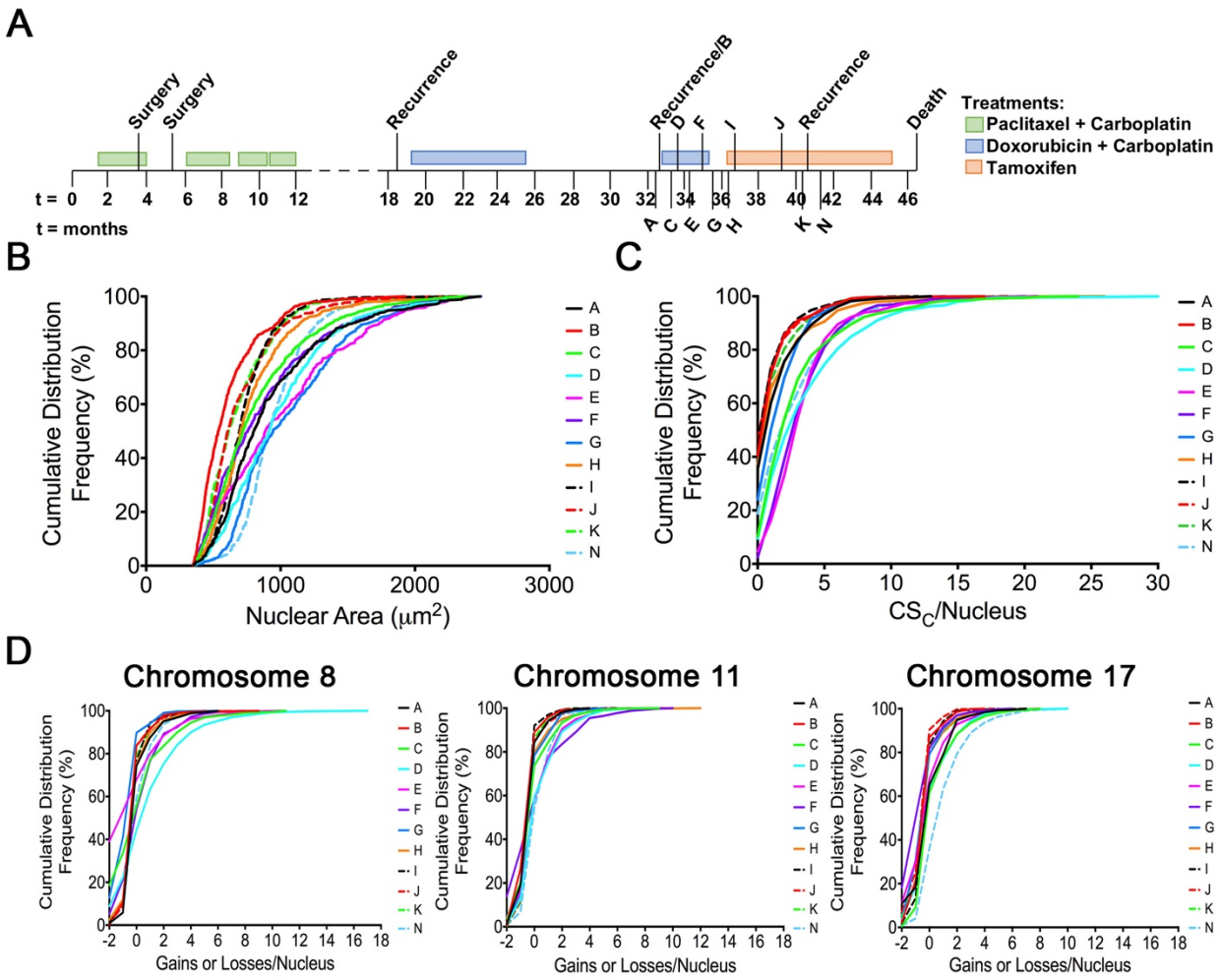


**Figure S5-15. Cumulative Distribution Frequencies for Patient OV183.**
***(A)*** Timeline indicating the collection times for 12 samples. ***(B)*** Cumulative NA distribution frequencies of 12 serial samples (N = 2; n >200). ***(C)*** Cumulative $CS_c$ distribution frequencies for each of the 12 serial samples evaluated. ***(D)*** Cumulative distribution frequencies for each individual *CS* value (*i.e.* $CS_8$ [left], $CS_{11}$ [middle], and $CS_{17}$ [right]) for all 12 samples.

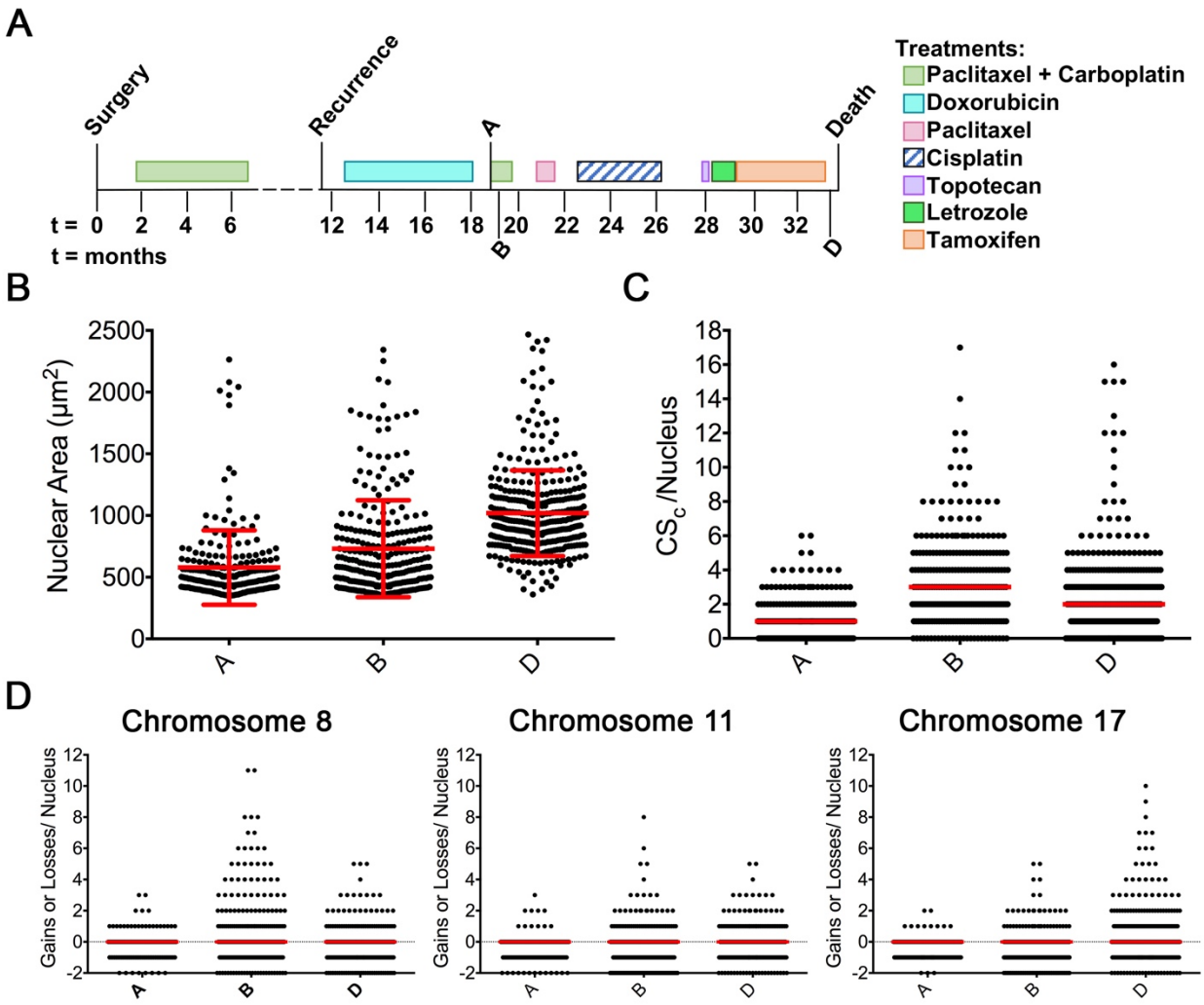


**Figure S5-16. CIN Increases as Disease Progresses in OV001.**
***(A)*** Timeline indicating the collection times for three samples. ***(B)*** Dot plot presenting the NAs determined from three serial samples. Red bars indicate the mean ± SD (N = 2; n >200). ***(C)*** Dot plot presenting the $CS_c$ values for each nucleus evaluated. Red bars indicate the median $CS_c$. ***(D)*** Dot plot presenting the individual *CS* values (chromosome 8 [left], 11 [middle], and 17 [right]) for each nucleus evaluated. Red bars indicate the individual *CS* values.

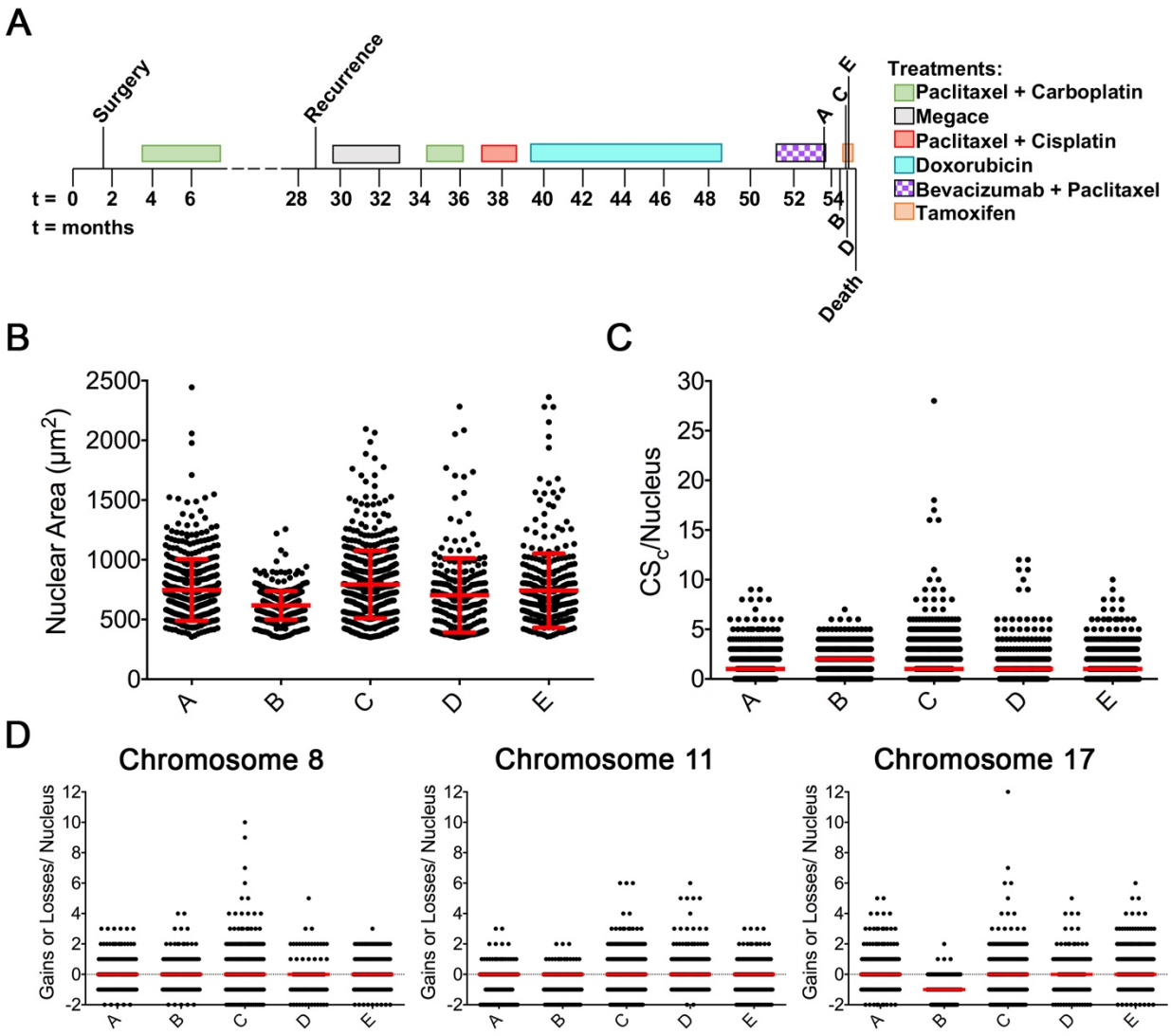


**Figure S5-17. CIN is Prevalent and Dynamic in OV299.**
***(A)*** Timeline indicating the collection times for five samples. ***(B)*** Dot plot presenting the NAs determined from five serial samples. Red bars indicate the mean ± SD (N = 2; n >200). ***(C*** Dot plot presenting the $CS_c$ values for each nucleus evaluated. Red bars indicate the median $CS_c$. ***(D)*** Dot plot presenting the individual *CS* values (chromosome 8 [left], 11 [middle], and 17 [right]) for each nucleus evaluated. Red bars indicate the individual *CS* values.

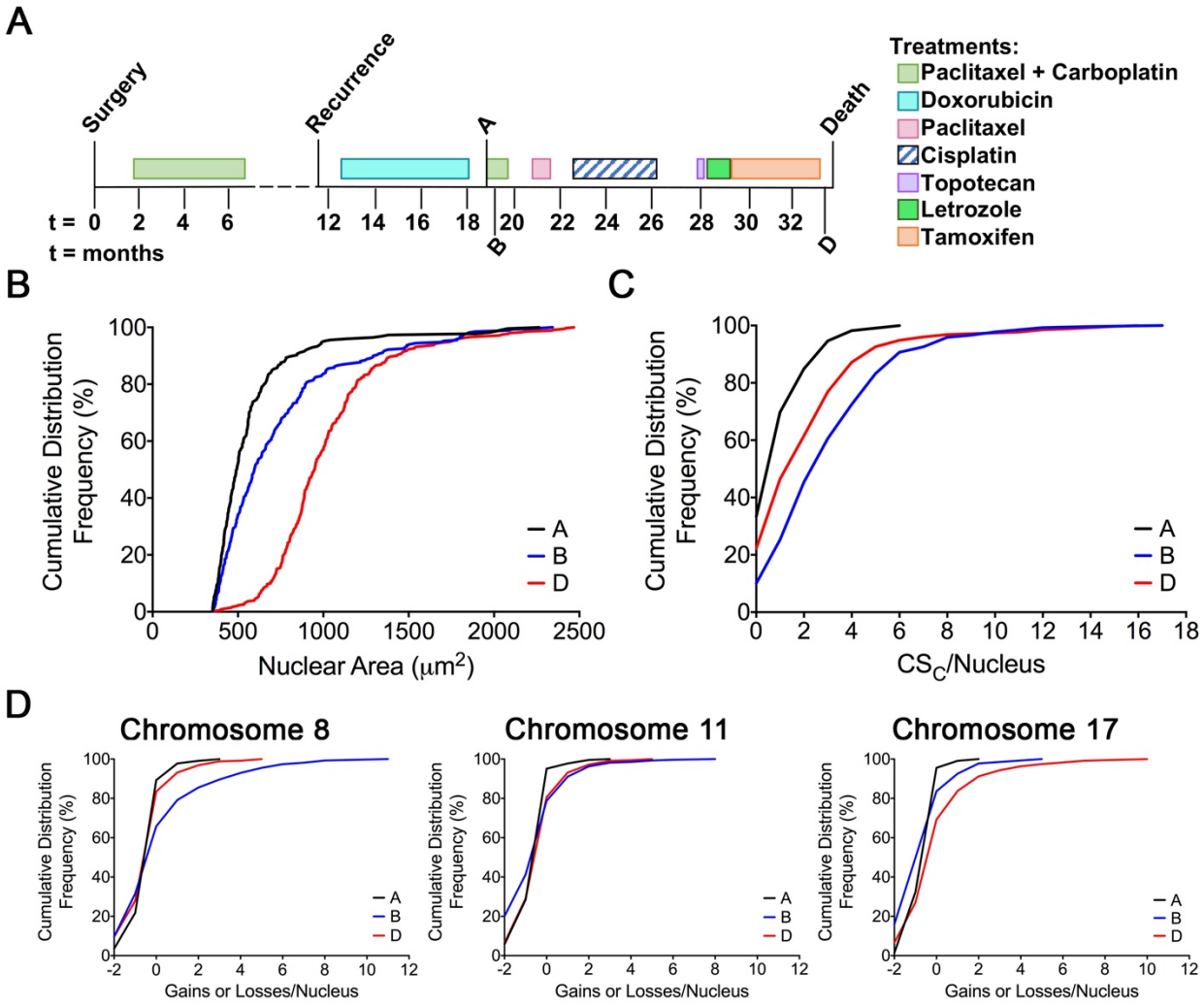


**Figure S5-18. Cumulative Distribution Frequencies for Patient OV001.**
***(A)*** Timeline indicating the collection times for three samples. ***(B)*** Cumulative NA distribution frequencies of three serial samples (N = 2; n >200). ***(C)*** Cumulative $CS_c$ distribution frequencies for each of the three serial samples evaluated. ***(D)*** Cumulative distribution frequencies for each individual *CS* value (*i.e.* $CS_8$ [left], $CS_{11}$ [middle], and $CS_{17}$ [right]) for the three samples.

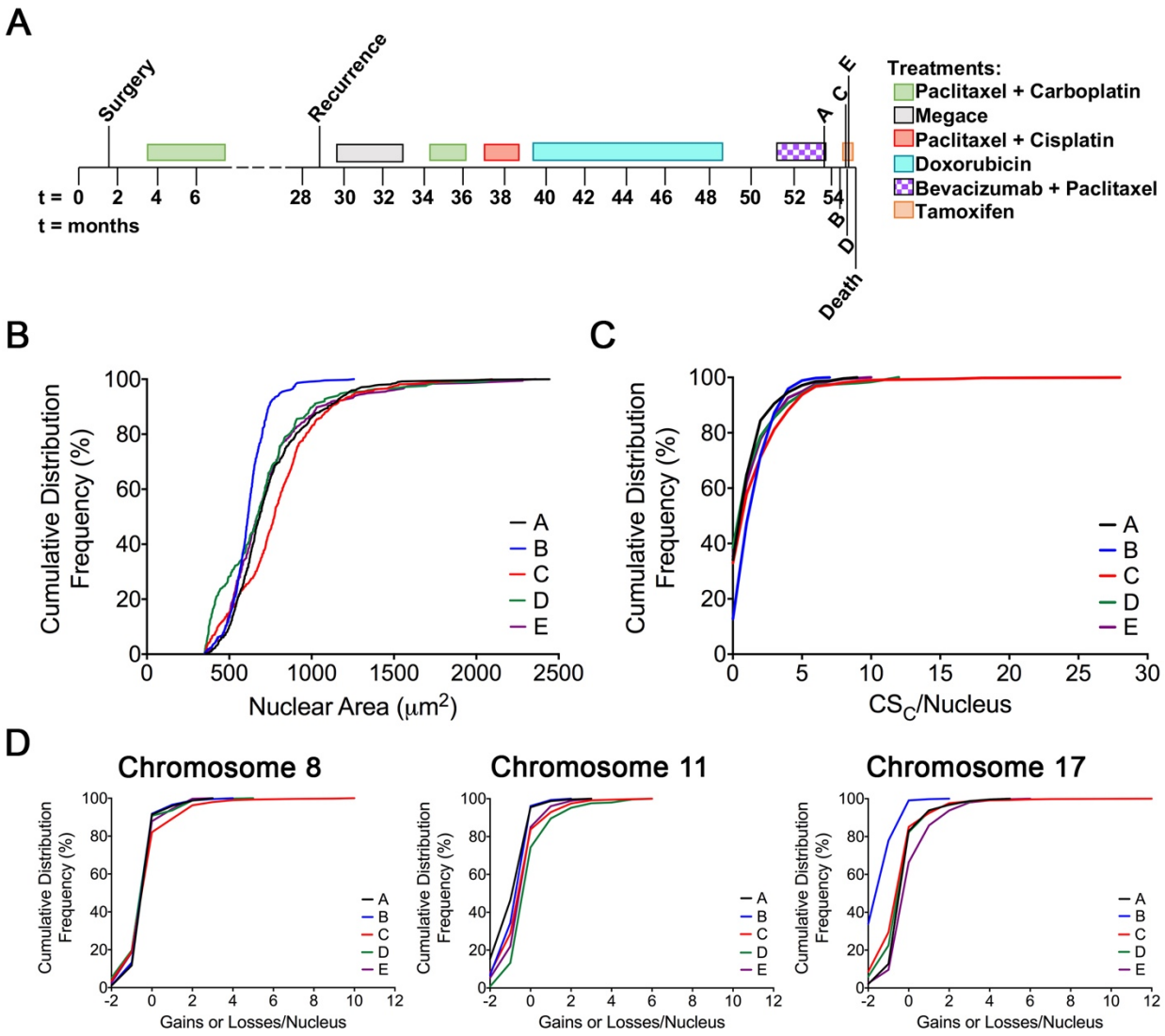


**Figure S5-19. Cumulative Distribution Frequencies for Patient OV299.**
***(A)*** Timeline indicating the collection times for five samples. ***(B)*** Cumulative NA distribution frequencies of five serial samples (N = 2; n >200). ***(C)*** Cumulative $CS_c$ distribution frequencies for each of the five serial samples evaluated. ***(D)*** Cumulative distribution frequencies for each individual *CS* value (*i.e.* $CS_8$ [left], $CS_{11}$ [middle], and $CS_{17}$ [right]) for the five samples.

# CHAPTER 6: AIM 3 RESULTS

## 6.1.0 Aim 3: To Determine the Prevalence of CIN in the Manitoba EOC Cohort TMA

***Rationale:*** The EOC patient TMA samples include various disease states, including both chemonaïve and chemosensitive disease, providing novel insight into CIN in HGSOC solid tumors.

## 6.1.1 Description of The Manitoba EOC Cohort

To assess the prevalence of CIN in the Manitoba EOC cohort comprised 36 type II (HGSOC) solid tumors (22 chemonaïve and 14 chemosensitive) (Table S6-1), *CS* values were determined using a previously optimized FISH-based approach[118] (*Section 3.7.3*). The HGSOC tumors were cored in duplicate and arrayed across two mini-TMAs (detailed in *Section 3.7.2*) (Fig 3-1). The overall goal of *Aim 3* was to evaluate CIN (*e.g. CS* values) in 100 nuclei/core, and thus a total of 200 nuclei/patient sample; however, this was not possible in two cores (20.2 and 34.1) due to high tissue auto-fluorescence or low cellularity. Nevertheless, it was possible to enumerate 100 nuclei within the duplicate core from both patients. The remaining 34 patient samples (34 patients x 2 cores = 68 total samples) were completely enumerated. Finally, it should be noted that 10 patient samples have associated ascites available, allowing for *CS* comparisons between the primary solid tumor and ascites, which represents metastatic tumors.

## 6.1.2 Both Chemonaïve and Chemosensitive Primary HGSOC Tumors Exhibit CIN

Chemonaïve HGSOC solid tumor samples are samples that were collected prior to receiving any chemotherapy treatment, while chemosensitive samples received neo-adjuvant chemotherapy prior to tumor collection. Figure 6-1 shows $CS_c$ values quantified from five

chemonaïve and five chemosensitive solid tumors cored in duplicate, which serve as representative examples of type II (HGSOC) solid tumors. Both chemonaïve and chemosensitive $CS_c$ values exhibited cell-to-cell heterogeneity and each core had a median $CS_c$ between 2 and 5 (Table S6-2). In general, each pair of duplicate cores have the same median $CS_c$ values (*e.g.* core 13.1 and 13.2 have a median $CS_c = 3$); however, 12 pairs of duplicate cores had different median $CS_c$ values (*e.g.* core 22.1 and 22.2 that had median $CS_c = 3$ and $CS_c = 4$, respectively), which may reflect ITH. Interestingly, ~95% of all nuclei evaluated have a $CS_c \neq 0$, indicating extreme levels of CIN within HGSOC tumor samples (Figure 6-1). Similar trends were also observed for the individual *CS* values (Table S6-2). In general, each sample exhibited gains and losses in chromosomes 8, 11, and 17 and had median individual *CS* values of $CS_8 = -1$, $CS_{11} = -1$, and $CS_{17} = -1$, respectively, indicating that losses of chromosomes 8, 11 and 17 are more frequent than chromosome gains. Overall, these data show that CIN is prevalent in 100% of HGSOC solid tumor samples and the majority (~96%) of samples exhibit extreme levels of aneuploidy as measured by median $CS_c$ values $\geq 3$.

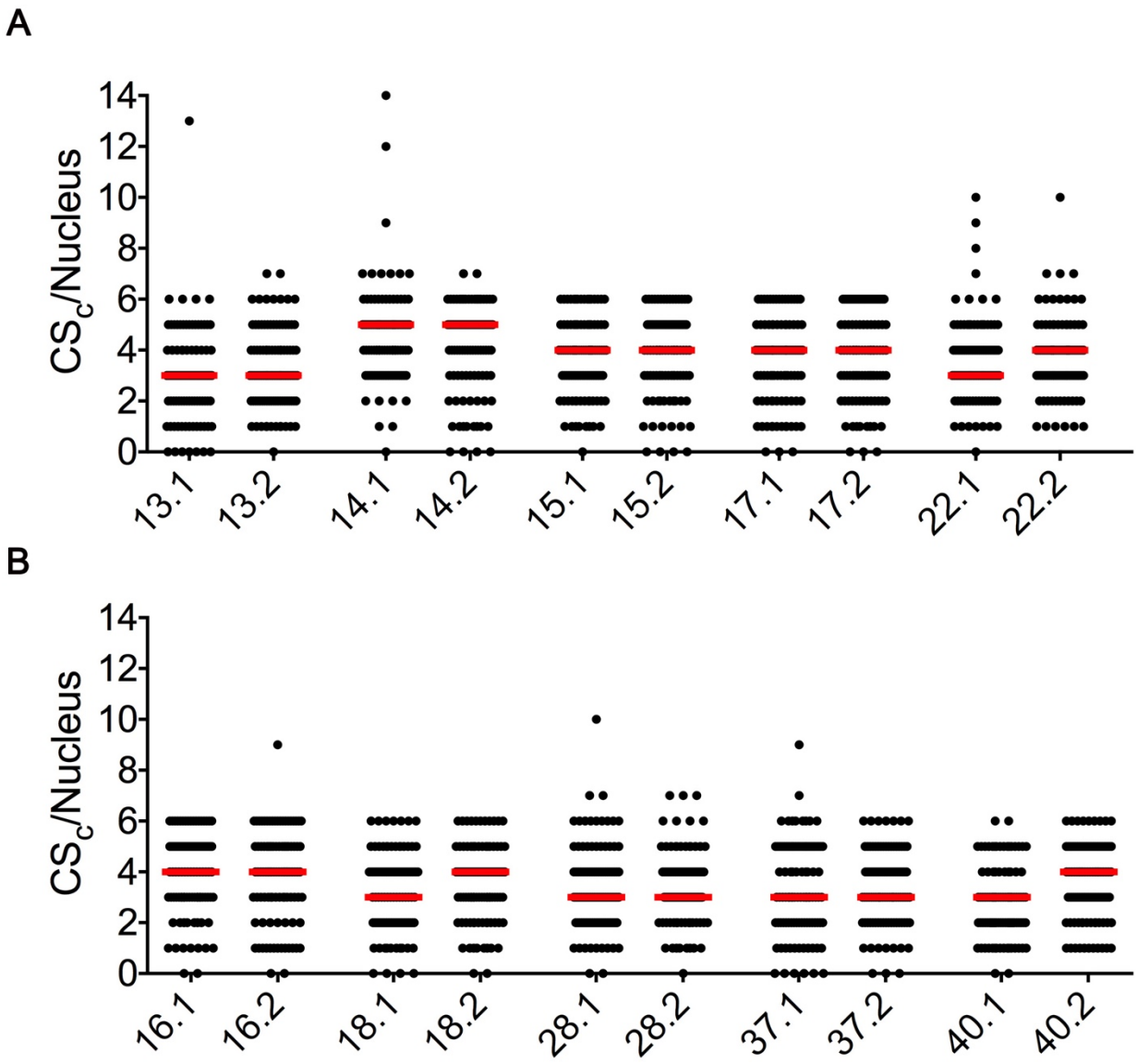


**Figure 6-1. Chemonaïve and Chemosensitive HGSOC Solid Tumors Exhibit CIN.**
**(*A*)** Dot plot presenting the $CS_c$ values for five representative chemonaïve patient samples (cored in duplicate; *i.e.* #-1 and #-2 are two cores from the same patient archived clinical FFPE tissue block). Red bars indicate the median $CS_c$ (n ≥ 100 nuclei/core). **(*B*)** Dot plot presenting the $CS_c$ values for five chemosensitive patient samples (cored in duplicate). Red bars indicate the median $CS_c$ (n ≥ 100 nuclei/core).

### 6.1.3 CIN is Higher in Primary Tumors Than in Ascites Collected from the Same Patient

The above suggests that extreme levels of CIN are associated with primary HGSOC solid tumors. To assess the differences in CIN between solid tumors and ascites derived patient samples, *CS* values were evaluated in 10 paired samples from the same patient diagnosed with HGSOC, including OV067, OV070, OV103, OV173, OV177, OV180, OV184, OV196, OV205, and OV299. Figure 6-2 shows a timeline of serial samples collected from patient OV0180 and quantified $CS_c$ values from both ascites and solid tumor, which serves as a representative example. Briefly, five serial ascites samples were isolated and analyzed (Fig 6-2A). In general, OV180 ascites samples have median $CS_c$ values = 1 (Fig 6-2B), while the solid tumor samples have median $CS_c$ values = 3 (Fig 6-2C). Similar results were observed for OV067 (Fig S6-1), OV070 (Fig S6-2), OV103 (Fig S6-3), OV173 (Fig S6-4), OV177 (Fig S6-5), OV184 (Fig S6-6), OV196 (Fig S6-7), OV205 (Fig S6-8), and OV299 (Fig S6-9). Overall these data show that 100% of HGSOC solid tumors have a higher median $CS_c$ values, therefore higher levels of aneuploidy, than the ascites derived patient samples collected from the same patient.

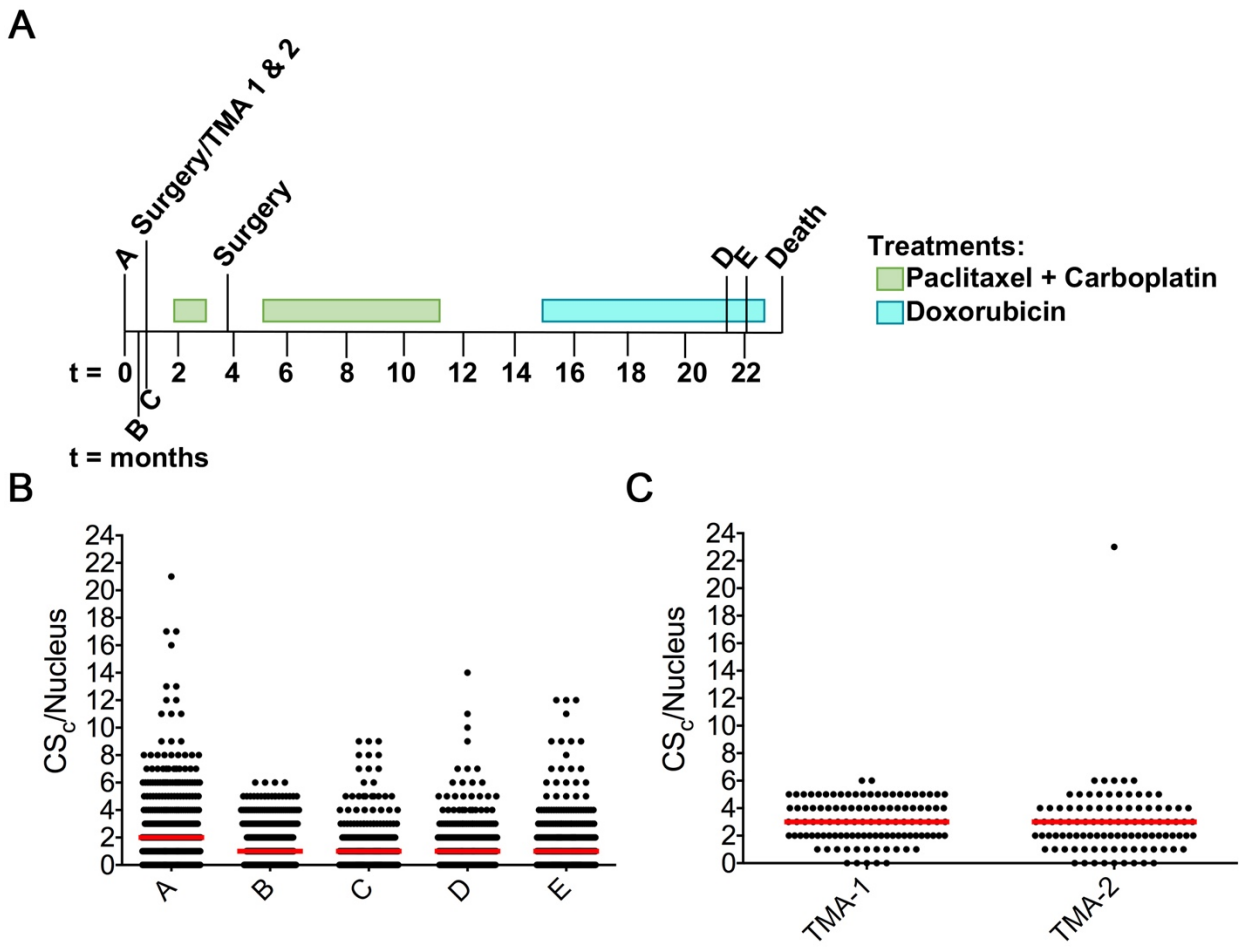


**Figure 6-2. OV180 has Higher *CS*$_c$ Values in Solid Tumors Than in Ascites Samples.**
**(*A*)** Timeline indicating the collection times for five serial samples. **(*B*)** Dot plot presenting the *CS*$_c$ values determined from five serial ascites samples. Red bars indicate the median *CS*$_c$ (N =2, n > 200 nuclei). **(*C*)** Dot plot showing the *CS*$_c$ values determined from the corresponding solid tumor samples (cored in duplicate; *i.e.* #-1 and #-2 are two cores from the same patient archived clinical FFPE tissue block). Red bars indicate the median *CS*$_c$ (n ≥ 100 nuclei/core).

### 6.1.4 Conclusion

The central goal of *Aim 3* was to evaluate the prevalence of CIN in HGSOC solid tumors. Overall, the above data show that CIN is prevalent in 100% of HGSOC solid tumors as measured by median $CS_c$ values ≥ 1. Importantly, CIN is prevalent at a high frequency in HGSOC solid tumors regardless of stage, grade, chemotherapy status, and background mutations and in general, the majority (54.2%) of CIN positive samples have a median $CS_c$ = 4 (4.1% of samples have a median $CS_c$ = 2, 38.9% of samples have a median $CS_c$ = 3, and 2.8% of samples have a median $CS_c$ = 5). Notably, 95.9% of samples exhibit extreme aneuploidy as measured by a $CS_c$ ≥ 3. Additionally, all 10 HGSOC solid tumors have a higher median $CS_c$ than the patient-matched ascites samples.

### 6.2.0 Supporting Information

### 6.2.1 Supporting Tables

**Table S6-1. HGSOC Solid Tumor Clinical Details.**

| Core ID | Histotype | Primary Site | Stage | Chemo- |
|---|---|---|---|---|
| 13[B] | Papillary serous cystadenocarcinoma | Ovary | IIC | Naïve |
| 14 | Serous cystadenocarcinoma | Ovary | IIC | Naïve |
| 15 | Papillary serous cystadenocarcinoma | Ovary | IIA | Naïve |
| 16 | Serous cystadenocarcinoma | Ovary | IC | Sensitive |
| 17 | Serous cystadenocarcinoma | Ovary | IIIC | Naïve |
| 18 | Serous cystadenocarcinoma | Ovary | IV | Sensitive |
| 19 | Serous cystadenocarcinoma | Ovary | IIIC | Sensitive |
| 20 | Mixed cell adenocarcinoma | Ovary | IIIC | Naïve |
| 21 | Serous cystadenocarcinoma | Ovary | IIIC | Sensitive |
| 22[C] | Mixed cell adenocarcinoma | Ovary | IC | Naïve |
| 23[C] | Serous cystadenocarcinoma | Ovary | IV | Naïve |
| 24 | Serous cystadenocarcinoma | Ovary | IIIC | Naïve |
| 25[C] | Serous cystadenocarcinoma | Ovary | IIIC | Sensitive |
| 26 | Serous cystadenocarcinoma | Ovary (Right) | IIINOS[D] | Sensitive |
| 27 | Serous cystadenocarcinoma | Ovary | IIIA | Naïve |
| 28[C] | Serous cystadenocarcinoma | Ovary | IIIC | Sensitive |
| 29 | Serous cystadenocarcinoma | Ovary | IIIB | Naïve |
| 30[B] | Serous cystadenocarcinoma | Ovary (Left) | IV | Sensitive |
| 31 | Serous cystadenocarcinoma | Ovary | IIIC | Sensitive |
| 32 | Serous cystadenocarcinoma | Ovary | IIIC | Naïve |
| 33[A] | Serous cystadenocarcinoma | Ovary (Left) | IIIC | Naïve |
| 34 | Serous cystadenocarcinoma | Ovary | IC | Naïve |
| 35 | Serous cystadenocarcinoma | Ovary | IV | Naïve |
| 36[A, C] | Serous cystadenocarcinoma | Omentum | IIIC | Naïve |
| 37[B, C] | Serous cystadenocarcinoma | Ovary | IIIC | Sensitive |
| 38 | Serous cystadenocarcinoma | Ovary | IIIC | Naïve |
| 39 | Serous cystadenocarcinoma | Ovary | IC | Naïve |
| 40[C] | Serous cystadenocarcinoma | Ovary (Right) | IV | Sensitive |
| 41[C] | Serous cystadenocarcinoma | Ovary | IIIB | Sensitive |
| 42[C] | Serous cystadenocarcinoma | Ovary | IIIC | Naïve |
| 43[A] | Serous cystadenocarcinoma | Ovary | IIIC | Sensitive |
| 44 | Serous cystadenocarcinoma | Ovary | IIIA | Sensitive |
| 45 | Serous cystadenocarcinoma | Ovary (Left) | IIA | Naïve |
| 46 | Serous cystadenocarcinoma | Ovary | IIIA | Naïve |
| 47 | Mixed cell adenocarcinoma | Ovary | IC | Naïve |
| 48[A, C] | Mixed cell adenocarcinoma | Ovary | IC | Naïve |

[A]*BRCA1* positive tumor
[B]*BRCA2* positive tumor
[C]Ascites samples collected from the same patient
[D]Not otherwise specified (NOS)

**Table S6-2. *CS* Descriptive Statistics for HGSOC Solid Tumor Patient Samples.**

| | | Median | | | | | | Median | | | |
|---|---|---|---|---|---|---|---|---|---|---|---|
| Core ID | n[A] | $CS_8$ | $CS_{11}$ | $CS_{17}$ | $CS_c$ | Core ID | n[A] | $CS_8$ | $CS_{11}$ | $CS_{17}$ | $CS_c$ |
| 13.1 | 100 | 0 | 0 | -1 | 3 | 31.1 | 100 | -1 | -1 | -2 | 4 |
| 13.2 | 100 | 0 | 0 | -1 | 3 | 31.2 | 100 | -1 | -1 | -2 | 4 |
| 14.1 | 100 | -0.5 | -2 | -1 | 5 | 32.1 | 100 | -0.5 | 0 | 1 | 4 |
| 14.2 | 100 | -1 | -1.5 | -2 | 5 | 32.2 | 100 | -1 | -1 | -2 | 4 |
| 15.1 | 100 | -1 | -1 | -1 | 4 | 33.1 | 100 | -1 | -0.5 | -1 | 3 |
| 15.2 | 100 | -1 | -1 | -1 | 4 | 33.2 | 100 | -1 | -1 | -1 | 4 |
| 16.1 | 100 | -1 | -1.5 | -2 | 4 | 34.1 | 26 | -0.5 | 0 | -0.5 | 4 |
| 16.2 | 100 | -1 | -1 | -2 | 4 | 34.2 | 100 | -1 | -1 | -1 | 4 |
| 17.1 | 100 | -1 | -1 | -1 | 4 | 35.1 | 100 | 1 | 1 | 0 | 3 |
| 17.2 | 100 | -1 | -1 | -1 | 4 | 35.2 | 100 | -1 | 0 | -1 | 3 |
| 18.1 | 100 | -1 | -1 | -1 | 3 | 36.1 | 100 | -1 | -1 | -1 | 3 |
| 18.2 | 100 | -1 | -1 | -1 | 4 | 36.2 | 100 | -1 | -1 | -1 | 3 |
| 19.1 | 100 | -1 | -1 | -1 | 4 | 37.1 | 100 | -1 | -1 | -1 | 3 |
| 19.2 | 100 | -1 | -1 | -1 | 4 | 37.2 | 100 | -1 | -1 | -1 | 3 |
| 20.1 | 100 | 0 | 0 | -1 | 3 | 38.1 | 100 | -1 | -1 | -1 | 4 |
| 20.2 | 68 | -1 | -1 | -1 | 4 | 38.2 | 100 | -1 | -1 | -1 | 4 |
| 21.1 | 100 | 0 | -0.5 | -1 | 4 | 39.1 | 100 | -1 | -1 | -2 | 4 |
| 21.2 | 100 | 0 | -1 | -1 | 4 | 39.2 | 100 | -1 | -1 | -1 | 4 |
| 22.1 | 100 | 0 | -1 | -1 | 3 | 40.1 | 100 | -1 | -1 | -1 | 3 |
| 22.2 | 100 | -1 | -1 | -1 | 4 | 40.2 | 100 | -1 | -1 | -2 | 4 |
| 23.1 | 114 | -0.5 | -1 | -1 | 3 | 41.1 | 100 | -1 | -1 | -2 | 4 |
| 23.2 | 100 | -1 | -1 | -1 | 3 | 41.2 | 100 | -1 | -2 | -2 | 4 |
| 24.1 | 100 | -1 | 0 | -1 | 3 | 42.1 | 100 | -1 | -1 | -1 | 4 |
| 24.2 | 100 | -1 | -1 | -1 | 3 | 42.2 | 100 | -1 | -1 | -1 | 3 |
| 25.1 | 100 | -1 | -1 | -1 | 3 | 43.1 | 100 | -1 | -1 | -1 | 3 |
| 25.2 | 100 | -1 | -1 | -1 | 4 | 43.2 | 100 | -1 | -1 | -1 | 4 |
| 26.1 | 100 | -1 | -1 | -1.5 | 4 | 44.1 | 100 | 0 | 0 | -1 | 4 |
| 26.2 | 100 | -1 | -1 | -1 | 4 | 44.2 | 100 | 0 | -1 | -1 | 3 |
| 27.1 | 100 | -1 | 0 | -1 | 4 | 45.1 | 100 | -1 | -1 | -1 | 3 |
| 27.2 | 100 | -1 | 0 | -1 | 3 | 45.2 | 100 | -1 | -0.5 | -1 | 2.5 |
| 28.1 | 103 | 0 | -1 | -1 | 3 | 46.1 | 100 | 1 | 0 | -1 | 3 |
| 28.2 | 102 | 0 | -1 | -1 | 3 | 46.2 | 100 | 0 | 0 | -1 | 3 |
| 29.1 | 100 | -1 | -1 | -1 | 4 | 47.1 | 100 | 0 | -1 | 0 | 2 |
| 29.2 | 100 | -1 | -1 | -2 | 4 | 47.2 | 100 | -1 | -1 | -1 | 3 |
| 30.1 | 100 | -1 | -1 | -2 | 4 | 48.1 | 100 | -1 | -1 | -1 | 4 |
| 30.2 | 100 | -1 | -1 | -1.5 | 4 | 48.2 | 100 | -1 | -1 | -1 | 4 |

[A]Number of nuclei analyzed (n)

### 6.2.2 Supporting Figures

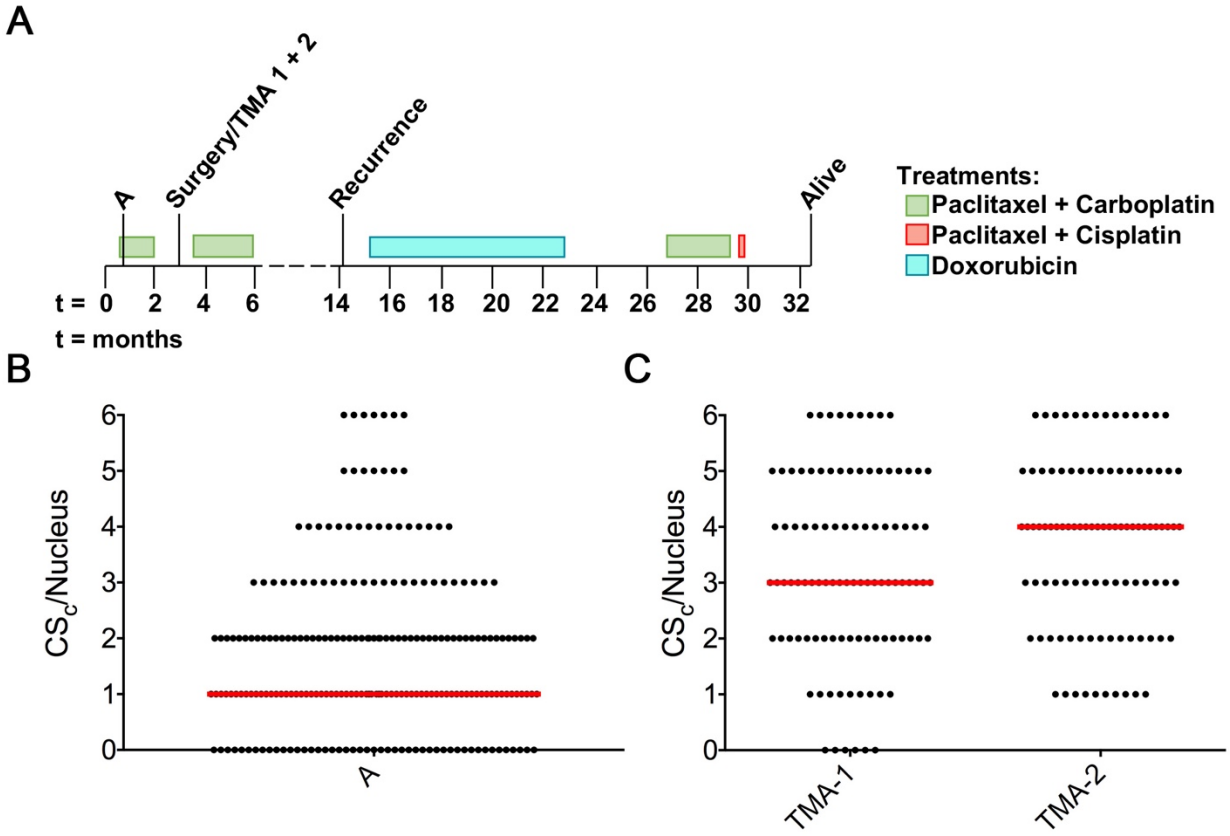


**Figure S6-1. OV067 has Higher *CS*$_c$ Values in Solid Tumors Than in Ascites Samples.** **(*A*)** Timeline indicating the collection times for one sample. Note this patient was alive as of their last known update (November 14, 2016). **(*B*)** Dot plot presenting the *CS*$_c$ values determined from one ascites sample. Red bars indicate the median *CS*$_c$ (N = 2; n > 200). **(*C*)** Dot plot showing the *CS*$_c$ values determined from the corresponding solid tumor samples isolated during surgery (cored in duplicate). Red bars indicate the median *CS*$_c$ (n ≥ 100 nuclei/core).

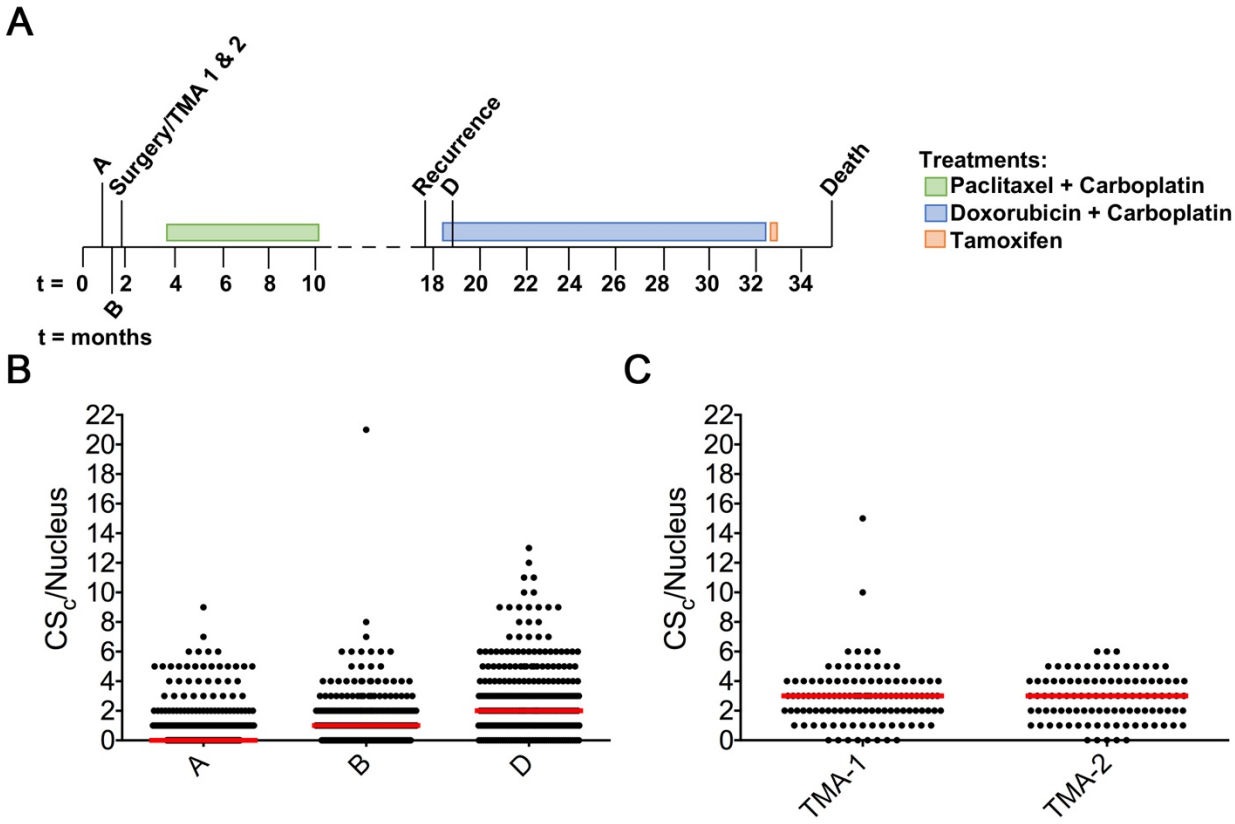


**Figure S6-2. OV070 has Higher $CS_c$ Values in Solid Tumors Than in Ascites Samples.**
**(*A*)** Timeline for patient OV070. **(*B*)** Dot plot presenting the $CS_c$ determined from three serial ascites samples (N = 2; n > 200). Red bars indicate the median. **(*C*)** Dot plot showing the $CS_c$ values determined from the corresponding solid tumor samples isolated during surgery (cored in duplicate). Red bars indicate the median $CS_c$ (n≥ ≥ 100 nuclei/core).

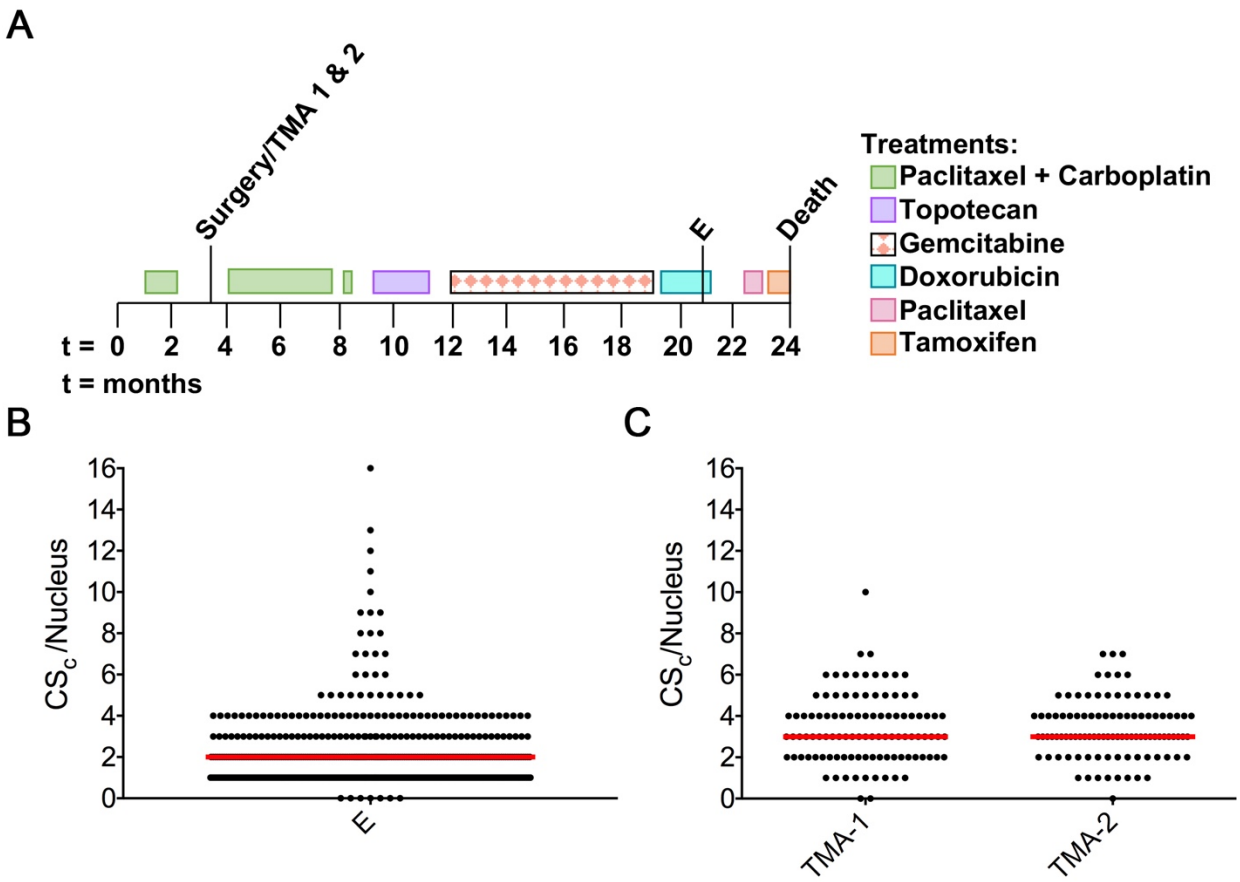


**Figure S6-3. OV103 has Higher *CS*$_c$ Values in Solid Tumors Than in Ascites Samples.**
**(*A*)** Timeline for patient OV103. **(*B*)** Dot plot presenting the *CS*$_c$ determined from one ascites sample (N = 2; n > 200). Red bars indicate the median. **(*C*)** Dot plot showing the *CS*$_c$ values determined from the corresponding solid tumor samples isolated during surgery (cored in duplicate). Red bars indicate the median *CS*$_c$ (n ≥ 100 nuclei/core).

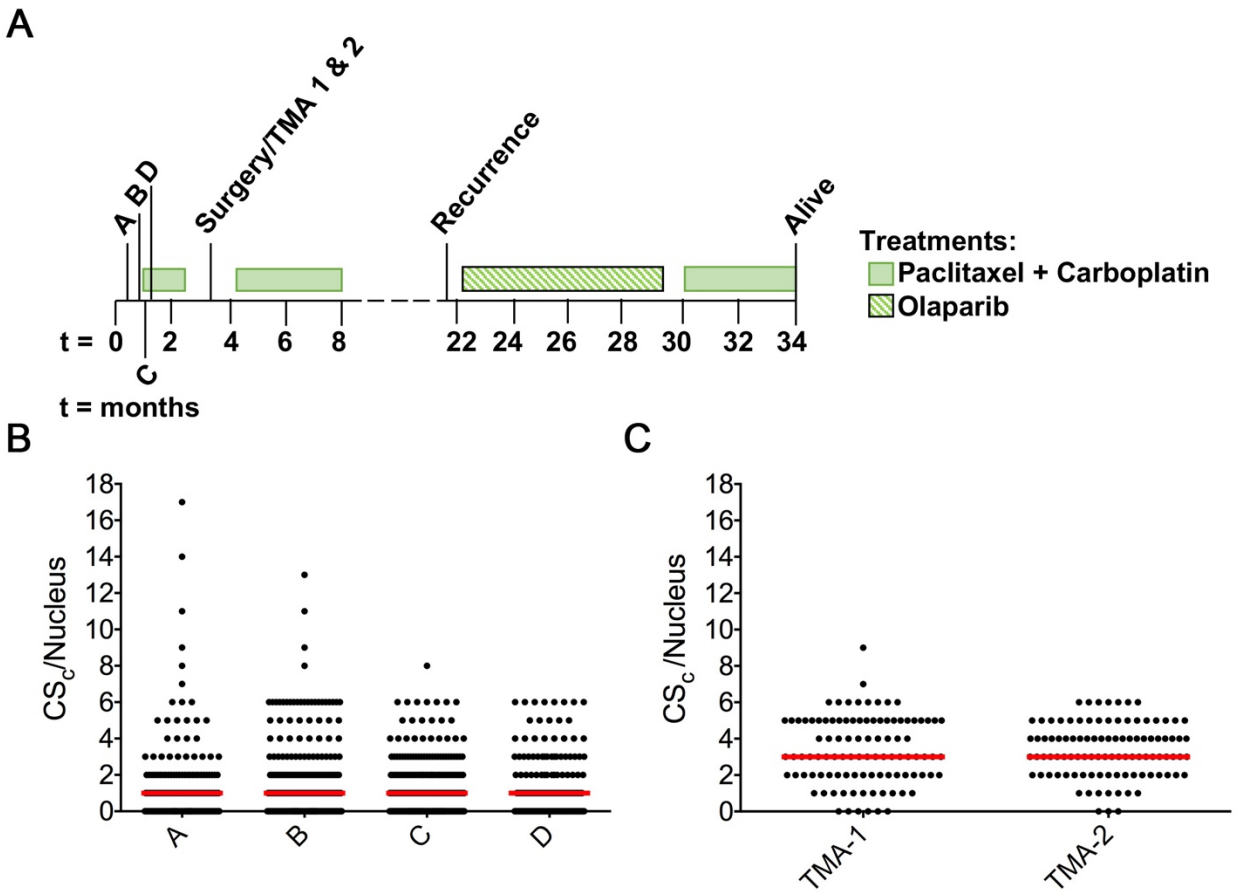


**Figure S6-4. OV173 has Higher *CS*$_c$ Values in Solid Tumors Than in Ascites Samples.** **(*A*)** Timeline indicating the collection times for four serial sample. Note this patient was alive as of their last known update (February 4, 2019). **(*B*)** Dot plot presenting the *CS*$_c$ determined from four serial ascites samples (N = 2; n > 200). Red bars indicate the median. **(*C*)** Dot plot showing the *CS*$_c$ values determined from the corresponding solid tumor samples isolated during surgery (cored in duplicate). Red bars indicate the median *CS*$_c$ (n ≥ 100 nuclei/core).

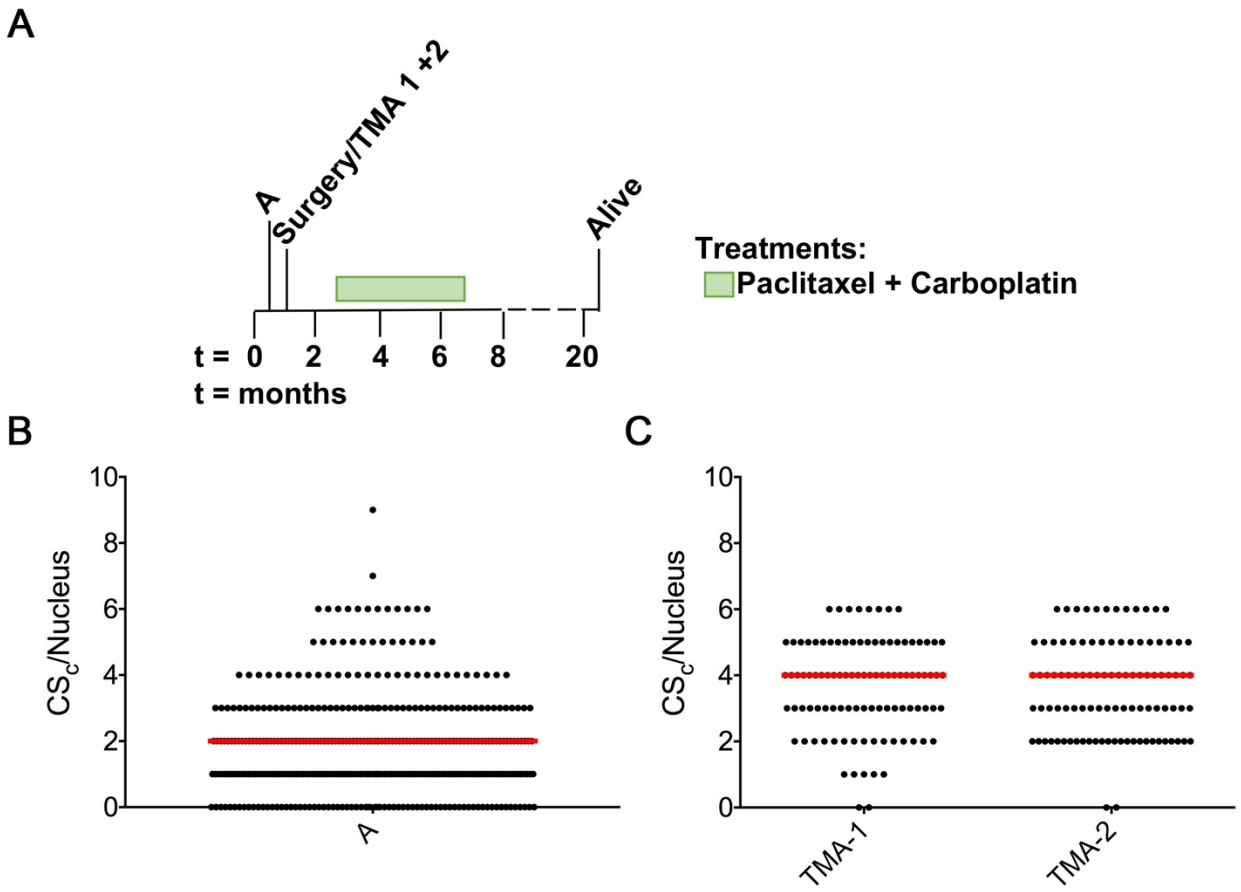


**Figure S6-5. OV177 has Higher *CS*$_c$ Values in Solid Tumors Than in Ascites Samples.**
**(*A*)** Timeline indicating the collection times for one sample. Note this patient was alive as of their last known update (February 22, 2018). **(*B*)** Dot plot presenting the *CS*$_c$ determined from one ascites sample (N = 2; n > 200). Red bars indicate the median. **(*C*)** Dot plot showing the *CS*$_c$ values determined from the corresponding solid tumor samples isolated during surgery (cored in duplicate). Red bars indicate the median *CS*$_c$ (n ≥ 100 nuclei/core).

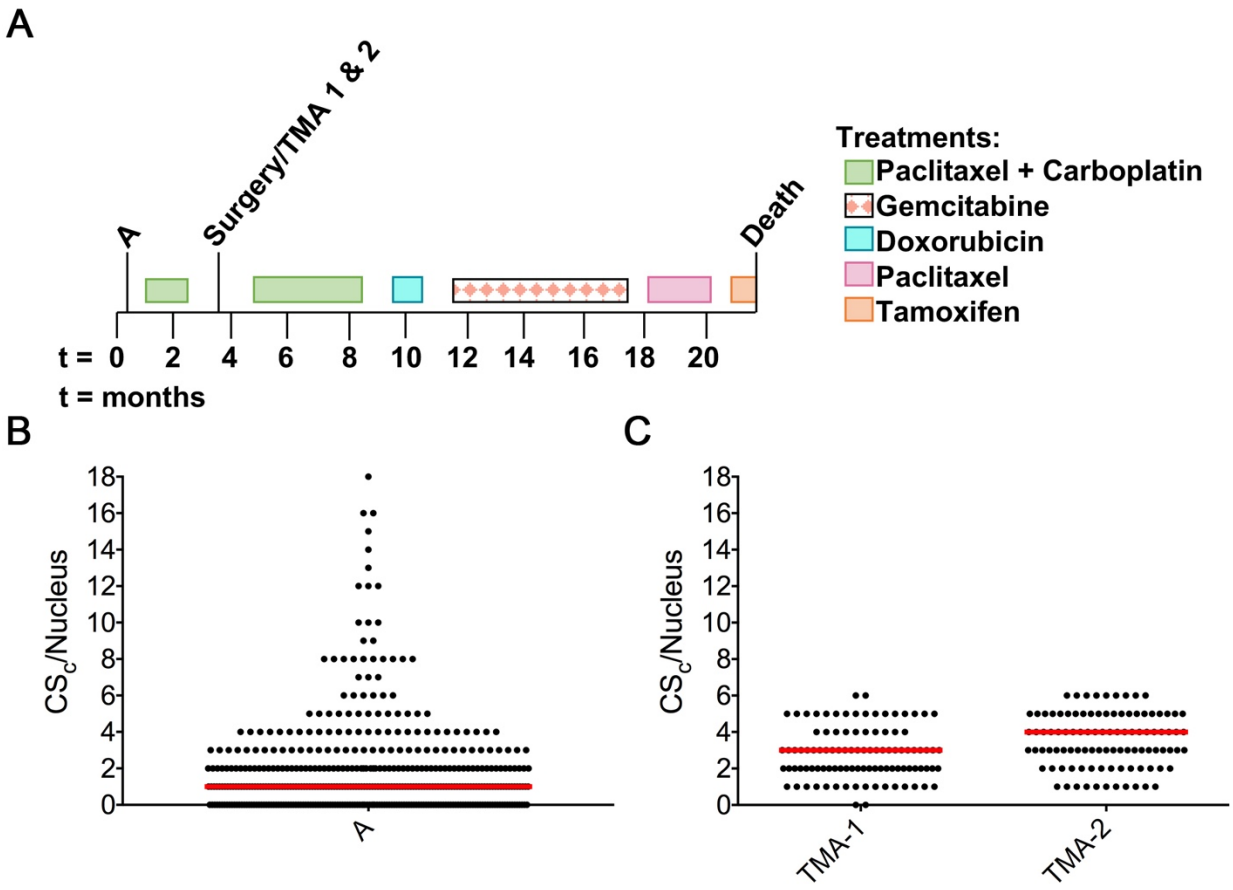


**Figure S6-6. OV184 has Higher *CS*$_c$ Values in Solid Tumors Than in Ascites Samples.**
**(*A*)** Timeline for patient OV184. **(*B*)** Dot plot presenting the *CS*$_c$ determined from one ascites sample (N = 2; n > 200). Red bars indicate the median. **(*C*)** Dot plot showing the *CS*$_c$ values determined from the corresponding solid tumor samples isolated during surgery (cored in duplicate). Red bars indicate the median *CS*$_c$ (n ≥ 100 nuclei/core).

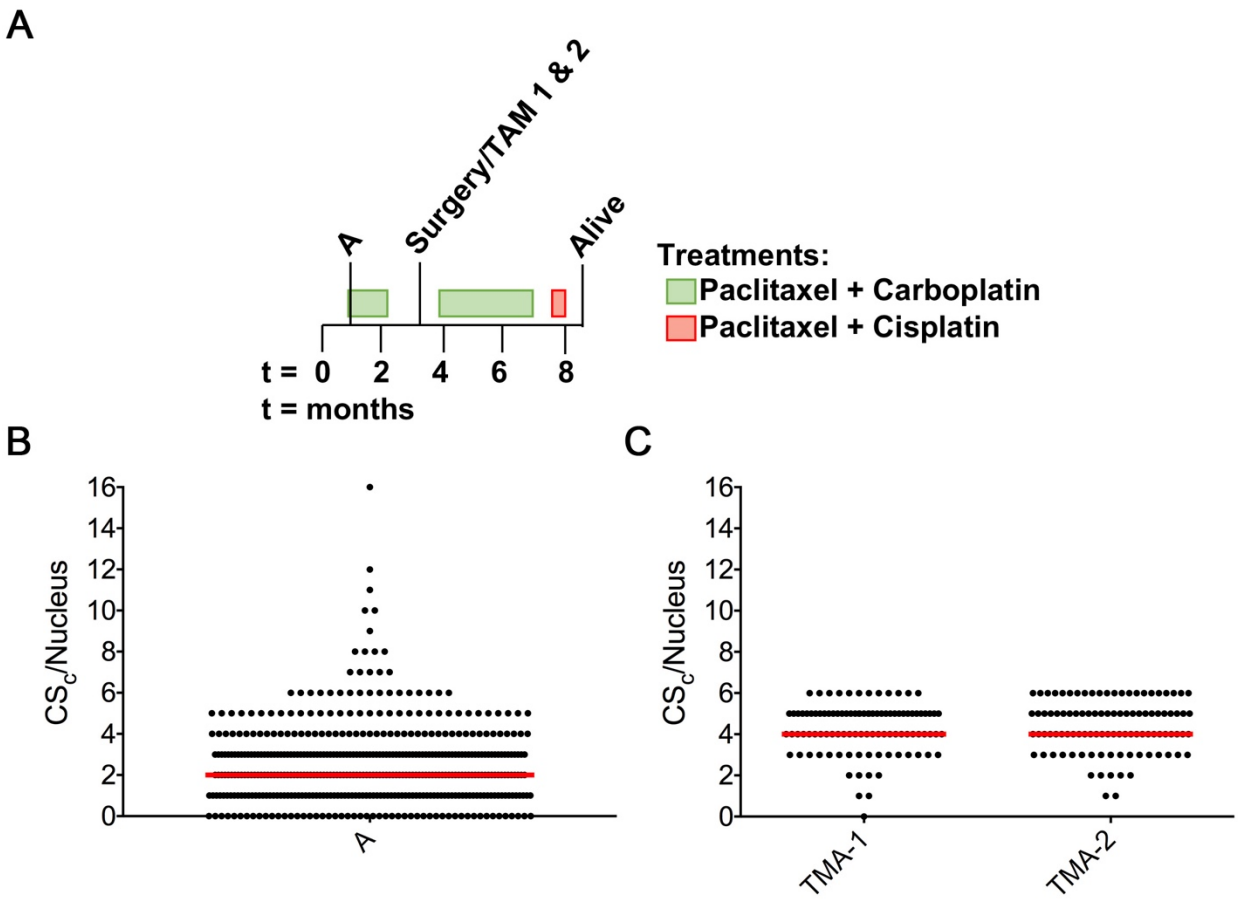


**Figure S6-7. OV196 has Higher *CS$_c$* Values in Solid Tumors Than in Ascites Samples.** **(*A*)** Timeline for patient OV196. Importantly, this patient was still alive as of November 29, 2018. **(*B*)** Dot plot presenting the *CS*$_c$ determined from one ascites sample (N = 2; n > 200). Red bars indicate the median. **(*C*)** Dot plot showing the *CS*$_c$ values determined from the corresponding solid tumor samples isolated during surgery (cored in duplicate). Red bars indicate the median *CS$_c$* (n ≥ 100 nuclei/core).

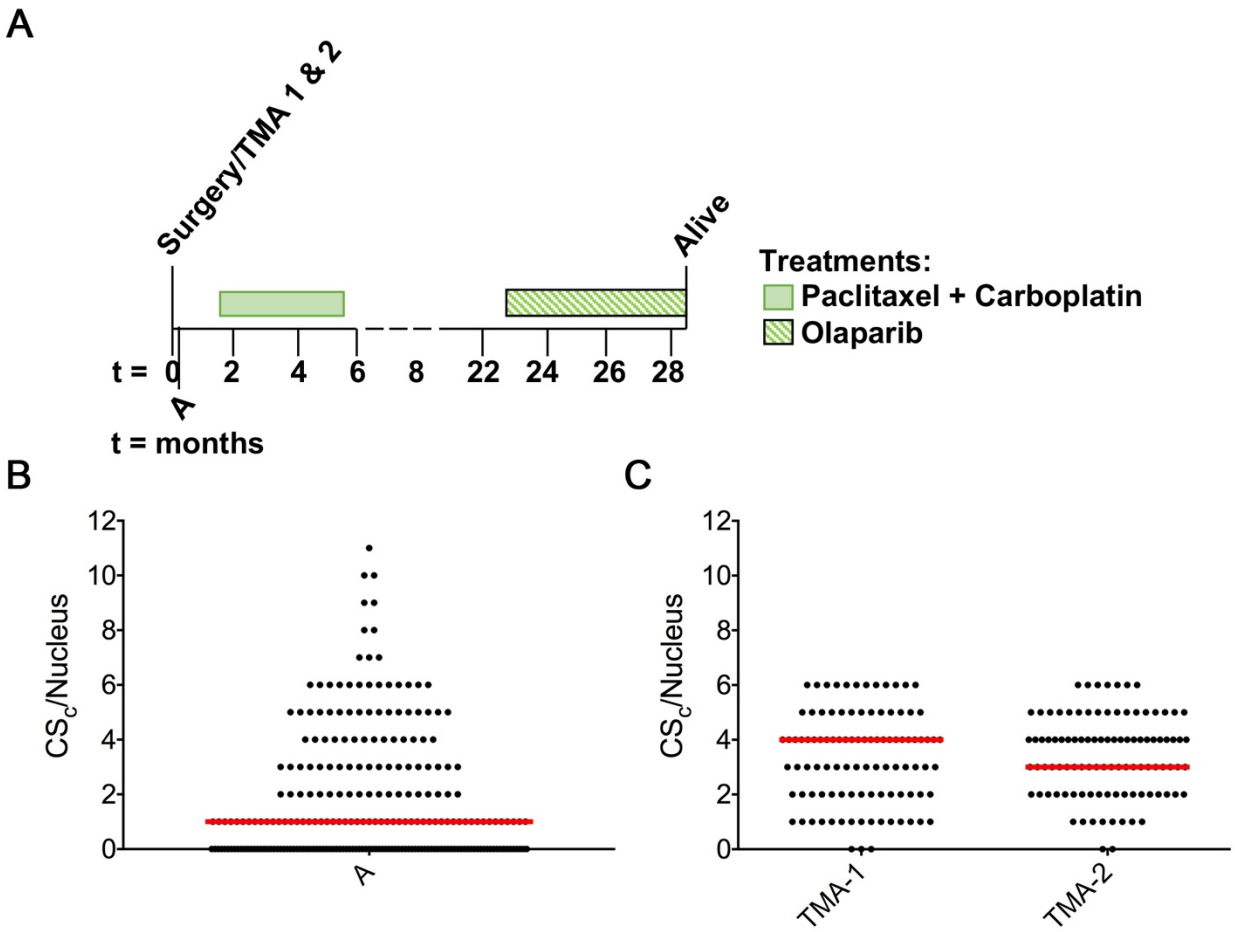


**Figure S6-8. OV205 has Higher *CS$_c$* Values in Solid Tumors Than in Ascites Samples.** **(*A*)** Timeline for patient OV205. Importantly, this patient was still alive as of March 19, 2019. **(*B*)** Dot plot presenting the *CS*$_c$ determined from one ascites sample (N = 2; n > 200). Red bars indicate the median. **(*C*)** Dot plot showing the *CS*$_c$ values determined from the corresponding solid tumor samples isolated during surgery (cored in duplicate). Red bars indicate the median *CS$_c$* (n ≥ 100 nuclei/core).

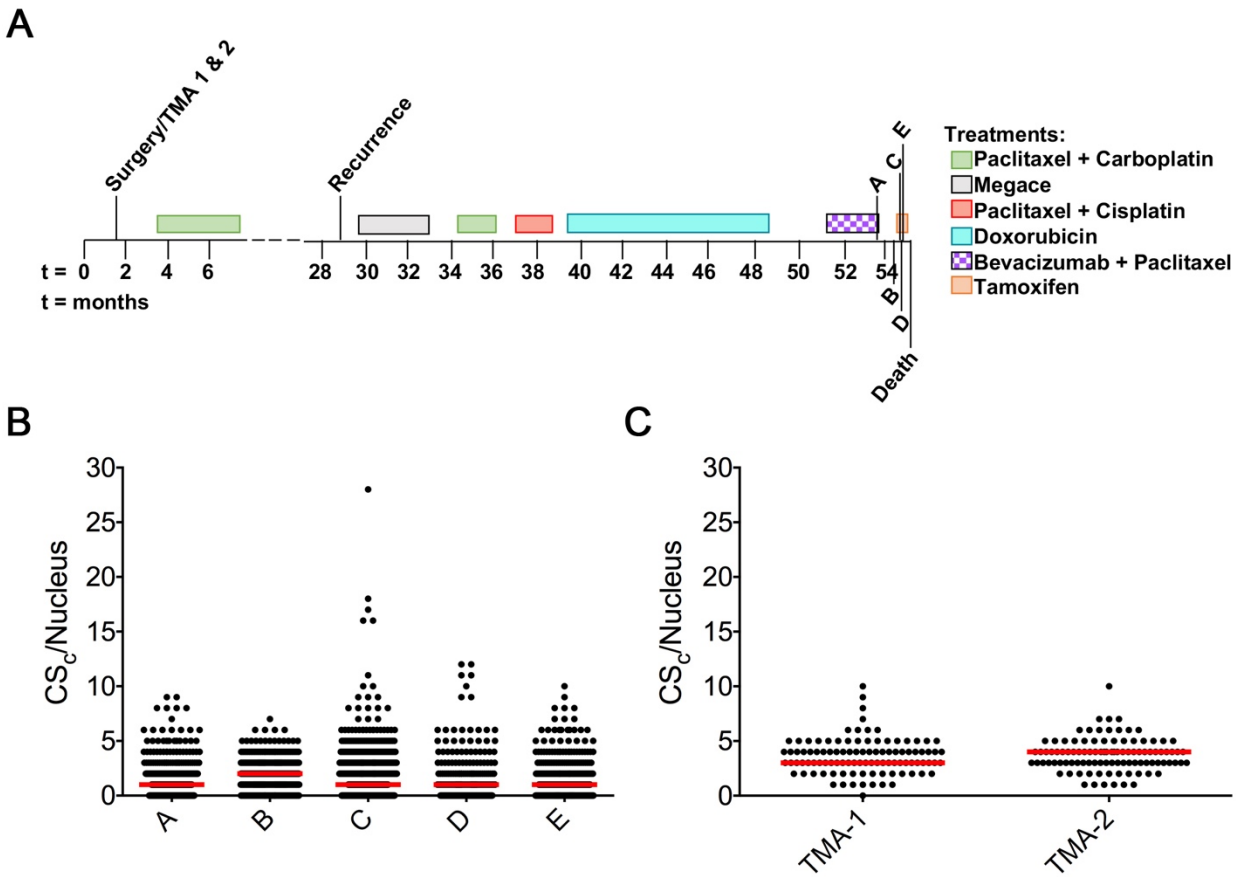


**Figure S6-9. OV299 has Higher $CS_c$ Values in Solid Tumors Than in Ascites Samples.** **(*A*)** Timeline for patient OV299. **(*B*)** Dot plot presenting the $CS_c$ determined from five serial ascites samples (N = 2; n > 200). Red bars indicate the median. **(*C*)** Dot plot showing the $CS_c$ values determined from the corresponding solid tumor samples isolated during surgery (cored in duplicate). Red bars indicate the median $CS_c$ (n ≥ 100 nuclei/core).

# CHAPTER 7: DISCUSSION

## 7.1.0 Summary and Conclusions

In this thesis, NA quantification and *CS* values were employed to characterize the prevalence and dynamics of CIN in HGSOC patient samples. Prior to evaluating patient samples, the first aim of this study was to validate the DNA probe set (*i.e.* CEPs) in FT cell lines and establish a *CS* threshold (Fig 7-1A). Importantly, the results from *Aim 1* (*Chapter 4*) determined that the CEPs are highly specific and are capable of enumerating interphase chromosomes in both diploid and aneuploid cell lines. Additionally, a *CS* threshold was established and samples with a median $CS_c = 0$ do not exhibit CIN and samples with a median $CS_c \geq 1$ indicate CIN is prevalent.

Following CEP validation, the second aim was to apply this approach and determine NAs and *CS* values in ascites samples derived from HGSOC patients, to gain further insight into the prevalence and temporal dynamics of CIN in response to disease progression, treatment and disease recurrence (Fig 7-1B). Importantly, the results from *Aim 2* (*Chapter 5*) determined that CIN is prevalent in 92.5% of HGSOC ascites derived patient samples, which was characterized by NA heterogeneity and median $CS_c$ values $\geq 1$. More specifically, 20/22 single patient samples (8/10 chemonaïve, 6/6 chemosensitive, and 6/6 chemoresistant) and 43/46 serial patient samples exhibited aneuploidy and CIN. In general, the majority (60.2%) of CIN positive samples had a median $CS_c = 1$, 25% of patients had a median $CS_c = 2$, and 7.4% of patients exhibited extreme aneuploidy and had a median $CS_c = 3$. Additionally, serial HGSOC patient samples exhibited statistically significant NA and *CS* changes over time (*i.e.* temporal dynamics). Generally, aneuploidy and CIN increased with disease progression and recurrence, and had varied dynamics during treatments and following chemotherapy.

Lastly, the third aim of this study determined *CS* values in 36 HGSOC solid tumors (22 chemonaïve and 14 chemosensitive), providing novel insight into CIN in HGSOC solid tumors (Fig 7-1C). Importantly, the results from *Aim 3* (*Chapter* 6) determined that CIN was prevalent in 100% of HGSOC solid tumors as measured by median $CS_c$ values ≥ 1. In general, 4% of CIN positive samples had a median $CS_c = 2$, 39% had a median $CS_c = 3$, 54% had a median $CS_c = 4$ and 3% of samples had a median $CS_c = 5$. Notably, 96% of samples exhibited extreme aneuploidy as measured by a $CS_c \geq 3$ and the majority of observed chromosome changes in solid tumors were losses of chromosomes 8, 11 and 17. Additionally, 10 patient samples had both ascites and solid tumors collected from the same individual, and all 10 HGSOC solid tumors had a higher median $CS_c$ than the patient-matched ascites samples.

Collectively, these data determined that CIN was prevalent at a high frequency in both ascites derived patient samples and HGSOC solid tumors and exhibited unique temporal dynamics. More specifically, aneuploidy and CIN increased with disease progression and recurrence, and had varied dynamics during treatments and following chemotherapy, thus supporting my hypothesis (*Section 2.2.0*, pg. 19).

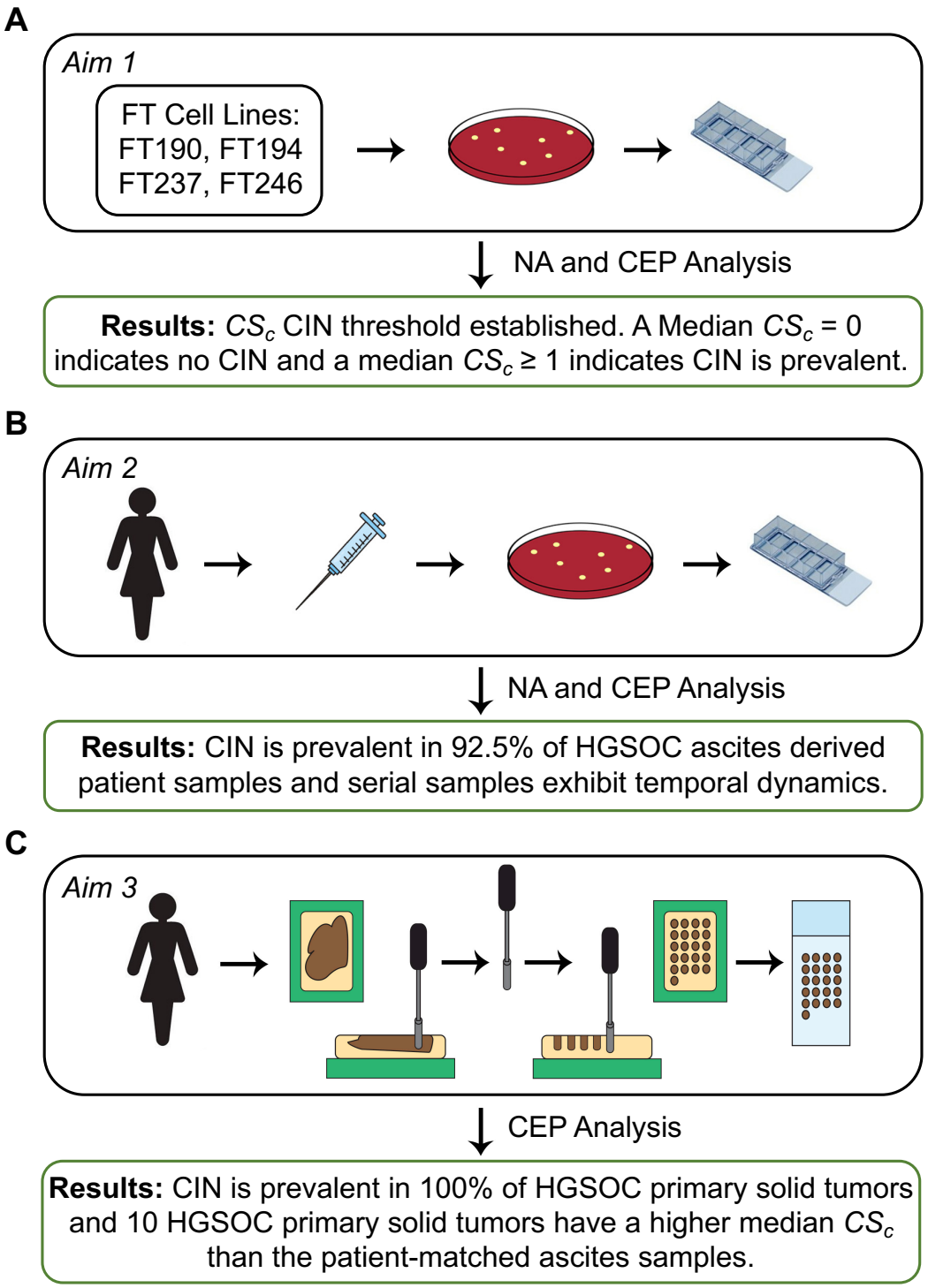


**Figure 7-1. Schematic Outlining General Methods and Results.**
***(A)*** Schematic of *Aim 1*. FT cell lines were used to validate CEP specificity, prior to NA and CEP analysis (top); general results are summarized (bottom). ***(B)*** Schematic of *Aim 2*. Briefly, ascites was collected via paracentesis, tumor cells are isolated and grown for NA and CEP analysis (top); general results are summarized (bottom). ***(C)*** Schematic of *Aim 3*. Briefly, solid tumors were collected during surgery, tumor samples are cored and transferred to Manitoba EOC TMA, and sectioned for CEP analysis (top); general results are summarized (bottom).

### 7.2.0 Benefits and Limitations of CIN Assays

This study utilizes two complementary approaches, namely single-cell QuantIM and cytogenetic approaches (FISH; CEPs) to identify and quantify CIN. Below, these approaches are described, their fundamental benefits and limitations are discussed, and recent representative examples of how the methods have been applied within EOC/HGSOC research/clinical settings are reviewed.

### 7.2.1 Nuclear Area (NA) Analysis

Rather than quantifying specific changes associated with N- or S-CIN, a more rapid way to assess CIN is to quantify phenotypes or surrogate markers of CIN. In this regard, single-cell QuantIM is highly effective at identifying significant changes in NAs[46,71,123–125]. There are a number of benefits that are associated with NA assays, including: 1) it can be performed in live or fixed cells; 2) it is low-cost; 3) it is simple to execute, as it requires labeling with only a standard DNA counterstain (DAPI)[71]; and 4) it is amenable to automation in 2D cell culture experiments. For example, Penner-Goeke *et al*.[46] and this thesis evaluated NA cell-to-cell heterogeneity to determine the prevalence and dynamics of CIN within recurrent and drug-resistant EOC/HGSOC ascites derived patient samples. Unfortunately, an inherent limitation of both studies is that there are no control cells evaluated (*i.e.* fallopian tube secretory epithelial cells [FTSECs]; *detailed further in Section 7.2.4*), resulting in an inability to establish a NA CIN threshold, as changes in NAs can also occur independent of CIN[71]. For example, NAs vary throughout the cell cycle, as G1 nuclei (*i.e.* pre-replication) are smaller than G2 nuclei (*i.e.* post-replication)[71,105]; however, the variation in NAs exhibited during cell cycle are minimal and cannot account for the extreme NA heterogeneity observed in CIN positive samples[105]. Additionally, there are no available

technologies or analysis software that are capable of measuring NAs in solid tumors contained on the TMAs following 3D imaging. Overall, the quantitative assessment of NAs is an indirect method of evaluating CIN, that is ideally suited to initial screen that will warrant further complementary approaches to validate N- and/or S-CIN phenotypes[71].

### 7.2.2 FISH and Chromosome Enumeration Probe (CEP) Analysis

FISH is a powerful tool used to evaluate cytogenetic abnormalities that involves the hybridization of a fluorescently labeled probe to a specific gene, region (*e.g.* CEP) or to the whole chromosome[71]. Since FISH can be applied to both mitotic and interphase populations, it enables the analysis of cell-to-cell heterogeneity, and it is ideally suited to CIN-based studies[71]. A fundamental benefit of FISH is that several probes can be multiplexed and enumerated automatically to concurrently assess multiple chromosomes[70,71,82,126]. For example, Penner-Goeke *et al*.[46] and the current study multiplexed three distinct CEPs to determine the prevalence and dynamics of N-CIN within recurrent and drug-resistant EOC/HGSOC patient samples. Unfortunately, multiplexing is typically limited to ≤ 3-4 probes due to the limited number of distinct fluorophores that can be individually imaged without spectral overlap on most conventional fluorescent microscopes[46,71,118]. Additionally, the CEPs employed within this thesis are only capable of assessing changes of N-CIN in 3 specific chromosomes interrogated (*i.e.* chromosomes 8, 11 and 17) and cannot identify instances of N- or S-CIN involving non-labeled chromosomes (*e.g.* chromosomes 1, 2, 3, etc.)[71,82,126,127]. For example, Worrall *et. al*[128] utilized CEPs to determine that specific chromosomes (chromosomes 1 and 2) are prone to non-random mis-segregation events following mitotic arrest in both h-TERT immortalized human retinal pigment and fallopian epithelium cells. Moreover, the Worrall study suggested

chromosomes 1 and 2 exhibited non-random chromosome mis-segregation due to their large chromosome size and cohesion fatigue during anaphase. Within the current thesis, chromosomes 8, 11, and 17 exhibited both gains and losses in chromosome numbers and did not exhibit chromosome specific aneuploidy. This may be due to a variety of reasons, including: 1) chromosomes 8, 11 and 17 are smaller and exhibit less cohesion fatigue; 2) this thesis was evaluating changes in late stage HGSOC patient samples and the study by Worrall *et al.*[128] was performed in non-transformed diploid cell lines (*i.e.* different cell types); and 3) chromosome mis-segregation mechanisms likely differ between early transformation events and late stage HGSOC. Finally, an inherent limitation of the current study is that CEP analysis in solid tumors contained on the TMAs are not amenable to automation and must be manually counted, which can be labour intensive and time consuming. Nonetheless, these approaches have been successfully employed in both research and clinical settings, including both solid and hematological (liquid) cancers[118,129].

### 7.2.3 Sensitivity of Single-cell Quantitative Imaging (QuantIM) Approaches

In general, there was good concordance between the NA and $CS_c$ values calculated for each of the HGSOC ascites derived patient samples. However, there were instances where the two metrics differ. For example, OV009 (Fig S5-3, pg. 105) did not exhibit statistically significant changes in NA (Table S5-9, pg. 89), but exhibited statistically significant changes in $CS_c$ values (Table S5-12, pg. 90). While differences between NA and $CS_c$ values are uncommon, it likely reflects the differences in the sensitivity of each approach, emphasizing why these approaches have been combined. For example, significant changes in NAs most likely reflects large scale changes in DNA content (*i.e.* ploidy changes), rather than small scale changes associated with the

gain or loss of 1 or 2 chromosomes[46]. On the other hand, $CS_c$ values are expected to reflect both small and large scale changes in chromosome 8, 11 and 17; however, it is not capable of distinguishing subtle differences that can occur between a tetraploid cell (*e.g.* 92 chromosomes total, with 4 copies of chromosomes 8, 11 and 17) and an aneuploid cell (*e.g.* 52 chromosomes total, with 4 copies each of chromosomes 8, 11, and 17)[46]. Moreover, $CS_c$ values are only capable of assessing changes N-CIN in chromosomes 8, 11 and 17 and cannot identify instances of aneuploidy involving non-labeled chromosomes. Therefore, it is important to evaluate both metrics of CIN concurrently, when possible, for a more comprehensive assessment of CIN and its dynamics within HGSOC patient samples[46].

### 7.2.4 Fallopian Tube Secretory Epithelial Cells (FTSECs) as a Negative Control

An additional limitation of the current study is that there are no negative control cells (*i.e.* FTSECs). In a research setting, it would be ideal to have access to the distal end of normal fallopian tube fimbriae (FTF), STIC lesions, solid tumor and ascites derived tumor samples isolated from the same patient. Unfortunately, accessing tissue at different stages of HGSOC development from each patient is unrealistic as patients are typically diagnosed at late stages when HGSOC tumors have grown large enough to encompass normal FTF and STIC lesions[7,19–23]. Therefore, the next best available resource for negative control tissue is normal FTF removed for treatment of other medical conditions, including: 1) prophylactic prevention (*i.e.* risk reducing surgery in women harbouring *BRCA1/2* germline mutations)[130–132]; 2) to treat other conditions (*i.e.* removal of fallopian tubes due to ectopic pregnancy or during total hysterectomy to treat endometriosis)[133–135]; or 3) tubal ligation as a form of birth control (*i.e.* opportunistic salpingectomy during caesarean delivery of babies)[134]. Following removal of the fallopian tubes,

the FTF can be preserved in FFPE blocks, which can be sectioned and analyzed using the protocol detailed above in *Materials and Methods* (*Chapter 3*). Alternatively, FTF collected can be investigated using the Sectioning and Extensively Examining the Fimbriated End (SEE-FIM) protocol, which has the potential of identifying STIC lesions[136] for novel CIN investigation. Importantly, normal FTF collected from healthy women and women harbouring *BRCA1/2* mutations would permit insight into baseline variation of NAs, aid in establishing a NA CIN threshold, and validate our *CS* threshold.

### 7.3.0 CIN is Highly Prevalent in HGSOC Ascites Samples and Exhibits Temporal Dynamics

In this study, I determined that CIN, as characterized by NA heterogeneity and median $CS_c$ values $\geq 1$, was associated with 92.5% of HGSOC ascites derived patient samples (20/22 single patient samples and 43/46 serial patient samples) regardless of age, stage or chemotherapy status. Moreover, serial HGSOC patient samples exhibit temporal dynamics and, in general, aneuploidy and CIN increase with disease progression and recurrence, and had varied dynamics during treatments and following chemotherapy, suggesting that changes in CIN reflects the underlying biology driving disease progression, recurrence and drug response. For example, OV200 (Fig 5-9, pg. 69) exhibited increases in CIN as the disease progresses prior to any treatment, while OV063 (Fig S5-11, pg. 113), OV070 (Fig 5-12, pg. 76) and OV183 (Fig 5-13, pg. 80) exhibited increases in CIN following disease recurrence and drug resistance, demonstrating the potential association between recurrence/resistance and increases in aneuploidy and CIN. Importantly, similar observations have been previously reported by Penner-Goeke *et al.*[46] within serial samples isolated from the ascites of women over time, including those with responsive, recurrent and drug resistant EOC.

In addition to previously established CIN dynamics, this thesis highlighted novel CIN dynamics during/following paclitaxel and carboplatin treatments in serial HGSOC samples. For example, CIN in OV009 (Fig S5-3, pg. 105) decreased during initial paclitaxel and carboplatin treatments, while OV173 (Fig 5-11, pg. 73) and OV203 (Fig S5-2, pg. 104) had persistent levels of aneuploidy and CIN. Additionally, aneuploidy and CIN were determined to increase during paclitaxel and carboplatin treatments when utilized as a 3rd line chemotherapy treatment in OV001 (Fig S5-16, pg. 118). There are a number of factors determined to impact genome instability, and these factors are speculated to impact the heterogenous responses to paclitaxel and carboplatin treatments detailed above, including: 1) changes in chromosomes numbers (N-CIN) and structural changes (S-CIN) not measured by the single-cell quantitative methods used to evaluate CIN within the current study; 2) the varying mechanisms of CIN that can occur between patient samples (*e.g.* supernumerary centrosomes, elevated microtubule dynamics and DNA replication stress[137]); 3) the different timing of sample collection between patients; and 4) the varying level/rate of CIN observed within tumors (*i.e.* ITH), between tumors within an individual patient (*i.e.* spatially separated tumors) and between patients[138]. Moreover, a previous study by Swanton *et al.*[139] suggested that the level of CIN (based on the expression of 70 known CIN genes [*i.e.* CIN70 signature]) predicts ovarian cancer sensitivity to taxanes (*e.g.* paclitaxel and docetaxel). Importantly, they determined that high median CIN70 signature expression was associated with paclitaxel resistance, and a low median CIN70 signature expression was associated with paclitaxel sensitivity[139]. However, this study did not directly evaluate chromosomal alterations (N-CIN or S-CIN) or cell-to-cell heterogeneity, utilizes population-averaging techniques (*detailed in Section 1.2.1*) and evaluated a single sample from patients. Therefore, the current thesis is the second study to characterize CIN dynamics over time and in response to paclitaxel and carboplatin treatments.

In addition to the unique temporal dynamics described above, serial HGSOC samples exhibited varied CIN dynamics during/following second-line chemotherapy treatments. For example, OV180 (Fig S5-12, pg. 114) exhibited persistent CIN during doxorubicin treatments, OV299 (Fig S5-17, pg. 119) exhibited increases in CIN following bevacizumab and paclitaxel treatment, OV001 (Fig S5-16, pg. 118) exhibited decreases in CIN following tamoxifen treatment, while OV125 (Fig S5-1, pg. 103), OV183 (Fig 5-13, pg. 80), and OV299 exhibited persistent CIN during/following tamoxifen, although, the heterogeneous response to these second-line chemotherapies is likely due to ITH and the different drug mechanisms of action. Additionally, OV070 (Fig 5-12, pg. 76) and OV183 exhibited increases in CIN during doxorubicin and carboplatin treatments raising the question of whether changes in CIN reflect the pathologic changes driving disease progression, or those induced by drug treatments. Therefore, further investigation in a larger HGSOC cohort are needed to determine the temporal dynamics of CIN in response to the wide variety of second-line chemotherapy treatments for HGSOC.

Another unique aspect of this study is the novel investigation of CIN (characterized by NA heterogeneity and median $CS_c$ values $\geq 1$) in HGSOC patient samples harbouring *BRCA1/2* mutations. Importantly, this thesis determined that CIN was prevalent in 94.7% of *BRCA* positive HGSOC patient samples (18/19 samples derived from 9 patients) and exhibited unique temporal dynamics. For example, OV063 (Fig S5-11, pg. 113) exhibited an increase in CIN as the disease progressed and remained stable at a median $CS_c = 1$ following disease recurrence and multiple treatments. OV173 (Fig 5-11, pg. 73) exhibited CIN dynamics as the disease progressed and persisted during paclitaxel and carboplatin treatment. OV180 (Fig S5-12, pg. 114) exhibited CIN dynamics following diagnosis and persisted as disease progressed and during doxorubicin treatment. Notably, many of the past studies in HGSOC utilize traditional population averaging

techniques[140], therefore, this thesis is the first study to characterize the prevalence of CIN and unique temporal dynamics in HGSOC patient samples harbouring *BRCA1/2* mutations.

### 7.4.0 Solid Tumors Exhibit Extreme Levels of CIN

The final aspect of my thesis was to characterize the prevalence of CIN (characterized by median $CS_c$ values $\geq$ 1) in 36 HGSOC solid tumors collected during cytoreductive (*e.g.* 22 chemonaïve) and interval debulking (*e.g.* 14 chemosensitive) surgery. Importantly, this study determined that CIN was prevalent in 100% of HGSOC solid tumor samples (*i.e.* 36 unique patient samples cored in duplicate; total 72 cores). In general, 24 pairs of duplicate cores had the same median $CS_c$ values; however, 12 pairs of duplicate cores had different median $CS_c$ values, which is likely due to ITH. These difference in median $CS_c$ values can be expected, as ITH has be described in different sites collected from the same tumor[141]. Importantly, previous studies have focused on characterizing genetic heterogeneity and genome instability[138,141–143], therefore, the current thesis is the first study to characterize the prevalence of extreme CIN in HGSOC solid tumor samples.

We also had a unique opportunity to investigate the level of CIN in solid tumor and ascites samples collected from the same individual diagnosed with HGSOC. While CIN was prevalent in both solid tumors and ascites samples, all 10 HGSOC solid tumors had a higher median $CS_c$ than the patient-matched ascites samples and were categorized as having extreme levels of CIN (*i.e.* $CS_c$ values $\geq$ 3). This thesis is the first study to investigate the level of CIN in paired samples; however, many studies have evaluated genomic instability and spatial heterogeneity between solid tumors and ascites. For example, Schwarz *et al.*[142] and Kim *et al.*[143] constructed phylogenetic trees and evaluated the spatial heterogeneity between solid tumors, liquid biopsies and ascites samples

collected from patients diagnosed with HGSOC[142,143]. Importantly, these studies determined that genome instability was prevalent in each of the patient samples, but there were differences in clonal evolution between HGSOC patients, there were varying rates of evolution within patient samples, and a high degree of genetic heterogeneity within individual tumors and between their metastases[142,143]. Therefore, it is unsurprising that there were differing levels of CIN between solid tumors and ascites derived patient samples (*i.e.* metastatic disease). Additionally, the level of CIN observed in patient samples may be impacted by the varying techniques used to investigate solid tumors and ascites samples. For example, following surgery solid tumors are fixed in FFPE blocks and no longer able to divide, likely resulting in a larger proportion of cells exhibiting high levels of CIN that are not lost from the population during cell culture techniques. On the other hand, ascites derived patient samples have gone through a number of selection pressures, including: 1) isolation and tumor selective growth (*i.e.* in vitro adaptation)[45]; and 2) liquid nitrogen preservation and revival (*Sections 3.4.1* and *3.4.2*). It is possible that during these technical manipulations, cells exhibiting extreme levels of CIN were not viable or robust enough to grow and were lost from the population, resulting in lower median $CS_c$ values.

### 7.5.0 Future Directions

In order to further this study, collection of negative control cells can be incorporated into the study design. Ideally, this study would have access to patient matched FTSECs located at the distant end of FTF; however, both patient matched FTF and HGSOC tumor are not often available. Therefore, normal FTF removed for other conditions would be the next best available resource for a negative control. Importantly, having access to a negative control would permit insight into baseline variation of NAs, aid in establishing a NA CIN threshold, and validate our *CS* threshold.

Additionally, the data presented above (*Section 7.3.0*) outlines unique temporal dynamics as the disease progresses, upon disease recurrence and during/following chemotherapy highlighting CIN as a potential biomarker of disease progression; however, the levels of CIN (as characterized by NAs and *CS* values) must first be correlated to patient outcomes and clinical protein biomarkers (*i.e.* CA125 and HE4). If an association is established between CIN and patient outcomes or clinical protein biomarkers, this study will need to be expanded into a larger patient cohort in order to validate specific temporal trends. Moreover, this project can be expanded to investigate CIN in circulating tumor cells and to compare the temporal dynamics of CIN to changes in chromosome copy numbers (*e.g.* aneuploidy) and protein biomarkers that have recently been determined to be early detection/diagnostic biomarkers[32,144,145] and biomarkers of treatment response[146,147] in circulating tumor DNA (ctDNA) collected EOC patients. Importantly, this would allow investigation into a larger proportion of HGSOC patients, as only ~30% of HGSOC present with ascites and circulating tumor cells and ctDNA can be collected via non-invasive liquid biopsy (*i.e.* phlebotomy) from all consenting patients; however, isolation and investigation of circulating tumor cells and ctDNA requires specialized technologies, can be technically challenging and expensive (review previously by Lowes *et al.*[148]). Furthermore, CIN investigation in HGSOC solid tumors can be expanded into the Canadian Ovarian Cancer Experimental Unified Resource (COEUR), which is a large cohort comprised of more that 2000 EOC patient tissue samples with associated clinical data, including 1246 HGSOC samples[149]. Importantly, this will improve the statistical power of this study for biomarker discovery, although, manual CEPs enumeration in 100 nuclei/sample, in 1246 HGSOC samples would be very labor intensive and time consuming.

### 7.6.0 Significance

HGSOC represents 70% of all EOC diagnoses (~60 Manitobans annually) and 70-80% of all EOC deaths (~50 Manitobans annually). The high mortality in HGSOC patients is due to the lack of screening modalities, asymptomatic disease until late stages and high proportion of chemoresistant disease. Unfortunately, our current understanding of recurrent and chemoresistant disease is limited and the mechanisms driving disease progression, recurrence and drug resistance need to be identified. My research has determined that CIN is highly prevalent in both HGSOC ascites derived patient samples and solid tumors. Additionally, this work has highlighted the potential relationship between the temporal dynamics of CIN in HGSOC, with disease progression and acquisition of drug resistance emphasizing that CIN could potentially be a novel biomarker of disease progression. Importantly, CIN has just begun to be characterized in HGSOC, and understanding CIN dynamics in response disease progression, treatment and recurrence may have implications for new treatment interventions and ultimately improve the lives and outcome of women living with HGSOC.

## CHAPTER 8: REFERENCES


1. Society, C. C. Canadian Cancer Statistics 2019. *Can. Cancer Soc.* 1–95 (2019).
2. Euscher, E. D. Germ Cell Tumors of the Female Genital Tract. *Surg. Pathol. Clin.* **12**, 621–649 (2019).
3. Young, R. H. Ovarian sex cord-stromal tumours and their mimics. *Pathology* **50**, 5–15 (2018).
4. Navaneelan, T. & Ellison, L. Health at a Glance Ovarian cancer : Survival statistics. (2015).
5. Ayhan, A. *et al.* High grade serous ovarian carcinomas originate in the fallopian tube. *Nat. Commun.* **8**, 1–10 (2017).
6. Rojas, V., Hirshfield, K. M., Ganesan, S. & Rodriguez-Rodriguez, L. Molecular characterization of epithelial ovarian cancer: Implications for diagnosis and treatment. *Int. J. Mol. Sci.* **17**, (2016).
7. Kroeger, P. T. & Drapkin, R. Pathogenesis and heterogeneity of ovarian cancer. *Curr. Opin. Obstet. Gynecol.* **29**, 26–34 (2017).
8. Singer, G. *et al.* BRIEF Mutations in BRAF and KRAS Characterize the. *Communication* **95**, 6–8 (2003).
9. Obata, K. *et al.* Frequent PTEN/MMAC mutations in endometrioid but not serous or mucinous epithelial ovarian tumors. *Cancer Res.* **58**, 2095–2097 (1998).
10. Singer, G. *et al.* Patterns of p53 mutations separate ovarian serous borderline tumors and low- and high-grade carcinomas and provide support for a new model of ovarian carcinogenesis: A mutational analysis with immunohistochemical correlation. *Am. J. Surg. Pathol.* **29**, 218–224 (2005).
11. Bowtell, D. D. Rethinking ovarian cancer II: reducing mortality from high-grade serous ovarian cancer. *Nat Rev Cancer* **15**, 668–679 (2016).
12. Lengyel, E. Ovarian cancer development and metastasis. *Am. J. Pathol.* **177**, 1053–1064 (2010).
13. Ahmed, N. & Stenvers, K. L. Getting to know ovarian cancer ascites: Opportunities for targeted therapy-based translational research. *Front. Oncol.* **3 SEP**, 1–12 (2013).
14. Coleman, R. L., Monk, B. J., Sood, A. K. & Herzog, T. J. Latest research and clinical treatment of advanced-stage epithelial ovarian cancer. *Natl. Rev. Clin. Oncol.* **10**, 211–224 (2013).
15. Network, C. G. A. Integrate Genomic Analyses of Ovarian Carcinoma. *Nature* **474**, 609–615 (2011).
16. Altman, A. D. *et al.* The diagnostic utility of TP53 and CDKN2A to distinguish ovarian high-grade serous carcinoma from low-grade serous ovarian tumors. *Mod. Pathol.* **26**, 1255–1263 (2013).
17. Köbel, M. *et al.* Ovarian carcinoma histotype determination is highly reproducible, and is improved through the use of immunohistochemistry. *Histopathology* **64**, 1004–1013 (2014).
18. LePage, C. *et al.* Optimized p53 immunohistochemistry is an accurate predictor of TP53 mutation in ovarian carcinoma . *J. Pathol. Clin. Res.* **2**, 247–258 (2016).
19. Karst, A. M., Levanon, K. & Drapkin, R. Modeling high-grade serous ovarian carcinogenesis from the fallopian tube. *Proc. Natl. Acad. Sci.* **108**, 7547–7552 (2011).
20. Kurman, R. & Shih, I. Molecular Pathogenesis and Extraovarian Origin of Epithelial

Ovarian Cancer. Shifting the Paradigm. *Hum Pathol* **42**, 918–931 (2011).
21. Nakamura, K. *et al.* Reconstitution of high-grade serous ovarian carcinoma from primary fallopian tube secretory epithelial cells. *Oncotarget* **9**, 12609–12619 (2018).
22. Lee, Y. *et al.* A candidate precursor to serous carcinoma that originates in the distal fallopian tube. *J. Pathol.* **211**, 26–35 (2007).
23. Kurman, R. J. & Shih, I. M. The Origin and Pathogenesis of Epithelial Ovarian Cancer - a Proposed Unifying Theory. *Am J Surg Pathol* **34**, 433–443 (2010).
24. Marquez, R. T. *et al.* Patterns of gene expression in different histotypes of epithelial ovarian cancer correlate with those in normal fallopian tube, endometrium, and colon. *Clin. Cancer Res.* **11**, 6116–6126 (2005).
25. Paul, A. & Paul, S. The breast cancer susceptibility genes (BRCA) in breast and ovarian cancers. *Front. Biosci. - Landmark* **19**, 605–618 (2014).
26. Gorodetska, I., Kozeretska, I. & Dubrovska, A. BRCA genes: The role in genome stability, cancer stemness and therapy resistance. *J. Cancer* **10**, 2109–2127 (2019).
27. Roberts, C. M., Cardenas, C. & Tedja, R. The role of intra-tumoral heterogeneity and its clinical relevance in epithelial ovarian cancer recurrence and metastasis. *Cancers (Basel).* **11**, (2019).
28. Rebbeck, T. R. *et al.* Association of type and location of BRCA1 and BRCA2 mutations with risk of breast and ovarian cancer. *JAMA - J. Am. Med. Assoc.* **313**, 1347–1361 (2015).
29. Doubeni, C., Doubeni, A. & Myers, A. Diagnosis and management of ovarian disorders. *Am. Fam. Physician* **93**, 937–944 (2016).
30. 2019, O. C. C. Ovarian Cancer Canada; Signs & Symptoms. (2019). Available at: https://ovariancanada.org/About-Ovarian-Cancer/Detection/Signs-Symptoms. (Accessed: 2nd March 2020)
31. Javadi, S., Ganeshan, D. M., Qayyum, A., Iyer, R. B. & Bhosale, P. Ovarian cancer, the revised FIGO staging system, and the role of imaging. *Am. J. Roentgenol.* **206**, 1351–1360 (2016).
32. Whitwell, H. J. *et al.* Improved early detection of ovarian cancer using longitudinal multimarker models. *Br. J. Cancer* (2020). doi:10.1038/s41416-019-0718-9
33. Id, O. *et al.* CA-125 reduction during neoadjuvant chemotherapy is associated with success of cytoreductive surgery and outcome of patients with advanced high-grade ovarian cancer. doi:10.1111/aogs.13814
34. Orr, B. & Edwards, R. P. Diagnosis and Treatment of Ovarian Cancer. *Hematol. Oncol. Clin. North Am.* **32**, 943–964 (2018).
35. Mutch, D. G. & Prat, J. 2014 FIGO staging for ovarian, fallopian tube and peritoneal cancer. *Gynecol. Oncol.* **133**, 401–404 (2014).
36. Narod, S. Can advanced-stage ovarian cancer be cured? *Nat. Rev. Clin. Oncol.* **13**, 255–261 (2016).
37. Torre, L. A. *et al.* Ovarian cancer statistics, 2018. *CA. Cancer J. Clin.* **68**, 284–296 (2018).
38. Kipps, E., Tan, D. S. P. & Kaye, S. B. Meeting the challenge of ascites in ovarian cancer: new avenues for therapy and research Europe PMC Funders Author Manuscripts. *Nat. Rev. Cancer* **13**, 273–282 (2013).
39. Bregenzer, M. E. *et al.* The role of cancer stem cells and mechanical forces in ovarian cancer metastasis. *Cancers (Basel).* **11**, 1–22 (2019).

40. Nwani, N. G., Sima, L. E., Nieves-Neira, W. & Matei, D. Targeting the microenvironment in high grade serous ovarian cancer. *Cancers (Basel).* **10**, 1–22 (2018).
41. Lane, D., Matte, I., Garde-Granger, P., Bessette, P. & Piché, A. Ascites IL-10 Promotes Ovarian Cancer Cell Migration. *Cancer Microenviron.* **11**, 115–124 (2018).
42. Kampan, N. C. *et al.* Interleukin 6 Present in inflammatory ascites from advanced epithelial ovarian cancer patients promotes tumor necrosis factor receptor 2-expressing regulatory T cells. *Front. Immunol.* **8**, 1–14 (2017).
43. Liang, B., Guo, Z., Li, Y. & Liu, C. Elevated VEGF concentrations in ascites and serum predict adverse prognosis in ovarian cancer. *Scand. J. Clin. Lab. Invest.* **73**, 309–314 (2013).
44. Ha, J. *et al.* LPA Induces Metabolic Reprogrammin in Ovarian Cancer via Pseudohypoxic Response. *Cancer Res* **78**, 1923–1934 (2018).
45. Shepherd, T. G., Thériault, B. L., Campbell, E. J. & Nachtigal, M. W. Primary culture of ovarian surface epithelial cells and ascites-derived ovarian cancer cells from patients. *Nat. Protoc.* **1**, 2643–2649 (2007).
46. Penner-Goeke, S. *et al.* The temporal dynamics of chromosome instability in ovarian cancer cell lines and primary patient samples. *PLoS Genet.* **13**, 1–24 (2017).
47. Lisio, M. A., Fu, L., Goyeneche, A., Gao, Z. H. & Telleria, C. High-grade serous ovarian cancer: Basic sciences, clinical and therapeutic standpoints. *Int. J. Mol. Sci.* **20**, (2019).
48. Brooks, S. Preoperative Evaluation of Patients with Suspected Ovarian Cancer. *Gynecol. Oncol.* **55**, S80–S90 (1994).
49. Mayba, J. *et al.* Examining the Selection Criteria of Neoadjuvant Chemotherapy Patients. *J. Obstet. Gynaecol. Canada* **40**, 595–603 (2018).
50. Gadducci, A. *et al.* Current strategies for the targeted treatment of high-grade serous epithelial ovarian cancer and relevance of BRCA mutational status. *J. Ovarian Res.* **12**, 1–8 (2019).
51. Wishart, D. S. *et al.* DrugBank 5.0: A major update to the DrugBank database for 2018. *Nucleic Acids Res.* **46**, D1074–D1082 (2018).
52. Monk, B. J., Randall, L. M. & Grisham, R. N. The Evolving Landscape of Chemotherapy in Newly Diagnosed Advanced Epithelial Ovarian Cancer. *Am. Soc. Clin. Oncol. Educ. B.* e141–e151 (2019). doi:10.1200/edbk_239007
53. Oken, M. M. *et al.* Toxicity and response criteria of the Easter Cooperative Oncology Group. *Am. J. Clin. Oncol.* **5**, 649–656 (1982).
54. Bommert, M., Harter, P., Heitz, F. & du Bois, A. When should Surgery be used for Recurrent Ovarian Carcinoma? *Clin. Oncol.* **30**, 493–497 (2018).
55. Cohen, S., Schwartz, M., Dottino, P. & Beddoe, A. M. Use of a multi-drug regimen gemcitabine, 5-fluorouracil, irinotecan, cisplatin, bevacizumab, docetaxel, and cyclophosphamide (GFIP/BDC) for heavily pretreated relapsed epithelial ovarian, fallopian tube and primary peritoneal cancer. *J. Ovarian Res.* **12**, 1–7 (2019).
56. Pendlebury, A., Debernardo, R. & Rose, P. G. Long-term use of pegylated liposomal doxorubicin to a cumulative dose of 4600 mg/m2 in recurrent ovarian cancer. *Anticancer. Drugs* **28**, 815–817 (2017).
57. Hyman, D. M. *et al.* Topotecan in patients with BRCA-associated and sporadic platinum-resistant ovarian, fallopian tube, and primary peritoneal cancers. *Gynecol. Oncol.* **123**, 196–199 (2011).
58. Sachdev, E., Tabatabai, R., Roy, V., Rimel, B. J. & Mita, M. M. PARP Inhibition in

Cancer: An Update on Clinical Development. *Target. Oncol.* **14**, 657–679 (2019).
59. Cojocaru, E., Parkinson, C. A. & Brenton, J. D. Personalising Treatment for High-Grade Serous Ovarian Carcinoma. *Clin. Oncol.* **30**, 515–524 (2018).
60. Monk, B. J., Minion, L. E. & Coleman, R. L. Anti-angiogenic agents in ovarian cancer: Past, present, and future. *Ann. Oncol.* **27**, i33–i39 (2016).
61. George, A. *et al.* The role of hormonal therapy in patients with relapsed high-grade ovarian carcinoma: A retrospective series of tamoxifen and letrozole. *BMC Cancer* **17**, 4–11 (2017).
62. Stanley, B. *et al.* Endocrine treatment of high grade serous ovarian carcinoma; quantification of efficacy and identification of response predictors. *Gynecol. Oncol.* **152**, 278–285 (2019).
63. Leditschke, J. *et al.* Whole–genome characterization of chemoresistant ovarian cancer. *Nature* **521**, 489–494 (2015).
64. Freimund, A. E., Beach, J. A., Christie, E. L. & Bowtell, D. D. L. Mechanisms of Drug Resistance in High-Grade Serous Ovarian Cancer. *Hematol. Oncol. Clin. North Am.* **32**, 983–996 (2018).
65. Binju, M. *et al.* Mechanisms underlying acquired platinum resistance in high grade serous ovarian cancer - a mini review. *Biochim. Biophys. Acta - Gen. Subj.* **1863**, 371–378 (2019).
66. Wimmel, A., Lucibello, F. C., Sewing, A., Adolph, S. & Müller, R. Inducible acceleration of G 1 progression through tetracycline-regulated expression of human cyclin E. *Oncogene* **9**, 995–997 (1994).
67. Siu, K. T., Rosner, M. R. & Minella, A. C. An integrated view of cyclin E function and regulation © 2012 Landes Bioscience . Do not distribute . © 2012 Landes Bioscience . Do not distribute . *Cell Cycle* 57–64 (2012).
68. Mayr, D. *et al.* Analysis of gene amplification and prognostic markers in ovarian cancer using comparative genomic hybridization for microarrays and immunohistochemical analysis for tissue microarrays. *Am. J. Clin. Pathol.* **126**, 101–109 (2006).
69. Hanahan, D. & Weinberg, R. A. Hallmarks of cancer: The next generation. *Cell* **144**, 646–674 (2011).
70. Geigl, J. B., Obenauf, A. C., Schwarzbraun, T. & Speicher, M. R. Defining 'chromosomal instability'. *Trends Genet.* **24**, 64–69 (2008).
71. Lepage, C. C., Morden, C. R., Palmer, M. C. L., Nachtigal, M. W. & McManus, K. J. Detecting chromosome instability in cancer: Approaches to resolve cell-to-cell heterogeneity. *Cancers (Basel).* **11**, (2019).
72. Sieber, O. M., Heinimann, K. & Tomlinson, I. Genomic instability — the engine of tumorigenesis ? **3**, 469–476 (2003).
73. Beckman, R. A. & Loeb, L. A. Genetic instability in cancer: Theory and experiment. *Semin. Cancer Biol.* **15**, 423–435 (2005).
74. Rajagopalan, H., Nowak, M. A. & Vogelstein, B. The significance of unstable chromosomes in colorectal cancer. **3**, 5–10 (2003).
75. Negrini, S., Gorgoulis, V. G. & Halazonetis, T. D. Genomic instability — an evolving hallmark of cancer. **11**, 220–228 (2010).
76. Michigami, Y., Watari, J., Ito, C., Nakai, K. & Yamasaki, T. Long-term effects of H. pylori eradication on epigenetic alterations related to gastric carcinogenesis. *Sci. Rep.* 1–13 (2018). doi:10.1038/s41598-018-32717-3

77. Bell, D. W. & Ellenson, L. H. Molecular Genetics of Endometrial Carcinoma. 337–365 (2019).
78. Gelsomino, F., Barbolini, M., Spallanzani, A., Pugliese, G. & Cascinu, S. The evolving role of microsatellite instability in colorectal cancer: A review. *Cancer Treat. Revews* **51**, 19–26 (2016).
79. Miller, B. F., Sánchez-Vega, F. & Elnitski, L. The emergence of pan-cancer CIMP and its elusive interpretation. *Biomolecules* **6**, 1–14 (2016).
80. Nowak, M. A. *et al.* The role of chromosomal instability in tumor initiation. *Proc. Natl. Acad. Sci. U. S. A.* **99**, 16226–16231 (2002).
81. Burrell, R. A. *et al.* Replication stress links structural and numerical cancer chromosomal instability. *Nature* **494**, 492–496 (2013).
82. Thompson, L. L., Jeusset, L. M. P., Lepage, C. C. & McManus, K. J. Evolving therapeutic strategies to exploit chromosome instability in cancer. *Cancers (Basel).* **9**, 1–23 (2017).
83. Cahill, D. P., Kinzler, K. W., Vogelstein, B. & Lengauer, C. Genetic instability and darwinian selection in tumours. *Trends Cell Biol.* **9**, M57-60 (1999).
84. Levine, M. S. & Holland, A. J. The impact of mitotic errors on cell proliferation and tumorigenesis. *Genes Dev.* **32**, 620–638 (2018).
85. Pavelka, N., Rancati, G. & Li, R. Dr Jekyll and Mr Hyde: role of aneuploidy in cellular adaptation and cancer. *Curr. Opin. Cell Biol.* **22**, 809–815 (2010).
86. Michor, F., Iwasa, Y., Vogelstein, B., Lengauer, C. & Nowak, M. A. Can chromosomal instability initiate tumorigenesis? *Semin. Cancer Biol.* **15**, 43–49 (2005).
87. Sakthianandeswaren, A. *et al.* MACROD2 haploinsufficiency impairs catalytic activity of PARP1 and promotes chromosome instability and growth of intestinal tumors. *Cancer Discov.* **8**, 988–1005 (2018).
88. Sansregret, L., Vanhaesebroeck, B. & Swanton, C. Determinants and clinical implications of chromosomal instability in cancer. *Nat. Rev. Clin. Oncol.* **15**, 139–150 (2018).
89. Duesberg, P., Stindl, R. & Hehlmann, R. Origin of multidrug resistance in cells with and without multidrug resistance genes: chromosome reassortments catalyzed by aneuploidy. *Proc. Natl. Acad. Sci. U. S. A.* **98**, 11283–11288 (2001).
90. Gao, C. *et al.* Chromosome instability, chromosome transcriptome, and clonal evolution of tumor cell populations. *Proc. Natl. Acad. Sci. U. S. A.* **104**, 8995–9000 (2007).
91. Bayani, J. *et al.* Genomic mechanisms and measurement of structural and numerical instability in cancer cells. *Semin. Cancer Biol.* **17**, 5–18 (2007).
92. Cunningham, C. E. *et al.* Targeting the CINful genome: Strategies to overcome tumor heterogeneity. *Prog. Biophys. Mol. Biol.* (2019). doi:10.1016/j.pbiomolbio.2019.02.006
93. Bakhoum, S. F. & Landau, D. A. Chromosomal instability as a driver of tumor heterogeneity and evolution. *Cold Spring Harb. Perspect. Med.* **7**, 1–14 (2017).
94. Lee, A. J. X. *et al.* Chromosomal Instability Confers Intrinsic Multi-Drug Resistance. **71**, 1858–1870 (2011).
95. Gerlinger, M. & Swanton, C. How Darwinian models inform therapeutic failure initiated by clonal heterogeneity in cancer medicine. *Br. J. Cancer* **103**, 1139–1143 (2010).
96. Bakhoum, S. F. & Cantley, L. C. The Multifaceted Role of Chromosomal Instability in Cancer and Its Microenvironment. *Cell* **174**, 1347–1360 (2018).
97. Stanta, G. & Bonin, S. Overview on Clinical Relevance of Intra-Tumor Heterogeneity. *Front. Med.* **5**, 1–10 (2018).
98. Burrell, R. A. & Swanton, C. Tumour heterogeneity and the evolution of polyclonal drug

resistance. *Mol. Oncol.* **8**, 1095–1111 (2014).
99. Wang, W. *et al.* Chromosomal instability and acquired drug resistance in multiple myeloma. *Oncotarget* **8**, 78234–78244 (2017).
100. Leontovich, A. A. *et al.* NOTCH3 expression is linked to breast cancer seeding and distant metastasis. *Breast Cancer Res.* **20**, 1–19 (2018).
101. Guo, X. *et al.* Geraniin selectively promotes cytostasis and apoptosis in human colorectal cancer cells by inducing catastrophic chromosomal instability. *Mutagenesis* **33**, 271–281 (2018).
102. Benhra, N., Barrio, L., Muzzopappa, M. & Milán, M. Chromosomal Instability Induces Cellular Invasion in Epithelial Tissues. *Dev. Cell* 1–14 (2018). doi:10.1016/j.devcel.2018.08.021
103. Giam, M. & Rancati, G. Aneuploidy and chromosomal instability in cancer: A jackpot to chaos. *Cell Div.* **10**, 1–12 (2015).
104. McGranahan, N., Burrell, R. A., Endesfelder, D., Novelli, M. R. & Swanton, C. Cancer chromosomal instability: Therapeutic and diagnostic challenges. *EMBO Rep.* **13**, 528–538 (2012).
105. McManus, K. J. & Thompson, L. L. A novel multiplexed, image-based approach to detect phenotypes that underlie chromosome instability in human cells. *PLoS One* **10**, 1–17 (2015).
106. Janssen, A., Kops, G. J. P. L. & Medema, R. H. Elevating the frequency of chromosome mis-segregation as a strategy to kill tumor cells. *Proc. Natl. Acad. Sci. U. S. A.* **106**, 19108–19113 (2009).
107. Bakhoum, S. F. & Compton, D. A. Chromosomal instability and cancer: A complex relationship with therapeutic potential. *J. Clin. Invest.* **122**, 1138–1143 (2012).
108. Cunningham, C. E. *et al.* Therapeutic relevance of the protein phosphatase 2A in cancer. *Oncotarget* **7**, 61544–61561 (2016).
109. Barresi, V. *et al.* Chromosomal instability analysis and regional tumor heterogeneity in colon cancer. *Cancer Genet.* **210**, 9–21 (2017).
110. Uehara, Y. *et al.* Integrated copy number and expression analysis identifies profiles of whole-arm chromosomal alterations and subgroups with favorable outcome in ovarian clear cell carcinomas. *PLoS One* **10**, e0128066 (2015).
111. Castagnola, P. *et al.* Genomic DNA Copy Number Aberrations, Histological Diagnosis, Oral Subsite and Aneuploidy in OPMDs/OSCCs. *PLoS One* **10**, e0142294 (2015).
112. Kohlruss, M. *et al.* A microsatellite based multiplex PCR method for the detection of chromosomal instability in gastric cancer. *Sci. Rep.* **8**, 12551 (2018).
113. Jones, A. M. *et al.* Analysis of copy number changes suggests chromosomal instability in a minority of large colorectal adenomas. *J. Pathol.* **213**, 249–256 (2007).
114. Bakker, B. *et al.* Single-cell sequencing reveals karyotype heterogeneity in murine and human malignancies. *Genome Biol.* **17**, 1–15 (2016).
115. Yuan, C. *et al.* The MTDH (-470G>A) Polymorphism Is Associated with Ovarian Cancer Susceptibility. *PLoS One* **7**, 3–7 (2012).
116. Taube, E. T. *et al.* Wilms tumor protein 1 (WT1) - Not only a diagnostic but also a prognostic marker in high-grade serous ovarian carcinoma. *Gynecol. Oncol.* **140**, 494–502 (2016).
117. Welcsh, P. L. BRCA1 and BRCA2 and the genetics of breast and ovarian cancer. *Hum. Mol. Genet.* **10**, 705–713 (2001).

118. Cisyk, A. L. *et al.* Characterizing the Prevalence of Chromosome Instability in Interval Colorectal Cancer. *Neoplasia* **17**, 306–316 (2015).
119. Cooper, G. M. *The Cell: A Molecular Approach. 2nd edition.* (2000).
120. Arends, M. J. Pathways of colorectal carcinogenesis. *Appl. Immunohistochem. Mol. Morphol.* **21**, 97–102 (2013).
121. Abdel-Rahman, W. M. *et al.* Spectral karyotyping suggests additional subsets of colorectal cancers characterized by pattern of chromosome rearrangement. *Proc. Natl. Acad. Sci. U. S. A.* **98**, 2538–2543 (2001).
122. Wilson, M. K. *et al.* Fifth ovarian cancer consensus conference of the gynecologic cancer intergroup: Recurrent disease. *Ann. Oncol.* **28**, 727–732 (2017).
123. Markossian, S., Arnaoutov, A., Saba, N. S., Larionov, V. & Dasso, M. Quantitative assessment of chromosome instability induced through chemical disruption of mitotic progression. *Cell Cycle* **15**, 1706–1714 (2016).
124. Nielsen, K., Petersen, S. & Orntoft, T. A comparison between stereological estimates of mean nuclear volume and DNA flow cytometry in bladder tumours. *APMIS* **97**, 949–56 (1989).
125. Capo-chichi, C. D. *et al.* Nuclear envelope structural defects cause chromosomal numerical instability and aneuploidy in ovarian cancer. *BMC Med.* **9**, 28 (2011).
126. Bakker, B., van den Bos, H., Lansdorp, P. M. & Foijer, F. How to count chromosomes in a cell: An overview of current and novel technologies. *BioEssays* **37**, 570–577 (2015).
127. Speicher, M. R. & Carter, N. P. The new cytogenetics: Blurring the boundaries with molecular biology. *Nat. Rev. Genet.* **6**, 782–792 (2005).
128. Worrall, J. T. *et al.* Non-random Mis-segregation of Human Chromosomes. *Cell Rep.* **23**, 3366–3380 (2018).
129. Roylance, R. *et al.* Expression of regulators of mitotic fidelity are associated with intercellular heterogeneity and chromosomal instability in primary breast cancer. *Breast Cancer Res. Treat.* **148**, 221–229 (2014).
130. Kotsopoulos, J. & Narod, S. Prophylactic salpingectomy for the prevention of ovarian cancer; who should we target? *Int. J. Cancer* 1–30 (2020). doi:10.1017/CBO9781107415324.004
131. Dilley, S. E., Straughn, J. M. & Leath, C. A. The evolution of and evidence for opportunistic salpingectomy. *Obstet. Gynecol.* **130**, 814–824 (2017).
132. Center, T. U. of T. M. A. C. A Study for Women at High-risk for Ovarian Cancer. WISP: Women Choosing Surgical Prevention. (2019). Available at: https://wisp.mdanderson.org/. (Accessed: 13th March 2020)
133. Rodgers, R. *et al.* The effect of laparoscopic salpingectomy for ectopic pregnancy on ovarian reserve. *Aust. New Zeal. J. Obstet. Gynaecol.* 1–6 (2020). doi:10.1111/ajo.13129
134. Hanley, G. E. *et al.* Examining indicators of early menopause following opportunistic salpingectomy: A cohort study from British Columbia, Canada. *Am. J. Obstet. Gynecol.* (2020). doi:10.1016/j.ajog.2020.02.005
135. Lamblin, G. *et al.* Opportunistic salpingectomy during vaginal hysterectomy for a benign pathological condition. *Int. Urogynecol. J.* **29**, 715–721 (2018).
136. Koc, N., Ayas, S. & Arinkan, S. A. Comparison of the classical method and SEE-FIM protocol in detecting microscopic lesions in fallopian tubes with gynecological lesions. *J. Pathol. Transl. Med.* **52**, 21–27 (2018).
137. Tamura, N. *et al.* Mechanisms of Chromosomal Instability in High-grade Serous Ovarian

Carcinoma. 1–36 (2019). doi:10.1101/727537
138. Lambrechts, S. *et al.* Genetic heterogeneity after first-line chemotherapy in high-grade serous ovarian cancer. *Eur. J. Cancer* **53**, 51–64 (2016).
139. Swanton, C. *et al.* Chromosomal instability determines taxane response. *Proc. Natl. Acad. Sci. U. S. A.* **106**, 8671–8676 (2009).
140. Lee, Y. J. *et al.* Genomic profiling of the residual disease of advanced high-grade serous ovarian cancer after neoadjuvant chemotherapy. *Int. J. Cancer* **146**, 1851–1861 (2020).
141. Bashashati, A. *et al.* Distinct evolutionary trajectories of primary high-grade serous ovarian cancers revealed through spatial mutational profiling. *J. Pathol.* **231**, 21–34 (2013).
142. Schwarz, R. F. *et al.* Spatial and Temporal Heterogeneity in High-Grade Serous Ovarian Cancer: A Phylogenetic Analysis. *PLoS Med.* **12**, 1–20 (2015).
143. Kim, S. *et al.* Evaluating Tumor Evolution via Genomic Profiling of Individual Tumor Spheroids in a Malignant Ascites. *Sci. Rep.* **8**, 1–11 (2018).
144. Vanderstichele, A. *et al.* Chromosomal instability in cell-free DNA as a highly specific biomarker for detection of ovarian cancer in women with adnexal masses. *Clin. Cancer Res.* **23**, 2223–2231 (2017).
145. Cohen, J. D. *et al.* Detection and localization of surgically resectable cancers with a multi-analyte blood test. **359**, 926–930 (2018).
146. Kim, Y. M. *et al.* Prospective study of the efficacy and utility of TP53 mutations in circulating tumor DNA as a non-invasive biomarker of treatment response monitoring in patients with high-grade serous ovarian carcinoma. *J. Gynecol. Oncol.* **30**, 1–13 (2019).
147. Arend, R. *et al.* Molecular Resonse to Neoadjuvant Chemotherapy in High-Grade Serous Ovarian Carcinoma. *Physiol. Behav.* **16**, 1–24 (2018).
148. Lowes, L. E. *et al.* Circulating tumor cells (CTC) and cell-free DNA (cfDNA)workshop 2016: Scientific opportunities and logistics for cancer clinical trial incorporation. *Int. J. Mol. Sci.* **17**, (2016).
149. Le Page, C. *et al.* Characteristics and outcome of the COEUR Canadian validation cohort for ovarian cancer biomarkers. *BMC Cancer* **18**, 1–18 (2018).

## APPENDIX A: SOLUTIONS

### CELL CULTURE

DMEM, F12 Complete Cell Culture Media (2% Ultroser G)

| Name | Amount |
|---|---|
| Dublecco's Modified Eagle's Medium Nutrient Mixture F-12 (1:1) | 1 pouch |
| $NaHCO_3$ | 2.4 g |
| $ddH_2O$ | up to 1.0 L total volume |
| Total Volume | 1.0 L |

- Titrate to pH 7.0
- Pass through 0.22 µm filter prior to use
- Store in 500 mL aliquots in fridge, bring to room temperature prior to use
- Add 10 mL of Ultroser G to 490 mL of media prior to use

Medium 199/MCDB 105 Medium Complete Cell Culture Media (10% fetal bovine serum [FBS])

| Name | Amount |
|---|---|
| Medium 199 | 1 pouch |
| MCDB105 Medium | 1 jar |
| $NaHCO_3$ | 2.2 g |
| $ddH_2O$ | up to 1.0 L total volume |
| Total Volume | 1.0 L |

- Titrate to pH 7.0
- Pass through 0.22 µm filter prior to use
- Store in 500 mL aliquots in fridge, bring to room temperature before use
- Add 50 mL of FBS to 450 mL of media prior to use

10x PBS (Stock Solution)

| Name | Amount |
|---|---|
| NaCl | 80.0 g |
| KCl | 2.0 g |
| $Na_2HPO_4$ | 14.4 g |
| $KH_2PO_4$ | 2.4 g |
| $ddH_2O$ | up to 1.0 L total volume |
| Total Volume | 1.0 L |

- Titrate to pH 7.4

1x PBS

| Name | Amount |
|---|---|
| 10x PBS (stock) | 100.0 mL |
| $ddH_2O$ | 900.0 mL |
| Total Volume | 1.0 L |

- Pass through 0.45 µm filter prior to use

**MITOTIC CHROMOSOME SPREADS**

1M KCl (Stock Solution)

| Name | Amount |
|---|---|
| KCl | 7.5 g |
| $ddH_2O$ | up to 100.0 mL total volume |
| Total Volume | 100.0 mL |

75mM KCl (Hypotonic Solution)

| Name | Amount |
|---|---|
| 1M KCl (stock) | 750.0 µL |
| $ddH_2O$ | up to 10.0 mL total volume |
| Total Volume | 10.0 mL |

**CELL FIXATION**

3:1 Methanol:Acetic Acid (Fixative)

| Name | Amount |
|---|---|
| Methanol | 3.0 mL |
| Acetic Acid | 1.0 mL |
| Total Volume | 4.0 mL |

**FLUORESCENCE *IN SITU* HYBRIDIZATION OF CELL LINES AND PRIMARY PATIENT SAMPLES**

20x SSC (Stock Solution)

| Name | Amount |
|---|---|
| NaCl | 175.3 g |
| NaCitrate (Dihydrate) | 88.2 g |
| $ddH_2O$ | up to 1.0 L total volume |
| Total Volume | 1.0 L |

- Titrate to pH 7.0 with NaOH
- Pass through 0.45 µm filter prior to use

2x SSC

| Name | Amount |
|---|---|
| 20x SSC (stock) | 100.0 mL |
| $ddH_2O$ | 900.0 mL |
| Total Volume | 1.0 L |

- Pass through 0.45 µm filter prior to use

1x SSC

| Name | Amount |
|---|---|
| 20x SSC (stock) | 50.0 mL |
| $ddH_2O$ | 950.0 mL |
| Total Volume | 1.0 L |

- Pass through 0.45 µm filter prior to use

1M HCl (Stock Solution)

| Name | Amount |
|---|---|
| HCl (concentrated, 36.5%) | 8.3 mL |
| $ddH_2O$ | 91.7 mL |
| Total Volume | 100.0 mL |

0.01M HCl

| Name | Amount |
|---|---|
| 1M HCl (stock) | 0.5 mL |
| $ddH_2O$ | 49.5 mL |
| Total Volume | 50.0 mL |

Pepsin

| Name | Amount |
|---|---|
| Pepsin (stock, 100 mg/mL) | 25 µL |
| 0.01 M HCl | 50.0 mL |
| Total Volume | ~50.0 mL |

1M $MgCl_2$

| Name | Amount |
|---|---|
| $MgCl_2$ | 20.3 g |
| $ddH_2O$ | up to 100.0 mL total volume |
| Total Volume | 100.0 mL |

1x PBS/50 mM $MgCl_2$

| Name | Amount |
|---|---|
| 1M $MgCl_2$ | 5.0 mL |
| 10x PBS (stock) | 10.0 mL |
| $ddH_2O$ | up to 100.0 mL total volume |
| Total Volume | 100.0 mL |

1% Formaldehyde/1x PBS/50 mM $MgCl_2$

| Name | Amount |
|---|---|
| 37% formaldehyde | 1.35 mL |
| 1x PBS/50 mM $MgCl_2$ | 48.3 mL |
| Total Volume | 50.0 mL |

70% Ethanol

| Name | Amount |
|---|---|
| 95% Ethanol | 73.7 mL |
| $ddH_2O$ | 26.3 mL |
| Total Volume | 100.0 mL |

90% Ethanol

| Name | Amount |
|---|---|
| 95% Ethanol | 94.7 mL |
| $ddH_2O$ | 5.3 mL |
| Total Volume | 100.0 mL |

70% deionized Formamide/2x SSC

| Name | Amount |
|---|---|
| Deionized formamide | 70.0 µL |
| 2x SSC | 30.0 µL |
| Total Volume | 100.0 µL |

50% Formamide/2xSSC

| Name | Amount |
|---|---|
| Formamide | 500.0 mL |
| 20x SSC (stock) | 50.0 mL |
| $ddH_2O$ | up to 1.0 L total volume |
| Total Volume | 1.0 L |

DAPI (Stock Solution, 50 µg/mL)

| Name | Amount |
|---|---|
| DAPI | 50.0 µg |
| 1x PBS | 1.0 mL |
| Total Volume | 1.0 mL |

DAPI for FISH (0.1 µg/mL)

| Name | Amount |
|---|---|
| DAPI (stock) | 10.0 µL |
| 1x PBS | 5.0 mL |
| Total Volume | ~5.0 mL |

**FLUORESCENCE *IN SITU* HYBRIDZATION OF FFPE TISSUE**

Citric Acid Buffer

| Name | Amount |
|---|---|
| Citric Acid | 0.525g |
| $ddH_2O$ | up to 250.0 mL total volume |
| Total Volume | 250.0 L |

- Titrate to pH 6.0

2x SSC pH 7.0

| Name | Amount |
|---|---|
| 20xSSC (stock) | 100.0 mL |
| $ddH_2O$ | up to 1.0 L total volume |
| Total Volume | 1.0 L |

- Titrate to pH 7.0
- Pass through 0.45 µm filter prior to use

0.2M HCl

| Name | Amount |
|---|---|
| 1M HCl (stock) | 10.0 mL |
| $ddH_2O$ | 40.0 mL |
| Total Volume | 50.0 mL |

- Titrate to pH 2.0

Pepsin

| Name | Amount |
|---|---|
| Pepsin (stock, 100 mg/mL) | 250 µL |
| 0.2M HCl (pH 2.0) | 50.0 mL |
| Total Volume | ~50.0 mL |

2x SSC/0.1% NP-40

| Name | Amount |
|---|---|
| 20x SSC (stock) | 50.0 mL |
| NP-40 | 0.5 mL |
| $ddH_2O$ | up to 500.0 mL total volume |
| Total Volume | 500.0 mL |